FINITE ELEMENT MODELING AND SIMULATIONS OF TRACTOR-TRAILER IMPACTS ON HIGHWAY MEDIAN BARRIERS

by

Matthew T. Gutowski

A dissertation submitted to the faculty of
The University of North Carolina at Charlotte
in partial fulfillment of the requirements
for the degree of Doctor of Philosophy in
Mechanical Engineering

Charlotte

2017

Approved by:

_____
Dr. Howie Fang

_____
Dr. Harish P. Cherukuri

_____
Dr. Ronald E. Smelser

_____
Dr. David C. Weggel

_____
Dr. Matthew J. Whelan

ABSTRACT

MATTHEW T. GUTOWSKI. Finite element modeling and simulations of tractor-trailer impacts on highway median barriers. (Under the direction of DR. HOWIE FANG)

Roadside safety hardware systems play a vital role in reducing both the number and severity of multi-vehicular collisions by preventing errant vehicles from traversing through an open median into oncoming traffic. The safety hardware used to prevent cross-median crashes are categorized into flexible, semi-rigid, and rigid barriers based on the allowable deflection and energy absorption of the barrier system. Various barrier systems exist in each category and are required to be evaluated using full-scale crash tests prior to installation approval. Although the majority of the barrier systems are only tested using small- and medium-sized passenger vehicles, impact scenarios involving heavy vehicles (i.e., tractor-trailers) should be investigated to further understand the performance limits of barrier systems and create a safer environment for all vehicles on the road. While full-scale crash tests are useful in understanding the post-impact behavior of a vehicle and a barrier system's redirection capabilities, they are expensive to conduct and are limited by the number of crash scenarios that can be investigated efficiently and effectively. In this research, a finite element model of a full-scale tractor-trailer was improved, validated against full-scale crash test data, and used to simulate crash scenarios on flexible, semi-rigid, and rigid median barriers installed on flat and sloped terrain. The standardized impact conditions and evaluation criteria were utilized for these crash scenarios to assess the median barrier performance, the tractor-trailer post-impact behavior, and the occupant injury risk based on impact severity.

ACKNOWLEDGEMENTS

Completing this dissertation has been a tremendous challenge which would not have been possible without the support and encouragement of my advisor, committee members, colleagues, family, and friends.

I would like to sincerely thank my advisor, Dr. Howie Fang, for his guidance, patience, and support throughout my graduate studies. Without the assistance of Dr. Fang, this dissertation would not have been possible.

I would also like to express my gratitude to Dr. Harish P. Cherukuri, Dr. Ronald E. Smelser, Dr. David C. Weggel, and Dr. Matthew J. Whelan for serving as committee members and providing their valuable time, insight, comments, and advice on my dissertation.

Special thanks to all of my colleagues I have had the pleasure of working with throughout my graduate studies. Additionally, I would like to thank my family and friends who have always believed in me and offered unending motivation, care, and direction.

TABLE OF CONTENTS

LIST OF TABLES

LIST OF FIGURES

LIST OF ABBREVIATIONS

AASHTO	American Association of State Highway and Transportation Officials
ASI	Acceleration Severity Index
ATD	Anthropomorphic Test Device
CEN	European Committee for Standardization
CG	Center of Gravity
CMB	Cable Median Barrier
CMV	Commercial Motor Vehicle
DOT	Department of Transportation
FAST	Fixing America's Surface Transportation [Act]
FE	Finite Element
FHWA	Federal Highway Administration
FMCSA	Federal Motor Carrier Safety Administration
FMVSS	Federal Motor Vehicle Safety Standard
FOIL	Federal Outdoor Impact Laboratory
GVWR	Gross Vehicle Weight Rating
ISOL	Impact and Structural Optimization Laboratory
LON	Length-of-Need
NCAC	National Crash Analysis Center
NCHRP	National Cooperative Highway Research Program
NHTSA	National Highway Traffic Safety Administration
NTRCI	National Transportation Research Center, Inc.

MAP-21	Moving Ahead for Progress in the 21st Century Act
MASH	Manual for Assessing Safety Hardware
MwRSF	Midwest Roadside Safety Facility
OIV	Occupant Impact Velocity
ORA	Occupant Ridedown Acceleration
PHD	Post-impact Head Deceleration
R	Redirected
RIC	Remained-in-Contact
RO	Rollover
SAE	Society of Automotive Engineers
THIV	Theoretical Head Impact Velocity
TL	Test Level
TTI	Texas Transportation Institute
USDOT	United States Department of Transportation

CHAPTER 1: INTRODUCTION

Transportation roadside safety relates to the hardware systems and operational procedures established to prevent and mitigate automotive accidents and fatalities. Although roadside safety is continually improving, with roadways becoming safer though improved safety hardware and stricter vehicle safety regulations, the severity and quantity of traffic-related incidents is still of great concern. According to the World Health Organization's 2015 Global Status Report on Road Safety, there are 1.25 million traffic related fatalities and up to 50 million traffic related non-fatal injuries annually. Traffic fatalities are the leading cause of death among those between the ages of 15-29 years old (WHO 2015). According to the National Highway Traffic Safety Administration's (NHTSA) National Center for Statistics and Analysis (NCSA) 2015 crash data report, there were 6.3 million reported traffic accidents in the United States that resulted in 35,092 fatalities and 2.44 million non-fatal injuries. Of the aforementioned traffic accidents, 433,000 involved heavy trucks, of which, 4,067 were fatal and 116,000 were non-fatal accidents (NCSA 2016).

The Federal Highway Administration (FHWA) categorizes vehicles into classes based on the gross vehicle weight rating (GVWR) in order to prevent trailer overloading and reduce failure of vehicular components. Class 8 vehicles (i.e., heavy trucks) have a GVWR of +33,001 lb (+14,969 kg) and encompass all semi-trailer trucks as well as other

specialized heavy-weight vehicles (AFDC 2012). Traffic accidents typically result in severe multifaceted consequences that include loss-of-life, wage and productivity losses, medical expenses, legal and administrative expenses, and vehicle and/or property damages. The total annual estimated economic cost of all traffic accidents in the United States was reported to be $288 billion in 2015 by the National Safety Council (NSC 2015).

The widely acknowledged ambition for constantly improving roadside safety to reduce collision severity and eliminate occupant injury is a continuous challenge and concern for researchers, safety hardware manufacturers, and vehicle manufacturing companies. As such, countless research efforts and developments have been implemented to improve collision mechanics and make the roads a safer place.

1.1 Transportation Roadside Safety

In order to reduce the total number of accidents, and subsequently, injuries and fatalities, traffic barrier systems are utilized to improve the safety of vehicles that depart the roadway. These barrier systems are used to safely contain and redirect errant vehicles, prevent traversing through a median into oncoming traffic, and reduce the possibility of impacting stationary objects such as trees, telephone poles, and bridge pillars. The barrier systems are categorized into the following three groups: flexible, semi-rigid, and rigid barrier systems. Flexible barrier systems typically include cable median barriers (CMB), semi-rigid barrier systems include double-faced W-beam and Thrie-beam guardrails, and rigid barrier systems include concrete barriers.

The classification of each barrier system is based on the structural rigidity of the barrier system, which determines the amount of deflection and impact energy absorption a

design would permit. All barrier systems installed on public federal, state, and local highways must be designed to the standards outlined in the American Association of State Highway and Transportation Officials (AASHTO) Roadside Design Guide (2006) and successfully assessed using full-scale crash tests according to the testing procedures of AASHTO's Manual for Assessing Safety Hardware (MASH) prior to installation (Sicking et al. 2009). The full-scale crash tests must meet or exceed the MASH performance standards in regard to guardrail adequacy, occupant risk, and post-impact trajectory, prior to being approved for installation on public roadways. The additional FHWA Eligibility Letter is a voluntary certification, typically sought after by hardware manufacturers, which federally recognizes the hardware system for meeting the MASH crash testing evaluation criteria (Alicandri 2017).

MASH specifies six different test levels (TL), which correspond to the vehicle weight class a barrier system is required to be able to safely contain and redirect. TLs 1-3 use compact and mid-sized passenger vehicles such as sedans and pickup trucks, while TLs 4-6 use heavy trucks such as single-unit trucks (i.e., TL-4), semi-trailer trucks (i.e., TL-5), and semi-tanker trucks (i.e., TL-6) in addition to the passenger vehicles used in the lower TLs. All flexible and semi-rigid barrier systems installed on interstate freeways and state highways are tested to at least a MASH TL-3 compliance and, thus, are not typically tested under impacts from larger vehicles. On the same aforementioned roadways, rigid barrier systems (i.e., concrete barriers), as well as bridge railings, are typically tested to a minimum of MASH TL-4 or TL-5 compliance in order to provide redirective capabilities to passenger vehicles as well as heavy trucks.

Semi-trailer trucks are referred to by multiple names in the United States, "tractor-trailer", "18-wheeler", "semi", "semi-truck", or "big rig". For consistency, the most common designation, "tractor-trailer," will be used when discussing semi-trailer trucks throughout the remainder of this research. Tractor-trailers consist of a tractor unit connected to a trailer though the use of a fifth-wheel and kingpin coupling connection. This cylindrical-joint connection adds additional degrees of freedom to the movement of the vehicle, allowing the trailer to articulate about this point to improve the overall mobility and maneuverability of the vehicle. Potential drawbacks to the articulating tractor-trailer include maneuvers not possible with non-articulating vehicles, such as trailer swing or jackknifing. Trailer swing is a recoverable yaw rotation of the trailer whereas jackknifing occurs when either the tractor or trailer independently rotates about the fifth-wheel/kingpin connection, which causes the two truck components to collide with one another. Modern-day tractor-trailers are available in many configurations and are largely dependent on the type of trailer payload. Trailer types include the tank chassis (e.g., oil tanker), flatbed, car carrier, and refrigerator tank trailers, with the most common trailer type being the dry-box/van trailer. The dry-box trailer is available in standard trailer lengths varying from 28 ft (8.5 m) to 57 ft (17.4 m), with the most common industry-standard lengths being 48 ft (14.6 m) and 53 ft (16.1 m) (STAA 1982).

In 2015, 3.63 million tractor-trailers traveled 169.8 billion miles (273.3 billion km), moving 70% of the freight in the United States and contributing to the traffic on 4,500 of the busiest interstates and highways throughout the country, according to the American Trucking Association (ATA 2016). There are an immense number of tractor-trailers on the

road each day, traveling along highways with flexible and semi-rigid barrier systems only tested to MASH TL-3. The performance of these barrier systems under impacts from larger vehicles has not been fully investigated. To this end, roadside safety in regard to the performance of redirection-type hardware systems utilized to contain errant passenger vehicles while minimizing occupant injury should be investigated in relation to Class 8 vehicles, in particular, tractor-trailers.

1.1.1 History of Tractor-Trailer Safety Legislation

Since the creation of the first heavy trucks, specifically tractor-trailers, in 1898 by Alexander Winston (Magoci 2017), the safety of these vehicles has slowly improved, albeit, at a much slower rate than passenger vehicles. Regulations have been implemented throughout the years to improve the operating conditions for truck drivers and create universal guidelines for tractor-trailer dimensions and gross weight limits. In 1935, the Motor Carrier Act was passed by Congress that implemented hours-of-service regulations for truck drivers (MOTOR 1935). The trucking industry was relatively small until 1956, when the Federal-Aid Highway Act authorized the creation of the Interstate Highway System (FEDERAL 1956). After implementation of this act, the trucking industry began to flourish. This act also implemented the first federal maximum GVWR of 73,280 lb (33,240 kg) for tractor-trailers. However, in 1974, the Federal-Aid Highway Amendments changed the federal maximum GVWR to 80,000 lb (36,287 kg) (FEDERAL 1974). The Motor Carrier Regulatory Reform and Modernization Act, also known as the Motor Carrier Act of 1980, deregulated the trucking industry leading to extreme growth, increased productivity, and increased competition between companies (MOTOR 1980). The Surface

Transportation Assistance Act of 1982 standardized the length and width of commercial motor vehicles (CMV) for use on the newly formed National Truck Network, or more commonly the National Network (STAA 1982). The National Network consists of approximately 200,000 miles (321,869 km) of approved state highways and Interstate Highway System designated for used by CMVs.

In an attempt to decrease the severity and quantity of accidents involving large trucks, the Federal Motor Carrier Safety Administration (FMCSA) was established within the USDOT on January 1, 2000, through the Motor Carrier Safety Improvement Act of 1999 (MOTOR 1999), which replaced the former FHWA's Office of Motor Carrier Committee. The FMCSA's primary mission is to issue and enforce Federal Motor Carrier Safety Regulations, gather industry related data from drivers, trucks, and companies to develop new methods and technologies to enhance CMV safety (GAO 2005).

The three-year Moving Ahead for Progress in the 21st Century Act (MAP-21) was passed in 2012 to address the many challenges facing the transportation system in the United States including: improving driver, passenger, and pedestrian safety, maintaining and improving infrastructure, reducing traffic congestion, and improving the efficiency of freight movement. MAP-21 targeted improvements in CMV safety through: stricter regulations to begin operating in the trucking industry, holding trucking companies and their drivers to higher safety standards, and preventing high-risk drivers, trucks, and companies from operating (MAP-21 2012). To continue building on MAP-21, in 2015, the five-year Fixing America's Surface Transportation (FAST) Act was approved to authorize funding for federal-aid highways, highway safety programs, improved mobility and

infrastructure, and environmental preservation (FAST 2015). Notable ongoing and planned research funded by the FAST Act to improve CMV safety includes: improvements to roadside inspection systems, the creation of the Motor Carrier Safety Research Analysis Committee to support the FMCSA's research and technology program, continued development of collision avoidance and automatic stability control systems, among others (Smith 2017).

1.1.2 Tractor-Trailer Crashworthiness

Vehicle crashworthiness is the ability of the vehicle compartment in combination with occupant safety devices to protect the occupant during an impact to reduce the number of fatalities and injuries. In 1966, the NHTSA was created under the Highway Safety Act that introduced Federal Motor Vehicle Safety Standards (FMVSS) to improve the crashworthiness and crash avoidance performance of vehicles (Bois et al. 2004). However, most of these FMVSS are only applicable to passenger vehicles and are not required for CMVs. In 1956, occupant restraints (i.e., seat belts), arguably the most significant occupant protection device, was introduced as an option but was not required in passenger vehicles until 1968 when FMVSS 208 was passed. It was not until 1972, when FMVSS 209 and 210 were introduced pertaining to seat belt assemblies and anchorages, respectively, that federal crashworthiness standards were applicable to tractor-trailers (Williams & Lund 1986).

In 1980, the Society of Automotive Engineers (SAE) formed the Truck Crashworthiness Committee, as a branch of the SAE Cab Occupant Environment Committee formed by truck manufacturers, research institutions, and the USDOT, to

address tractor-trailer occupant crash protection in CMVs. This committee funded a multi-year study to develop test procedures pertaining to occupant restraint performance, maintenance of the occupant's survivable space, and compliance of cab interior surfaces. Results from this study led to the creation of seven SAE Recommended Practices, which provided voluntary procedures to promote the crashworthiness of new tractor cabin designs. The Recommended Practices include: 1) J2418 Occupant Restraint System Evaluation - Frontal Impact Component-Level; 2) J2419 Occupant Restraint System Evaluation - Frontal Impact System-Level; 3) J2420 COE Frontal Strength Evaluation - Dynamic Loading; 4) J2422 Cab Roof Strength Evaluation - Quasi-Static Loading; 5) J2424 Free Motion Headform Impact Tests of Heavy Truck Cab Interiors; 6) J2425 Steering Control Systems - Laboratory Test Procedure; and 7) J2426 Occupant Restraint System Evaluation - Lateral Rollover System-Level (SAE 1997). Each Recommended Practice has been updated at least once since their initial release.

Throughout the years, many aspects of the tractor-trailer have been investigated, studied, and improved to increase the safety and crashworthiness of the vehicle and occupant. For instance, Tobler and Krauter (1972) utilized a derived set of nonlinear equations of motion for a tractor-trailer to investigate the fifth-wheel/kingpin connection and found a geometrical modification to the fifth-wheel design could reduce the jackknifing behavior during turning and braking maneuvers. However, the mechanically derived jackknife prevention systems became obsolete, with the introduction of electronically controlled brake systems (Kawabe & Kawai 1973), minimum stopping

distance requirements using air brakes specified in FMVSS 121 (GAO 1996), and the use of antilock brake systems to improve directional stability and control (GAO 1998).

Under-riding protection for passenger vehicles colliding with tractor trailers is an area of research that has been implemented to improve the overall safety of vehicles on the road. In 1998, FMVSS 223 and 224 were enacted, requiring the use of rear underride guard protection specifications and requirements, respectively. Studies conducted by NHTSA (Bean et al. 2009; Allen 2010) and the University of Michigan Transportation Research Institute (Blower & Woodrooffe 2013) evaluated crash data between 1980-2008, which resulted in a motion for FMVSS updates to improve the safety and performance of the rear underride guards (NHSTA 2015-A). In addition to rear underride protection devices, front and side underride protection devices have been shown to be beneficial and regulations are set in Europe and other countries (Brumbelow 2012). However, no current regulations for such devices are implemented in the United States (Galipeau-Bélair et al. 2013; Cook 2016; IIHS 2017).

As part of MAP-21, the NHTSA composed a report to the House Committee on Transportation and Infrastructure and the Senate Committee on Commerce, Science, and Transportation addressing the need for further heavy truck crashworthiness standards and additional updates to the SAE Recommended Practices (NHSTA 2015-B; 2015-C). As a result, the NHTSA announced FMVSS 136, which requires electronic stability control systems on large trucks and buses by 2019 to help mitigate rollover and loss of control (GAO 2015-A). The NHTSA also funded a grant to evaluate the effectiveness of Forward Collision Avoidance and Mitigation systems in heavy trucks, specifically the use of

Adaptive Cruise Control, Lane Departure Warning, Blind Spot Monitoring, and Forward Collision Warning in combination with Automatic Emergency Braking and/or Collision Mitigation Braking technology (Woodrooffe et al. 2013; GAO 2015-B). The most recent proposed research collaboration between the NHTSA, FMCSA, and USDOT is the investigation of implementing speed limiting devices in CMVs to reduce accident severity (GAO 2016).

1.2 Full-Scale Crash Testing Guidelines and Criteria

Roadside safety hardware systems, by design, have the functional requirements to contain a vehicle that left the roadway by preventing vehicles from penetrating though, vaulting over, or under-riding the barrier system. The barrier systems should also allow the vehicle to redirect smoothly with a low exit angle without causing snagging or vehicle rollover. Additionally, the barriers should absorb enough impact energy to permit tolerable occupant impact forces while minimizing the deformation on the occupant's survivable space (i.e., interior compartment). In order to evaluate roadside safety hardware systems, full-scale crash tests are utilized to classify the performance prior to installation.

In 1962, the Highway Research Board Correlation Service Circular 482 published the first formalized set of full-scale testing guidelines and procedures for evaluating roadside safety hardware (HRB 1962). These guidelines were extremely limited, taking up less than a page, in which a single car under a specified speed and angle, would achieve 'tolerable lateral acceleration'. Over a decade later, the Transportation Research Board's National Cooperative Highway Research Program (NCHRP) Report 153, "Recommended Procedures for Vehicle Crash Testing of Highway Appurtenances," expanded the crash

testing guidelines to two passenger-sized vehicles and expanded the evaluation criteria from the singular criterion of the antiquated Highway Research Board 482 guidelines (Bronstad & Michie 1974). It was not until the creation of the NCHRP Report 230, "Recommended Procedures for the Safety Performance Evaluation of Highway Appurtenances," that tractor-trailers were added as test vehicles to the crash testing guidelines (Michie 1981).

The next iteration of testing procedures, NCHRP Report 350: "Recommended Procedures for the Safety Performance Evaluation of Highway Features" (1993), established six TLs for different vehicle weight classes, as well as refined the roadside hardware evaluation criteria into three categories: structural adequacy, occupant risk, and post-impact vehicle response. In 1998, AASHTO and FHWA collaboratively agreed that all newly installed safety hardware along the National Highway System must meet NCHRP Report 350 safety-performance evaluation criteria (USDOT 1998).

The successor of NCHRP Report 350 began in 1997 as NCRHP project 22-14 "Improvement of the Procedures for the Safety-Performance Evaluation of Roadside Features" (Bligh 2001) and was completed under NCHRP Project 22-14(02), "Improved Procedures for Safety-Performance Evaluation of Roadside Features" in 2008 (Sicking). The results from this 11-year study were formally published by AASHTO in 2009 as the MASH (Sicking et al. 2009). MASH contained revisions for criteria of safety-performance evaluation for virtually all roadside safety features in addition to updates of the vehicle classes to more accurately represent present-day vehicles.

More recently, AASHTO released the second revision of MASH (2016), (i.e., MASH-2) which ended the approval of NCHRP Report 350 compliant roadside safety hardware, in addition to requiring all previously approved NCHRP Report 350 hardware installed on the National Highway System be replaced or retested under MASH-2 evaluation criteria as part of the AASHTO/FHWA Joint Implementation Agreement (USDOT 2016). To assist hardware manufacturers and state DOTs in fulfilling the AASHTO/FHWA Joint Implementation Agreement, procedures for evaluating non-proprietary roadside safety hardware under MASH evaluation criteria were developed through NCHRP 22-14(03) (Bullard et al. 2010).

Due to the feasibility limitations of conducting full-scale crash tests for an array of impact scenarios, the criteria set forth by MASH and its successors established the impact conditions of the crash tests to emulate the 'worst practical conditions.' This postulation is based on the fact that, if the roadside hardware performed satisfactorily under severe impact conditions, all other impact scenarios will result in adequate performance from the roadside hardware (AASHTO 2016). However, limitations to the full-scale crash tests conducted under laboratory conditions do not account for a number of variables that may be present when the roadside safety hardware systems are installed along roadways. Some of the factors include: installations on uneven or sloped terrain, damaged or improperly repaired hardware, weather conditions, and driver responses. Due to these limitations, the need for in-service performance evaluation has been recognized by AASHTO and FHWA. However, the difficulties of performing and monitoring in-service evaluation has prevented

establishment of requirements in the roadside safety hardware testing manuals (Carrigan et al. 2017).

1.3 Full-Scale and Numerical Tractor-Trailer Crash Testing

Roadside safety hardware systems developed by manufacturers, state DOTs, and university research centers are required to be crash tested to assess the safety performance. There are currently nine crash-testing facilities in the United States, accredited and recognized by FHWA, for conducting full-scale crash tests of roadside safety hardware to determine if AASHTO performance standards are met. These testing facilities include: California Department of Transportation, E-TECH Testing Services, Inc., KARCO Engineering, Midwest Roadside Safety Facility (MwRSF), FHWA/NHTSA National Crash Analysis Center (NCAC), Safe Technologies, Inc., Southwest Research Institute, Texas Transportation Institute (TTI), and Transportation Research Center, Inc. (Faller 2017)

Beginning in 1981, 17 full-scale crash tests have been conducted using tractor-trailers of different configurations, all of which, excluding the most recent in 2016, were impacted against a rigid concrete structure. The concrete structures include a variety of bridge railing types (i.e., Texas C202, T5, and T224, F-shape, Vertical, and Aesthetic open) ranging in height from 42-54 in (1.1-1.4 m), concrete barriers (i.e., 42-in (1.1-m) New Jersey, Ontario Tall Wall, Vertical slope, and a 32-in (0.8-m) F-Shape), and a 90-in (2.3-m) instrumented wall. The aforementioned excluded crash test conducted in 2016 utilized a proprietary 59.6-in (1.5-m) combined steel Thrie- and W-beam guardrails stacked on top of each other (Clausius 2016). Twelve crash tests were conducted at TTI, two crash tests

were conducted at MwRSF, one crash test was conducted at NCAC's Federal Outdoor Impact Facility (FOIL), and the most recent steel guardrail crash test was conducted at Holmes Solutions, an FHWA accredited international testing facility in New Zealand.

The crash test conducted at FOIL was the only full-scale test using a tractor without a trailer unit attached (Marzougui 2003). Two of the early tests conducted at TTI used cab-over-engine tractors instead of the more common conventional tractor where the engine is located in front of the cab (Campise & Buth 1986; Mak et al.1988). Three of the full-scale tests used 50,000-lb (22,680-kg) tractor-trailers opposed to the more commonly used fully-laden 80,000-lb (36,287-kg) tractor-trailers (Beason & Hirsch 1989; Buth et al.1997-A; 1997-B). Another full-scale test conducted at the same time as the TTI cab-over-engine crash test used a conventional tractor with a 36.5-ft (11.1-m) tanker-trailer (i.e., TL-6, although TLs were not implemented until NCHRP Report 350 (1993)) . The remaining full-scale crash tests consisted of conventional tractors with trailers ranging in lengths from 40-48 ft (12.2-14.6 m) (Hirsch & Fairbanks 1984; Hirsch et al. 1986; Mak & Campise 1990; Alberson et al. 1997; Polivka et al. 2005; Rosenbaugh et al. 2007; Saez et al.2015; Williams et al. 2015; Clausius 2016; Rosenbaugh et al. 2016)un. All of the crash tests, except for the tractor-only FOIL test, used uniform impact conditions of 15° impact angle and 50-mph (80-km/h) impact speed. The aforementioned FOIL impact used a 25° impact angle and an impact speed of 31 mph (50 km/h).

In regard to conducting full-scale finite element (FE) simulations of crash tests, extremely limited research has been conducted. Historically, numerical analysis has been limited to the use of studying, improving, and developing individual systems or regions of

tractor-trailers. Simplified lumped-mass-spring dynamic models have been used to analytically assess the vehicle vibrations (Gadala et al. 1986), leaf-spring suspension response (Ibrahim 1999; 2004), braking performance (Suh et al. 2002), and tire forces (Cole & Cebon 1992) on different road conditions. More recent FE simulations were used to analyze tractor leaf spring designs (Dhoshi et al. 2011; Lakshmi & Satyanarayana 2012; Ghodake & Patil 2013) and individual front suspension designs (Yarmohamadi & Berbyuk 2013). FE analysis has also been used to structurally assess the design of the tractor frame rails (Kurdi et al. 2008; Vallejo 2008; Paul et al. 2012), trailer floor (Högberg 2001), trailer frame (Tohti et al. 2012; Abad et al. 2013), the tractor-trailer fifth-wheel/kingpin connection (Schoffner et al. 2007; Shoffner 2008; Cinar 2012), and the fuel tank placement (Friedman et al. 2016). In another study, the suspension system on a simplified tractor-trailer FE model was developed (Li et al. 2006) and used to assess the dynamic response of highway bridges subjected to a moving tractor-trailer (Szurgott et al. 2010).

Additional FE modeling and simulation work has been conducted pertaining to the occupant safety of tractor-trailer drivers. Parnell et al. modeled a tractor-cabin to evaluate the structural integrity of the frame during a 180° rollover event as part of the SAE's Heavy Truck Crashworthiness study (1999). In 2015, TTI and the University of Michigan Transportation Research Institute conducted a study in which a FE model consisting of a tractor cabin, simplified anthropomorphic test device (ATD) (i.e., crash test dummy), seat, restraint system, and airbag was used to assess the occupant safety during a full-frontal impact and a 90° rollover. The authors experienced several limitations in the research including only modeling the tractor cabin, using a reduced element ATD model, and

estimation of the interior compartment materials and dimensions due to the lack of publicly available information. These limitations, among others, appeared to be the leading cause of the occupant injury responses from the full-frontal impact exceeding the allowable threshold values. Additional limitations were encountered with the rollover impact scenario resulting in occupant injury criteria not being assessed. The authors proposed further research be conducted to surmount the limitations the abovementioned study experienced in order to better evaluate the safety of a tractor-trailer occupants using FE simulations (Dobrovolny et al. 2015).

Beyond the 2007-2010 development of the full-scale tractor-trailer FE model through a USDOT Research and Innovative Technology Administration sponsored project conducted at the National Transportation Research Center, Inc. (NTRCI) University Transportation Center collaborating with Battelle, Oak Ridge National Laboratory, and the University of Tennessee at Knoxville (Plaxico et al. 2007; 2009; Miele et al. 2010), to date, no published research utilizing the full-scale tractor-trailer FE model for redirective impact scenarios publicly exists. However, Plaxico and Ray (2015) used a version of an unladen tractor-trailer FE model to simulation a head-on impact into a bridge pier for an ongoing NCHRP study to develop guidelines for shielding bridge pillars in the AASHTO Load and Resistance Factor Design (LRFD) Bridge Design Specifications manual (Ray et al. 2012).

In the remainder of this research, the improvement and validation of a full-scale tractor-trailer FE model is conducted for use in assessing the performance of in-service flexible, semi-rigid, and rigid median barrier systems, with the use of nonlinear dynamic numerical simulations, using MASH TL-5 impact conditions. CHAPTER 2 will briefly

discuss one of the most important aspects of numerical simulations, the handling of contact interfaces. CHAPTER 3 elaborates on the development and improvement of FE models for a conventional day-cab tractor, a 48-ft (14.6-m) dry-box trailer, and a 50,000-lb (22,680-kg) trailer ballast load and the subsequent validation of said FE models against experimental full-scale crash test data. CHAPTER 4 discusses the creation of the models for the flexible, semi-rigid, and rigid median barrier systems used in this research. CHAPTER 5 conveys the evaluation criteria used to assess impact scenarios and presents the FE simulation results by barrier type. CHAPTER 6 analyzes all impact scenarios by comparing the evaluation criteria results and CHAPTER 7 provides a summary of the research findings. Appendices are provided postscript as a supplemental reference to CHAPTER 5.

CHAPTER 2: CONTACT THEORY

The handling of contact analysis is a fundamental part of simulating FE vehicle crashes as well as other engineering applications. Modeling interactions between parts and the subsequent deformations of various components is not possible without accurate contact handling methods. The contact algorithms used to define an interface between neighboring entities as well as self-contact is arguably one of the most important and computationally expensive aspects of conducting numerical simulations. Properly defining appropriate contact formulations and contact handling techniques will ultimately control the accuracy and validity of the FE analysis results. Throughout the development of FE software, various contact methods have been implemented to improve the efficiency and accuracy of contact handling, primarily the Lagrangian multiplier method and the penalty method. In this chapter, the advantages and disadvantages of these contact formulations will be discussed in section 2.1 and the implementation of the contact algorithms in LS-DYNA is presented in section 2.2.

2.1 Contact Methods and Formulations

Due to the severe deformations that typically occur in vehicle-to-barrier crashes, establishing appropriate contact formulations between neighboring interfaces is a major controlling factor in determining the stability and accuracy of the numerical simulation.

The most common contact formulations used to enforce contact constraints are the Lagrangian multiplier method and the penalty method.

In the Lagrangian multiplier method, contact forces are introduced as unknowns in the form of Lagrangian multipliers (Kikuchi & Oden 1988) and the non-penetration condition is explicitly enforced (Zhong & Mackerle 1992). Although this method has relatively high accuracy, the introduction of the unknown Lagrangian multipliers and the subsequent solving of additional variables in the contact force equations is computationally inefficient and costly. It was observed by Hallquist et al. (1985) that the Lagrangian multiplier method did not preserve a smooth force distribution across contact interfaces and excited zero energy modes in the elements involved.

The penalty method was originally developed both theoretically and computationally as a solution for equality constrained optimization problems (Fiacco & McCormick 1964; 1966). The penalty method was implemented into LS-DYNA by Hallquist et al. (1985) to calculate the contact force as a function of deformation. Unlike the Lagrangian multiplier method, the penalty method does not introduce new unknown variables making it the most commonly used contact formulation due to its relative simplicity and high efficiency in contact problems for both explicit and implicit FE codes. The penalty method was used exclusively for all numerical simulations and will be discussed herein.

2.1.1 The Penalty Method

The penalty method's main advantage compared to other contact formulations lies in its fast convergence, solution accuracy, and ease of implementation within numerical FE

codes. The penalty method algorithm is achieved by assuming that the normal load

magnitude is proportional to the residual of the impenetrability constraints using penalty

coefficients. The penalty coefficients are applied by hypothetical normal interface springs,

which apply a repulsive force to contacting bodies proportional to the penetration depth to

prevent bodies from occupying the same physical space. The stiffness of the interface

springs is known as the contact stiffness. The contact stiffness along with the penetration

depth is used to define the contact force expressed by

$$\boldsymbol{F}^c = kD \tag{2.1}$$

where k is the contact stiffness and D is the penetration depth. Figure 2.1 illustrates the

determination of the penetration depth used for the contact force equation above.
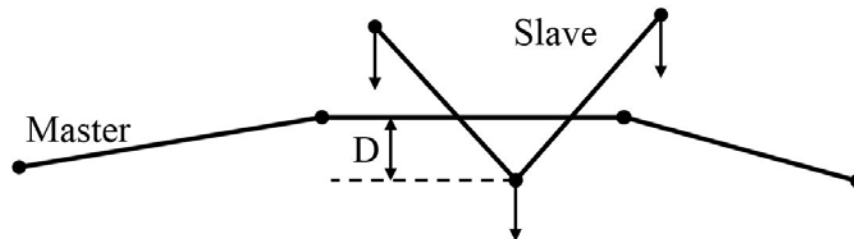
Figure 2.1: Determining penetration depth

The contact forces for each penetrating body are assembled into a vector that is

added to the global equation of motion (Laursen 2003), given by

$$\boldsymbol{M}\ddot{\boldsymbol{d}}(t) + \boldsymbol{F}^{int}\big(\boldsymbol{d}(t)\big) + \boldsymbol{F}^c\big(\boldsymbol{d}(t)\big) = \boldsymbol{F}^{ext}(t) \tag{2.2}$$

where t is the time, $\boldsymbol{M}$ is the mass matrix, $\ddot{\boldsymbol{d}}(t)$ is the acceleration vector, $\boldsymbol{F}^{int}$ is the

internal force vector, $\boldsymbol{d}(t)$ is the displacement vector, $\boldsymbol{F}^c$ is the contact force vector, and

F^{ext} is the external force vector. The aforementioned equation is typically nonlinear for impact related applications. For example, the internal forces have a nonlinear relationship to displacements due to material nonlinearities as well as the nonlinear function of displacements in the contact force from nonlinearities of the contact interfaces. The different penalty formulation methods differ primarily in the way the penalty coefficients are assigned. The penalty coefficients have three distinct formulations for calculating the contact stiffness, these include the standard penalty formulation, the soft-constraint penalty formulation, and the segment-based penalty formulation.

2.1.1.1 Standard Penalty Formulation

The standard penalty formulation is the default method in which the contact stiffness is calculated using material constants and the geometry of the discretized body (i.e., elements). In this method, penetrations of each slave node to the master segment is checked at each time step. If no penetration is detected, the calculation moves on. Otherwise, an interface force is applied between the slave node and the master segment. Since the penalty coefficient is dependent on material properties and element size, the contact stiffness is calculated differently for shell and solid elements. For shell elements, the contact stiffness is defined by

$$k_p = \frac{S_{sl}KA}{\max(shell\ diagonal)} \tag{2.3}$$

where S_{sl} is the sliding interface penalty scale factor, K is the material's bulk modulus, A is the element contact area, and the denominator is the length of the largest diagonal shell element. For solid elements, the contact stiffness is defined by

$$k_p = \frac{S_{sl}KA^2}{V} \tag{2.4}$$

where V is the volume of the element (Hallquist 2017). The standard penalty contact

formulation is most effective and stable when the contacting surfaces have similar material

properties. Therefore, the standard penalty formulation is not recommended for contacting

materials that have highly dissimilar elastic bulk moduli, such as soft foams contacting

metals. Additionally, this formulation is not affected by the time step size since the

penetration check between the slave nodes and master surface is conducted at each time

step.

2.1.1.2 Soft-Constraint Penalty Formulation

The soft-constraint penalty formulation is an alternative approach that is capable of

handling contacting surfaces of dissimilar materials and dissimilar mesh densities. This

penalty formulation utilizes the same slave node to master surface penetration checking

and calculation of the contact stiffness using the default standard penalty formulation.

However, an alternative soft contact stiffness using nodal masses and the initial time step

is used. This soft contact stiffness is determined by

$$k_s = 0.5 S_{sc} \frac{m^*}{\Delta t_c{}^2} \tag{2.5}$$

where S_{sc} is the soft constraint scale factor, m^* is a function of the mass of the slave and

master nodes, and Δt_c is the initial time step. The time step variable is updated to the

current time step if the solution time step grows, in order to prevent unstable behavior

(LSTC 2017). This soft-constraint contact stiffness is compared to the standard penalty

contact stiffness and the maximum of the two contact stiffness values is used to calculate the contact force.

2.1.1.3 Segment-Based Penalty Formulation

Contrary to the previous two penalty formulation methods, the segment-based penalty formulation uses segments on the slave and master surfaces when checking for penetration as opposed to the slave node to master segment penetration checking of the previous two methods. The segment-based penalty formulation method is useful for applications where penetrations occur in such a way that the slave nodes do not intersect with the master segment, which can occur during edge-to-edge and surface-to-surface contacts. This method of contact formulation is more robust than the aforementioned methods and is capable of handling contacting surfaces with sharp corners and unequal mesh densities. The segment-based penalty formulation is able to distribute the contact forces more realistically to all nodes equally throughout the segments in contact. The contact stiffness calculation in the segment-based formulation is similar to the soft-constraint based formulation except the mass variable uses the segment masses instead of nodal masses. The segment mass variable is equal to the element mass for shell elements and half the element mass for solid elements. The segment-based contact stiffness is calculated by

$$k_s = .5 S_{sl} \begin{Bmatrix} SFS \\ or \\ SFM \end{Bmatrix} \left(\frac{m_s \cdot m_m}{m_s + m_m} \right) \frac{1}{\Delta t_c^2} \tag{2.6}$$

where SFS is the slave segment penalty stiffness scale factor, SFM is the master segment penalty stiffness scale factor, and m_s and m_m are the respective masses of the slave and master segments. This formulation also differs from the soft-constraint formulation in the method of updating the time step variable. The initial time step variable is only updated when the solution time step increases by more than 5%; therefore, the time step variable in this formulation usually remains constant. Another difference between the two previous penalty formulations and the segment-based penalty formulation is that initial penetrations are not eliminated at the beginning of the analysis. Instead, the initial position of the segments in penetration are used as a baseline and any further penetrations are calculated from the initial baseline position. This method is useful for extremely large models consisting of hundreds of components that may have several initial penetrations. However, this feature should not be used as an alternative to properly configured FE models.

2.2 Contact Modeling in LS-DYNA

The continual development and improvement of contact handling algorithms in LS-DYNA has been ongoing since Livermore Software Technology Corporation was founded in 1987 by John O. Hallquist to commercialize DYNA3D, developed at the Lawrence Livermore National Laboratory (Hallquist 1976). To date, there are over 60 different methods for handling various contact situations implemented in LS-DYNA (LSTC 2017). Modeling accurate numerical simulations in LS-DYNA relies highly on the proper definitions of contact between neighboring bodies that will touch, push, and/or slide against each other. In LS-DYNA, contact between the slave and master surfaces can be defined using nodes, node sets, parts, part sets, segments, or segment sets. Traditionally, contact is

checked between slave nodes and the master surface (i.e., segment) in contact methods categorized as node-to-surface contacts. A slightly different group of contact methods called surface-to-surface contacts use the slave surface instead of the slave nodes to check for contact with the master surface. The third and most commonly used group of contacts for crash applications is the single surface contacts, in which all entities are defined in a single slave set and self-contact, in addition to contact between all defined entities, is checked. Each contact group has its own benefits and shortcomings, and will be discussed in the following sections.

2.2.1 Nodes-to-Surface Contacts

Node-to-surface contacts are categorized as one-way treatment contacts, meaning only penetration of the slave nodes through the master surface is checked at each time step. Contact forces are applied to the slave nodes to eliminate penetrations through the master surface. In addition, tangential contact forces can be applied using the Coulomb friction formulation with an exponential interpolation function to transition from static to dynamic friction defined by

$$\mu_c = \mu_d + (\mu_s - \mu_d)e^{-DC|v_{rel}|} \tag{2.7}$$

where μ_c is the Coulomb coefficient of friction, μ_d is the dynamic coefficient of friction, μ_s is the static coefficient of friction, DC is the exponential decay coefficient, and v_{rel} is the relative velocity of the contacting surfaces.

The node-to-surface group of contacts are the simplest method of handling contact detection but has its limitations. For instance, penetrations may not be detected with an

extremely coarse mesh on the slave surface. Great care should be taken when defining slave and master entities. It is recommended that the coarser mesh entities should be selected as the master surface when defining contact (Bala 2001). Additional recommendations include selecting a master surface for parts with larger material stiffness and larger surface area (Stelzmann 2012). Due to the asymmetric penetration searching of the node-to-surface contacts, these computationally efficient contact methods are useful when the direction of contact will remain constant throughout the numerical simulation, such as with tires contacting the road surface. However, penetration is only checked on slave nodes pointed in the normal direction from the master surface; therefore, these types of contacts are not recommended for highly deformable and/or geometrically complex parts. Figure 2.2 illustrates the one-way treatment of the nodes-to-surface contact algorithm.
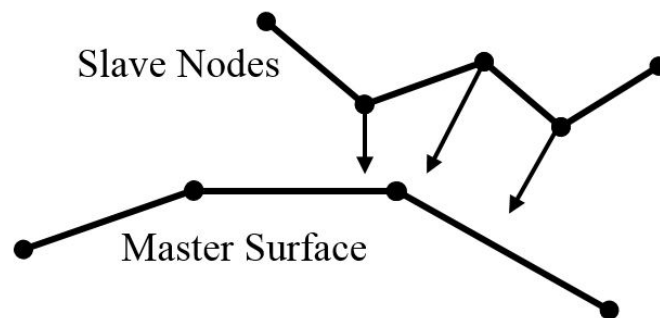
Figure 2.2: One-way Nodes-to-Surface contact treatment

The following contacts are implemented in LS-DYNA as one-way contacts: NODES_TO_SURFACE, ONE_WAY_SURFACE_TO_SURFACE, AUTOMATIC_ BEAMS_TO_SURFACE, AUTOMATIC_NODES_TO_SURFACE, and AUTOMATIC_

ONE_WAY_SURFACE_TO_SURFACE. The addition of the 'AUTOMATIC' term to the contact method enables the detection of contact on either side of the master surface. The majority of commonly used contacts utilized in LS-DYNA, particularly in crash analysis, use the 'AUTOMATIC' option, as they are better suited at handling contacts with disjointed meshes.

2.2.2 Surface-to-Surface Contacts

The surface-to-surface group of contacts, also known as two-way contacts, check for penetrations in essentially the same way as the one-way contacts except, after checking for penetrations between the slave nodes and master surface, penetrations are then checked for between the master nodes and the slave surface. Due to the symmetric nature of the contact checking, the selection of the slave and master surfaces is arbitrary, since all nodes on both surfaces are checked against the other surface Although the two-way contacts are twice the computational cost of one-way contacts, they benefit from being able to handle contact between surfaces in which the orientation is not initially known. The only two-way contact defined in LS-DYNA that is recommended for crash-related numerical simulations is AUTOMATIC_SURFACE_TO_SURFACE. Figure 2.3 illustrates the two-way treatment of the surface-to-surface contact algorithm.
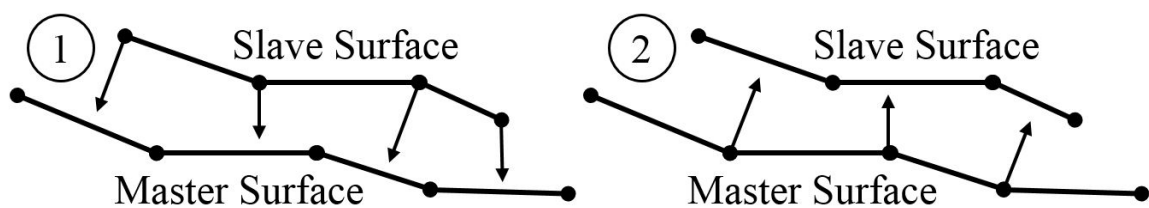
Figure 2.3: Two-way surface-to-surface contact treatment

2.2.3 Single Surface Contacts

The single surface group of contacts are the most widely utilized contact definitions in LS-DYNA, especially for crash analysis applications. These contact methods, implemented by Benson and Hallquist (1990), use two-way contact treatment with no master surface defined. Only a single slave set, typically a part list, is required. Contact is checked between external surfaces in all parts defined, including self-contact. Caution is advised when defining which parts will be included in the contact definition, since over-defining the contact will increase the computational time and cost. The two main contacts in this group are AUTOMATIC_SINGLE_SURFACE and AUTOMATIC_GENERAL. Both of these contacts have non-automatic versions but are outdated and not recommended for most applications. Although the two contacts in this group are defined the same way by only selecting a slave set, the way contact is checked between parts vastly differs. While AUTOMATIC_SINGLE_SURFACE is able to use node-to-segment and segment-to-segment penetration checking methods, AUTOMATIC_GENERAL only uses the segment-to-segment method when checking for penetrations. Figure 2.4 shows the segment-to-segment contact checking of the single surface contact types.
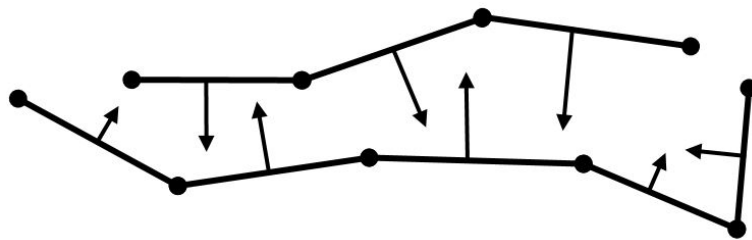
Figure 2.4: Single surface segment-to-segment contact treatment

One of the main fundamental differences between these two contacts is how beam element contacts and external shell edge contacts are handled. The default AUTOMATIC_SINGLE_SURFACE contact checks for penetrations only at node locations of beam and external shell elements instead of along the entire length of the beam or shell element edge as the AUTOMATIC_GENERAL contact does. The contact treatment of shell edge-to-edge and beam-to-beam contact is exclusive to the AUTOMATIC_GENERAL contact. The number of master segments stored to check for penetrations between each slave node or segment differs with each contact; AUTOMATIC_SINGLE_SURFACE uses two segments while AUTOMATIC_GENERAL uses three segments. In addition, the AUTOMATIC_GENERAL contact identifies and updates these master segments in the contact search at a frequency tenfold to that of the AUTOMATIC_SINGLE_SURFACE contact. The AUTOMATIC_GENERAL contact also has an additional 'INTERIOR' option (i.e., AUTOMATIC_GENERAL_INTERIOR) that includes all interior shell edges in the contact penetration checks. Figure 2.5 illustrates the distinction between exterior and interior edges.
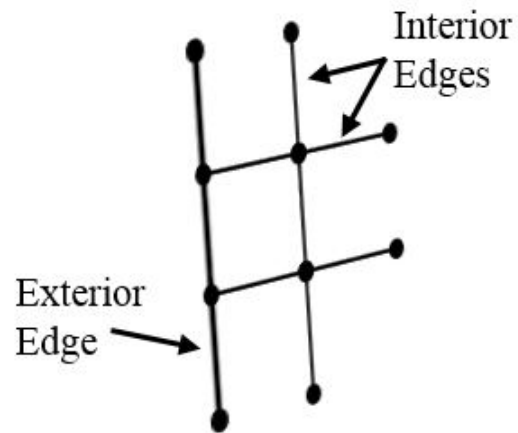
Figure 2.5: Exterior and interior edges

The addition of the interior edges in the penetration checking incurs an additional computational cost, but greatly improves the robustness and usefulness in applications where the contact surfaces experience large deformations, such as crash-related numerical simulations (LSTC 2017).

CHAPTER 3: FINITE ELEMENT MODELING OF A TRACTOR-TRAILER

While full-scale crash testing has been used for evaluating new vehicle models and roadside safety hardware designs, the use of numerical simulations to explore and evaluate performance improvements to new designs as well as investigate additional crash scenarios not evaluated using full-scale crash testing has increased. In this chapter, the FE models used for testing and validation of tractor-trailer impact scenarios are discussed. In particular, the FE models of a 1991 White/GMC WG64T conventional day-cab tractor, a 1990 Stoughton 48-ft (14.6-m) dry-box trailer, and a 50,000-lb (22,680-kg) ballast trailer load are reviewed.

On a fundamental level, vehicles are comprised of a multitude of individual components, connected together using welds, rivets, and bolts. Although most structural components in a vehicle are typically steel, other parts are made of aluminum, metallic foam, and composite materials such as fiberglass. The increasing complexity of newer vehicles imposes a challenge to accurately depict and numerically model these vehicles. A typical passenger sedan has as many as 30,000 parts, with larger vehicles consisting of even more parts. Because of the large number of parts in these vehicles, simplified FE models are created to accurately model the most important aspects of the vehicles, usually the structural components, to represent the vehicle deformation and energy absorption capabilities. In general, the selection of mesh density, mesh quality, element selection, and

element size of vehicular components can greatly affect the computational cost, and are of great importance regarding the reliability of crash-related numerical simulation results. For vehicle crashworthiness evaluation, the main objective is to assess the ability for a vehicle's structural components to protect the occupants during a collision. Extensive detail is typically included for structural components, the interior compartment, and occupant restraint systems, to more accurately represent the vehicle's occupant safety capabilities (Marzougui et al. 2012). For example, the powertrain system of a tractor, presented in Figure 3.1, includes the engine, transmission, multiple drive-shafts, engine mounts, and three axles, and is a critical system that greatly affects the vehicle kinematics during a collision (Fancher et al. 1986). Accordingly, attention to accurately modeling this system is of great importance.
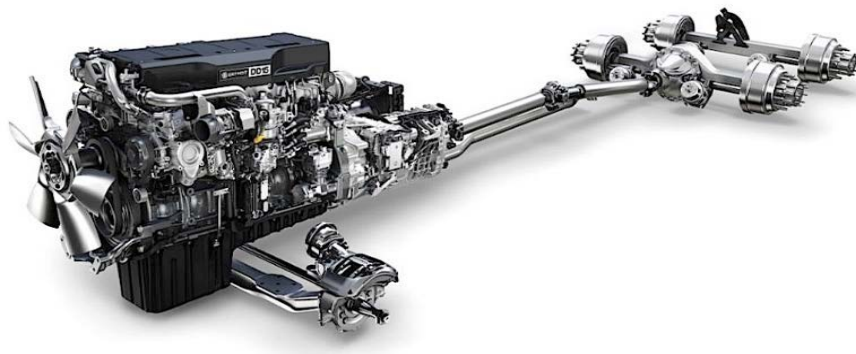
Figure 3.1: Tractor powertrain system (URL1)

Contrary to the vehicle models used for crashworthiness analysis, where high levels of detail are used for multiple regions of the vehicle, the vehicle models used for roadside safety hardware evaluation are often simplified, 'bullet' models, which do not include

certain aspects, such as the interior compartments or restraint systems. Since these FE models are not primarily used to examine the crashworthiness of the vehicle, but rather evaluate the overall crash performance through the analysis of the kinematic behavior and energy transfer throughout the impact, these simplified models are accepted as the industry standard for roadside safety hardware evaluation (Plaxico et al. 2007). In addition, simplifications to bolted and spot weld connections, where deformation is negligible and not of primary interest, are often represented without failure mechanisms. However, newly developed vehicle FE models often include an enormous amount of detail, representing the minutest detail in order to capture more realistic vehicle kinematics and dynamic loading conditions encountered in a variety of impact scenarios. These extremely detailed FE models currently only exist for smaller passenger vehicles. For larger vehicles, such as a tractor-trailer simplifications are still made in order to maintain a computationally efficient FE model due to the overall size of the vehicle. The following chapter will discuss the development and improvement of a tractor and trailer model, followed by the validation of the FE models using full-scale crash test data. The FE modeling work conducted in this research was completed at UNC Charlotte's Impact and Structural Optimization Laboratory (ISOL).

3.1 Finite Element Model of a Day-Cab Tractor

The initial tractor FE model was created at NCAC, and modeled after a 1992 Freightliner FLD120 sleeper-cab tractor, with a wheelbase of 16.9 ft (5.2 m) and a test inertia weight of 14,683 lb (6,660 kg) (Plaxico et al. 2007). The initial tractor FE model was elementary in its development and fidelity. The FE model was determined to be

inaccurate due to over-simplifications throughout the vehicle, such as the omission of structural components and lack of geometrical detail in key aspects of the tractor. Some limitations of this original model included: distribution of the mass of non-modeled parts to neighboring components by adjusting material properties, omission of failure criteria in the tractor's front axle and suspension components, use of extremely large mesh elements for critical components, and use of overly simplified contact definitions.

Before this FE model was validated against full-scale tests, NTRCI made major improvements to the model. The improvements included mesh refinement for critical structural components to improve element quality and computational efficiency, assigning appropriate material properties based on material classifications from the vehicle, and improving the geometrical detail by comparing the FE model to full-scale tractors. Improvements were also made to accurately represent the tractor's front and rear suspension systems. The tractor's front leaf-spring suspension assembly was purchased and force-velocity laboratory testing of the assembly was used to define the material properties for the model. Additionally, the shock absorbers from the suspension system were purchased to determine the force-velocity responses to characterize the material properties of the front and rear shock absorbers. The last suspension system improvement was to define the material parameters for an unloaded tractor and a loaded 80,000-lb (36,287-kg) tractor-trailer of the rear Air-Ride suspension components. These improvements, as well as other minor modifications, resulted in an enhanced tractor FE model that was suitable for use for validation against full-scale crash test data. Figure 3.2 shows the enhanced sleeper-cab tractor FE model provided by NTRCI (Plaxico et al. 2007).

Figure 3.2: NTRCI enhanced FE model of a sleeper-cab tractor

The NTRCI tractor FE model had a wheelbase of 16.9 ft (5.2 m) and a test inertia weight of 16,255 lb (7,373 kg). This model contained 459 parts, discretized into 115,816 elements, utilizing 11 constitutive models. The 11 constitutive models included: the piecewise linear plasticity model defined for steel components, the rigid model for mounting hardware, the elastic model for the tires and other rubber components, the nonlinear elastic spring model and Maxwell spring model for the rear axle's air-ride suspension, the linear and nonlinear viscous damping models for the front and rear axle's shock absorbers, the thermal elastic-plastic model for the front suspension U-bolts, the laminated glass model for the windows, the simplified rubber with damage model for the rubber cushions between the front axles and frame rails, and the null material model for contact purposes.

Before the NTRCI tractor FE model could be validated against the full-scale tractor-only test data from a 1992 Freightliner FLD120 impacting a 32-in (813 mm) rigid

F-shape concrete barrier, conducted at NCAC's FOIL in McLean, Virginia on August 28, 2003 (Marzougui 2003), additional numerical modifications to the tractor FE model were required. Throughout the entire NTRCI tractor FE model, numerous initial penetrations and crossed edges were present that greatly affected the numerical stability and performance of FE simulation results. Figure 3.3 illustrates the initial penetrations and crossed edges that were present in the NTRCI tractor FE model and subsequently removed, at ISOL, to improve the numerical model's robustness, stability, and fidelity.
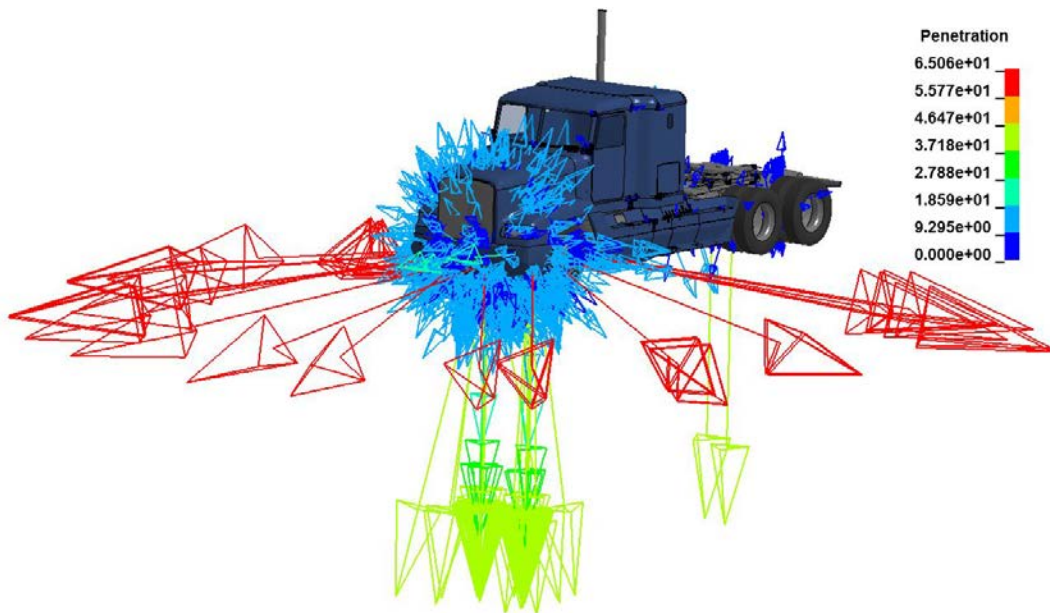
Figure 3.3: Initial penetrations (mm) present in the NTRCI tractor FE model

In the NTRCI tractor FE model, the propeller shaft of the second driveshaft, connecting the rear tandem axles together, was not modeled. The omission of this core structural component resulted in inaccurate kinematic responses during redirective impact

scenarios. To resolve this, the propeller shaft on the rear tandem driveshaft was introduced to the ISOL FE model. In Figure 3.4, a top-down view of the rearmost portion of the NTRCI and ISOL tractor FE models are shown with the drive shafts highlighted in yellow. The missing propeller shaft in the NTRCI model is seen in Figure 3.4a and the modeled propeller shaft in the ISOL model seen in Figure 3.4b.

a. NTRCI FE model   b. ISOL FE model
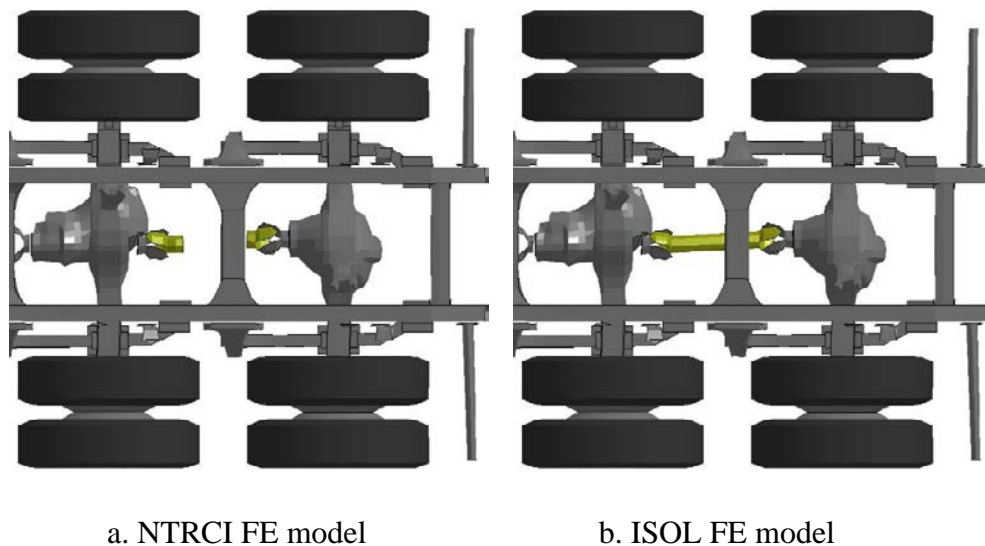
Figure 3.4: Tractor FE model's second driveshaft

Additional in-house FE model revisions were made to convert the NTRCI FE sleeper-cab tractor to a day-cab tractor and remove additional components in order to correspond with the FOIL full-scale test tractor configuration. The ISOL tractor FE model of the 1992 Freightliner FLD120 tractor was modified to remove the sleeper-cabin, exhaust stack, hood, fenders, mud flaps, and other miscellaneous components to more accurately correlate with the full-scale crash test tractor. Other modifications made to the ISOL tractor

FE model included, general keyword reorganization and further mesh refinement of critical

components that experience large deformations during redirective impacts against flexible,

semi-rigid, and rigid median barriers. For example, the mesh on the tractor fuel tanks was

too large for a component which experienced a direct impact. Figure 3.5a shows the mesh

of the fuel tank on the NTRCI FE model and the subsequent inaccurate deformations after

being impacted in Figure 3.5b. In the ISOL FE model, the mesh was refined for structural

components and parts which would be subjected to severe deformations during an impact

scenario (see Figure 3.6a and Figure 3.6b). Figure 3.7 shows the test tractor from the full-

scale FOIL tractor crash test as well as the corresponding enhanced and modified ISOL

tractor FE model used for validation.

a. NTRCI fuel tank   b. NTRCI deformed fuel tank
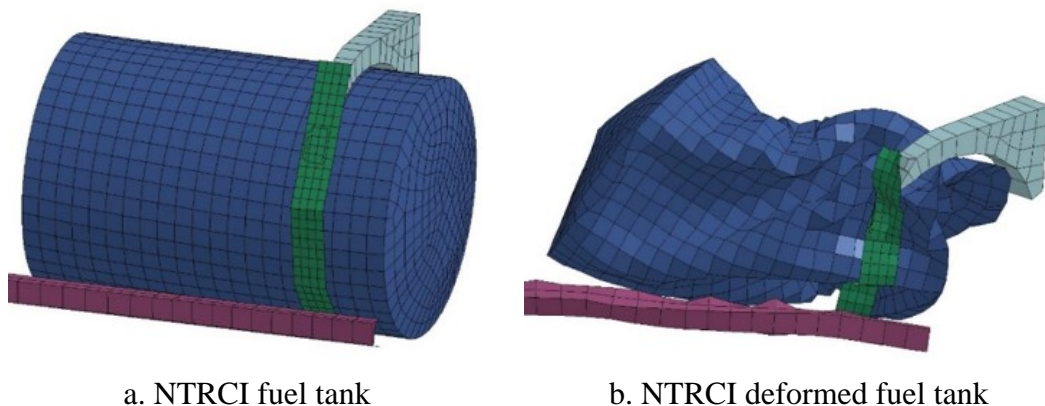
Figure 3.5: NTRCI FE model fuel tank original mesh
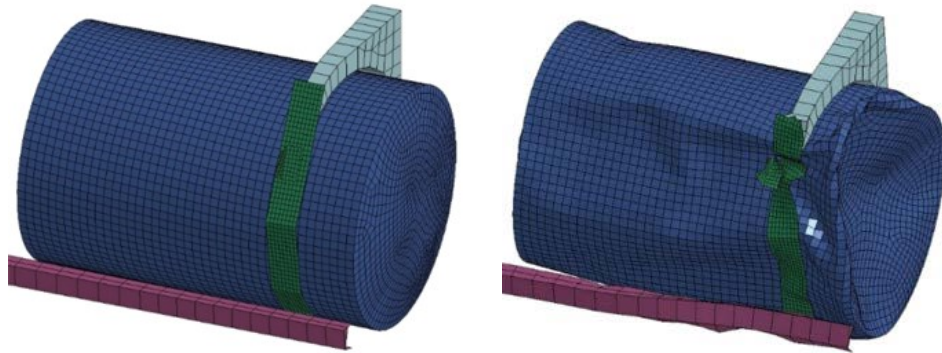
a. ISOL fuel tank   b. ISOL deformed fuel tank

Figure 3.6: ISOL FE model fuel tank mesh improvement

a. FOIL tractor
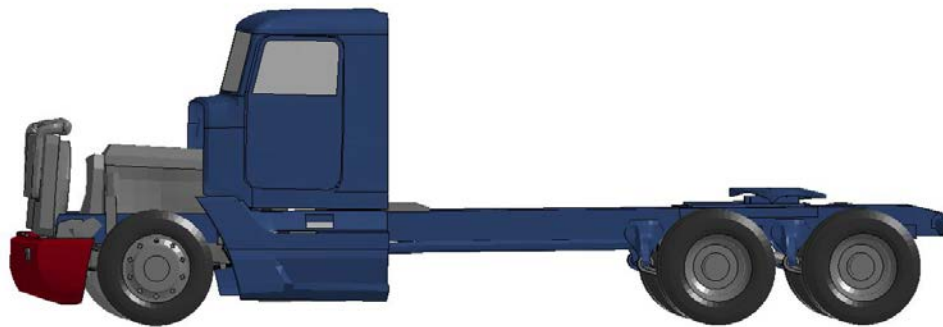
b. ISOL tractor FE model

Figure 3.7: Tractor side view

The test vehicle in Figure 3.7a had a wheelbase of 214 in (5.44 m) and curb weight of 16,852 lb (7,644 kg) prior to removal of the nonstructural components like the hood, fenders, mud flaps, sleeper cabin, exhaust stack, passenger seats, battery box and batteries, all fluids, gear shift, and other miscellaneous components. After the removal of the aforementioned components, and the addition of test instrumentation, the tractor had a test inertial weight of 14,682 lb (6,660 kg). The enhanced and modified ISOL tractor FE model in Figure 3.7b has a test inertial weight of 14,608 lb (6,626 kg) and a wheelbase of 217 in (5.51 m). This enhanced and modified tractor FE model contained 334 parts, discretized into 179,376 elements, utilizing ten constitutive models. The ten constitutive models used include: a piecewise linear plasticity model defined for steel components, a rigid model for mounting hardware, an elastic model for the tires and other rubber components, a nonlinear elastic spring model and an Maxwell spring model for the rear axle's air-ride suspension, linear and nonlinear viscous damping models for the front and rear axle's shock absorbers, a thermal elastic-plastic model for the front leaf-spring suspension U-bolts, a simplified rubber with damage model for the rubber cushions between the front axles and frame rails, and the null material model for contact purposes. The material model for the windows in this model were simplified to a piecewise linear plasticity model using the same material properties as the previous laminated glass constitutive model. This simplification was made because an ATD was not present in the vehicle and the crack propagation and failure of the glass was not of primary concern.

For the FOIL full-scale crash test, the impact speed of the tractor was 31.25 mph (50.3 km/h) with an impact angle of 25°. The results from this full-scale crash test was not

compiled into a written report, although video and accelerometer data was obtained for the validation of the ISOL tractor FE model (Marzougui 2003). The impact speed of the crash test simulation was 31.25 mph (50.3 km/h) with an impact angle of 25°. Figure 3.8 shows the impact location of the full-scale test and of the ISOL tractor FE model in the validation simulation.

a. FOIL full-scale test   b. ISOL FE model
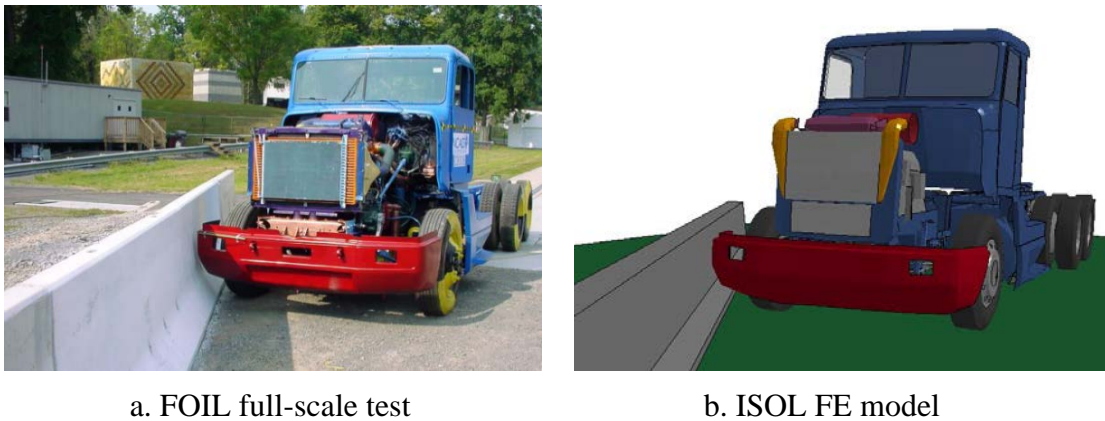
Figure 3.8: Tractor impact location

As mentioned previously, a full report was not written for the full-scale crash test; therefore, a limited amount of data was available. As a result, in addition to comparing the longitudinal acceleration profiles and yaw, pitch, and roll rotations using the limited data available, a qualitative analysis was conducted by comparing various states throughout the impact sequence to aid in the model validation. Figure 3.9, Figure 3.10, and Figure 3.11 illustrate the comparison of impact sequences for the FOIL full-scale crash test and the ISOL tractor FE model validation simulation from front, top, and side views, respectively.

0.0 seconds
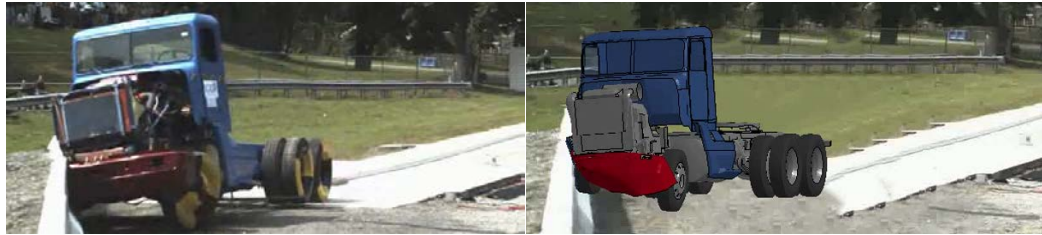
0.15 seconds

0.35 seconds

0.65 seconds

0.75 seconds

Figure 3.9: Front view impact sequence of the FOIL full-scale test and ISOL tractor FE model validation simulation
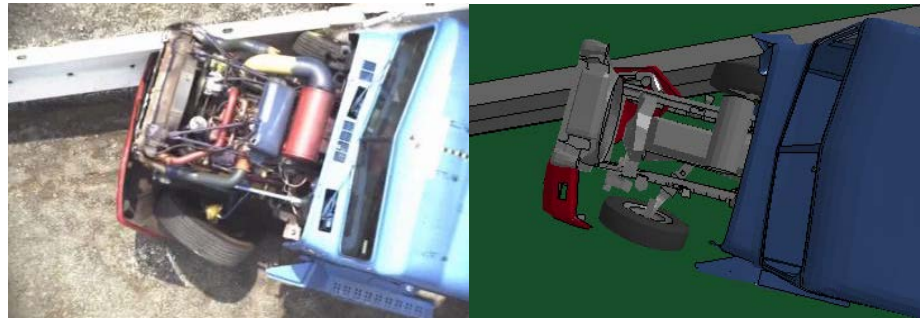
0.15 seconds
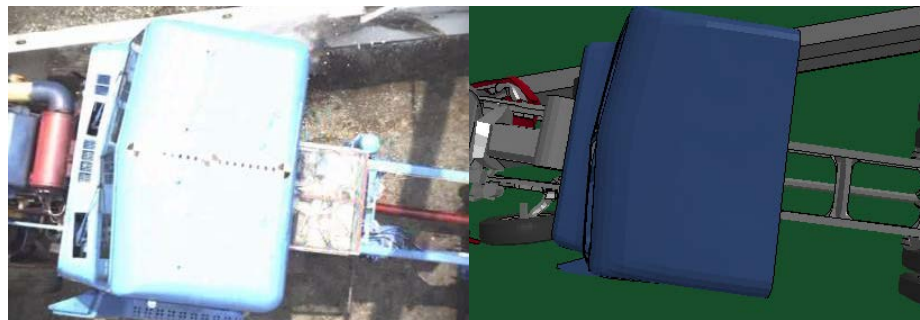
0.35 seconds
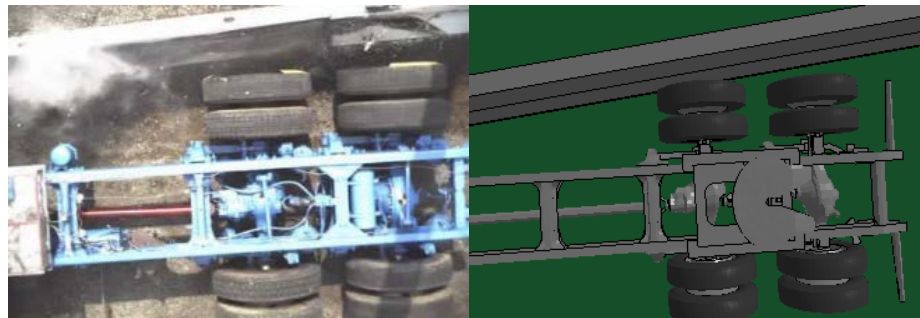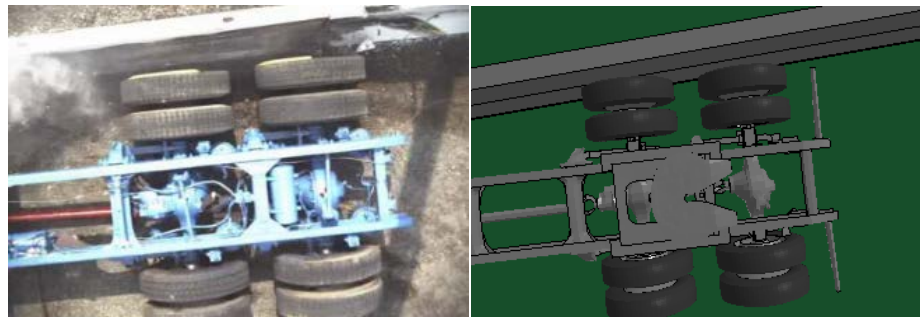
0.65 seconds

0.75 seconds

Figure 3.10: Top view impact sequence of the FOIL full-scale test and ISOL tractor FE model validation simulation

0.0 seconds

0.15 seconds

0.35 seconds

0.50 seconds

0.65 seconds

0.75 seconds

Figure 3.11: Side view impact sequence of the FOIL full-scale test and ISOL tractor FE model validation simulation

Based on the visual comparison of qualitative analysis between the crash tests, there is relatively good agreement throughout the impact with the ISOL tractor FE model replicating the front axle ascending the concrete barrier and the rear tandem axles impacting the barrier at 0.65 seconds. Video footage from the ISOL full-scale crash test was only recorded for 1 second. The post-impact trajectory of both the FOIL tractor and the ISOL tractor FE model were identical. The damage to the passenger-side front axle present in the FOIL tractor was present in the ISOL tractor FE model as well, caused by the failure of the U-bolt on the front axle.

Quantitatively comparing the longitudinal acceleration and rotational angles measurements from the full-scale test, to the results from the initial NTRCI tractor FE model and the improved ISOL tractor FE model, the ISOL tractor FE model more strongly correlated with the FOIL tractor behavior. Figure 3.12 presents the longitudinal acceleration profiles, measured at the center of gravity (CG) of the tractor, for the FOIL full-scale crash test, NTRCI FE simulation, and the ISOL FE validation simulation. Figure 3.13, Figure 3.14, and Figure 3.15 show the comparisons of the yaw, pitch, and roll angles, respectively, measured at the tractor CG, between the FOIL full-scale crash test, and the NTRCI and ISOL FE simulations.
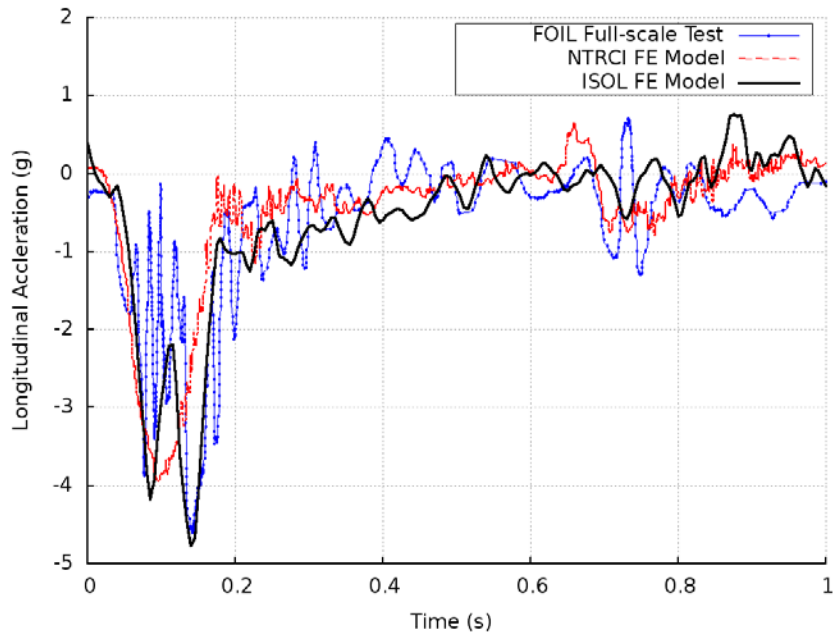
Figure 3.12: Longitudinal acceleration profiles of the FOIL full-scale tractor, NTRCI tractor FE model, and ISOL tractor FE model
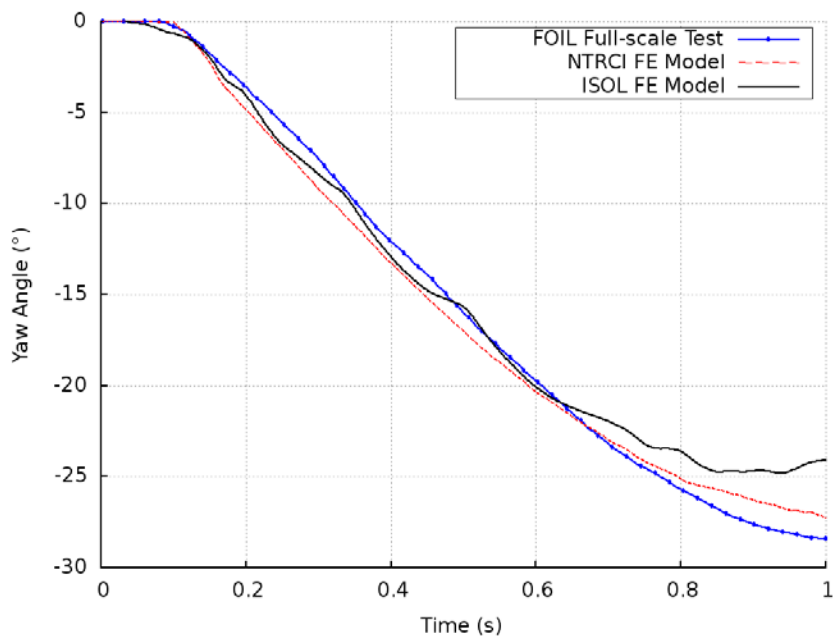
Figure 3.13: Yaw angle profiles of the FOIL full-scale tractor, NTRCI tractor FE model, and ISOL tractor FE model
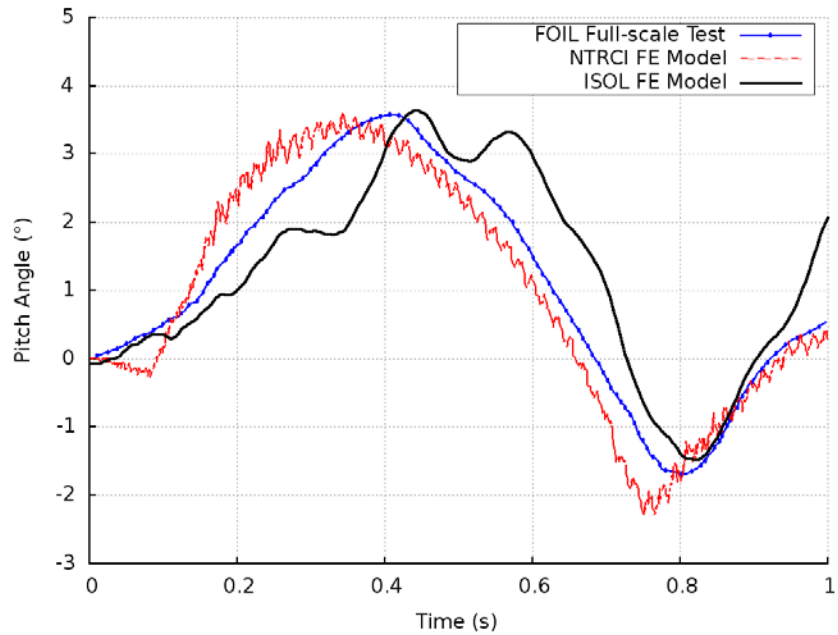
Figure 3.14: Pitch angle profiles of the FOIL full-scale tractor, NTRCI tractor FE model, and ISOL tractor FE model
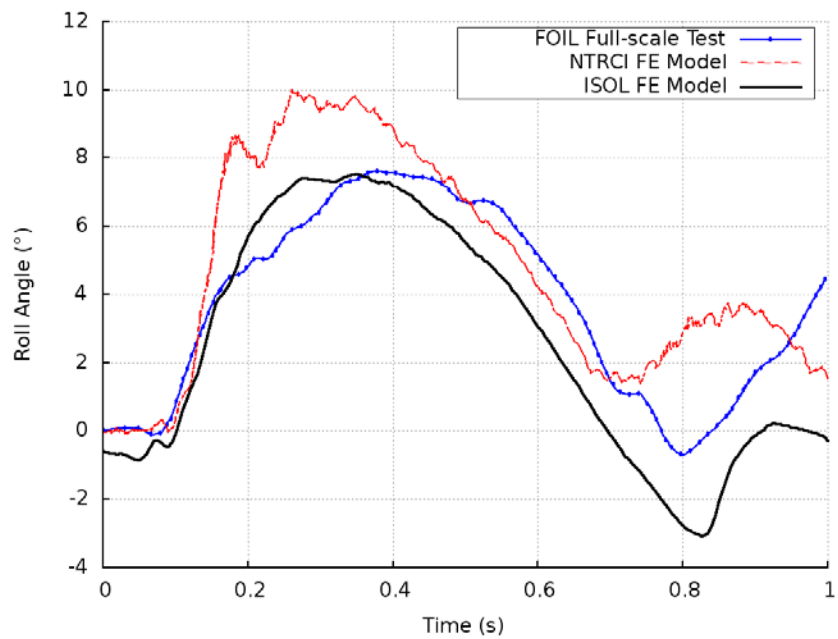
Figure 3.15: Roll angle profiles of the FOIL full-scale tractor, NTRCI tractor FE model, and ISOL tractor FE model

The longitudinal accelerations in Figure 3.12 represent the 50-ms moving average acceleration profiles of the FOIL tractor, NTRCI tractor FE model, and ISOL tractor FE model. The acceleration profile of the ISOL tractor FE model corresponded well with the FOIL tractor, with a 2.2% variation between the maximum longitudinal accelerations, as shown in Table 3.1. The yaw, pitch, and roll angles in the validation simulation of the ISOL tractor FE model followed the overall trend of the FOIL tractor throughout the impact scenario; however, slight discrepancies between the exact values of the rotational angles were present.

The most prominent difference between the FOIL full-scale crash test and the ISOL tractor FE model validation simulation was the fixture and connections of the 42-in (1.1-m) F-shape concrete barrier. The FOIL full-scale crash test's barrier consisted of seven concrete barrier segments, connected together and staked into the ground using steel rods to hold the barrier rigid. In addition to the steel-rod fixture holding the concrete barrier rigid, additional support behind the barrier was added for additional rigidity. Despite the attempt to keep the concrete barrier rigid during the full-scale impact, the concrete barrier experienced a lateral displacement during the impact, resulting in impact energy being absorbed and deflecting the concrete barrier by 0.78 in (20 mm). In the ISOL validation simulation, the F-shape concrete barrier was rigidly constrained; therefore, during the impact, the concrete barrier did not deflect or absorb any impact energy.

In terms of post-impact vehicle behavior, the non-rigid concrete barrier in the FOIL full-scale crash test resulted in the tractor briefly snagging on the deflected concrete barrier segment and resulted in a larger maximum yaw angle compared to the ISOL tractor FE

model. As seen in Table 3.1, the maximum yaw angle experienced by the tractor in the FOIL full-scale crash test and the ISOL validation simulation was -28.5° and -24.82°, respectively. When analyzing the pitch and roll angles, although the overall trend of the ISOL tractor FE model deviated from the FOIL tractor's rotations slightly both before and after impact, the maximum pitch and roll angles of the ISOL tractor FE model were within 0.05° of the FOIL tractor.

Additional parameters used to validate the ISOL tractor FE model included comparing the occupant safety between the FOIL full-scale crash test and the ISOL FE model validation simulation. The occupant safety evaluation criteria utilize a number of standardized United States and European metrics, which use the vehicle's acceleration profiles and in some cases, the yaw rotation, to correlate accident severity to occupant safety. These metrics will be explained in greater detail in Section 5.1.2. However, for the sake of clarity, the occupant safety metrics used are summarized herein. The Acceleration Severity Index (ASI) uses the x-, y-, and z-acceleration profiles of the tractor CG and compared to their respective component limit accelerations, 12 g, 9 g, and 10 g in the longitudinal (x-axis), lateral (y-axis), and vertical (z-axis) directions, respectively, to provide a measure of collision severity that is assumed to be proportional to occupant risk. An ASI value of 1.0 corresponds to "light injury, if any", although a value of 1.4 is acceptable. The Occupant Impact Velocity (OIV) represents the velocity a hypothetical 'occupant' would impact the tractor's interior compartment. The tractor interior is defined by the Flail Space Model, which is a region a hypothetical occupant can move either 2 ft (0.6 m) forward or 1 ft (0.3 m) laterally before contacting the interior compartment. The

corresponding Occupant Ridedown Acceleration (ORA) is maximum acceleration the occupant would experience, after the OIV occurs. The OIVs and ORAs are both calculated in the x and y directions. The OIVs have an allowable limit of 30 ft/s (9.1 m/s), and ORAs have an allowable limit of 15 *g*. The Theoretical Head Impact Velocity (THIV) and corresponding Post-Impact Head Deceleration (PHD) determine the same impact velocity and maximum acceleration as OIV and ORA, respectively, except the resultant of the x and y components is used and the yaw rotation of the vehicle is considered. THIV has an allowable limit of 30 ft/s (9.1 m/s) and the PHD has an allowable limit of 20 *g*.

In Table 3.1, the occupant safety evaluation criteria is compared between the FOIL full-scale crash test, the NTRCI FE simulation and the ISOL FE validation simulation. The ASI of the ISOL tractor FE model correlated extremely well with the FOIL tractor. Comparing the OIV and corresponding ORA values, a moderate variation exists between the individual x- and y-component impact velocities and corresponding maximum ridedown accelerations between the FOIL tractor and the ISOL tractor FE model. The discrepancy can be attributed to the deflection of the concrete barrier in the FOIL full-scale crash test. Conversely, when assessing the resultant impact velocity and ridedown acceleration in the THIV and PHD metrics, the ISOL tractor FE model corresponded well with the FOIL tractor.

Table 3.1: Tractor specifications, impact parameters, and evaluation criteria for the full-scale crash test and FE simulations

Testing Location	FOIL	NTRCI	ISOL
Test Vehicle	1992 Freightliner FLD120	Tractor FE Model	Tractor FE Model
Test Inertial Weight	14,682 lb (6,660 kg)	16,255 lb (7,373 kg)	14,608 lb (6,626 kg)
Tractor Wheelbase	214 in (5.44 m)	202.8 in (5.15 m)	217 in (5.51 m)
Longitudinal CG Location	95.52 in (2.35 m)	100 in (2.54 m)	90.5 in (2.3 m)
Impact Speed	31.25 mph (50.3 km/h)	31.25 mph (50.3 km/h)	31.25 mph (50.3 km/h)
Impact Angle	25°	25°	25°
Post-impact Behavior:			
Maximum Yaw Angle	-28.5°	-29.3°	-24.82°
Maximum Pitch Angle	3.6°	3.6°	3.65°
Maximum Roll Angle	7.6°	10°	7.55°
Occupant Safety:			
Maximum 50-ms Moving Average Acceleration (g):			
X-axis (Longitudinal)	-4.5	-3.9	-4.6
Y-axis (Transverse)	-4	-5.7	-4.5
ASI	0.54	0.69	0.56
OIV ft/s (m/s):			
X-axis (Longitudinal)	12.1 (3.7)	11.2 (3.4)	9.4 (2.88)
Y-axis (Transverse)	6.9 (2.1)	9.5 (2.9)	8.8 (2.68)
THIV ft/s (m/s)	13.9 (4.25)	13.5 (4.11)	14.0 (4.28)
ORA (*g*):			
X-axis (Longitudinal)	-1.7	-4.2	-1.17
Y-axis (Transverse)	-3.9	-6.2	-4.13
PHD (*g*)	9.9	34	8.35

After assessing the improved and enhanced ISOL tractor FE model and validating against the FOIL full-scale crash test data, it was determined with relatively high

confidence that the ISOL tractor FE model could be used for future numerical simulations. In order to validate the whole tractor-trailer FE model, the tractor wheelbase needed to be modified to match the wheelbase of the day-cab tractor used in the full-scale tractor-trailer test (Test No. TL5CMB-2) conducted at MwRSF on July 12, 2007 (Rosenbaugh et al. 2007). This full-scale tractor-trailer test was selected for validation as it was the most recent full-scale test to be conducted against a concrete barrier that had publicly available crash test data. The tractor used in the MwRSF full-scale test was a 1991 White/GMC WG64T conventional day-cab tractor, seen in Figure 3.16, and had a test inertial weight of 15,133 lb (6,864 kg).

Figure 3.16: 1991 White/GMC WG64T conventional day-cab tractor used in the MwRSF full-scale crash test

The ISOL tractor FE model that was validated against the FOIL tractor-only full-scale crash test had a wheelbase of 217 in (5.5 m) and was modified to correspond to the 154.9-in (3.9-m) wheelbase of the MwRSF 1991 White/GMC WG64T conventional day-cab tractor. In addition to modifying the wheelbase, all of the components that were

removed for the FOIL validation test (i.e., hood, fenders, battery box, batteries, and other miscellaneous components), with the exception of the sleeper-cab and exhaust stack, were restored to correspond with the MwRSF tractor in Figure 3.16. Figure 3.17a illustrates the 217-in (5.5-m) wheelbase of the ISOL tractor FE model used in the FOIL tractor-only model validation full-scale crash test and Figure 3.17b shows the modified ISOL tractor FE model with a wheelbase of 154.7 in (3.9 m) to match the tractor's wheelbase in the MwRSF full-scale crash test.

a. 217-in (5.5-m) wheelbase ISOL tractor FE model

b. 154.7-in (3.9-m) wheelbase ISOL tractor FE model

Figure 3.17: ISOL tractor FE model wheelbases

The day-cab tractor in Figure 3.17b is the FE model that was used in the MwRSF tractor-trailer validation simulation and all subsequent impact scenarios throughout the remainder of this research. The ISOL day-cab tractor FE model consisted of 374 parts discretized into 186,425 elements and utilizing the same ten constitutive models used in the previous FE model validation simulation. The test inertial weight of the ISOL tractor FE model was 15,067 lb (6,834 kg). In addition to the FE model improvements mentioned above, other numerical changes were made to increase the usability, stability, and robustness of the ISOL tractor FE model. A complete list of improvements to the ISOL day-cab tractor FE model are listed in Table 3.2.

Table 3.2: Numerical improvements made to the ISOL tractor FE model

Contact	1) All initial penetrations and crossed edges were eliminated. 2) Added INTERIOR option to handle beam elements in the *CONTACT_AUTOMATIC_GENERAL_INTERIOR contact defined for the front and rear suspension 3) Added both sets of tandem tires and wheels to the vehicle-self-contact part set. 4) Added the driver-side suspension stop (omitted in NTRCI FE model) to the frame-rail contact definition.
Elements	5) Most shell elements were switched to a full integration element formulation. 6) Rubber bump stops on the front suspension were remodeled to eliminate severe penetrations into the suspension stop 7) Mesh quality was improved by correcting severely warped quadrilateral elements and triangular elements with poor aspect ratios. 8) Average mesh size was reduced from 100 mm to 40 mm for parts which experienced severe deformation during impacts.

3.2 Finite Element Model of a 48-ft (14.6-m) Dry-Box Trailer

An initial trailer FE model was developed by NCAC; although, the model was quite elementary in its development, many structural components were not present and material properties were not defined. MASH recommends the following dimensions for trailers: the overall length of the trailer should not exceed 50 ft (15.2 m), the trailer overhang behind the tandem axles should not exceed 87 in (2.2 m), and the cargo bed height should fall within 50-54 in (1.3-1.4 m) when measured without a ballast. Figure 3.18a shows the dimensions of the initial NCAC trailer FE model compared to the actual dimensions, in Figure 3.18b, of the 48-ft (14.6-m) dry-box trailer used in the MwRSF full-scale crash test.
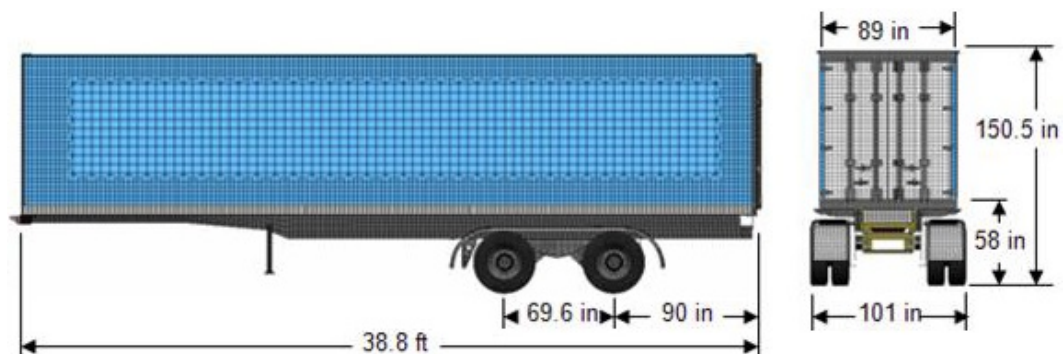
a. Initial NCAC trailer FE model dimensions
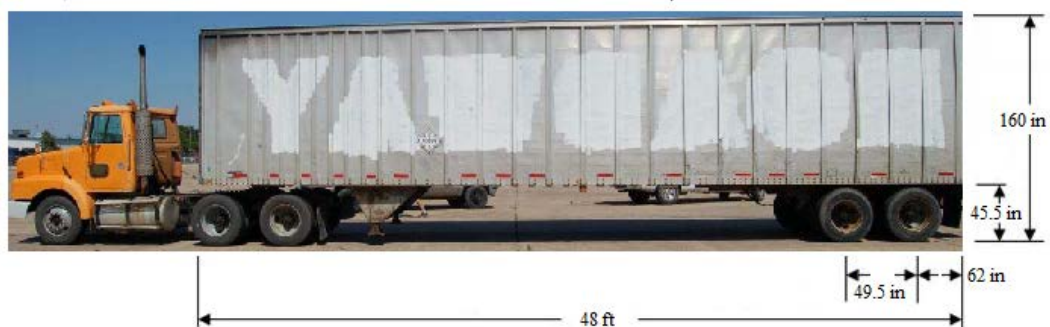
b. MwRSF trailer dimensions

Figure 3.18: Trailer dimensions

Although the NCAC trailer FE model in Figure 3.18a was not publicly available, NTRCI assessed the trailer FE model and determined that the size and dimensions of the trailer were inconsistent with most production trailers on the road today. Consequently, NTRCI concluded that the creation of a new trailer FE model, consistent with present-day trailer dimensions, was the proper route to take instead of modifying the NCAC FE model. For the creation of a new trailer FE model, NTRCI surveyed numerous trailers to gather pictures and dimensions to ensure the accuracy of the FE model development. NTRCI enlisted an external 3D modeling company, Digimation, to develop the CAD model based on the dimensions of a 53-ft (16.1-m) dry-box Stoughton trailer. The CAD model was delivered to NRTCI and imported into HyperMesh to create the FE mesh of the new trailer FE model. However, at this phase in the trailer FE model creation, certain details pertaining to material properties, connections between components, and specifics about structural components that would affect the overall kinematic behavior of the trailer were missing. The absent aforementioned details were unable to be obtained from privately-owned trailer manufacturers since their detailed CAD drawings and material specifications are proprietary. Consequently, the next stage in the trailer FE model development involved NTRCI purchasing a 1990 48-ft (14.6-m) dry-box Stoughton trailer to disassemble in order to get precise measurements of critical components and connection methods between components. Figure 3.19 shows the NTRCI purchased trailer used for the creation of a detailed trailer FE model (Plaxico et al. 2009).

Figure 3.19: 1990 48-ft (14.6-m) dry-box Stoughton trailer purchased by NTRCI

Fundamentally, a typical dry-box trailer is composed of a wood-planked floor, bolted to steel I-beams, with an exterior aluminum side-wall and roof, riveted to vertical steel beams, and lined with plywood panels on the interior. A translatable duel-axle (i.e., tandem) wheelset is used to adjust for various loading conditions, and a king pin assembly connects a trailer and a tractor together. One of the main components that required detailed modeling was the king pin assembly, as this is the sole connection to the tractor and the structural configuration would affect the tractor-trailer response during impact scenarios. NTRCI removed the king pin assembly from the trailer, seen in Figure 3.20a, and dissected sections of the exterior king pin box in order to record the location, thickness, and dimensions of the internally located baffles, L-braces, and the king pin mount (Plaxico et al. 2009). Figure 3.20b shows the FE model of the king pin assembly, with the exterior sheet-metal surface shown as translucent to view the interior components.
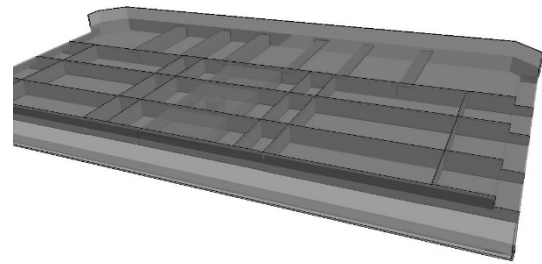
| a. NTRCI purchased trailer | b. FE model |

Figure 3.20: King pin assembly

Similar dissection procedures were conducted for accurate modeling of the trailer floor, sidewalls, roof, and the connections between the sidewalls to the trailer floor and roof. The last main system on the trailer that needed detailed modeling was adjustable bogie, which is composed of the rear tandem axles, tires, wheels, frame, and suspension system connected to longitudinal rails affixed to the underside of the trailer floor I-beams. All of the aforementioned components were able to be measured directly without the need to dissect components except for the tandem axles, whereby a hole was drilled into the axle to determine the thickness. Figure 3.21a shows the trailer tandem bogie assembly of the purchased NTRCI 48-ft (14.6-m) dry-box Stoughton trailer and the corresponding FE model created in Figure 3.21b.

a. NTRCI purchased trailer   b. FE model
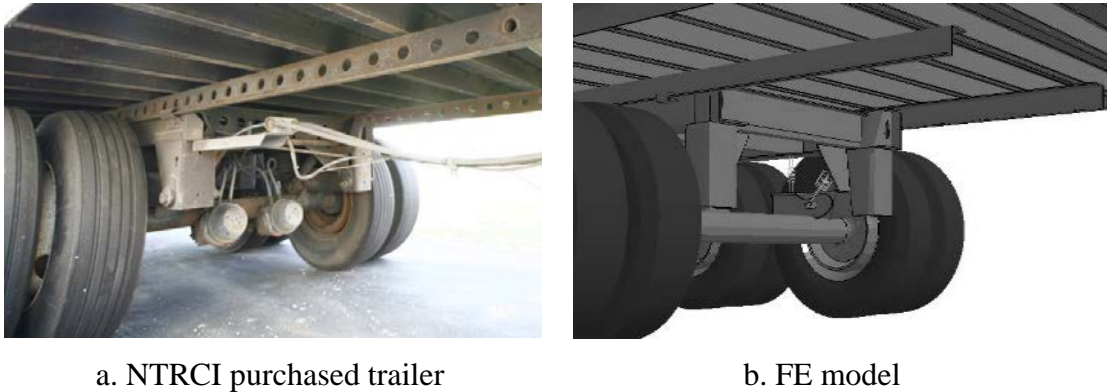
Figure 3.21: Trailer tandem bogie assembly

The suspension system and shock absorbers of the trailer as well as the tandem axles of the tractor needed to be modeled accurately due to the significant influence these components have on the overall vehicle kinematics during redirective maneuvers. As mentioned above in Section 3.1, during the tractor FE model development, the Air-Ride suspension and shock absorber components were purchased by NTRCI to determine the force-displacement and force-velocity characteristics of the spring and damper components, respectively, in order to apply the characterization curves to discrete elements in the FE model. The Air-Ride suspension system was able to be modeled using a three-parameter Maxwell model for the linear response with discrete spring and damper elements and an additional discrete elastic spring element to account for the nonlinear response. The shock absorber was modeled using a discrete nonlinear viscous damper element. Figure 3.22a shows one of the four sets of the Air-Ride suspension and shock absorber located at each wheelset on the NTRCI purchased trailer tandem axles (Plaxico et al. 2009). Figure 3.22b shows the two discrete spring elements (i.e. the Maxwell model and nonlinear spring), that

were used to replicate the Air-Ride suspension behavior and the discrete nonlinear viscous damper element used to replicate the shock absorber.
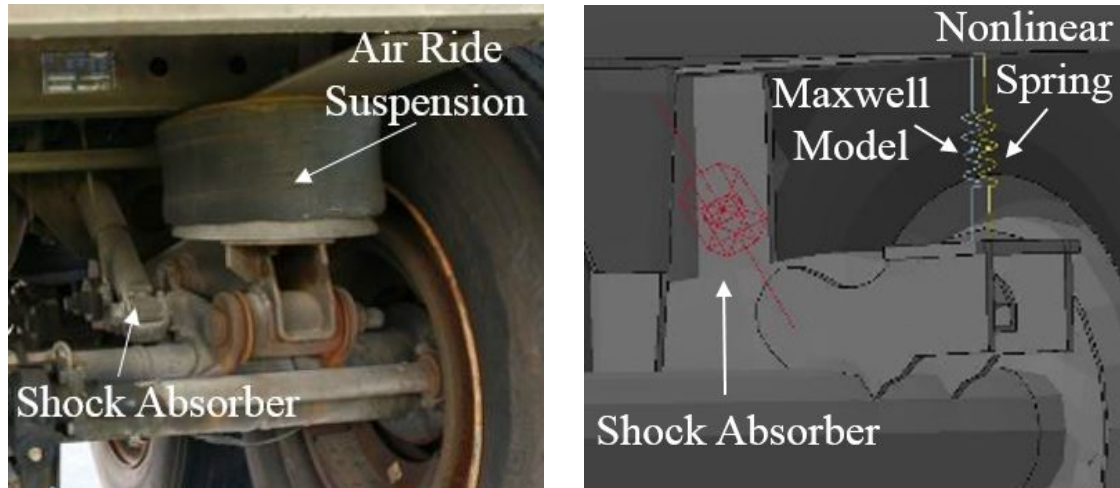
a. NTRCI purchased trailer   b. FE model

Figure 3.22: Trailer suspension and shock absorber

Once the trailer FE model was properly represented dimensionally, material properties needed to be assigned to each trailer component. The materials used in the trailer were classified into four categories, steel, aluminum, wood, and rubber; with each category utilizing a number of material classifications. The material properties for each component were gathered from various sources including ASTM standards (ASTM 2008; 2009), online databases (MatWeb 2009), reference books (Nicholas 1981; Walton & Opar 1981; Mullins 1990; Blair & Stevens 1995; Hoge 1996), and published stress-strain data (Moosbrugger 2002). In total, 17 classifications of steel, three classifications of aluminum, two classifications of wood, and one classification of rubber were defined.

The complete trailer FE model of the 1990 48-ft (14.6-m) dry-box Stoughton trailer had a test inertial weight of 13,616 lb (6,176 kg), a wheelbase of 49 in (1.2 m), a rear trailer overhang of 59 in (1.5 m), an unladen trailer bed height of 51 in (1.3 m), and a total trailer height of 153 in (3.9 m). The trailer FE model contained 103 parts, discretized into 243,007 elements, utilizing nine constitutive models. The nine constitutive models used included, the piecewise linear plasticity model defined for steel components, the rigid model for the kingpin and tandem axles, the elastic model for the tires and wood components, the simplified Johnson Cook model for the sidewalls, roof and rear door, the spot-weld model for the sidewall welds, the nonlinear elastic spring model and Maxwell spring model for the tandem axle's air-ride suspension, the nonlinear viscous damping model for the tandem axle's shock absorbers, and the null material model for contact purposes. The complete NTRCI 48-ft (14.6-m) dry-box trailer FE model with dimensions is shown in Figure 3.23.
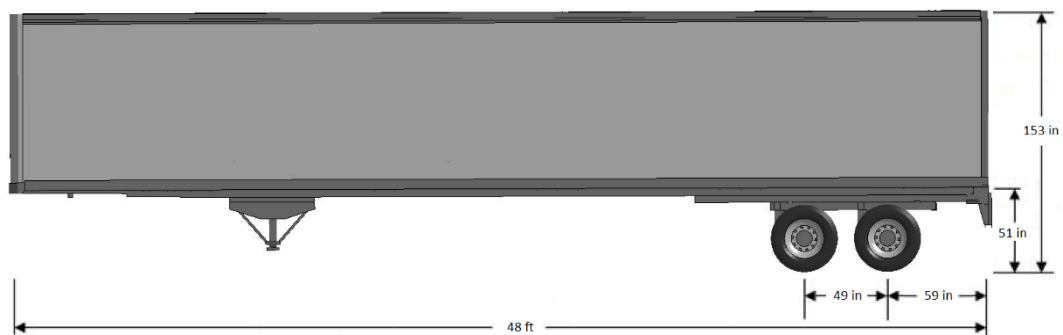
Figure 3.23: NTRCI 48-ft (14.6-m) dry-box trailer FE model dimensions

Although extensive modeling and preparation was done by NTRCI in the creation of the trailer FE model, additional modifications were needed to correct numerical

instabilities and modify dimensions to more accurately represent the MwRSF full-scale test's trailer. Figure 3.24 illustrates the initial penetrations and crossed edges that were present in the NTRCI trailer FE model.
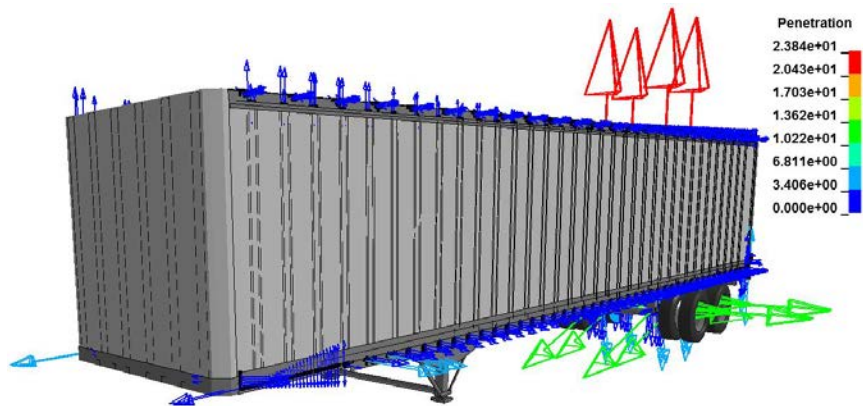
Figure 3.24: Initial penetrations (mm) present in the NTRCI trailer FE model

The initial penetrations and crossed edges were eliminated from the NTRCI trailer FE model in order to improve the numerical stability and robustness. Additionally the overall height of the ISOL trailer FE model was modified from 153 in (3.9 m) to 160 in (4.1 m) to match the trailer height of the MwRSF full-scale test's trailer. The additional height added to the ISOL trailer FE model increased the total element count to 251,863. The ISOL trailer FE model used for the MwRSF full-scale crash test validation simulation is shown in Figure 3.25, with the overall dimensions denoted.
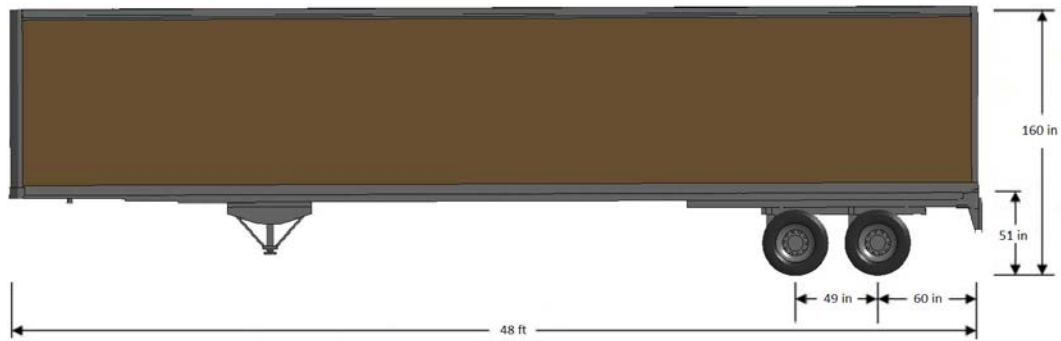
Figure 3.25: ISOL trailer FE model dimensions

3.3 Finite Element Model of a Trailer Ballast Load

The trailer ballast load used to create the complete 80,000-lb (36,287-kg) test vehicle was composed of F-shape concrete barriers that were padded with extruded polystyrene foam along the sides and floor as to not artificially add stiffness to the trailer (Plaxico et al. 2007). Figure 3.26a shows the ballast load configuration of the MwRSF full-scale test's ballast load configuration and Figure 3.26b shows the corresponding FE model created by NTRCI to replicate the ballast loading conditions.

a. MwRSF full-scale test   b. NTRCI FE model

Figure 3.26: Ballast load configuration

Similar to the NTRCI tractor and trailer FE models, the ballast model had initial penetrations and crossed edges, seen in Figure 3.27, which were removed prior to running the ISOL FE model validation simulation. The final ballast model contained 18 parts, discretized into 28,290 elements, utilizing three constitutive models. The three constitutive models used included: a piecewise linear plasticity model defined for the steel rods holding adjacent concrete barriers together, a rigid model for the F-shape concrete barriers, and an elastic model for the foam components.
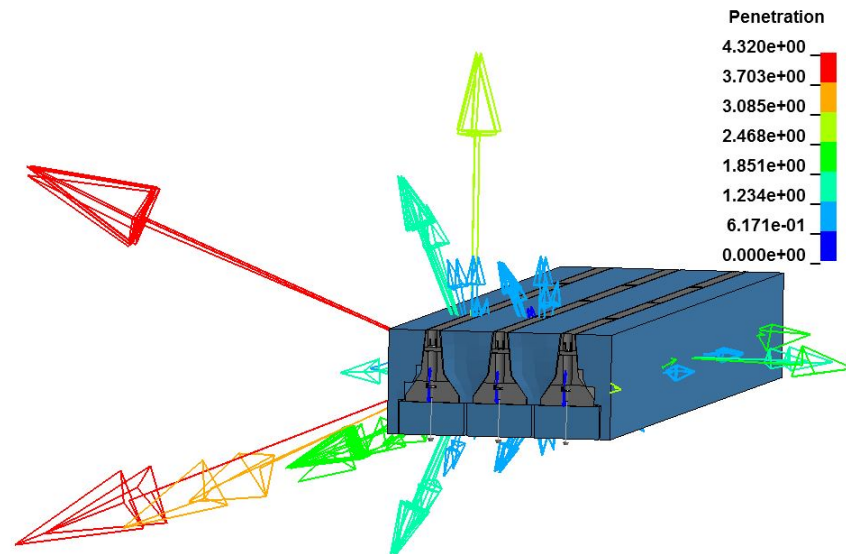
Figure 3.27: Initial penetrations (mm) present in the NTRCI FE ballast model

3.4 Validation of the Tractor-Trailer Finite Element Model

In order to validate the ISOL tractor-trailer FE model, the most recent full-scale crash test against a rigid concrete barrier conducted at MwRSF in 2007 was used. This full-scale crash test was selected to compare the vehicle redirection kinematics both qualitatively and quantitatively since crash test data was available. The MwRSF full-scale test was conducted to evaluate the crash performance of a new vertical-faced concrete median barrier design according to the testing guidelines of NCHRP Report 350 for TL-5 impact conditions. The test involved a 79,705-lb (36,153-kg) tractor-trailer impacting the concrete barrier at 52.7 mph (84.9 km/h) and impact angle of 15.5°. The test vehicle was a 1991 White/GMC WG64T tractor with a 1988 Pines 48-ft (14.6-m) trailer. The test article was a 42-in (1.1-m) vertical-faced concrete barrier with an installation length of 200 ft (60.9 m). The test vehicle used is shown in Figure 3.28 and the vertical-faced concrete

barrier is shown in Figure 3.29. The continuous concrete barrier was cast in-place with

Grade 60 rebar reinforcement throughout with the width tapering from the bottom and top,

24.1 in (613 mm) to 20 in (508 mm). The barrier face had a height of 34 in (864 mm) before

narrowing to the 4-in (102-mm) wide ridge along the top of the barrier (Rosenbaugh et al.

2007).

Figure 3.28: 1991 White/GMC WG64T tractor with a 1988 Pines 48-ft (14.6-m)
trailer used in the MwRSF full-scale crash test

Figure 3.29: Vertical-faced concrete barrier used in the MwRSF full-scale crash
test

The tractor, trailer, and ballast FE models from Sections 3.1, 3.2, and 3.3,

respectively, compiled into a complete tractor-trailer FE model used in the validation

simulation is shown in Figure 3.30. The complete tractor-trailer FE model was composed

of 495 parts, discretized into 466,578 elements. Figure 3.31 shows the FE model of the vertical-faced concrete barrier modeled after the full-scale test's barrier shown in Figure 3.29. Since there was no observed permanent deflection in the MwRSF full-scale test's barrier, the FE model of the concrete barrier was rigidly constrained and consisted of 66,056 solid elements using concrete material properties.
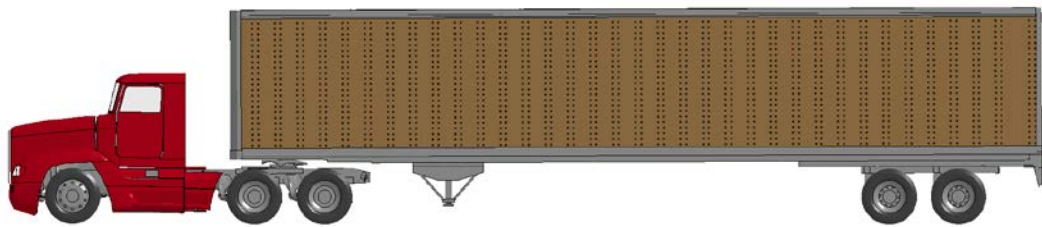
Figure 3.30: FE model of the ISOL modified 1992 Freightliner FLD120 day-cab tractor and 1990 48-ft (14.6-m) dry-box Stoughton trailer used in the validation simulation
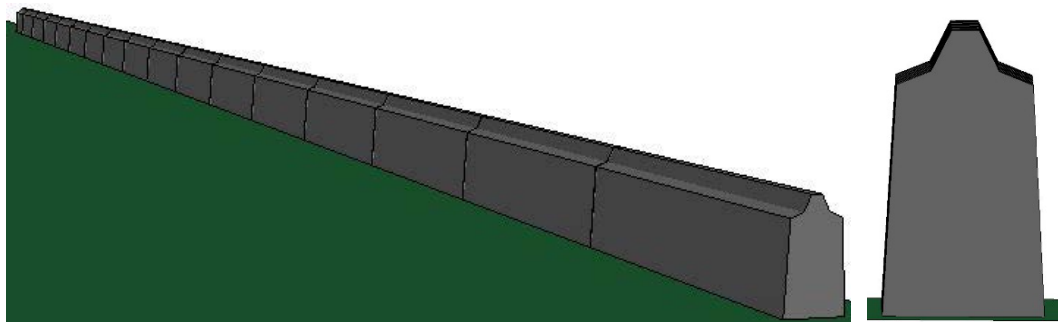
Figure 3.31: Vertical-faced concrete barrier used in the ISOL FE simulation

The tractor fifth-wheel to trailer kingpin connection was another important aspect requiring accurate modeling to realistically represent the articulating kinematics of the tractor-trailer interface. The tractor's fifth-wheel is a horseshoe-shaped coupling device in

which the trailer's kingpin, typically a 2-3.5-in (50.8-88.9-mm) diameter steel shaft, is inserted to allow yaw rotation between the tractor and trailer to facilitate easier turning maneuvers. This connection is achieved in the FE model through the use of a constrained spherical joint in which only yaw rotation is allowable. Figure 3.32a shows the FE model of the tractor's fifth-wheel highlighted in light blue, Figure 3.32b shows the trailer's kingpin highlighted in yellow, and Figure 3.32c shows the coupling of the tractor-trailer connection.

a. Tractor fifth-wheel

b. Trailer kingpin

c. Tractor-trailer fifth-wheel/kingpin coupling
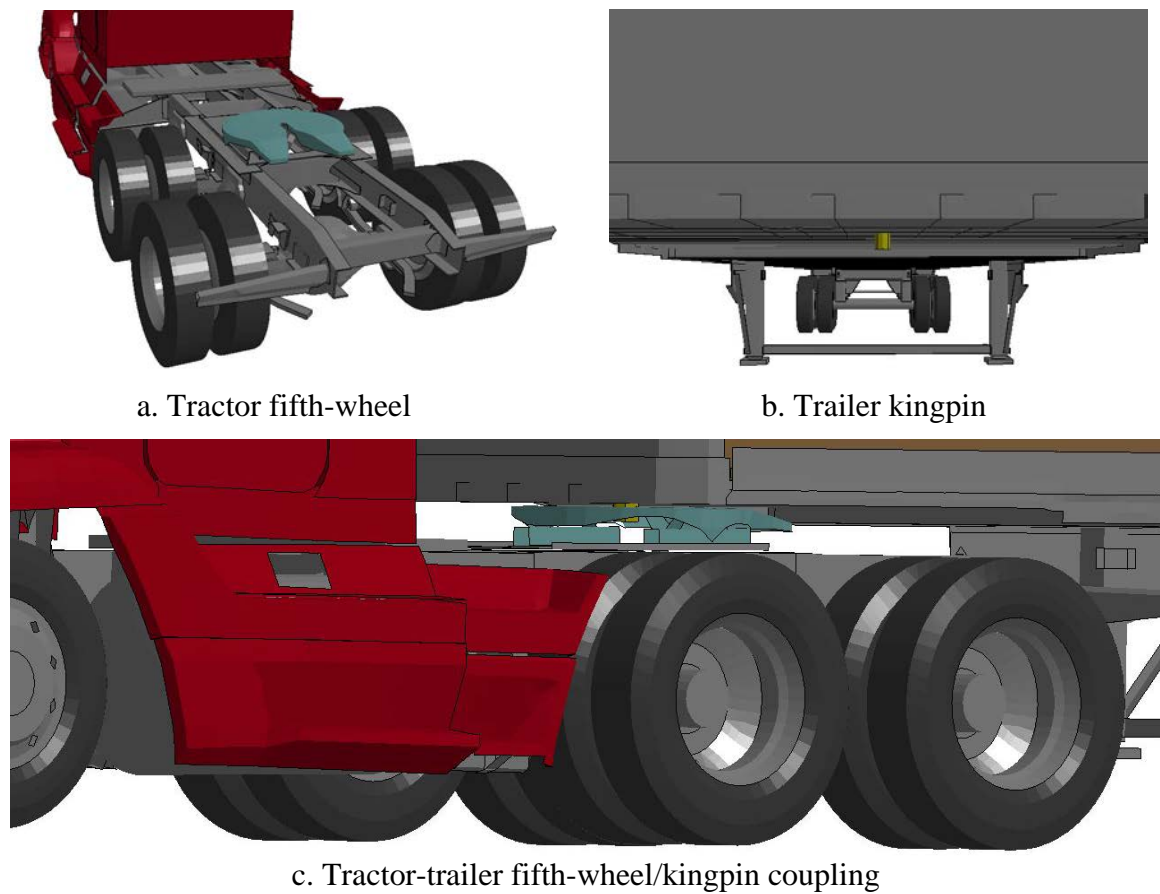
Figure 3.32: Tractor to trailer connection

In addition to removing all initial penetrations to improve the numerical stability of the ISOL tractor-trailer FE model, robust and stable contact definitions were defined to increase the overall computational efficiency of the numerical simulations. One-way contact treatment types (i.e., AUTOMATIC_NODES_TO_SURFACE) were used when the direction of contact was known beforehand, such as the ballast load to trailer walls. Two-way contact treatment types (i.e., AUTOMATIC_SURFACE_TO_SURFACE) were utilized for interactions with large contact areas that experienced sliding and rolling, such as the tractor-trailer tires to road surface. Single surface contact types (i.e., AUTOMATIC_SINGLE_SURFACE and AUTOMATIC_GENERAL_INTERIOR) were used when, a large number of neighboring components would interact with each other, large deformations would be present, and the direction of contact was unknown. The interior contact type was used for the rubber bump stop on the tractor's front suspension to prevent numerical instabilities which can occur when rubber or foam materials experience large compressive forces. The tied contact types were used to constrain neighboring components and only allow translational degrees of freedom. Force transducer contact types were used to record the contact force output of single surface contact types, as these contact interfaces do not output contact forces by default. It should be noted the force transducer contacts used do not produce any contact forces, and therefore do not influence the simulation results. Table 3.3 summarizes the contact types and corresponding use in the ISOL tractor-trailer FE model.

Table 3.3: Tractor-trailer contact types used

Contact Type	Use
Nodes to Surface	Tractor front suspension leaf springs to shackle
Automatic Nodes to Surface	Fifth-wheel/kingpin connection; ballast to trailer floor/walls
Automatic Surface to Surface	Tractor-trailer tires to ground; exterior body panels to ground;
Automatic Single Surface	Tractor self-contact; tractor front suspension-stop to frame; tractor tandem axle tires to kingpin assembly; trailer self-contact
Automatic General Interior	Tractor front suspension; neighboring ballast bolted connection; ballast to surrounding foam; tractor-trailer to barrier
Interior	Tractor front suspension rubber bump stop
Tied Nodes to Surface	Tractor frame rail/suspension stop contact location; trailer sidewalls to frame
Tied Nodes to Surface Offset	Trailer lateral I-beams to H-frame and lower side rail; ballast constrained connection to trailer floor
Tied Surface to Surface	Weld connections for trailer step guard; trailer tandem bogie to frame rail
Force Transducer	Contact force output for Single Surface and General Interior contact types

The MwRSF full-scale tractor-trailer test conducted under NCHRP Report 350 TL-5 impact conditions were conducted on July 12, 2007. The tractor-trailer was propelled using a reverse cable tow system to ensure an accurate impact speed of 52.7 mph (84.9 km/h) and an impact angle of 15.4°. The tractor-trailer was outfitted with two accelerometers, one located at the tractor's tandem axle and the other at the trailer's tandem axle. A rate transducer was located in conjunction with the trailer tandem axle

accelerometer to record rotational measurements. Ten high-speed cameras were configured to record the crash test from different vantage points throughout the impact scenario.

The ISOL tractor-trailer FE model contained 13 accelerometers throughout the vehicle, namely, in the tractor cabin, at the /kingpin connection, and the trailer tandem axle. The remaining accelerometers were located at the engine top, along the tractor frame rails, and at each tire on the tractor. Figure 3.33 shows the locations of the accelerometers, noted in orange, as well as the CG locations for the individual tractor-trailer units (i.e., tractor, trailer, and ballast) and the whole vehicle CG.
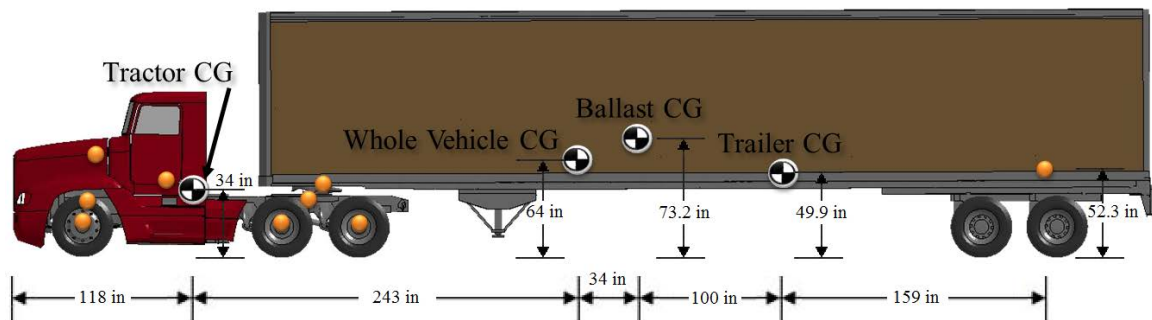
Figure 3.33: ISOL tractor-trailer FE model accelerometer and CG locations

To validate the ISOL tractor-trailer FE model, the MwRSF full-scale crash test was replicated and used to compare the vehicle redirection kinematics both qualitatively and quantitatively. Table 3.4 shows the tractor-trailer specifications of the MwRSF full-scale crash test, the initial NTRCI tractor-trailer FE model, and the ISOL tractor-trailer FE model. It should be noted that the individual tractor and trailer inertial weights were not reported in the MwRSF full-scale test and the combined inertial weight of the tractor and trailer was

deduced by subtracting the ballast load from the total vehicle inertial weight and estimating

the individual tractor and trailer inertial weights from a typical tractor/trailer weight ratio.

Table 3.4: Tractor-trailer specifications for the full-scale crash test and FE simulations

Testing Location	MwRSF Full-scale Test	NTRCI FE Simulation	ISOL FE Simulation
Tractor Model	1991 White/GMC WG64T	1992 Freightliner FLD120	1992 Freightliner FLD120
Tractor Wheelbase	154.9 in (3.93 m)	153.5 in (3.89 m)	154.7 in (3.93 m)
Tractor Test Inertial Weight	15,133 lb (6,864 kg)	15,203 lb (6,896 kg)	15,067 lb (6,834 kg)
Trailer Model	1988 48-ft (14.6-m) dry-box Pines	1990 48-ft (14.6-m) dry-box Stoughton	1990 48-ft (14.6-m) dry-box Stoughton
Trailer Test Inertial Weight	13,689 lb (6,209 kg)	13,616 lb (6,176 kg)	13,769 lb (6,246 kg)
Ballast Weight	50,885 lb (23,081 kg)	50,938 lb (23,105 kg)	50,878 lb (23,078 kg)
Tractor-trailer Inertial Weight	79,705 lb (36,154 kg)	79,757 lb (36,177 kg)	79,714 lb (36,158 kg)
Tractor-trailer Wheelbase	607 in (15.42 m)	604 in (15.3 m)	606.4 in (15.4 m)
Tractor-trailer Total Length	745.2 in (18.93 m)	734.7 in (18.66 m)	737.7 in (18.74 m)
Ballast C.G Longitudinal Location	401.5 in (10.2 m)	415.1 in (10.54 m)	394.9 in (10.03 m)
Ballast C.G Height	72.1 in (1.83 m)	76.5 in (1.94 m)	73.2 in (1.86 m)
Impact Speed	52.7 mph (84.9 km/h)	52.7 mph (84.9 km/h)	52.7 mph (84.9 km/h)
Impact Angle	15.4°	15.5°	15.4°

The modifications made to the NTRCI tractor-trailer FE model to create the ISOL tractor-trailer FE model allowed a closer comparison to the MwRSF full-scale test's vehicle in all aspects listed in Table 3.4. The ISOL FE model validation simulation was conducted on UNC Charlotte's computing cluster using LS-DYNA R9.0.1 with 16 processors. Figure 3.34 through Figure 3.37 shows comparison views of 250-ms incremented sequential states throughout the impact scenario of the MwRSF full-scale crash test and ISOL FE model validation simulation. Figure 3.34 shows the front view comparison, Figure 3.35 shows a head-on view from behind the concrete barrier, Figure 3.36 shows a rear view from a viewpoint located downstream from the impact location, and Figure 3.37 shows a top view located at the impact location. The ISOL FE model validation simulation sequence images in Figure 3.34 though Figure 3.37 were overlaid onto the MwRSF background images to aid in the visual comparisons.

0.0 seconds

0.25 seconds

0.50 seconds

0.75 seconds

1.0 seconds

Figure 3.34: Front view impact sequence of the MwRSF full-scale test and ISOL
FE model validation simulation

1.25 seconds

1.5 seconds

1.75 seconds

2.0 seconds

Figure 3.34 (continued): Front view impact sequence of the MwRSF full-scale
test and ISOL FE model validation simulation

0.0 seconds

0.25 seconds

0.50 seconds

0.75 seconds

1.0 seconds

1.25 seconds

1.5 seconds

Figure 3.35: Head-on view impact sequence of the MwRSF full-scale test and ISOL FE model validation simulation
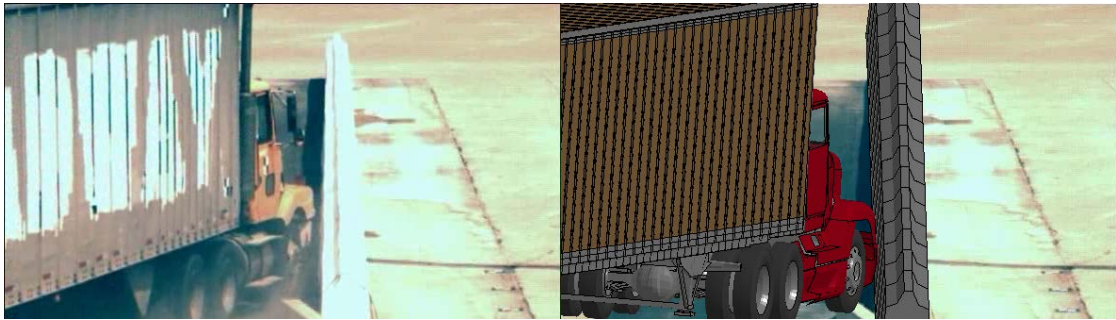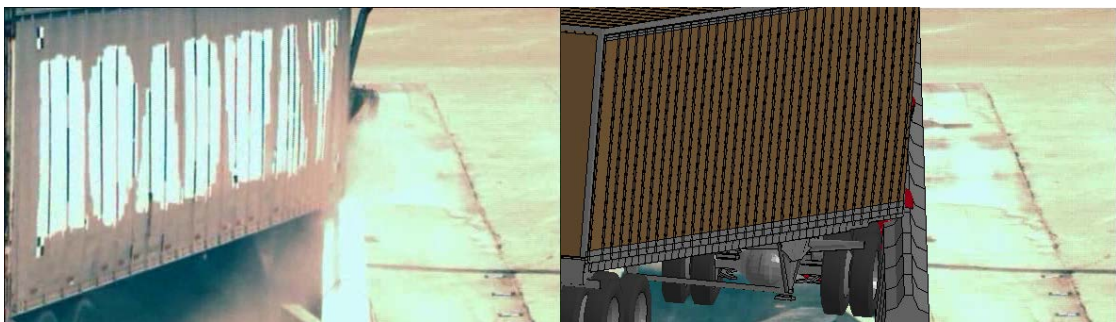
0.0 seconds
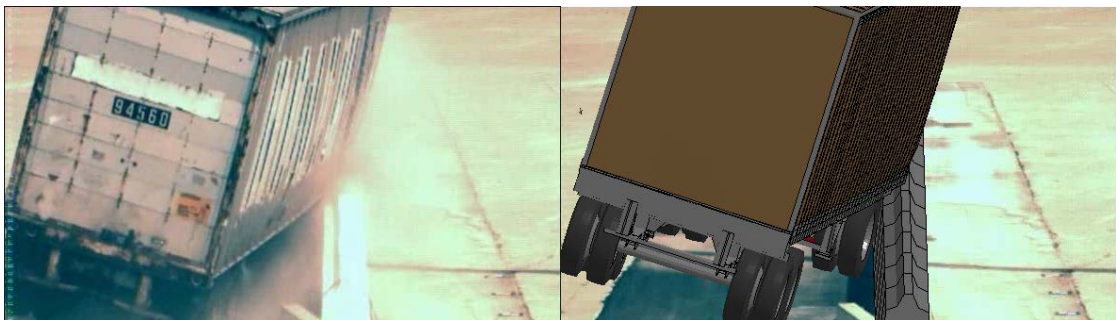
0.25 seconds
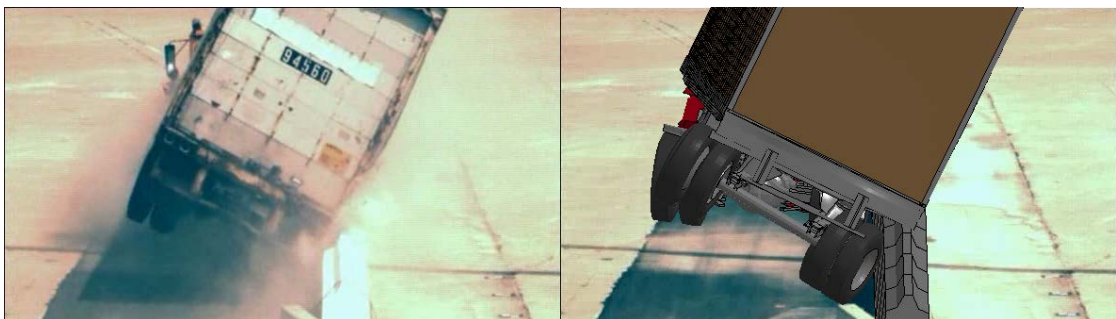
0.50 seconds

0.75 seconds

Figure 3.36: Back view impact sequence of the MwRSF full-scale test and ISOL FE model validation simulation

1.0 seconds
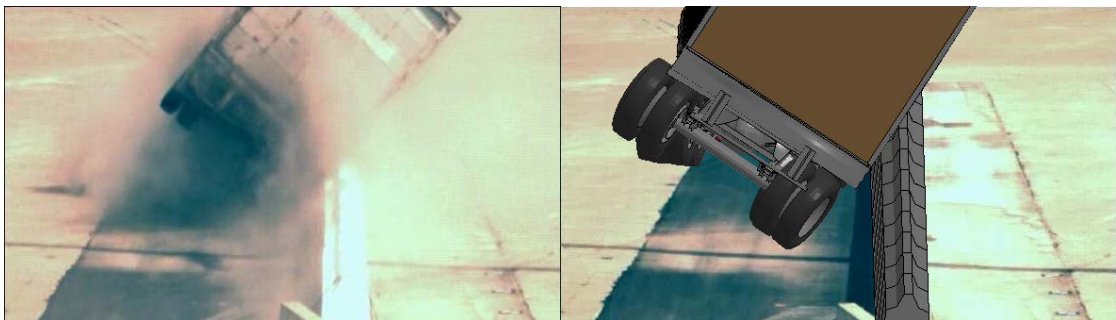
1.25 seconds
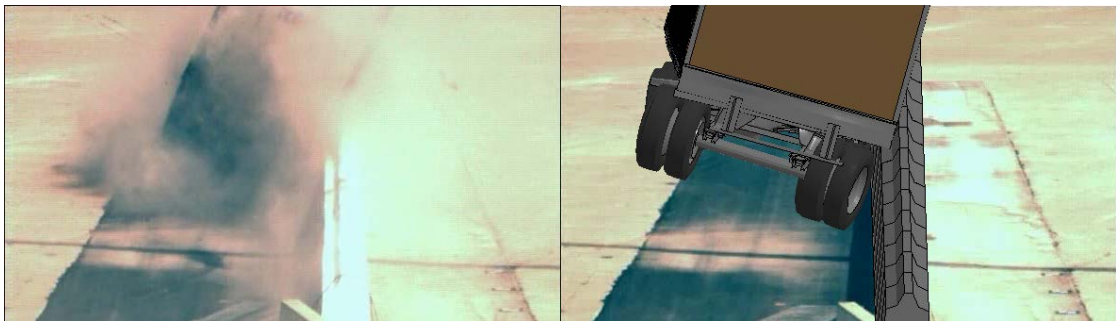
1.5 seconds

Figure 3.36 (continued): Back view impact sequence of the MwRSF full-scale
test and ISOL FE model validation simulation

0.0 seconds

0.25 seconds

0.50 seconds

0.75 seconds

1.0 seconds

1.25 seconds

1.5 seconds
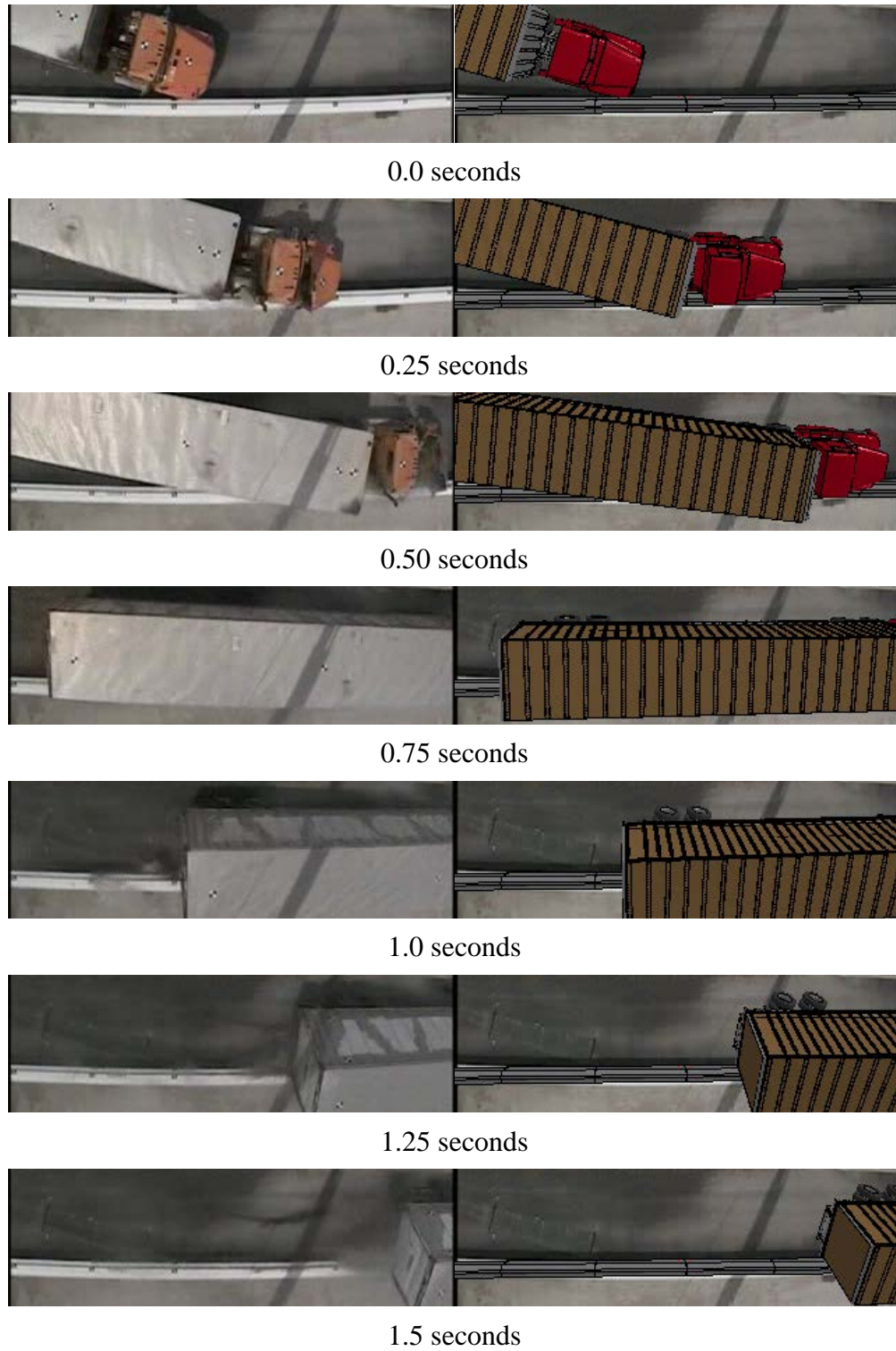
Figure 3.37: Top view impact sequence of the MwRSF full-scale test and ISOL FE model validation simulation

Based on the sequential image sequences from Figure 3.34 to Figure 3.37, the ISOL FE model validation simulation conducted in accordance with the MwRSF full-scale crash testing conditions match extremely well with key phenomenological events throughout the two-second impact sequence. During the first 0.25 seconds of the impact, the front-right corner of the tractor impacted the concrete barrier, causing the tractor to roll in the transverse direction, which resulted in the front-left tractor tire becoming airborne while the tractor is redirected parallel with the barrier. Between 0.25-0.5 seconds, the front-left corner of the trailer's kingpin assembly impacted the barrier while the tail-end of the trailer articulated around the fifth-wheel/kingpin connection and began to roll transversely towards the barrier with the trailer tandem tires becoming airborne. Between 0.5-0.75 seconds, the trailer tandem axles impacted the concrete barrier and the entire tractor-trailer was parallel with the barrier and began to roll on top of the barrier. Between 0.75-1.0 seconds, as the trailer continued to roll onto the barrier, the fixed fifth-wheel/kingpin connection between the tractor and trailer caused the tractor to roll with the trailer and resulted in all left-side tires becoming airborne. Between 1.0-1.25 seconds, the tractor and trailer both reached their respective maximum roll angles before beginning to return upright and the tractor's left-side tires returning to the roadway. Between 1.25-1.75 seconds, the trailer's tandem tires returned to the roadway as the roll angle approached zero and continued to roll transversely away from the barrier, although all tires remained grounded. For the remainder of the impact sequence, the tractor-trailer remained upright and continued to travel longitudinally along the face of the concrete barrier with an extremely low exit angle.

During the MwRSF full-scale crash test, the secondary accelerometer located at the tractor tandem axle failed to record data during the impact sequence due to being configured incorrectly. Therefore, only acceleration and rotational data was extracted from the trailer tandem axle's accelerometer for use in validating the ISOL tractor-trailer FE model to the MwRSF full-scale crash test. However, the tractor's roll angle data was able to be extracted manually through high speed camera footage throughout the impact scenario. Figure 3.38 shows the estimated tractor roll angle of the MwRSF full-scale crash test, compared to the NTRCI and ISOL FE simulations. The overall trend of the roll angles from the ISOL tractor FE model matches that of the MwRSF full-scale test tractor, with the maximum roll angle of the tractor being almost identical and occurring at the same instance in time. However, the tractor's counter-clockwise roll rotation occurring between 0.4-0.7 seconds was not consistent between the MwRSF and ISOL impact scenarios. A potential source for this discrepancy could be related to the fifth-wheel/kingpin connection being stiffer in the ISOL FE model compared to the MwRSF full-scale tractor-trailer.
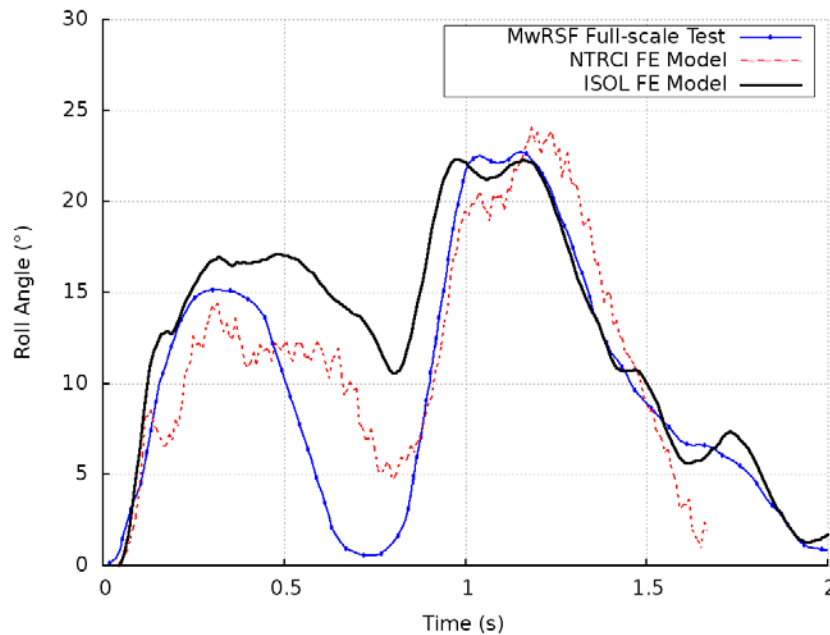
Figure 3.38: Roll angle profiles at the tractor CG for the MwRSF full-scale test,
NTRCI FE model, and ISOL FE model

Figure 3.39 through Figure 3.41 shows the yaw, pitch, and roll angles of the trailer

tandem axle, respectively, for the MwRSF full-scale crash test and the NTRCI and ISOL

FE simulations. In the yaw rotation profiles of the trailer tandem axle in Figure 3.39, the

ISOL trailer's tandem axle began yawing at the same time instance (0.2 seconds) as the

MwRSF trailer tandem axle. The yaw rotation of the ISOL trailer continued to grow to a

maximum yaw angle of -16.3°, whereas, the MwRSF trailer's maximum yaw angle was

-13.3°. Figure 3.40 shows that the pitch angle rotations of the MwRSF full-scale crash test

and the ISOL FE model validation simulation correlate well with each other compared to

the NTRCI FE simulation, with the MwRSF and ISOL trailer maximum pitch angles of

2.8° and 5.1°, respectively. The abrupt change in the pitch angle that occurred at 0.6

seconds corresponds to the trailer tandem axles impacting the concrete barrier. Figure 3.41

shows the roll angles experienced by the trailer in the MwRSF full-scale crash test and the NTRCI and ISOL FE simulations. The deviation of the roll angles at 0.6 seconds corresponds to the trailer tandem axles impacting the concrete barrier. Due to the slightly higher cargo-bed height in the ISOL trailer FE model compared to the MwRSF trailer, (i.e., 51 in (1.3 m) vs 45.5 in (1.16 m)), the tail-end of the trailer was able to climb on top of the barrier initially before continuing to roll which reduced the maximum roll angle the ISOL trailer experienced. The MwRSF trailer's maximum roll angle was 38.5° at 1.05 seconds and the ISOL trailer experienced a 35° maximum roll angle slightly later, at 1.1 seconds. Due to the ISOL trailer's lower roll angle compared to the MwRSF trailer, the ISOL trailer returned to an upright position sooner than the MwRSF trailer and had less momentum to continue to roll in the opposite direction. The post-impact difference in the roll angle profiles between the MwRSF and ISOL trailer can also be attributed to the stiffer fifth-wheel/kingpin connection in the numerical model as mentioned previously when discussing the tractor roll angles in Figure 3.38.
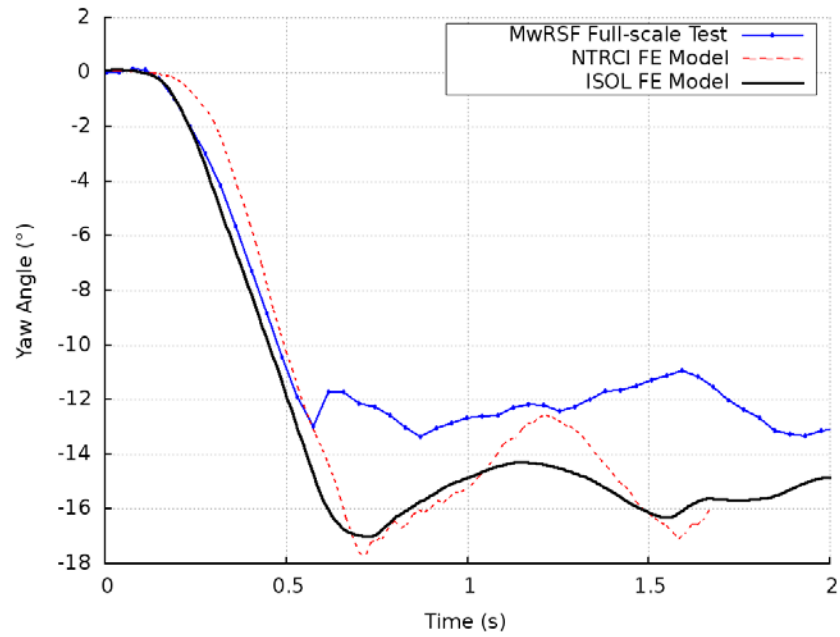
Figure 3.39: Yaw angle profiles at the trailer tandem axle for the MwRSF full-scale test, NTRCI FE model, and ISOL FE model
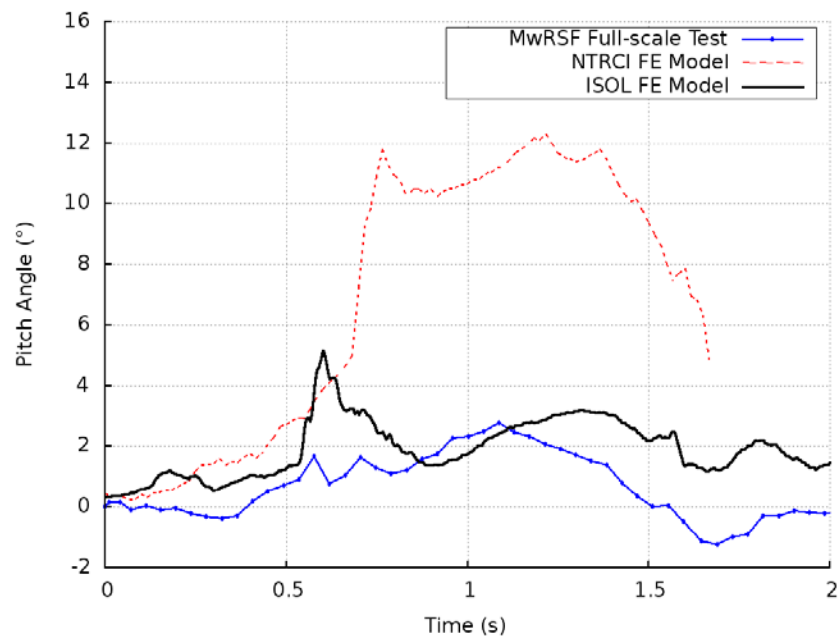
Figure 3.40: Pitch angle profiles at the trailer tandem axle for the MwRSF full-scale test, NTRCI FE model, and ISOL FE model
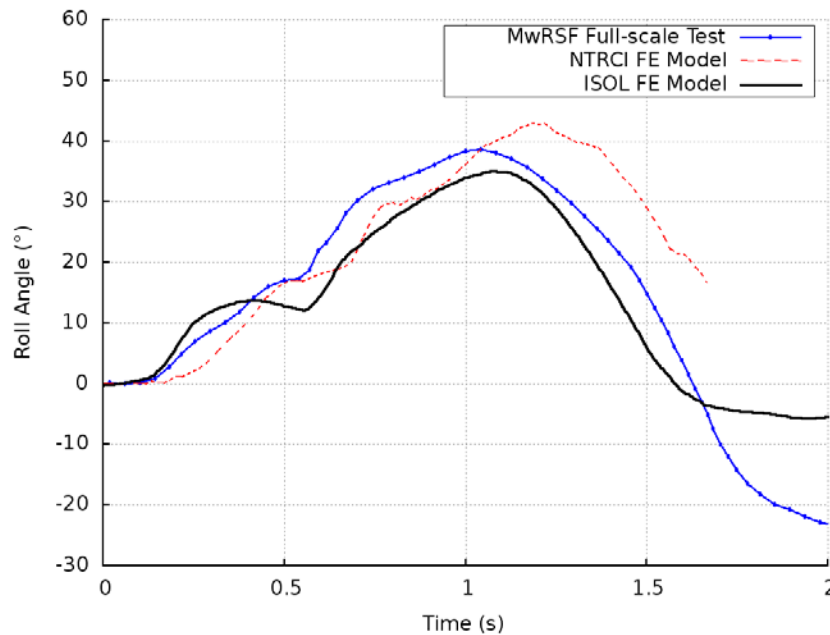
Figure 3.41: Roll angle profiles at the trailer tandem axle for the MwRSF full-scale test, NTRCI FE model, and ISOL FE model

Figure 3.42 through Figure 3.44 shows the longitudinal, transverse, and vertical acceleration profiles of the trailer tandem axle, respectively, for the MwRSF full-scale crash test and the NTRCI and ISOL FE simulations. The acceleration profiles in the aforementioned figures were filtered using Channel Frequency Class (CFC) 60 and show the 50-ms moving average accelerations to provide additional filtering of the raw data captured at a high frequency. In the acceleration profiles of the subsequent three figures, four tractor-trailer snapshots of the ISOL FE model validation simulation are overlaid at the corresponding peak accelerations throughout the impact scenario. In Figure 3.42 throughFigure 3.44, the ISOL tractor-trailer snapshots labeled 1-4 correspond to the following events: 1) tractor tandem axles impact barrier; 2) trailer tandem axles impact barrier; 3) rear-end of trailer impacts barrier; 4) trailer tandem axles return to roadway.
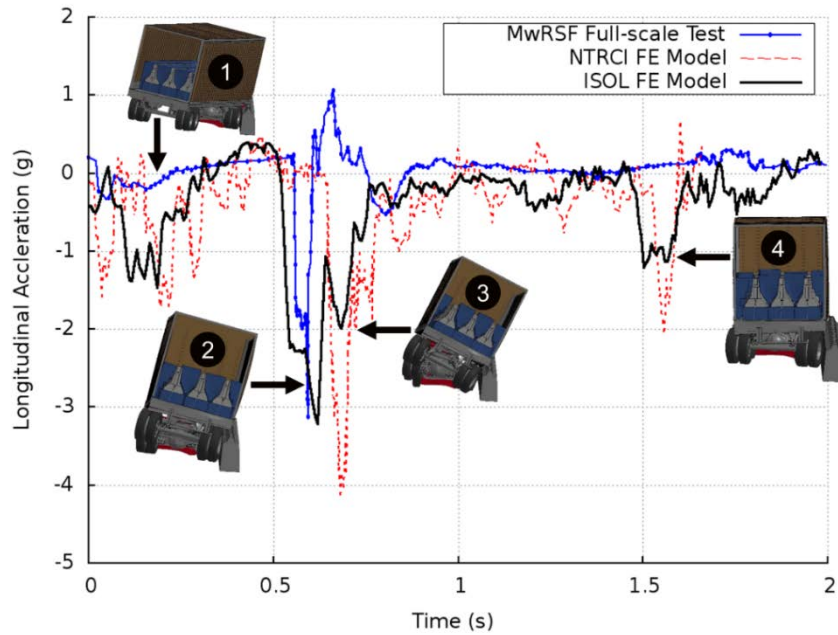
Figure 3.42: Longitudinal acceleration profiles at the trailer tandem axle for the MwRSF full-scale test, NTRCI FE model, and ISOL FE model
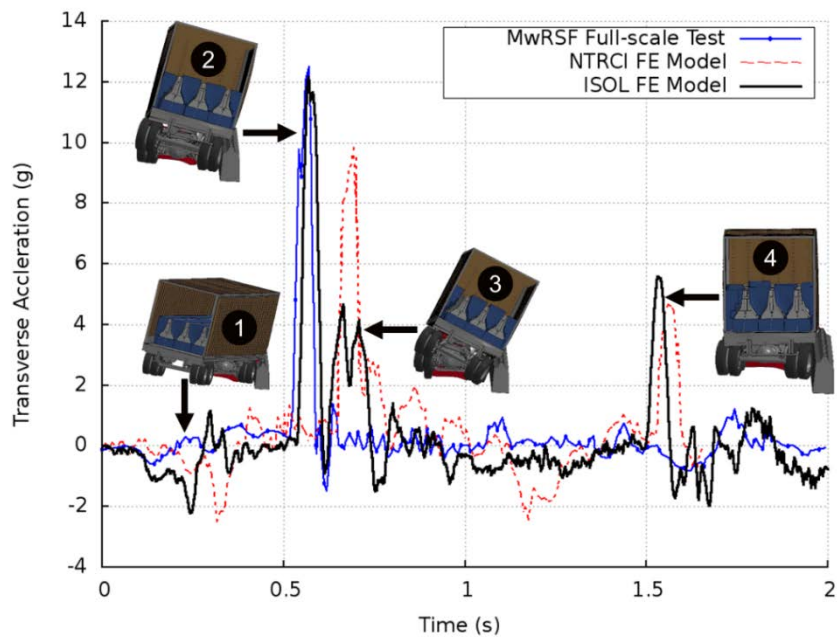
Figure 3.43: Transverse acceleration profiles at the trailer tandem axle for the MwRSF full-scale test, NTRCI FE model, and ISOL FE model
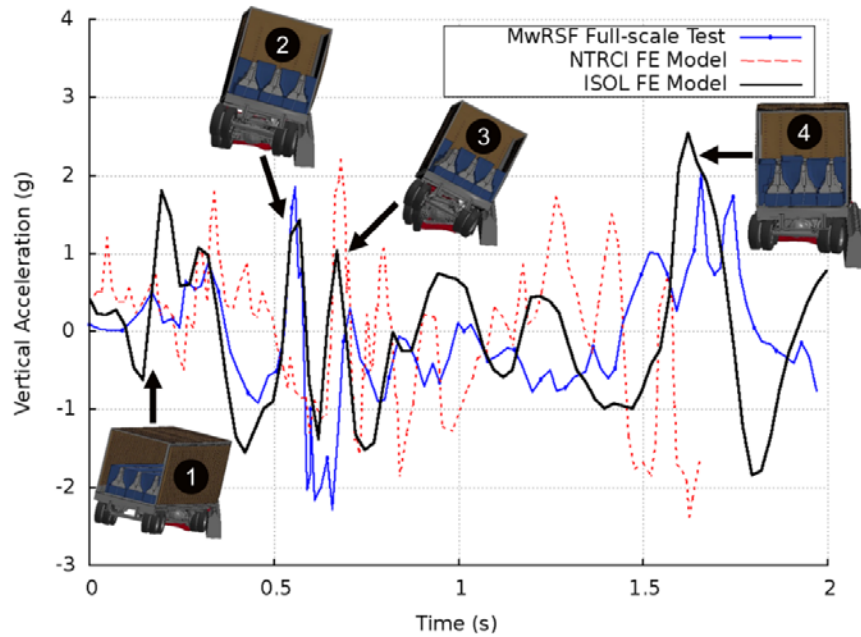
Figure 3.44: Vertical acceleration profiles at the trailer tandem axle for the
MwRSF full-scale test, NTRCI FE model, and ISOL FE model

The 50-ms moving average x-, y-, and z-axis acceleration profiles of the ISOL

trailer tandem axle matches the peak acceleration at 0.6 seconds of the MwRSF full-scale

crash test, at snapshot #2, where the trailer tandem axle impacts the concrete barrier. When

the fifth-wheel/kingpin connection at the tractor's tandem axle impacts the concrete barrier,

at snapshot #1, the 50-ms moving average x-, y-, and z-axis acceleration profiles of the

ISOL trailer tandem axle experienced on average a +1 *g* higher forces than the MwRSF

trailer. Due to the lower ride-height of the cargo-bed in the MwRSF trailer, snapshot #3

acceleration forces were not present in the MwRSF full-scale crash test; although, the

magnitude of the acceleration forces experienced at 0.7 seconds by the ISOL trailer were

significantly less than that of the initial trailer impact. At snapshot #4, when the trailer

tandem tires returned to the roadway, the vertical (z-axis) acceleration forces matched

reasonably well between the MwRSF trailer and the ISOL trailer, while the longitudinal (x-axis) and transverse (y-axis) acceleration forces were indistinguishable in the MwRSF trailer.

Overall, the acceleration profiles of the ISOL trailer matched reasonably well to the MwRSF full-scale test's trailer in terms of the time sequencing and magnitudes of phenomenological events throughout the impact scenario. Table 3.5 summarizes the post-impact behavior of the maximum rotational angles from Figure 3.38 through Figure 3.41 as well as the maximum 50-ms moving average accelerations from Figure 3.42 through Figure 3.44. In addition, the occupant safety evaluation criteria were determined based on the available acceleration profiles from the MwRSF full-scale crash test and compared to the NTRCI and ISOL FE simulations in Table 3.5.

Table 3.5: Evaluation criteria for the full-scale crash test and FE simulations

Testing Location	MwRSF	NTRCI	ISOL
Test Vehicle	Full-scale Test	Tractor-trailer FE Model	Tractor-trailer FE Model
Post-impact Behavior:			
Tractor Maximum Roll Angle	22.7°	24.3°	22.8°
Trailer Maximum Yaw Angle	-13.3°	-17.9°	-16.3°
Trailer Maximum Pitch Angle	2.8°	12.3°	5.1°
Trailer Maximum Roll Angle	38.5°	42.9°	35.0°
Occupant Safety - Trailer Tandem Axle:			
Maximum Accelerations (*g*):			
x-Axis (Longitudinal)	-13.7	-11.1	-12.0
y-Axis (Transverse)	39.9	33.2	27.1
z-Axis (Vertical)	-17.1	-58.9	-15.9
Resultant	40.0	59.5	30.8
ASI	1.37	1.23	1.29
Maximum 50-ms Moving Average Acceleration (*g*):			
x-Axis (Longitudinal)	-3.1	-4.2	-3.2
y-Axis (Transverse)	12.4	9.9	12.2
z-Axis (Vertical)	-2.2	-2.4	2.5
OIV ft/s (m/s):			
x-Axis (Longitudinal)	1.8 (0.56)	-4.9 (-1.48)	7.3 (2.24)
y-Axis (Transverse)	17.8 (5.11)	-3.0 (-0.92)	5.3 (1.62)
THIV ft/s (m/s)	11.3 (3.46)	1.7 (0.51)	9.3 (2.85)
ORA (g):			
x-Axis (Longitudinal)	-2.19	-1.09	-0.70
y-Axis (Transverse)	5.65	-0.38	2.97
PHD (*g*)	3.52	9.16	4.22

In terms of post-impact behavior, the maximum tractor roll angles and trailer yaw, pitch, and roll angles of the ISOL tractor-trailer FE model compared well with the MwRSF tractor-trailer and are a significant improvement compared to the NRTCI tractor-trailer FE

model. In regard to the occupant safety, although the ASI, OIV, ORA, THIV, and PHD evaluation criteria are not directly applicable as occupants are not typically located in the trailer, using the evaluation criteria aids in assessing the validation of the ISOL tractor-trailer FE model when compared to the MwRSF tractor-trailer. The MwRSF and ISOL maximum 50-ms moving average and non-averaged accelerations in the longitudinal, transverse, and vertical directions, shown in Table 3.5, correlate well with each other compared to the NTRCI accelerations. The ASI, as mentioned previously in the tractor-only model validation section, uses the x-, y-, and z-axis acceleration profiles and the respective acceleration limit values to compute a non-dimensional 'severity index' which is assumed to be proportional to occupant injury. An ASI of 1.0 corresponds to 'little to no injury', although an ASI less than or equal to 1.4 is acceptable. The ASI of the MwRSF and ISOL trailer were 1.37 and 1.29, respectively. Although the ASI is generally represented as a singular value, the ASI profile throughout the impact scenario is represented in Figure 3.45 for the MwRSF full-scale crash test and the NTRCI and ISOL FE simulations.
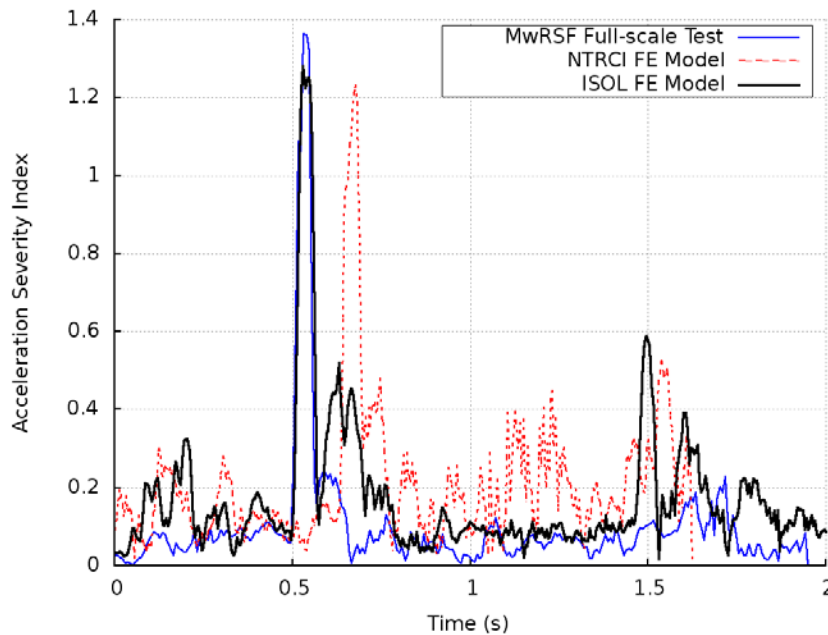
Figure 3.45: ASI calculated at the trailer tandem axle for the MwRSF full-scale test, NTRCI FE model, and ISOL FE model

The OIVs in the longitudinal and transverse directions and the resultant THIV were all below the allowable limit of 30 ft/s (9.1 m/s) in the MwRSF full-scale crash test and the NTRCI and ISOL FE simulations seen in Table 3.5. Similarly, the ORAs in the longitudinal and transverse directions and the resultant PHD were all below their respective allowable limit of 15 g and 20 g in the MwRSF full-scale crash test and the NTRCI and ISOL FE simulations. Comparing the OIV and corresponding ORA values, there is a moderate variation between the individual x- and y-component impact velocities and corresponding maximum ridedown accelerations of the MwRSF full-scale crash test compared to the ISOL FE simulation. However, when assessing the impact velocity and ridedown acceleration using the THIV and PHD metrics, the ISOL FE simulation corresponds well with the MwRSF full-scale crash test.

In all, the extensive geometrical modifications and numerical improvements made to the NTRCI tractor-trailer FE model to create the ISOL tractor-trailer FE model resulted in improved correlation both qualitatively and quantitatively in the validation against the MwRSF full-scale crash test data. To this end, the ISOL tractor-trailer FE model was deemed appropriate to be used for other full-scale impact scenarios. The following chapter will discuss the various flexible, semi-rigid, and rigid highway median barriers developed to assess the tractor-trailer impact behavior and guardrail performance during redirective impact scenarios under MASH TL-5 impact conditions.

CHAPTER 4: FINITE ELEMENT MODELING OF MEDIAN BARRIERS

Throughout the 223,000 miles of the National Highway System in the United States, thousands of miles of roadways in each state are equipped with flexible, semi-rigid, and rigid roadside and median barrier systems. These barrier systems cover the broad spectrum of safety hardware including, flexible (e.g., cable barriers), semi-rigid (e.g., W- and Thrie-beam guardrails), and rigid (e.g., concrete) barrier systems, with each barrier type having their own benefits and drawbacks.

Flexible barrier systems, such as cable barriers, are typically installed along roadways with medians greater than 30 ft (9.1 m) wide (AASHTO 2006) due to the large deflection that may occur when redirecting an errant vehicle. By design, the cables are intended to dislodge from the J-bolt housing on the steel posts to allow for increased impact energy absorption during a redirection; thus, reducing the severity of the deceleration forces on the vehicle and lowering the likelihood of occupant injury. A benefit of cable barrier systems is the lower installation cost compared to semi-rigid and rigid barrier systems, as well as the ability to be installed on curved, uneven, and sloped terrain of 4H:1V or flatter (AASHTO 2006). Conversely, drawbacks to the cable barrier systems include a higher propensity of vehicle penetration if the cables do not engage with the vehicle and either underride or override the vehicle. Additionally, cable barrier systems

incur higher repair costs due to longer sections of the barrier being damaged during an impact.

Semi-rigid barrier systems include widely used corrugated steel guardrails attached to a steel or wooden post. A blockout is typically used between the guardrail and post to offset the guardrail face and reduce the probability of the impacting vehicle's tire engaging directly with a post. These semi-rigid guardrail barrier systems allow a moderate amount of impact energy absorption through guardrail deflection and plastic deformation. The impact energy absorption is less than that of flexible barrier systems, as the additional rigidity of the steel guardrail reduces the allowable deflection while redirecting an impacting vehicle. Semi-rigid median barriers also have the versatility of being installed on flat or sloped terrain, as well as along curved roadways. The original single-faced (i.e., one-sided) design of semi-rigid guardrails were only applicable for roadside installations, unless two separate guardrails were used on either side of the roadway. With the development and approval of double-faced (i.e., two-sided) semi-rigid guardrails, the use these double-faced semi-rigid guardrails along medians has become increasingly more common (AASHTO 2006). Common double-faced semi-rigid barrier systems include W-beam and Thrie-beam guardrail systems. These semi-rigid barriers can be installed on flat and sloped terrain, and along roadways where narrower medians do not permit the use of flexible median barriers. A drawback of the semi-rigid barrier systems includes the higher repair costs to replace the deformed guardrail, blockout, mounting hardware, and/or posts after each accident.

Rigid barrier systems are the most effective barriers at preventing vehicles from crossing the median into oncoming traffic and are typically used in areas with high traffic volume and limited width medians. Rigid barriers, by design, do not allow deflection; therefore, extremely limited impact energy absorption occurs, resulting in the majority of impact energy dissipation occurring through severe vehicle deformation and vehicle redirection. The stiffness of the rigid barriers results in a higher occupant injury risk compared to flexible and semi-rigid barrier system impacts. Rigid barriers can only be installed on flat terrain and require very low maintenance; however, the initial installation cost is typically 10-15% higher than double-faced semi-rigid guardrail systems.

Each category of redirection-type median barriers has been shown to be effective at safely containing and redirecting vehicles. However, all of the aforementioned median barrier systems do not require full-scale crash test performance evaluations for all vehicle classes, prior to installation. Most flexible and semi-rigid barrier systems are evaluated using full-scale crash test of passenger vehicles, while rigid barrier systems are typically evaluated using full-scale crash test of heavy trucks and passenger vehicles.

4.1 Median Terrain Selection

Prior to the release of MASH-2, full-scale crash test evaluations of median barrier systems were conducted exclusively on flat terrain; however, in-service installations of the median barrier systems are commonly installed on uneven or sloped terrain. MASH-2 introduced guidelines for evaluating flexible median barriers on sloped terrain for TL-3 impact conditions, which does not include heavy vehicles in the crash testing scenarios (AASHTO 2016).

Sloped medians are categorized into the following groups based on an impacting vehicle's response: recoverable, non-recoverable, traversable, or critical. Recoverable sloped terrain includes embankments of 4H:1V or flatter, in which a vehicle on these slopes can usually be stopped and returned to the roadway. A non-recoverable slope, between 3H:1V and 4H:1V, is traversable but presents difficulties for vehicles to return to the roadway. Terrain with slopes steeper than 3H:1V are classified as critical and likely results in a rollover of vehicle that enter these critical slopes (AASHTO 2006). In practice, flatter and more recoverable sloped terrains are ideal to provide the most favorable conditions for increased passenger safety.

The terrain selected for this research included a flat median, in addition to a 6H:1V sloped median. These two terrain configurations were selected to represent both full-scale crash testing and in-service scenarios of flexible, semi-rigid, and rigid barrier systems to evaluate the barrier performance, vehicle behavior, and occupant injury risk of tractor-trailer impacts. Figure 4.1 illustrates the 46-ft (14-m) wide flat median, representative of a divided highway with traffic lanes along either side. The flexible, semi-rigid, and rigid barriers were placed along the mid span of the median width.
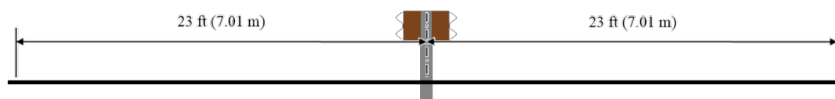
Figure 4.1: Flat median dimensions

Figure 4.2 shows the dimensions of the 46-ft (14-m) wide 6H:1V sloped median, which includes 6-ft (1.8-m) wide shoulders along either side of the median, bordered by traffic lanes. The flexible and semi-rigid median barriers were placed 4 ft (1.22 m) from the median ditch centerline, as MASH-2 specifies this placement can increase the propensity of vehicle penetration for passenger vehicles (AASHTO 2016). The off-center placement of the flexible and semi-rigid median barriers permitted the evaluation of front-side and backside impact scenarios, shown in Figure 4.2a. The front-side impact was defined as the impact scenario with the barrier located 4 ft (1.2 m) closer to the shoulder. Since rigid barriers can only be installed on flat terrain, the rigid median barrier was placed at the slope break point of the sloped median. The front-side impact was equivalent to that of the flat median impact and the backside impact required the tractor-trailer to traverse through the entire sloped median before impacting the backside of the rigid median barrier. Figure 4.2b shows the placement of the rigid barrier when installed on a sloped median.
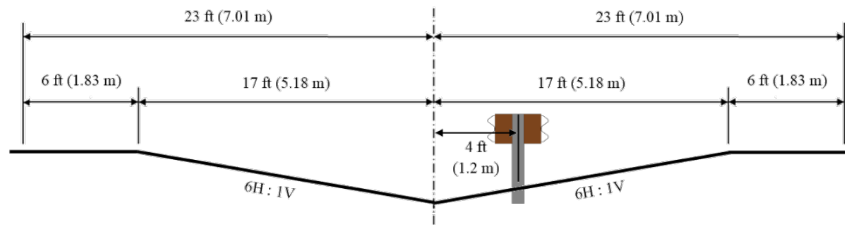
a. Flexible and semi-rigid guardrail placement on sloped medians
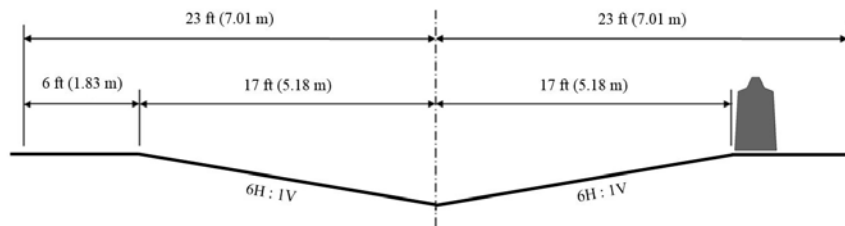
b. Rigid guardrail placement on sloped medians

Figure 4.2: Sloped median dimensions

Figure 4.3a and Figure 4.3b show the respective FE models created of the flat and sloped medians, with the median represented in green, the shoulder denoted in grey, and roadways designated in black. The entire ground surface (i.e., median, shoulder, and roadway) FE models were represented with rigidly constrained shell elements. As a result, the potential behavioral influences between the vehicle tires and the ground were neglected; with the exception of the frictional forces established in the contact definitions.

a. Flat median
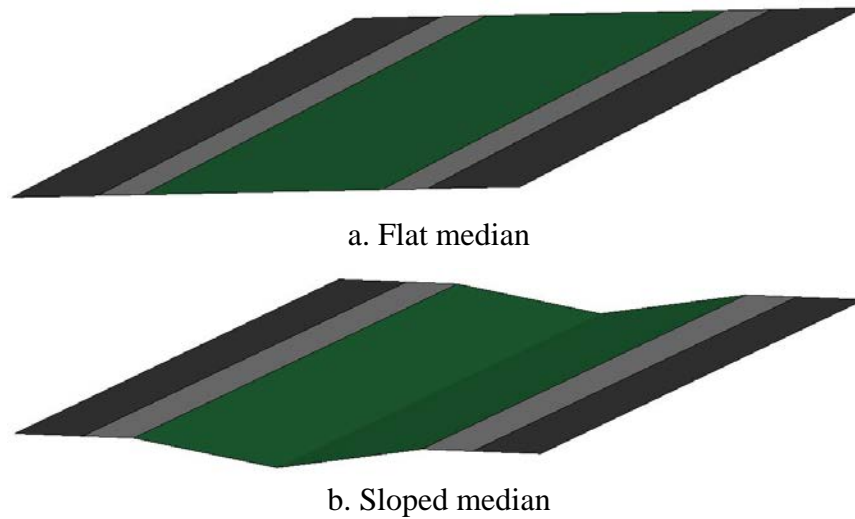
b. Sloped median

Figure 4.3: Flat and sloped median FE models

The remainder of this chapter will discuss the development of the flexible, semi-rigid, and rigid barrier FE models, placed on flat and sloped medians.

4.2 Flexible Median Barriers

The flexible median barrier systems used in this research included low-tension three- and four-CMBs. Development of the CMB FE model imparted significant challenges in modeling the cable to J-bolt interaction as well as the post-soil interaction. An FE model was created by Nawrocki and Labrosse (2000), where individual wire strands of a cable were modeled. However, utilizing this FE model would be too computationally expensive to use in full-scale crash testing simulations. Alternatively, a simplified model commonly used by the roadside safety community, represents the cable strand as a continuous body and is modeled using beam or solid elements. The low-tension three-CMB was originally created and validated at NCAC by Mohan et al. (2005). Where the J-bolts and cables were modeled using beam elements, with material properties based on the work

of Kirkpatrick (1999). The original Mohan et al. (2005) CMB FE model used additional null shell elements around the J-bolts and cables to handle the contact interface between the components. The post-soil interaction was modeled with each post encased in a soil block sufficiently large enough to allow for the post to be deflected or deform. The soil was modeled conforming to the characteristics of a standard foundation soil as outlined in NCHRP Report 350 and MASH (Marzougui et al. 2007).

The NCAC CMB FE model was modified at ISOL to create the three- and four-CMB FE models (Fang et al. 2009; 2012), according to North Carolina DOT design specifications (NCDOT 2002; 2012). A substantial modification to the CMB FE models made at ISOL was the removal of the contact-only null shell elements from the J-bolts and cables. This modification simplified the FE model and improved numerical stability and accuracy by allowing for the use of the beam-to-beam AUTOMATIC_GENERAL contact algorithm in LS-DYNA. The height of the cables on the CMBs, measured in descending order, from top to bottom are: 30 in (763 mm), 25.3 in (642 mm), and 20.5 in (522 mm); with a 4th cable height of 17 in (433 mm) on the four-CMB. Figure 4.4 shows single segments of the three- and four-CMBs. The J-bolts have a diameter of 0.314 in (8 mm) and the cable's diameter is 0.748 in (19 mm).

a. Three-cable barrier   b. Four-cable barrier
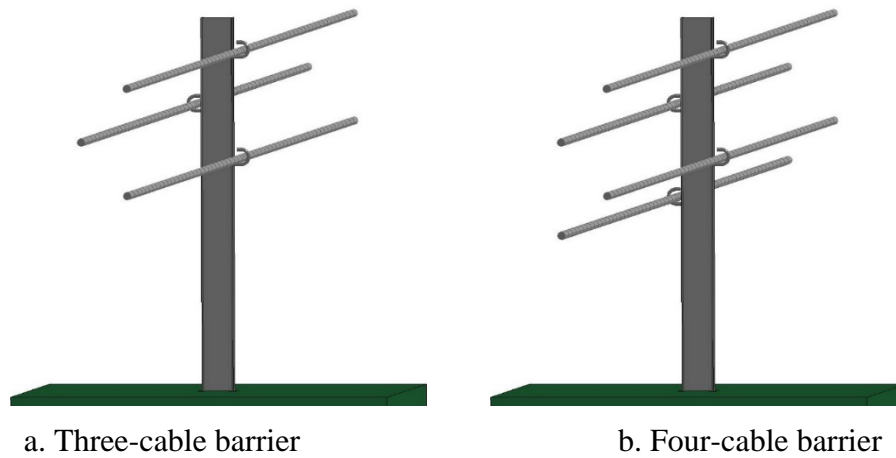
Figure 4.4: CMB FE model segments

The FE models of the single CMB segments were duplicated to create the entire 400-ft (122-m) length-of-need (LON) section of barriers, with posts spaced 16 ft (4.9 m) apart. The duplication of the barrier segments was completed using an ISOL-developed code to efficiently and effectively replicate all necessary LS-DYNA keywords (i.e., self-contacts, part, node, and element numbers). Each duplication referenced the original segment's material properties, element formulation, cross-sectional thickness, defined contact definitions between neighboring barrier segments, and merged nodes in adjacent segments. The ISOL code was also capable of placing terminals at either end of the LON section and connecting them to the adjacent barrier segments with properly defined contact definitions. This in-house code was used to generate all barrier FE models in this research. Figure 4.5 and Figure 4.6 show the complete flat and sloped median three- and four-CMB FE models, respectively.
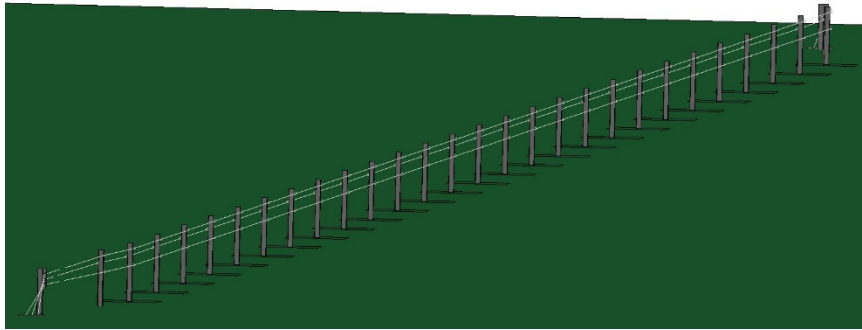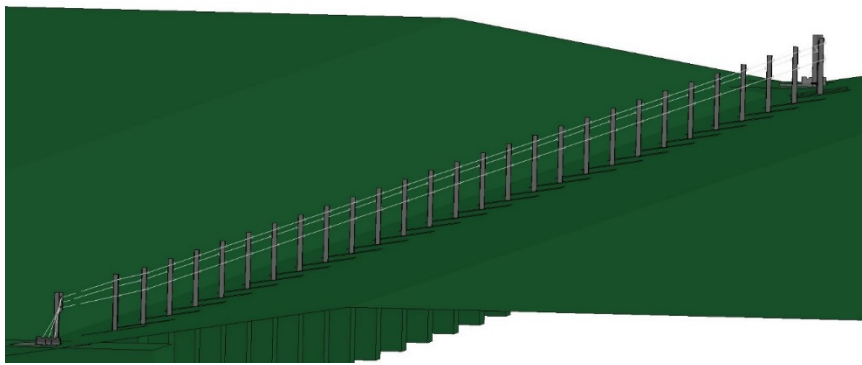
a. Flat median

b. Sloped median

Figure 4.5: three-CMB FE models
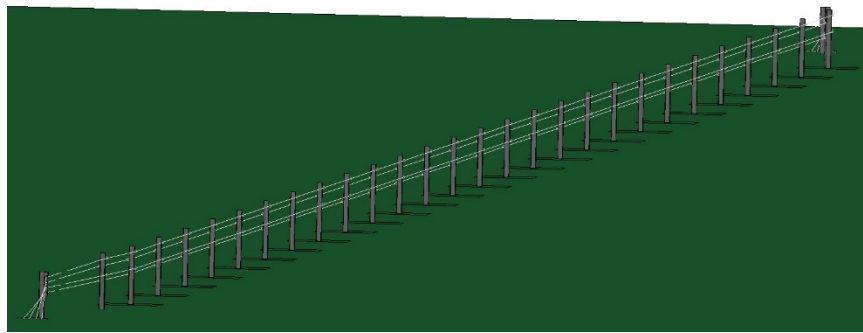
a. Flat median
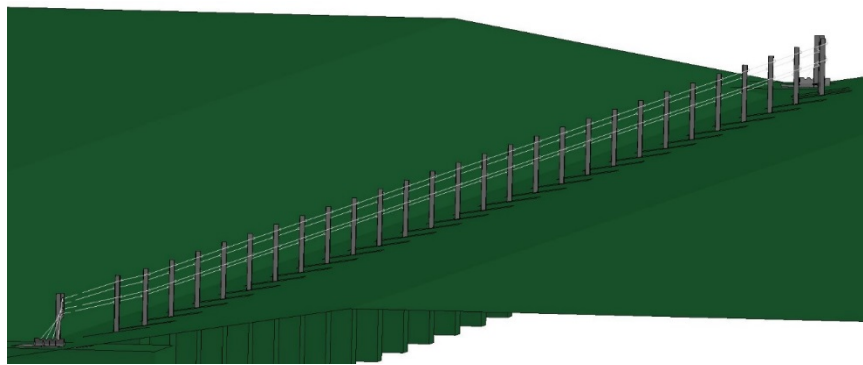
b. Sloped median

Figure 4.6: four-CMB FE models

The three- and four-CMB FE models utilized the same constitutive models throughout their respective 325 and 387 parts. The three- and four-CMB FE models consisted of 285,634 and 293,205 elements, respectively. The constitutive models utilized in the CMB FE models include, an elastic model for the cables, a piecewise linear plasticity model for the steel I-beam post, J-bolt, and anchoring hardware on the terminals, an elastic spring model for the cable-tensioning spring located at the terminal, a soil and foam model for the soil surrounding each post, a concrete model for the concrete anchoring blocks at the terminals, and a null material model for efficient contact handling between the post and soil.

4.3 Semi-Rigid Median Barriers

Unlike the flexible median barriers, the double-faced W-beam and Thrie-beam barriers are more complex systems that include many different components interacting with each other, such as, the soil foundations, steel guardrails, steel or wood blockouts, steel posts, numerous bolts to connect adjacent guardrail segments together and long-bolts to mount the guardrail and blockout to the posts. The FE modeling of the semi-rigid median barriers was more involved due to the additional components and the finer mesh required on the mounting hardware and steel guardrail to accurately capture the deformation during an impact scenario.

The FE models of the semi-rigid barriers used in this research included 31-in (787-mm) tall, double-faced wood-blockout W-beam, double-faced wood-blockout Thrie-beam, and double-faced steel-blockout Thrie-beam guardrails. The FE model of the single-faced G4(1S) W-beam guardrail, with posts spaced 6.25 ft (1.9 m) apart, was originally developed at NCAC and validated using crash test data from a full-scale crash test conducted at TTI under NCHRP Report 350 TL-3 conditions (Opiela et al. 2007). The double-faced wood-blockout W-beam guardrail was modeled and validated at ISOL for use during previous North Carolina DOT research projects (Fang et al. 2010; 2013; 2015). Figure 4.7 shows a segment of the double-faced W-beam guardrail that was duplicated using the ISOL code to generate the complete barrier FE model.
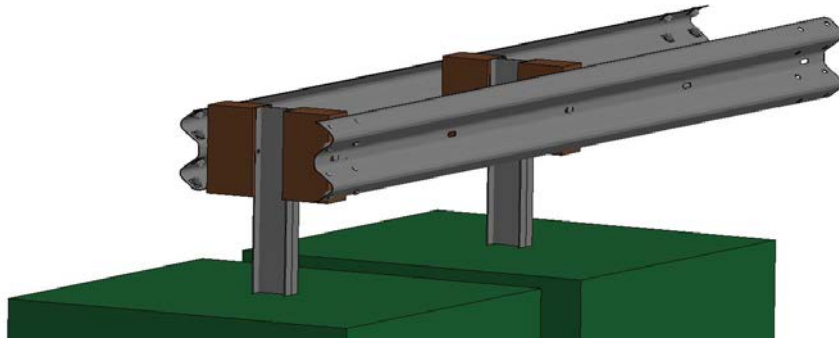
Figure 4.7: Double-faced W-beam guardrail FE model segment

The two variations of the double-faced Thrie-beam guardrails were created from existing FE models in accordance with AASHTO's Roadside Design Guide (AASHTO 2006) and the North Carolina DOT Roadway Standard Drawings (NCDOT 2012). The Thrie-beam guardrail FE models utilized the soil and post components from the W-beam guardrail FE model. The steel Thrie-beam guardrail was obtained from NCAC's model of a W-to-Thrie-beam transition barrier used to transition from a semi-rigid W-beam guardrail to a rigid concrete barrier. The ISOL Thrie-beam guardrail FE model was verified to be consistent with the TTI test 404211-5 (Buth & Menges 1999) and FE simulation results from Atahan and Cansiz (2005) prior to use in simulating impact scenarios. Two different blockout types for the Thrie-beam guardrail FE model were created, a wood-blockout and a steel-blockout. Figure 4.8 and Figure 4.9 illustrate the segments of the double-faced wood- and steel-blockout Thrie-beam guardrail FE models, respectively. These Thrie-beam guardrail FE model segments were used to generate the complete barrier FE models.
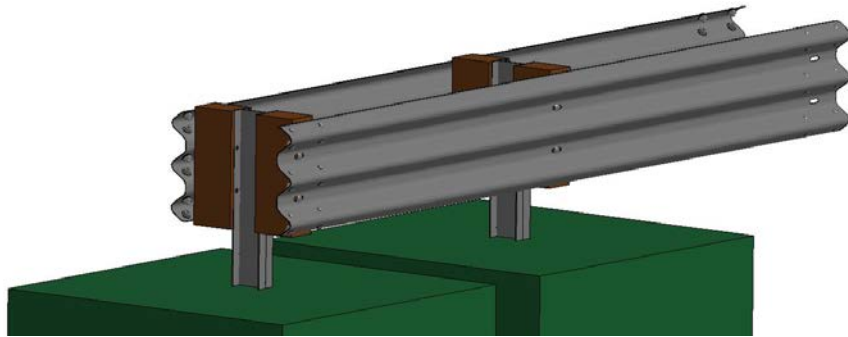
Figure 4.8: Double-faced wood-blockout Thrie-beam guardrail FE model segment
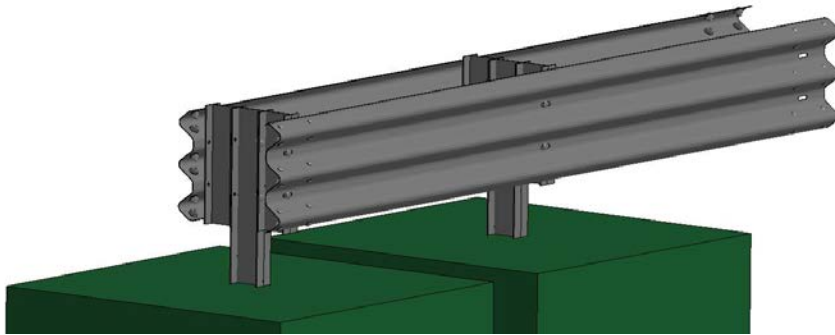
Figure 4.9: Double-faced steel-blockout Thrie-beam guardrail FE model segment

The FE model of the double-faced W-beam guardrail contains six constitutive models: a piecewise linear plasticity model for the steel components (i.e., I-beam posts and guardrail), an elastic model for the wood blockouts, a soil and foam model for the soil foundations surrounding the posts, a rigid model for the mounting hardware, a nonlinear elastic spring model for the bolt-tensioning spring in the short-bolts connecting adjacent guardrail segments together and long-bolts attaching the guardrails and blockouts to the posts, and a null material model for contact purposes. The FE model of the double-faced wood-blockout Thrie-beam guardrail contains the same six constitutive models as the W-

beam guardrail FE model. The double-faced steel-blockout Thrie-beam guardrail FE model

contained five of the six constitutive models the previous two aforementioned guardrail FE

models used, omitting the elastic model used for the wood blockouts. Figure 4.10, Figure

4.11, and Figure 4.12 show the complete flat and sloped median W-beam, wood-blockout

Thrie-beam, and steel-blockout Thrie-beam guardrail FE models, respectively.
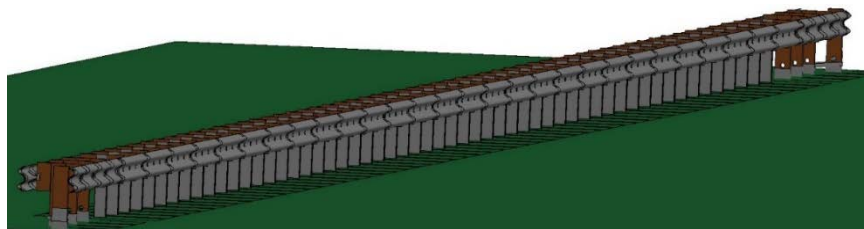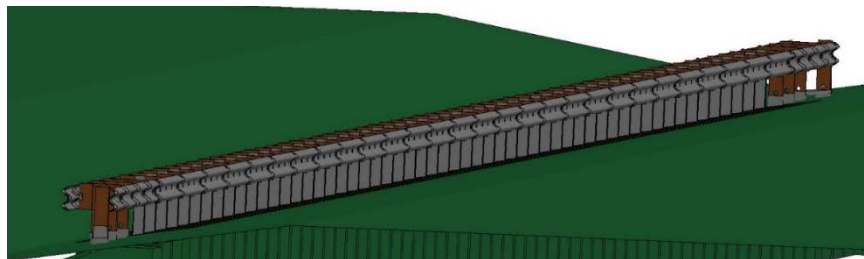
a. Flat median

b. Sloped median

Figure 4.10: Double-faced W-beam guardrail FE models
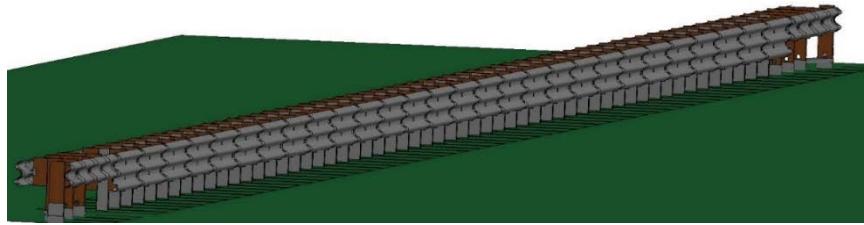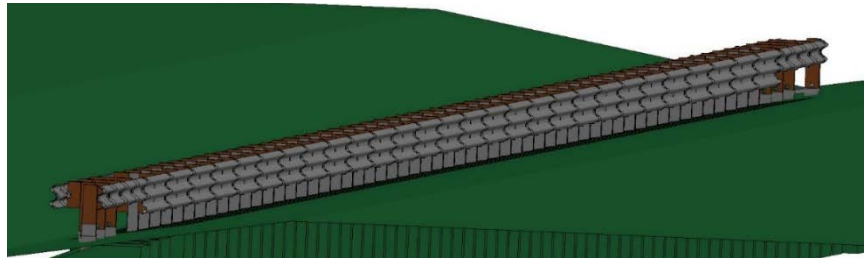
a. Flat median

b. Sloped median

Figure 4.11: Double-faced wood-blockout Thrie-beam guardrail FE models
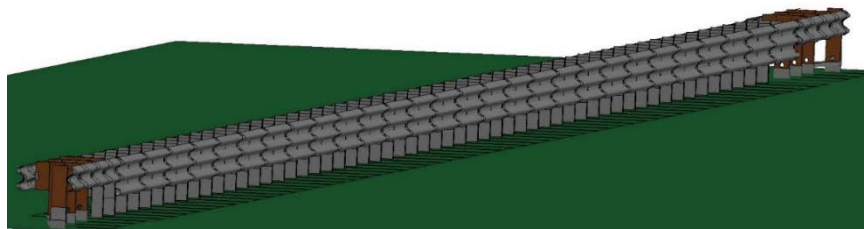
a. Flat median
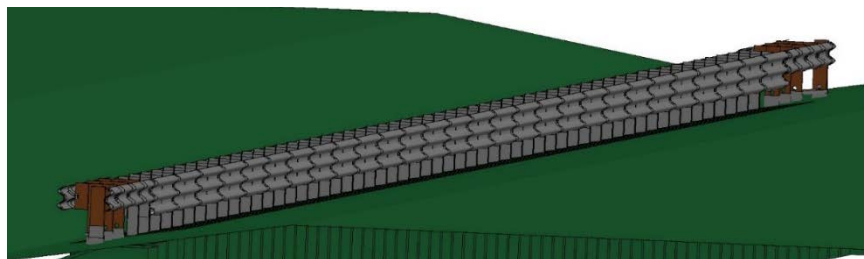
b. Sloped median

Figure 4.12: Double-faced steel-blockout Thrie-beam guardrail FE models

4.4 Rigid Median Barriers

Concrete barriers rarely deform even under severe impact conditions, and if damage does occur, it is usually limited to cosmetic damage. The MwRSF concrete barrier FE model used for tractor-trailer FE model validation was used to simulate the rigid median barrier impacts. The 42-in (1.1-m) concrete barrier was rigidly constrained and modeled with 114,210 solid elements using an elastic constitutive model to represent concrete. The exterior surface was surrounded with 64,250 null shell elements for contact purposes. The complete flat and sloped median concrete barrier FE models are shown in Figure 4.13.

a. Flat median
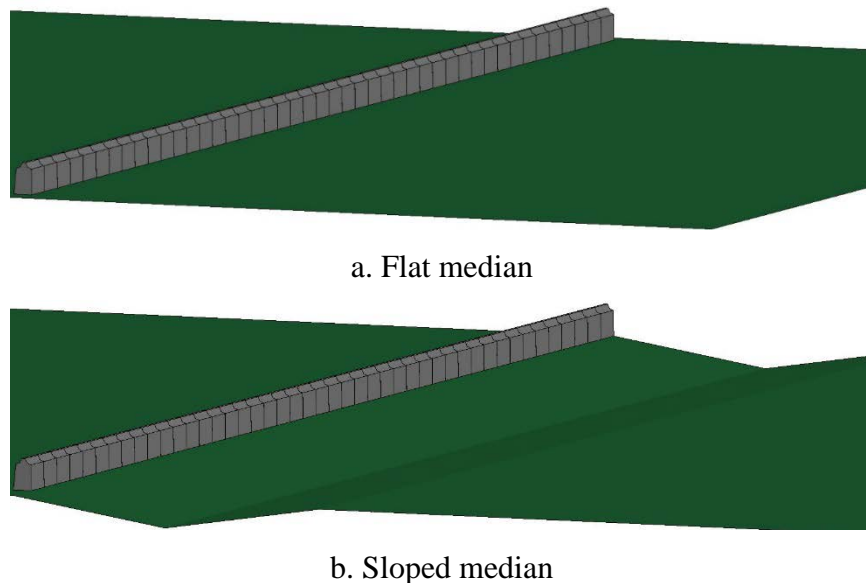
b. Sloped median

Figure 4.13: Concrete median barrier FE models

In all, four flexible median barriers (i.e., flat and sloped three- and four-CMBs), six double-faced semi-rigid median barriers (flat W-beam guardrail, sloped W-beam guardrail, flat wood-blockout Thrie-beam guardrail, sloped wood-blockout Thrie-beam guardrail, flat

steel-blockout Thrie-beam guardrail, and sloped steel-blockout Thrie-beam guardrail), and two rigid median barriers (i.e., flat concrete barrier and sloped concrete barrier) were created in order to evaluate the guardrail performance, vehicle behavior, and occupant risk when impacted by a 79,714-lb (36,158-kg) tractor-trailer. The subsequent chapter will discuss the impact scenarios and impact conditions in which the median barrier and tractor-trailer were used to evaluate the full-scale FE model crash test simulations.

CHAPTER 5: SIMULATIONS OF TRACTOR-TRAILER IMPACTS ON HIGHWAY
MEDIAN BARRIERS

An adequately designed median barrier system is effective at preventing vehicles

from traversing through the median into oncoming traffic and is capable of being impacted

from both sides to redirect errant vehicles in the safest way possible to lessen the risk of

occupant injury. When occupant safety evaluation is the primary objective, the use of an

ATD is mandatory. However, evaluating the barrier performance and vehicle behavior

from a full-scale crash test can be used to assess the accident severity and be correlated to

occupant safety when an ATD is not included. As stated in MASH, although the

relationship between vehicle dynamics during impact scenarios and occupant risk is

difficult to quantify, standardized safety metrics to assess occupant risk using vehicle

accelerations, developed by Jarvis D. Michie (1981), can be used as a high confidence

indication of potential occupant injury risk (Sicking et al. 2009).

The performance evaluation of highway median barrier systems has primarily been

performed through full-scale crash testing; however, in recent years, numerical simulations

have been used to support and supplement full-scale crash tests. Numerical simulations

have the advantage of precise control of every aspect in an impact scenario, afford cost-

effective parametric analyses, and can be analyzed in greater detail than a full-scale crash

test. Ultimately, both full-scale crash tests and numerical simulations are capable of

providing the necessary information to evaluate the structural adequacy, occupant risk, and vehicle trajectory of highway median barrier systems.

The process of conducting full-scale crash tests is complicated by the number of variables present in each impact scenario that can influence the test results, such as, weather conditions, ground type, vehicle model, and type of barrier. Continuous effort from the roadside safety community has created standardized testing procedures for conducting and evaluating the performance of highway safety barrier systems. AASHTO's MASH defines six TLs, each with specific vehicles classes, impact speeds, and impact angles. All TLs use a 2,420-lb (1,100-kg) small passenger sedan and 5,000-lb (2,270-kg) pickup truck. The impact speeds for TL-1, -2 and -3 are 31 mph (50 km/h), 43 mph (70 km/h), and 62 mph (100 km/h), respectively, all using an impact angle of 25°. TL-4, -5 and -6 use TL-3 impact conditions but add the use of heavy vehicles in addition to the passenger vehicles. TL-4 adds a 22,000-lb (10,000-kg) single-unit truck, TL-5 adds a 79,300-lb (36,000-kg) tractor-trailer, and TL-6 a 79,300-lb (36,000-kg) tractor-tanker-trailer. The impact speed for the TL-4 single-unit truck is 56 mph (90 km/h) with an impact angle of 15°. TL-5 and TL-6 tractor-trailers use an impact speed of 50 mph (80 km/h) and a 15° impact angle.

Section 5.1 will discuss the evaluation criteria used to assess the tractor-trailer impact scenarios in this research. Sections 5.2, 5.3, and 5.4 will present the tractor-trailer impacts on flexible, semi-rigid, and rigid median barriers, respectively. All impact scenarios in this research utilized MASH TL-5 impact conditions for the tractor-trailer (i.e., a 50-mph (80-km/h) impact speed and a 15° impact angle).

5.1 Tractor-Trailer Impact Evaluation Criteria

The tractor-trailer impacts on flexible, semi-rigid, and rigid median barriers were evaluated to assess the median barrier's structural adequacy, the tractor-trailer post-impact behavior, and the potential risk an occupant would be exposed to during the impact scenario. Each of these evaluation categories has respective criteria defined in MASH to classify the impact scenario as either satisfactory or unsatisfactory. This section will discuss the evaluation criteria used to analyze the tractor-trailer impact scenarios in Sections 5.2-5.4.

5.1.1 Vehicle Response Evaluation Criteria

Due to the extended interaction between the tractor-trailer and median barrier during an impact scenario, the evaluation of the post-impact vehicle behavior and the barrier's ability to contain and redirect the impacting vehicle are intertwined and will be evaluated in unison. The criteria used to evaluate the barrier performance and tractor-trailer response are as follows:

5.1.1.1 Tractor-Trailer Barrier Interaction Time

The interaction time is defined as the total engagement time that the tractor-trailer is in contact with the barrier. The interaction time will differ greatly based on the rigidity and amount of deflection the median barrier type allows; in general, the more flexible the barrier, the longer the interaction time. Longer interaction times also correlate with more impact energy being absorbed.

5.1.1.2 Maximum Dynamic Barrier Deflection

The maximum dynamic deflection is defined as the barrier's largest transverse displacement from the initial barrier placement throughout the duration of the impact

scenario. The maximum dynamic barrier deflection is only applicable for flexible and semi-rigid median barriers, since the rigid barriers are rigidly constrained and do not deflect.

5.1.1.3 Longitudinal Barrier Damage

The longitudinal barrier damage is defined as the longitudinal length of damage the median barrier experienced during an impact. The amount of damage a barrier develops during an impact scenario is important to classify, as the damaged section of barrier would not perform adequately in the subsequent interactions without being repaired or replaced. The longitudinal barrier damage length is further correlated with the maximum dynamic deflection of the barrier, by which, larger barrier deflections result in longer damaged barrier sections. It should be noted, for the rigidly-constrained concrete median barriers, the tractor-trailer-to-barrier interaction distance was reported as a surrogate for longitudinal barrier damage.

5.1.1.4 Tractor-Trailer Exit Angle and MASH Exit Box Criteria

The tractor-trailer's post-impact response is important to evaluate as it is preferred that the vehicle does not reenter the roadway if redirected by the barrier. One measure of the vehicle's post-impact response is the exit angle, which is defined as the angle between the barrier's longitudinal axis and the tractor-trailer's yaw angle when contact with the barrier ends. The preferred, but not required, exit angle should be less than 60% of the initial impact angle as specified by MASH, which equates to 9°, based on the 15° impact angle. However, assessing only the exit angle is not sufficient when evaluating the post-impact behavior because the tractor-trailer may continue to yaw after losing contact with the barrier. Hence, the exit box criterion was implemented in MASH, adopted from the

European Committee for Standardization (CEN) crash-testing standards (2010). The exit

box criterion is used to classify the vehicle redirection characteristics based on the vehicle's

post-impact trajectory. Figure 5.1 illustrates the application of the exit box criterion. An

impact scenario is considered safely redirected if the vehicle tires travel the longitudinal

distance of the exit box, B, without traveling a transverse distance, A, away from the barrier.

A safe redirection quantified by the exit box criteria corresponds to the impacting vehicle

having a small enough exit angle as to effectively eliminate the possibility of the vehicle

returning to the roadway and causing a secondary accident. The placement of the exit box

occurs at the last point of contact of the tire tracks with the initial location of the barrier

face. The dimensions of the exit box are based on the vehicle type and are a function of the

vehicle's size. Table 5.1 gives the equation for defining the exit box sides, A and B, as

defined in MASH, where V_W and V_L represent the vehicle width and length, respectively.
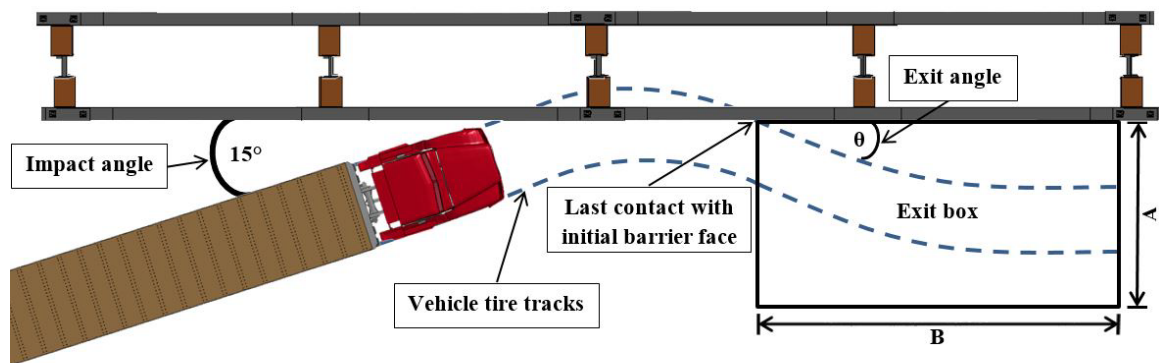
Figure 5.1: MASH exit box criterion

Table 5.1: Tractor-trailer MASH exit box dimensions

Vehicle Type	Exit Box Dimension	
	A	B
Cars or Pickup Trucks	$7.2 + V_W + 0.16V_L$ (ft)	32.8 ft (10 m)
Other Vehicles (i.e., Tractor-trailer)	$14.4 + V_W + 0.16V_L$ (ft)	65.6 ft (20 m)
ISOL Tractor-trailer FE Model	32.9 ft (10 m)	65.6 ft (20 m)

There are certain impact scenarios in which the exit box criteria is not applicable. One such scenario being when the impacting vehicle remains in contact with the barrier and upright while the impacting velocity is reduced to zero. This aforementioned scenario is deemed safe according to MASH since the threat of causing a secondary accident has been eliminated. Another scenario in which an exit box is not applicable is when the impacting vehicle fails to remain upright and rolls onto the barrier. In this scenario, based solely on the evaluation of barrier performance, the barrier performs as intended by eliminating the possibility of the impacting vehicle penetrating through the barrier into oncoming traffic. However, assessing the rollover impact scenario in terms of occupant injury, a potentially higher risk of injury could be present. Although the exit box criterion is a useful tool for classifying post-impact vehicular trajectories, use of this criterion alone is not sufficient to determine if the vehicle has been safely redirected.

5.1.1.5 Tractor-Trailer Rotational Angles

The yaw, pitch, and roll angles of the tractor-trailer were used to examine the vehicle's redirection, stability, and orientation throughout the impact scenarios. Figure 5.2 shows the orientation of the yaw, pitch, and roll angles for the ISOL tractor-trailer FE

model. The yaw angle indicates the angle of vehicle redirection, where the pitch and roll angles indicate the stability and orientation of the vehicle throughout the impact. A large pitch or roll angle implies an unstable response from the vehicle. MASH states the pitch and roll angles should not exceed 75°. However, an exception to this criterion applies to heavy vehicles, in which MASH states that this requirement is not applicable for tests involving the 10000S (i.e., single-unit truck) and 36000V (i.e., tractor-trailer) vehicles although it is preferable all vehicles remain upright. This exception allows for a 90° roll of the heavy vehicle during impacts, based on the fact that the primary goal of the impact scenario is to demonstrate the guardrail's ability to contain and redirect the impacting vehicles. Furthermore, MASH also states that quarter-turn rollovers of heavy vehicles do not necessarily correlate with increased occupant risk as they do in smaller passenger-sized vehicles (i.e., small sedan and pickup truck).
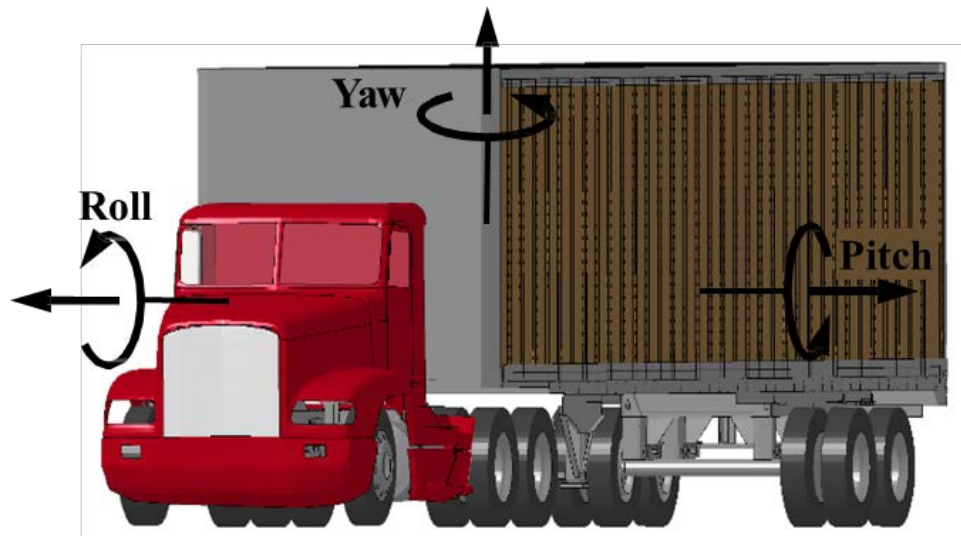
Figure 5.2: Yaw, pitch, and roll angle orientation

5.1.1.6 Longitudinal and Transverse Displacement and Velocities

The final evaluation criteria used to evaluate the vehicle response includes the longitudinal and transverse displacements and velocities of the tractor and trailer. The longitudinal and transverse displacements of the tractor-trailer throughout the impact scenarios are used to evaluate the trajectory of the vehicle as well as determine at what point the vehicle was redirected (if applicable). The longitudinal and transverse velocities were used to assess the post-impact speed of the tractor-trailer and determine the likelihood of traveling back onto the roadway to potentially cause a secondary accident.

5.1.2 Occupant Risk Evaluation Criteria

The other main category of evaluation criteria used to assess the tractor-trailer impact scenarios was occupant risk analysis. Although an ATD was not present in the tractor-trailer impact scenarios, the acceleration profiles of the tractor cabin CG can be correlated with the occupant injury risk using industry-standardized metrics that have proven to be valuable supplementary tools for designing, testing, and assessing highway safety hardware systems. The occupant injury risk is established based on the notion that, the more severe an impact is, the higher the likelihood of occupant injury. The following sections elaborate on the occupant safety metrics used to assess the occupant injury risk.

5.1.2.1 Tractor-Trailer Acceleration Profiles

In addition to the raw acceleration profiles of the tractor and trailer, the 50-ms moving average longitudinal and lateral forces of the tractor-trailer were used as measures for assessing impact severity (Council & Stewart 1993).

5.1.2.2 Occupant Impact Velocity and Occupant Ridedown Acceleration

MASH, as well as the two predecessors, NCHRP 230 and NCHRP 350, adopted the use of the flail space model to correlate impact severity to occupant risk. A "hypothetical" unrestrained occupant is assumed to be located at the vehicle CG. This assumption on occupant location is based on passenger-sized vehicles and, if applied to the tractor-trailer, the "hypothetical" occupant would be located outside of the tractor cabin. For the purpose of this research, the location of the "hypothetical" occupant was assumed to be located at the tractor cabin CG in order to provide more applicable occupant risk evaluations. Michie (1981) stated, the "hypothetical" occupant freely moves through the vehicle compartment (flail space) before striking the interior (i.e., instrument panel, windshield, or door) and is assumed to remain in contact with the vehicle interior for the duration of the impact. The velocity at which the occupant makes contact with the vehicle interior is the OIV and the subsequent maximum acceleration the occupant experiences after contact occurs is the ORA. The larger the OIV/ORA values, the higher the impact severity and the more likely the occupant would experience injuries. The OIV and ORA are standard occupant injury evaluation criteria defined in MASH and used in most full-scale roadway hardware system crash tests.
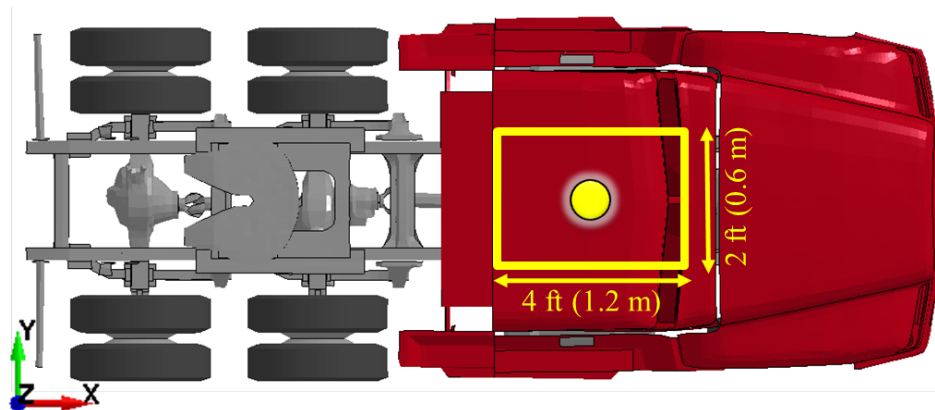
Figure 5.3: Flail space model of the tractor cabin

Figure 5.3 shows the location of the flail space model as designated for the tractor cabin. The OIV and ORA are calculated in both the longitudinal and lateral directions, neglecting the yaw rotation of the vehicle. The occupant is assumed to be able to travel 2 ft (0.6 m) in the longitudinal direction (x-axis) and 1 ft (0.3 m) in the lateral direction (y-axis) before impacting the vehicle's interior. The procedure for calculating the OIVs and ORAs in the longitudinal and lateral directions are as follows.

$$\int_0^{t_x} dt \int_0^{t_x} a_x dt = 0.6 \tag{5.1}$$

and

$$\int_0^{t_y} dt \int_0^{t_y} a_y dt = 0.3 \tag{5.2}$$

where t_x and t_y are the time instances in which longitudinal and lateral displacement limits are reached, respectively, and a_x and a_y are the longitudinal and lateral acceleration

profiles of tractor cabin CG, respectively. After t_x and t_y are determined, the OIV in the longitudinal and lateral directions are calculated by

$$OIV_x = \int_0^{t_0} a_x dt \tag{5.3}$$

and

$$OIV_y = \int_0^{t_0} a_y dt \tag{5.4}$$

where $t_0 = \min\{t_x, t_y\}$. The subsequent ORA$_x$ and ORA$_y$ in the longitudinal and lateral directions, respectively, are determined as the maximum 10-ms moving average tractor cabin CG acceleration after t_0 occurs. MASH specifies preferred limit OIVs of 30 ft/s (9.1 m/s) and ORAs of 15.0 g; although maximum limit OIVs of 40 ft/s (12.2 m/s) and ORAs of 20 g are acceptable.

5.1.2.3 Acceleration Severity Index

CEN utilizes the ASI and THIV as measures of occupant risk (CEN 2010). Although these occupant risk evaluation criteria are not required by MASH, they are strongly recommended. The ASI uses the x, y, and z acceleration profiles of tractor cabin CG to represent collision severity that is assumed to be proportional to occupant risk. The ASI is calculated by

$$ASI(t) = \left[\left(\frac{\bar{a}_x}{\hat{a}_x} \right)^2 + \left(\frac{\bar{a}_y}{\hat{a}_y} \right)^2 + \left(\frac{\bar{a}_z}{\hat{a}_z} \right)^2 \right]^{\frac{1}{2}} \tag{5.5}$$

where $\bar{a}_x$, $\bar{a}_y$, and $\bar{a}_z$ are the 50-ms moving average vehicle accelerations and $\hat{a}_x$, $\hat{a}_y$, and $\hat{a}_z$ are the threshold accelerations ($\hat{a}_x = 12$ g, $\hat{a}_y = 9$ g, and $\hat{a}_z = 10$ g). Normally the maximum value of $ASI(t)$ is used to represent the single non-dimensional index value. An ASI of 1.0 corresponds to "light injury, if any", although a value of 1.4 is acceptable.

5.1.2.4 Theoretical Head Impact Velocity and Post-Impact Head Deceleration

The THIV and PHD are analogous to OIV and ORA, respectively, except the THIV and PHD utilize coupled equations of motion, including the vehicle's yaw rotation and the resultant impact velocity of the hypothetical occupant making contact with the flail space model and the corresponding resultant maximum post-impact acceleration of the longitudinal and lateral components. The THIV restricts the maximum allowable impact velocity to 30 ft/s (9.1 m/s). The PHD, which limits the maximum post-impact acceleration to below 20 g, was previously required in CEN EN 1317-2, however, as of the most recent 2010 edition, this criteria has been removed as a result of extensive empirical evidence showing it to be unreliable as an index (CEN 2010; Hubbell 2012). The PHD is still recommended to be determined by MASH, although not required. Using ASI and THIV together, CEN defines three impact severity levels, A, B and C, as seen in Table 5.2. Ascending letters correspond to increased injury potential; therefore, lower impact severity levels (i.e., A or B) are generally desired to ensure a lower risk of occupant injury.

Table 5.2: CEN EN 1317-2: impact severity levels

Impact Severity Level	Index Values		
A	ASI ≤ 1.0		
B	ASI ≤ 1.4	and	THIV ≤ 30 ft/s (9.1 m/s)
C	ASI ≤ 1.9		

5.2 Tractor-Trailer Impacts on Flexible Median Barriers

Combining the ISOL tractor-trailer FE model discussed in Section 3.4 as well as the three- and four-CMBs from Section 4.2, a total of eight impact scenarios were conducted on flat and sloped medians, with impacts from the front-side and backside of the barrier. Table 5.3 shows the simulation matrix of the impact scenarios for tractor-trailer impacts on flexible median barriers and summarizes the overall impact performance based on the vehicle behavior. The impact scenarios were labeled in sequential alphabetical order for ease of referencing scenario results throughout this dissertation. If the tractor-trailer was successfully redirected by the barrier and remained upright, the impact scenario was designated as redirected (R). If the tractor-trailer remained upright and in contact with the barrier throughout the impact scenario, it was designated as remained-in-contact (RIC).

Table 5.3: Tractor-trailer responses for flexible median barrier impacts

Barrier	Impact Side	Impact Outcome	
		Flat Median	Sloped Median
Three-CMB	Front-side	*a. R*	*e. R*
	Backside	*b. R*	*f. R*
Four-CMB	Front-side	*c. RIC*	*g. R*
	Backside	*d. R*	*h. R*

5.2.1 Tractor-Trailer Impact Response

The tractor-trailer impact scenarios against flexible median barriers resulted in mostly favorable outcomes. The flexibility of the three- and four-CMBs allowed for substantial deflection ensuring that the tractor-trailer had ample time to be redirected from its original trajectory. Table 5.4 shows the total interaction time between the tractor-trailer

and the CMBs. The interaction time for the flat median front-side four-CMB impact, which resulted in the tractor-trailer remaining in contact through the duration of the simulation, was calculated from the difference between the simulation end time and the impact time.

Table 5.4: Tractor-trailer to flexible median barrier impact interaction time

Barrier	Impact Side	Impact Interaction Time (s)	
		Flat Median	Sloped Median
Three-CMB	Front-side	4.11	4.10
	Backside	4.46	5.60
Four-CMB	Front-side	5.84*	4.25
	Backside	4.86	5.35

RIC case's interaction time calculated using the simulation end time.

Omitting the *RIC* scenario, the front-side impacts resulted in lower interaction times compared to the backside impacts; as well as the sloped median impacts having longer interaction times compared to their respective flat median impact counterpart of the same impact side. The cable's alterable height after disengaging from the J-bolts on the post allows the cables to be shifted and make more thorough engagement with the tractor-trailer. The cable engagement prevented all impact scenarios from penetrating through the barrier and resulted in large dynamic deflections, summarized in Table 5.5. In general, the longer the interaction time between the tractor-trailer and the CMB, the greater the maximum dynamic deflection. Figure 5.4 shows a sequence of instances throughout impacts on the flat median backside three-CMB impact (i.e., Case *b*) and sloped median front-side four-CMB (i.e., Case *g*).

a. Case *b*   b. Case *g*
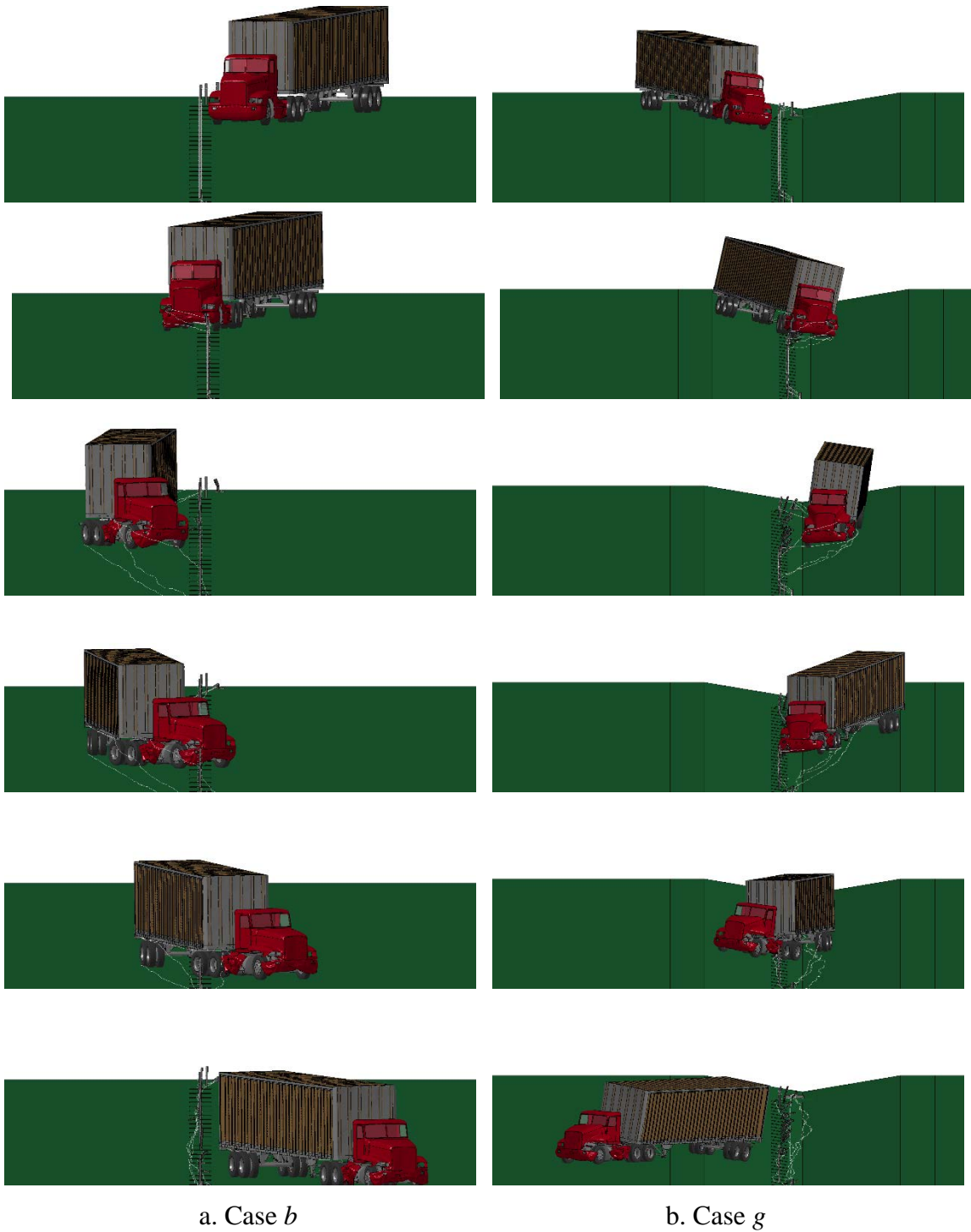
Figure 5.4: Front view sequences of tractor-trailer impacts on flexible median barriers

Table 5.5: Flexible median barrier maximum dynamic deflection

Barrier	Impact Side	Maximum Dynamic Deflection (ft (m))	
		Flat Median	Sloped Median
Three-CMB	Front-side	10.71 (3.27)	22.15 (6.75)
	Backside	16.46 (5.02)	25.78 (7.86)
Four-CMB	Front-side	16.52 (5.04)	21.74 (6.63)
	Backside	16.83 (5.13)	22.39 (6.83)

Again, using the flat median backside three-CMB impact (i.e., Case *b*) and sloped median front-side four-CMB impact (i.e., Case *g*) scenarios as examples, Figure 5.5 shows the instances when the CMBs in these impact cases experienced their respective maximum dynamic deflection. The tractor-trailers were hidden for ease of viewing the deformed CMBs. The rest of the maximum dynamic deflection figures for the other flexible median barrier impact scenarios (i.e., Cases *a-h*) are shown in APPENDIX A.
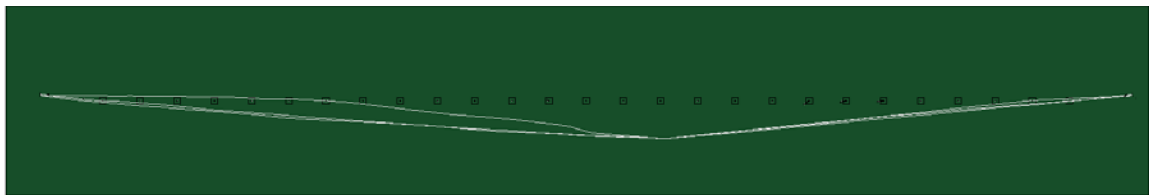
a. Case *b*: flat median three-CMB backside impact
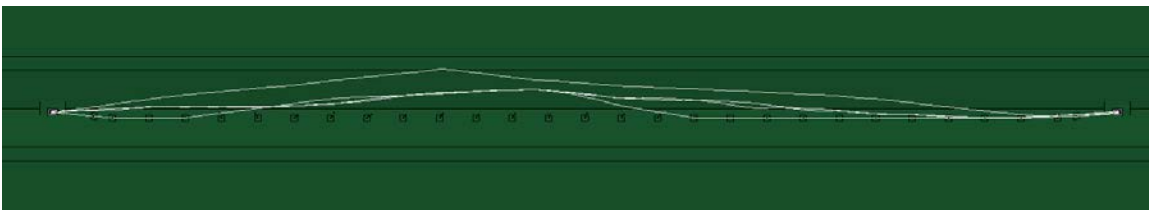
b. Case *g*: sloped median four-CMB front-side impact

Figure 5.5: Flexible median barrier maximum dynamic deflections from tractor-trailer impacts

For all of the tractor-trailer impacts on flexible median barrier, the length of the damaged sections of the barrier system spanned beyond the directly impacted barrier section listed in Table 5.6. The damaged region which includes components and/or hardware that would need to be repaired or replaced after an impact, typically extended the entire span of the CMB system with the cables being released from the J-bolts and posts, upstream and downstream, being deformed due to the severe deflection of the cables. The damage lengths listed in Table 5.6 refer to the longitudinal distance over which the tractor-trailer began and ended interaction with the CMB.

Table 5.6: Length of longitudinal damage for flexible median barrier impacts

Barrier	Impact Side	Length of Longitudinal Damage (ft (m))	
		Flat Median	Sloped Median
Three-CMB	Front-side	191.8 (58.5)	207.9 (63.4)
	Backside	223.9 (68.2)	304.9 (92.9)
Four-CMB	Front-side	363.1 (110.7)	225.5 (68.7)
	Backside	240.8 (73.4)	288.8 (88.0)

The exit angle is measured using the vehicle's last point of contact with the barrier. Typically, the exit angle for passenger vehicles and large trucks is measured between the longitudinal axis of the vehicle and the longitudinal barrier face. However, in the case of the tractor-trailer, due to the fifth-wheel/kingpin articulating connection that allows for yaw rotation, the exit angle would not be consistent between the tractor and trailer at the last point of contact of the trailer. As a point of reference, the tractor's last point of contact with the barrier transpired on average one second prior to the trailer's last point of contact with the barrier. Therefore, the exit angles for both the tractor and trailer are reported separately

in Table 5.7. Exit angles for the impact scenario that resulted in a *RIC* outcome were not applicable (n/a). Based solely on the exit angles, the post-impact behavior cannot be determined. The impact trajectories were assessed by overlaying the tractor-trailer path and tracing the tire tracks in order to utilize the MASH exit box criteria to categorize the post-impact trajectories. Figure 5.6a-h shows the tractor-trailer post-impact trajectories of flexible median barrier impacts (i.e., Cases *a-h*), with the MASH exit box placed at the last point of contact with the initial barrier face for the impact scenarios that were redirected. As seen from Figure 5.6a-h, of the impact scenarios in which the exit box criteria were used to assess the post-impact trajectory, two of the seven cases (i.e., Cases *d* and *h*) failed the exit box criteria due to large exit angles and continuous yaw rotation, respectively. Table 5.8 summarizes the exit box criteria performance for the flexible median barrier impacts.

Table 5.7: Tractor and trailer exit angles for flexible median barrier impacts

Barrier	Impact Side	Tractor and Trailer Exit Angles (°)	
		Flat Median	Sloped Median
Three-CMB	Front-side	4.29/4.69	43.7/10.5
	Backside	25.9/16.1	7.9/0.2
Four-CMB	Front-side	n/a	44.1/16.4
	Backside	49.2/18.4	9.3/5.0

Table 5.8: Tractor-trailer exit box criteria for flexible median barrier impacts

Barrier	Impact Side	Tractor-trailer Exit Box Criteria	
		Flat Median	Sloped Median
Three-CMB	Front-side	Pass	Pass
	Backside	Pass	Pass
Four-CMB	Front-side	n/a	Pass
	Backside	Fail	Fail

a. Case *a*: flat median three-CMB front-side impact
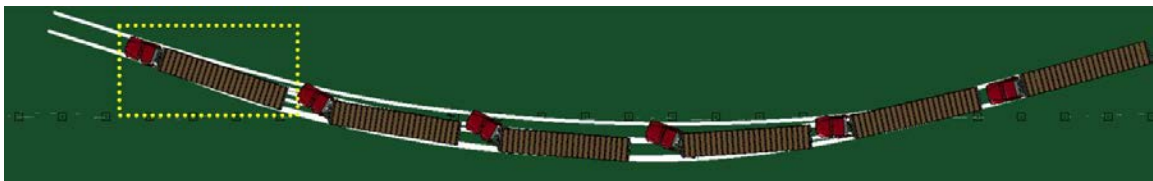
b. Case *b*: flat median three-CMB backside impact
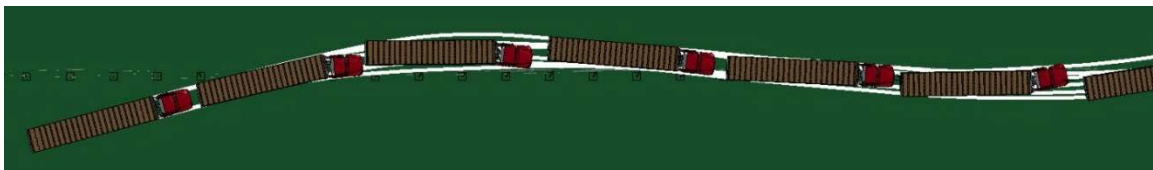
c. Case *c*: flat median four-CMB front-side impact
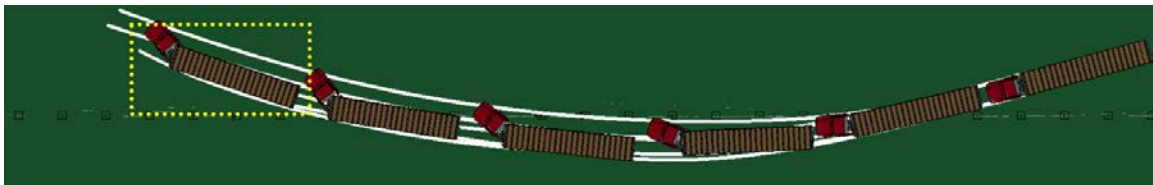
d. Case *d*: flat median four-CMB backside impact

Figure 5.6: Tractor-trailer post-impact trajectories of flexible median barriers
with MASH exit boxes placed (when applicable)

e. Case *e*: sloped median three-CMB front-side impact
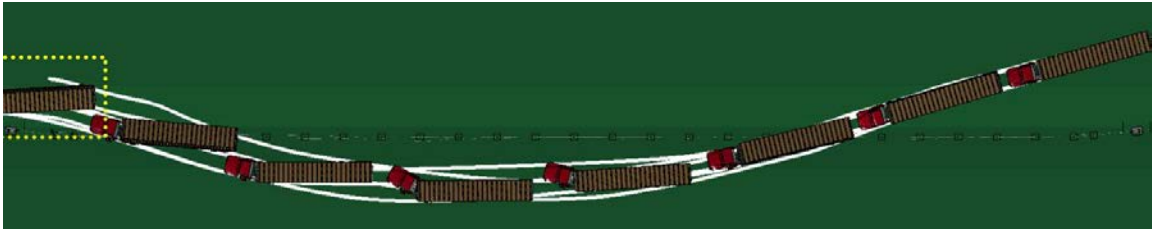
f. Case *f*: sloped median three-CMB backside impact
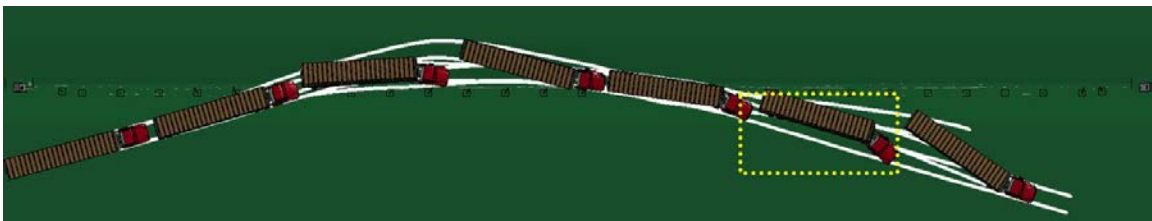
g. Case *g*: sloped median four-CMB front-side impact
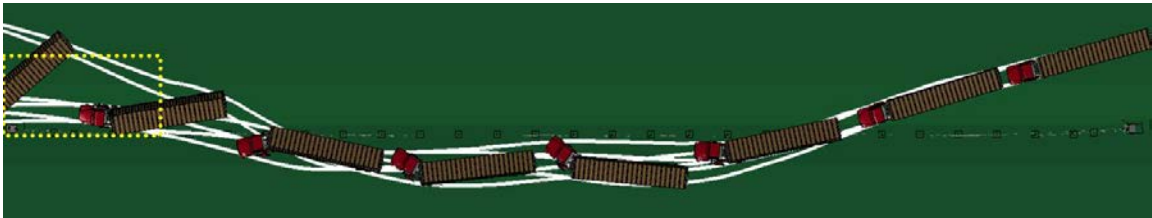
h. Case *h*: sloped median four-CMB backside impact

Figure 5.6 (continued): Tractor-trailer post-impact trajectories of flexible median barriers with MASH exit boxes placed (when applicable)
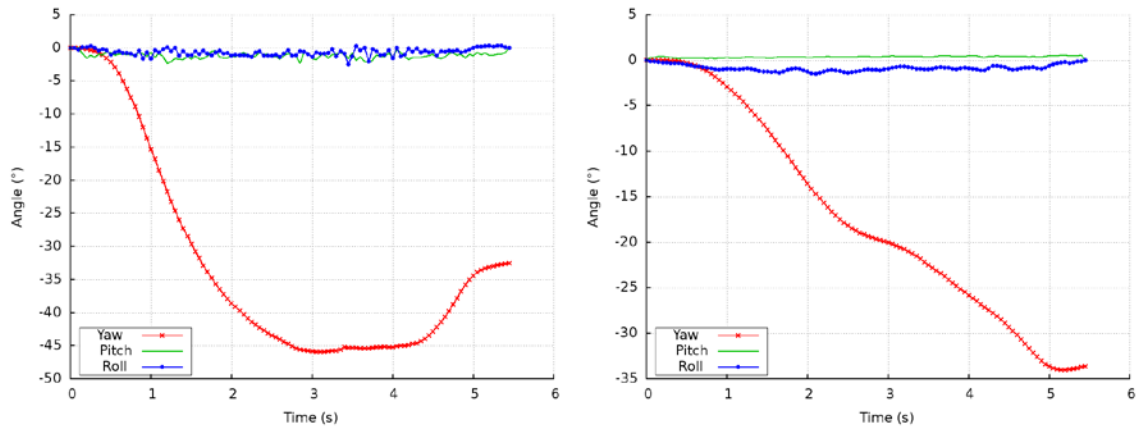
a. Tractor cabin CG

b. Trailer tandem axle

Figure 5.7: Case *b*: yaw, pitch, and roll angles for the flat median three-CMB backside impact
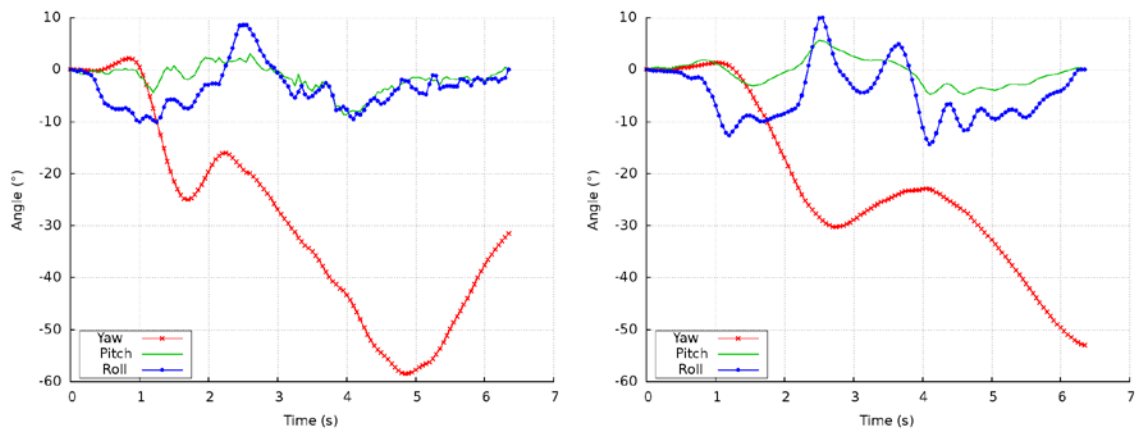
a. Tractor cabin CG

b. Trailer tandem axle

Figure 5.8: Case *g*: yaw, pitch, and roll angles for the sloped median four-CMB front-side impact

To assess the tractor-trailer's stability throughout the impact scenarios, the yaw, pitch, and roll angles were evaluated. Figure 5.7 and Figure 5.8 show the yaw, pitch, and roll angles of both the tractor CG and the trailer tandem axle of Case *b* and *g*, respectively. The flat median impact from Case *b* in Figure 5.7 shows that pitch and roll angle rotations

are negligible compared to the yaw angle rotations, whereas, in Case *g* (Figure 5.8) the pitch and roll angle rotations are more significant due to the impact occurring at a sloped median. The other yaw, pitch, and roll angle figures for the remaining flexible median barrier impact scenarios (i.e., Cases *a-h*) are shown in APPENDIX B. The maximum yaw, pitch, and roll angles experienced by the tractor and trailer are tabulated in Table 5.9 and Table 5.10, respectively. For all flexible median barrier impacts, the maximum pitch and roll angles were below ±10° and ±17°, respectively.

Table 5.9: Tractor maximum rotational angles for flexible median barrier impacts

Barrier	Impact Side	Tractor Maximum Rotational Angles (°)					
		Flat Median			Sloped Median		
		Yaw	Pitch	Roll	Yaw	Pitch	Roll
Three-CMB	Front-side	-25.8	-3.8	-10.5	-57.1	-9.7	-9.5
	Backside	-45.9	-2.6	-2.6	-43.9	-5.9	-11.0
Four-CMB	Front-side	-24.2	2.9	-3.4	-58.5	-8.7	-10.4
	Backside	-70.8	-2.7	-2.5	-57.2	-6.0	-15.4

Table 5.10: Trailer maximum rotational angles for flexible median barrier impacts

Barrier	Impact Side	Trailer Maximum Rotational Angles (°)					
		Flat Median			Sloped Median		
		Yaw	Pitch	Roll	Yaw	Pitch	Roll
Three-CMB	Front-side	-23.8	-2.8	-16.1	-56.8	5.3	-13.5
	Backside	-34.0	0.6	-1.5	-19.6	3.9	-14.6
Four-CMB	Front-side	-20.8	0.9	-2.2	-52.9	5.8	-14.5
	Backside	-37.8	0.6	-1.9	35.1	5.7	-21.3

The last tractor-trailer post-impact response criteria used to assess the flexible median barrier impacts was to determine the post-impact residual resultant velocity at the

end of the impact scenarios. The residual velocity of the tractor-trailer after being redirected by the median barriers can be used as an indicator of the potential for a secondary collision if the vehicle had a large exit angle or continuously growing yaw rotation after disengaging from the barrier. Table 5.11 shows the residual velocity of the tractor trailer after impacting the three- and four-CMBs.

Table 5.11: Tractor-trailer residual velocity for flexible median barrier impacts

Barrier	Impact Side	Post-Impact Residual Velocity (mph (km/h))	
		Flat Median	Sloped Median
Three-CMB	Front-side	41.4 (66.9)	33.8 (54.4)
	Backside	38.0 (61.2)	35.5 (57.2)
Four-CMB	Front-side	40.9 (65.9)	34.2 (55.0)
	Backside	28.6 (46.0)	32.5 (52.3)

Combining the post-impact trajectory, exit angle, yaw rotation, and residual velocity, it can be concluded that Cases *d* and *h* have a high probability of reentering the roadway and possibly causing a secondary collision with other vehicles on the road. Some impact cases, such as Cases *b*, *e*, and *g*, may have the possibility of causing a secondary collision, even though the exit box criteria was met, due to continually growing yaw rotations during the post-impact trajectory.

5.2.2 Occupant Risk Evaluation

Using the tractor cabin CG accelerations profiles, the occupant safety risk was evaluated. Table 5.12 shows the maximum accelerations at the tractor cabin CG in the x, y, and z directions during the tractor-trailer impact scenarios on flexible median barriers. Figure 5.9 and Figure 5.10 show the time histories of the x-, y-, and z-axis accelerations at the tractor cabin CG for Cases *b* and *g*, respectively. The remaining acceleration time histories of the tractor cabin CG during the flexible median barrier impact scenarios (i.e., Cases *a-h*) are located in APPENDIX C.

Table 5.12: Tractor cabin CG maximum accelerations for flexible median barrier impacts

Barrier	Impact Side	Maximum x-, y-, and z-axis accelerations (*g*)					
		Flat Median			Sloped Median		
		x	y	z	x	y	z
Three-CMB	Front-side	2.8	-5.2	16.5	3.3	-3.7	12.8
	Backside	2.8	3.9	-12.4	-2.2	3.5	9.5
Four-CMB	Front-side	2.7	8.6	-17.4	2.8	-3.7	-10.3
	Backside	-3.5	-5.1	-12.9	-4.6	-5.5	16.6

a. x-axis   b. y-axis   c. z-axis
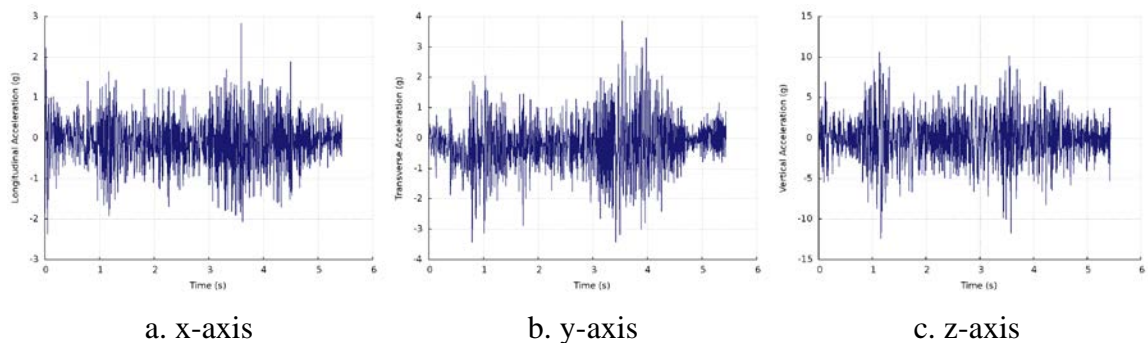
Figure 5.9: Case *b*: time histories of the tractor cabin CG x-, y-, and z-axis accelerations for the flat median three-CMB backside impact

a. x-axis   b. y-axis   c. z-axis
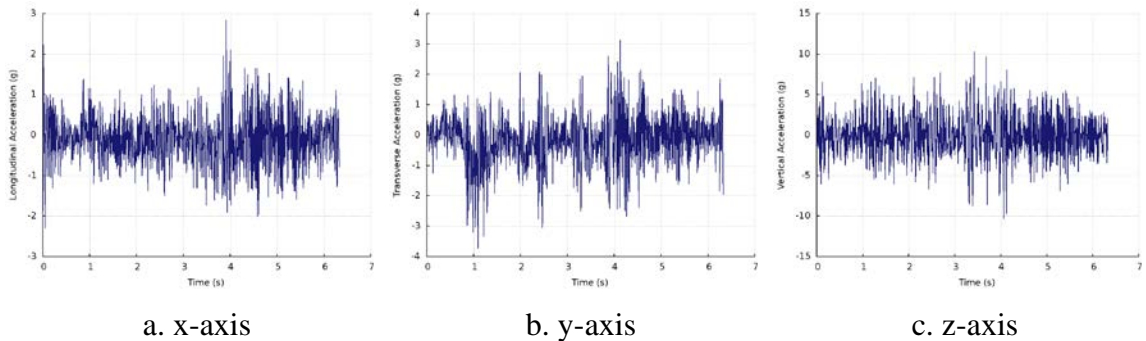
Figure 5.10: Case *g*: time histories of the tractor cabin CG x-, y-, and z-axis
accelerations for the sloped median four-CMB front-side impact

The tractor cabin CG acceleration profiles were used to evaluate the OIV and
corresponding ORA in the longitudinal and lateral directions. Table 5.13 compiles the
calculated OIV_x and OIV_y for the tractor cabin CG during the flexible median barrier
impacts. Table 5.14 shows the corresponding ORA_x and ORA_y after the respective OIV_x
and OIV_y was determined. All OIV and ORA values were far below the allowable threshold
values (i.e., OIV < 30 ft/s (9.1 m/s) and ORA < 15 *g*), signifying a low likelihood of
occupant injury risk.

Table 5.13: Tractor cabin CG OIV_x and OIV_y for flexible median barrier impacts

Barrier	Impact Side	OIV (ft/s (m/s))			
		Flat Median		Sloped Median	
		OIV_x	OIV_y	OIV_x	OIV_y
Three-CMB	Front-side	-4.5 (-1.37)	7.15 (2.18)	-3.4 (-1.04)	6.9 (2.10)
	Backside	-2.3 (-0.70)	7.78 (2.37)	-1.67 (-0.51)	-4.27 (-1.30)
Four-CMB	Front-side	-3.15 (-0.96)	7.58 (2.31)	-3.58 (-1.09)	8.27 (2.52)
	Backside	-2.62 (-0.80)	7.55 (2.30)	-3.44 (-1.05)	-4.86 (-1.48)

Table 5.14: Tractor cabin CG ORA_x and ORA_y for flexible median barrier impacts

Barrier	Impact Side	ORA (*g*)			
		Flat Median		Sloped Median	
		ORA_x	ORA_y	ORA_x	ORA_y
Three-CMB	Front-side	2.47	1.73	-1.08	-0.36
	Backside	-2.59	2.04	-2.01	1.18
Four-CMB	Front-side	1.30	0.87	-0.10	1.91
	Backside	-2.85	2.78	0.58	1.93

Using the time histories of the x-, y-, and z-axis accelerations of the tractor cabin CG, the ASIs were evaluated. Although the ASI is typically represented as a singular maximum value, the ASI can be investigated throughout the impact scenario. Figure 5.11 shows the ASI time histories for Cases *b* and *g* and Table 5.15 shows the ASIs for the tractor cabin CG for the flexible median barrier impact scenarios. The ASI time histories for the remaining cases are shown in APPENDIX D. For all flexible median barrier impacts, the tractor cabin experienced moderately low ASI values, with no impact scenarios approaching the allowable limit of 1.0, which also indicates a low risk of occupant injury.

a. Case *b*   b. Case *g*
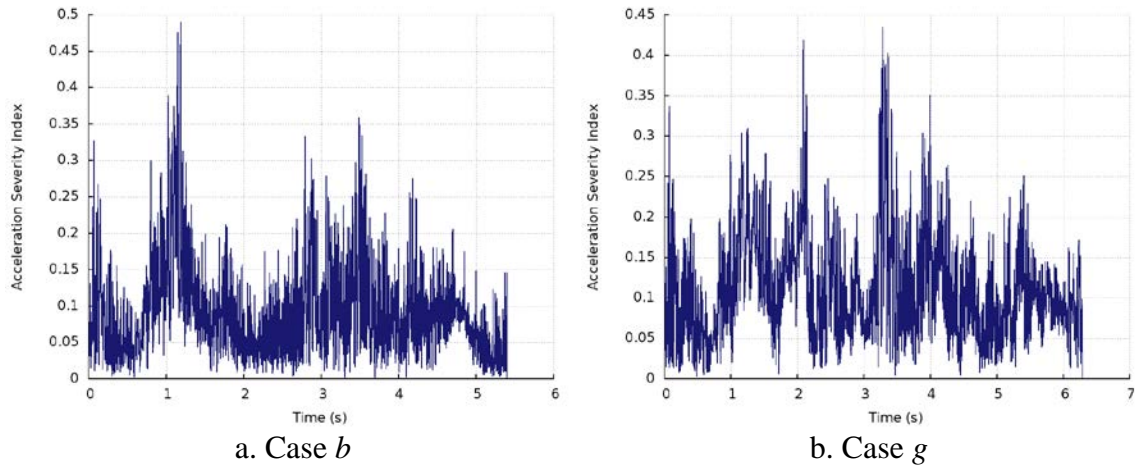
Figure 5.11: ASI profiles of tractor-trailer impacts on flexible median barriers

Table 5.15: Tractor cabin CG ASI for flexible median barrier impacts

Barrier	Impact Side	ASI	
		Flat Median	Sloped Median
Three-CMB	Front-side	0.63	0.49
	Backside	0.49	0.35
Four-CMB	Front-side	0.58	0.43
	Backside	0.54	0.49

The remaining occupant risk evaluation of the tractor-trailer impacts on flexible median barriers used the CEN's THIV and the obsolete PHD, in Table 5.16 and Table 5.17, respectively. All impact scenarios had THIV and PHD values well below the threshold limits, THIV < 30 ft/s (9.1 m/s) and PHD < 20 *g*, which also signifies low occupant risk potential.

Table 5.16: Tractor cabin CG THIV for flexible median barrier impacts

Barrier	Impact Side	THIV (ft/s (m/s))	
		Flat Median	Sloped Median
Three-CMB	Front-side	7.12 (2.17)	1.02 (0.31)
	Backside	6.2 (1.89)	1.02 (0.31)
Four-CMB	Front-side	7.48 (2.28)	1.18 (0.36)
	Backside	7.71 (2.35)	4.85 (1.48)

Table 5.17: Tractor cabin CG PHD for flexible median barrier impacts

Barrier	Impact Side	PHD (g)	
		Flat Median	Sloped Median
Three-CMB	Front-side	5.50	4.42
	Backside	5.96	3.91
Four-CMB	Front-side	5.87	3.84
	Backside	5.24	7.05

The CEN impact severity level criteria that uses the ASI and THIV to classify impact scenarios into groups based on the occupant risk severity. Consistent with all previously evaluated occupant risk criteria, all tractor-trailer impact scenarios against flexible median barriers received an impact severity level of A (i.e., lowest occupant risk)., It may be concluded by assessing all occupant risk evaluation criteria that, due to the size and weight of the tractor-trailer combined with the flexible median barrier's ability to absorb impact energy through considerable deflection, both CMBs resulted in safe conditions for an occupant in a tractor-trailer during MASH TL-5 impacts.

Table 5.18: CEN impact severity for tractor-trailer impacts on flexible median barriers

Barrier	Impact Side	CEN Impact Severity Level	
		Flat Median	Sloped Median
Three-CMB	Front-side	*A*	*A*
	Backside	*A*	*A*
Four-CMB	Front-side	*A*	*A*
	Backside	*A*	*A*

5.3 Tractor-Trailer Impacts on Semi-Rigid Median Barriers

Combining the ISOL tractor-trailer FE model discussed in Section 3.4 as well as the double-faced W- and Thrie-beam guardrails from Section 4.3, a total of nine impact scenarios were conducted on flat and sloped medians involving impacts from the front-side and backside of the barrier. Due to the symmetry of the front and back side of the double-faced semi-rigid median barrier models, the front-side and backside impact cases were assumed to be identical and therefore eliminated the need to conduct the flat backside impact cases for each of the guardrail models. Table 5.19 shows the simulation matrix of the impact scenarios for tractor-trailer impacts on double-faced semi-rigid median barriers and summarizes the overall impact performance based on the vehicle behavior. The impact scenario alphabetical designation is continued from Table 5.3. In addition to the *R* and *RIC* simulation outcomes, if the tractor-trailer fails to remain upright throughout the impact scenario, it was designated as a rollover (*RO*).

Table 5.19: Tractor-trailer responses for semi-rigid median barrier impacts

Barrier	Impact Side	Impact Outcomes	
		Flat Median	Sloped Median
W-beam Guardrail	Front-side	*i. R*	*l. RO*
	Backside	-	*m. RO*
Wood-blockout Thrie-beam Guardrail	Front-side	*j. R*	*n. RO*
	Backside	-	*o. RO*
Steel-blockout Thrie-beam Guardrail	Front-side	*k. RO*	*p. RO*
	Backside	-	*q. RO*

5.3.1 Tractor-Trailer Impact Response

The tractor-trailer impact scenarios against semi-rigid median barriers resulted in primarily simulation outcomes where the tractor-trailer rolled onto the barrier (*RO*). This post-impact behavior primarily contributed to a combination of the semi-flexible deflection capabilities, low guardrail height, and the median terrain. Table 5.20 shows the interaction time between the tractor-trailer and the various semi-rigid median barriers used to evaluate the impact performance. Impact Cases *k-q*, which resulted in a *RO* outcome, used the difference between the simulation end time and the impact time to determine the interaction time. Due to the less compliant response of the semi-rigid guardrails compared to the flexible median barriers, the interaction times were, on average, less than half of the duration of the flexible median barrier impact scenarios.

Table 5.20: Tractor-trailer to semi-rigid median barrier impact interaction time

Barrier	Impact Side	Impact Interaction Time (s)	
		Flat Median	Sloped Median
W-beam Guardrail	Front-side	2.22	2.18*
	Backside	-	1.56*
Wood-blockout Thrie-beam Guardrail	Front-side	2.56	1.76*
	Backside	-	2.16*
Steel-blockout Thrie-beam Guardrail	Front-side	1.75*	2.09*
	Backside	-	1.61*

RO impact case's interaction time calculated using simulation end time.

The front-side impact Cases *i* and *j*, which were redirected by W-beam guardrail and wood-blockout Thrie-beam guardrails, respectively, resulted in the longest interaction times of all semi-rigid median barrier impact scenarios. The wood blockout used on the W- and Thrie-beam guardrails is a less rigid material and allowed the guardrails to deflect further compared to the stiffer steel blockout. Figure 5.12 shows front view sequences of the flat median wood-blockout Thrie-beam guardrail front-side impact (i.e., Case *j*) and the sloped median W-beam guardrail backside impact (i.e., Case *m*) throughout the impact scenarios.

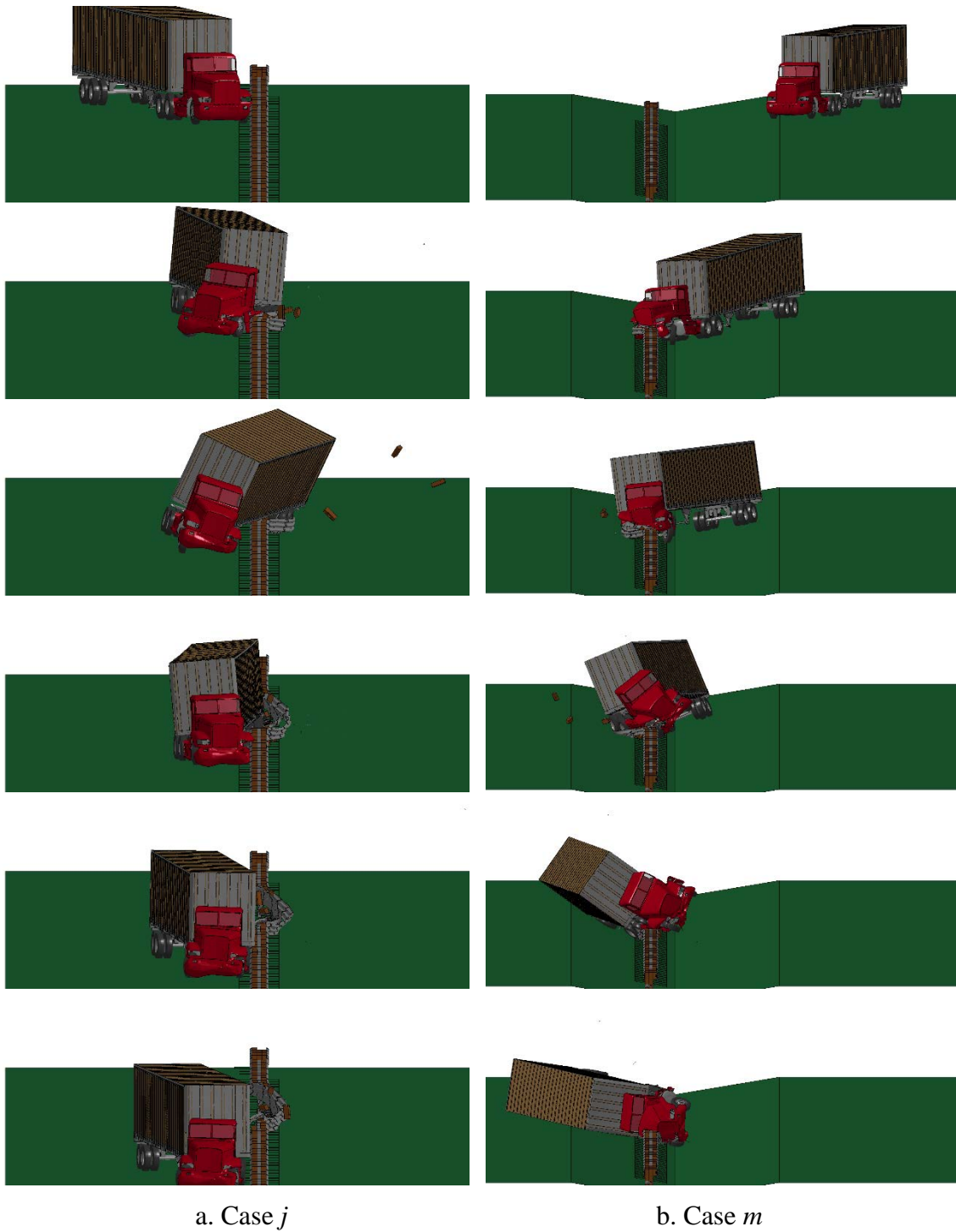a. Case *j*   b. Case *m*

Figure 5.12: Front view sequences of tractor-trailer impacts on semi-rigid median barriers

Table 5.21 shows the maximum dynamic deflections experienced during the tractor-trailer impact scenarios on the semi-rigid median barriers. The redirected front-side impact Cases *i* and *j* also resulted in the largest maximum dynamic deflections for their respective semi-rigid median barrier. Figure 5.13 shows the time instance that the maximum dynamic deflection occurred in impact Cases *j* and *m*. A complete set of maximum dynamic deflection for all impact cases is shown in APPENDIX A.

Table 5.21: Semi-rigid median barrier maximum dynamic deflection

Barrier	Impact Side	Maximum Dynamic Deflection (ft (m))	
		Flat Median	Sloped Median
W-beam Guardrail	Front-side	8.62 (2.63)	8.56 (2.61)
	Backside	-	7.51 (2.29)
Wood-blockout Thrie-beam Guardrail	Front-side	6.29 (1.92)	4.99 (1.52)
	Backside	-	5.17 (1.57)
Steel-blockout Thrie-beam Guardrail	Front-side	3.91 (1.19)	3.70 (1.13)
	Backside	-	2.64 (0.80)

a. Case *j*: flat median wood-blockout Thrie-beam guardrail front-side impact

b. Case *m*: sloped median W-beam guardrail backside impact

Figure 5.13: Semi-rigid median barrier maximum dynamic deflections from tractor-trailer impacts

The extent of the damage that the semi-rigid barrier systems experienced in the tractor-trailer impacts was localized to the impact location and did not extend longitudinally beyond the impacted area. The reduced longitudinal damage length compared to the flexible median barrier impacts is beneficial in reducing the length of barrier that needs to be repaired or replaced. Smaller damaged guardrail sections are beneficial by reducing the length of guardrail that would be potentially inadequate in containing and/or redirecting a subsequent impact. The impact scenarios with *RO* (i.e., Cases *k-q*) resulted in longer damaged barrier sections due to the tractor-trailer landing on top of the barrier, as seen in Table 5.22

Table 5.22: Length of longitudinal damage for semi-rigid median barrier impacts

Barrier	Impact Side	Length of Longitudinal Damage (ft (m))	
		Flat Median	Sloped Median
W-beam Guardrail	Front-side	118.9 (36.2)	143.6 (43.8)
	Backside	-	125.0 (38.1)
Wood-blockout Thrie-beam Guardrail	Front-side	131.1 (39.9)	124.9 (38.0)
	Backside	-	150.0 (45.7)
Steel-blockout Thrie-beam Guardrail	Front-side	112.5 (34.3)	175.0 (53.3)
	Backside	-	137.5 (41.9)

Only two impact scenarios (Cases *i* and *j*) remained upright throughout the entire impact durations; therefore, they were the only impact cases in which exit angles could be determined and the exit box criteria could be used to evaluate the post-impact trajectory. Table 5.23 shows the exit angles of the tractor and trailer for the *R* impact cases and Table 5.24 shows that both *R* impact cases passed the exit box criteria. Figure 5.14a-i shows the tractor-trailer post-impact trajectories of semi-rigid median barrier impacts (i.e., Cases *i-*

q), with the MASH exit box placed at the last point of contact with the initial barrier face for the impact cases that were redirected.

Table 5.23: Tractor and trailer exit angles for semi-rigid median barrier impacts

Barrier	Impact Side	Tractor and Trailer Exit Angles (°)	
		Flat Median	Sloped Median
W-beam Guardrail	Front-side	7.5/6.6	n/a
	Backside	-	n/a
Wood-blockout Thrie-beam Guardrail	Front-side	2.5/2.7	n/a
	Backside	-	n/a
Steel-blockout Thrie-beam Guardrail	Front-side	n/a	n/a
	Backside	-	n/a

Table 5.24: Tractor-trailer exit box criteria for semi-rigid median barrier impacts

Barrier	Impact Side	Tractor-trailer Exit Box Criteria	
		Flat Median	Sloped Median
W-beam Guardrail	Front-side	Pass	n/a
	Backside	-	n/a
Wood-blockout Thrie-beam Guardrail	Front-side	Pass	n/a
	Backside	-	n/a
Steel-blockout Thrie-beam Guardrail	Front-side	n/a	n/a
	Backside	-	n/a
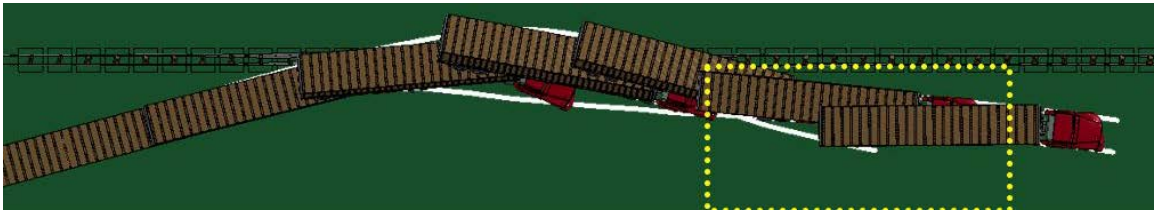
a. Case *i*: flat median W-beam guardrail front-side impact

b. Case *j*: flat median wood-blockout Thrie-beam guardrail front-side impact
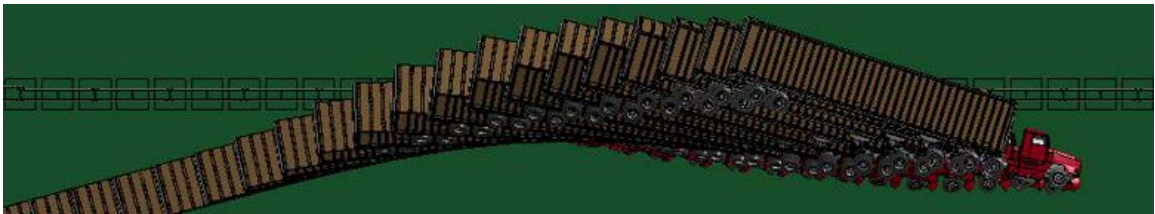
c. Case *k*: flat median steel-blockout Thrie-beam guardrail front-side impact
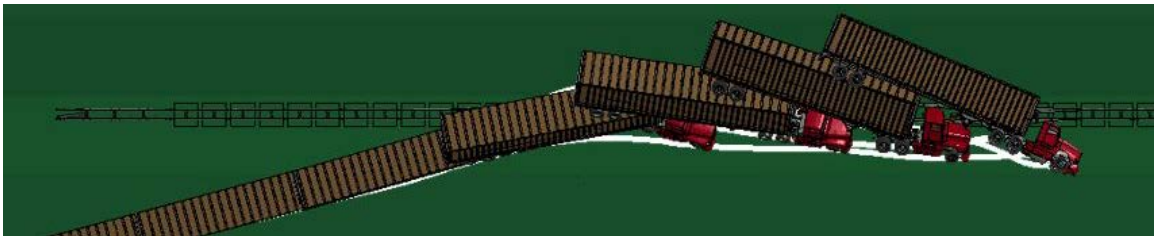
d. Case *l*: sloped median W-beam guardrail front-side impact

e. Case *m*: sloped median W-beam guardrail backside impact

Figure 5.14: Tractor-trailer post-impact trajectories of semi-rigid median barriers with MASH exit boxes placed (when applicable)
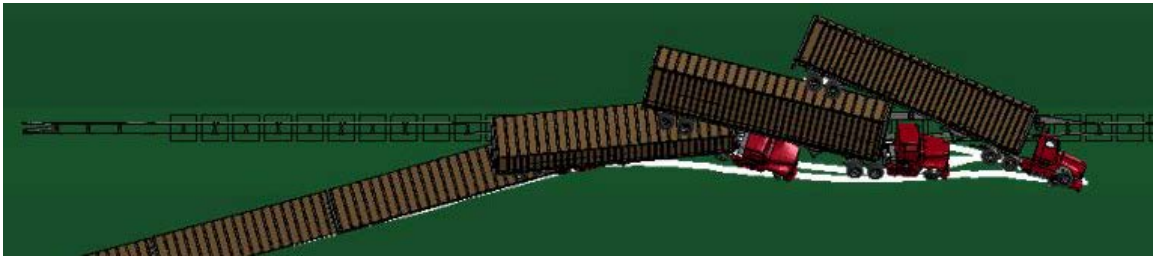
f. Case *n*: sloped median wood-blockout Thrie-beam guardrail front-side impact

g. Case *o*: sloped median wood-blockout Thrie-beam guardrail backside impact

h. Case *p*: sloped median steel-blockout Thrie-beam guardrail front-side impact

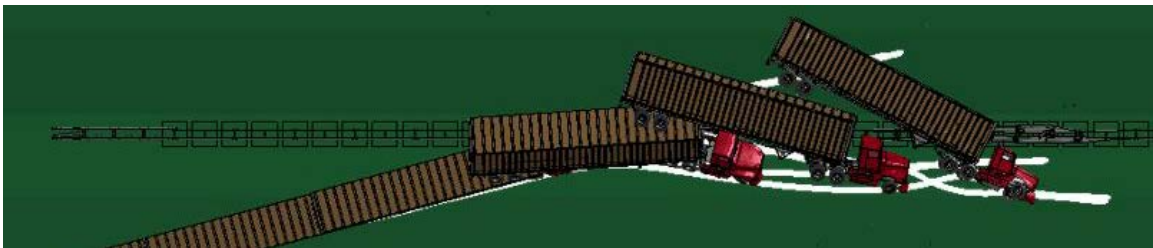i. Case *q*: sloped median steel-blockout Thrie-beam guardrail backside impact

Figure 5.14 (continued): Tractor-trailer post-impact trajectories of semi-rigid median barriers with MASH exit boxes placed (when applicable)

The two impact scenarios that were successfully redirected from the semi-rigid median barrier cases had both tractor and trailer pitch and roll angles of less than ±6° and

±27°, respectively. The impact scenarios that experienced a quarter-turn rollover can be concluded from the roll angles in excess of 80°. Typically, once an impacting vehicle's roll angle exceeds 45°, a rollover of at least a quarter-turn is inevitable. In terms of guardrail performance, MASH states that, although it's preferable for all vehicle to remain upright throughout redirective impact scenarios, heavy vehicles, such as tractor-trailers, are not required to remain upright and may undergo a quarter-turn rollover. This outcome may increase the possibility of occupant injury risk, which will be assessed in the following section. However, in terms of guardrail performance, the semi-rigid median barrier systems were able to prevent the tractor-trailer from overriding the guardrail and entering oncoming traffic lanes. Figure 5.15 and Figure 5.16 show the yaw, pitch, and roll angles of the flat median wood-blockout Thrie-beam guardrail front-side impact (i.e., Case *j*) and the sloped median W-beam guardrail backside impact (i.e., Case *m*) throughout the impact scenarios, respectively.

Table 5.25: Tractor maximum rotational angles for semi-rigid median barrier impacts

Barrier	Impact Side	Tractor Maximum Rotational Angles (°)					
		Flat Median			Sloped Median		
		Yaw	Pitch	Roll	Yaw	Pitch	Roll
W-beam Guardrail	Front-side	-40.7	-4.21	-10.9	-37.8	-15.4	-105
	Backside	-			-37.3	-17.4	-84.5
Wood-blockout Thrie-beam Guardrail	Front-side	-33.8	-4.4	-20.8	-33.6	-15.0	-95.2
	Backside	-			-34.6	-9.5	-98.2
Steel-blockout Thrie-beam Guardrail	Front-side	-31.2	-14.6	-96.5	-33.2	-17.0	-108
	Backside	-			-20.7	-8.7	-90.4

Table 5.26: Trailer maximum rotational angles for semi-rigid median barrier impacts

Barrier	Impact Side	Trailer Maximum Rotational Angles (°)					
		Flat Median			Sloped Median		
		Yaw	Pitch	Roll	Yaw	Pitch	Roll
W-beam Guardrail	Front-side	-30.3	-2.4	-14.5	-26.4	-15.4	-91.6
	Backside	-			-18.6	-12.9	-78.8
Wood-blockout Thrie-beam Guardrail	Front-side	-26.2	-5.3	-26.9	-25.3	-17.0	-85.5
	Backside	-			-30.7	-15.7	-94.1
Steel-blockout Thrie-beam Guardrail	Front-side	-23.7	-11.0	-89.4	-36.6	-16.0	-99.1
	Backside	-			-22.5	-13.4	-90.8
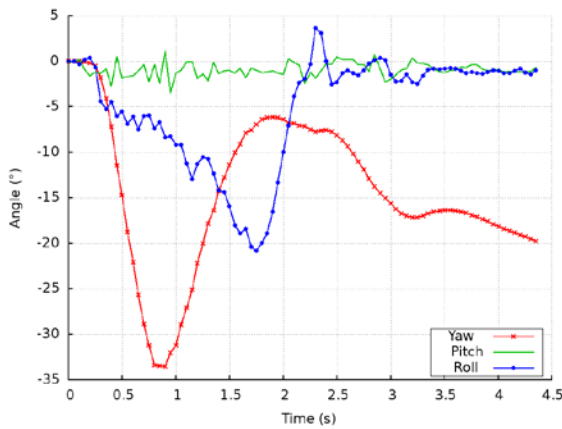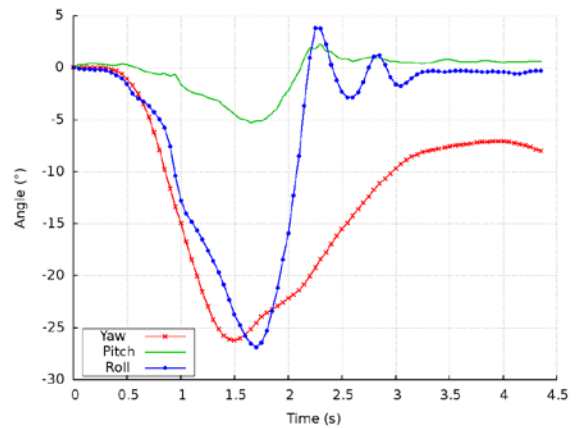
a. Tractor cabin CG   b. Trailer tandem axle

Figure 5.15: Case *j*: yaw, pitch, and roll angles for the flat median W-beam guardrail front-side impact

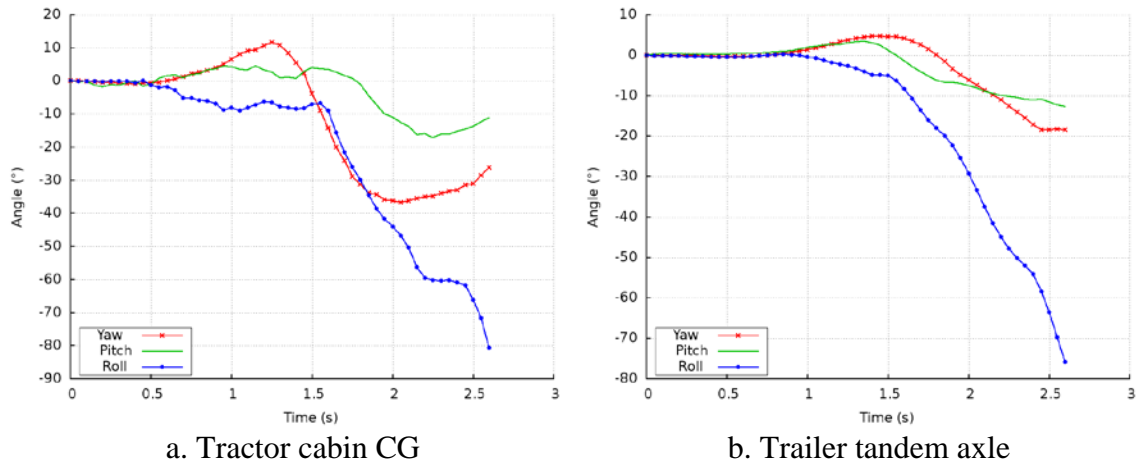a. Tractor cabin CG   b. Trailer tandem axle

Figure 5.16: Case *m*: yaw, pitch, and roll angles for the sloped median W-beam guardrail backside impact

Table 5.27 shows the post-impact residual velocities of the tractor-trailer impacts against the semi-rigid median barrier systems. The redirected impact scenarios from the flat median semi-rigid barrier impact cases had lower residual velocities compared to the flat median flexible barrier impacts. These reduced post-impact velocities, combined with low exit angled post-impact trajectories of Cases *i* and *j* indicate a low probability of reentering the travel lane and causing a secondary collision. The residual velocity of the *RO* impact cases is typically not of grave concern for causing a secondary collision due to the immense frictional force applied to the entire side of the tractor-trailer slowing the vehicle to rest.

Table 5.27: Tractor-trailer residual velocity for semi-rigid median barrier impacts

Barrier	Impact Side	Post-Impact Residual Velocity (mph (km/h))	
		Flat Median	Sloped Median
W-beam Guardrail	Front-side	35.5 (57.1)	34.2 (55.0)
	Backside	-	38.2 (61.5)
Wood-blockout Thrie-beam Guardrail	Front-side	33.2 (53.5)	37.9 (61.0)
	Backside	-	34.8 (56.0)
Steel-blockout Thrie-beam Guardrail	Front-side	37.3 (60.0)	34.6 (55.7)
	Backside	-	37.3 (60.0)

5.3.2 Occupant Risk Evaluation

Using the tractor cabin CG accelerations profiles, the occupant safety risk was evaluated for the semi-rigid median barrier impact scenarios. Table 5.28 shows the maximum accelerations, at the tractor cabin CG, in the x, y, and z directions during the tractor-trailer impact scenarios on semi-rigid median barriers. Figure 5.17 and Figure 5.18 show the time histories of the x-, y-, and z-axis accelerations at the tractor cabin CG for Cases *j* and *m*, respectively. The remaining acceleration time histories of the tractor cabin CG during the semi-rigid median barrier impact scenarios (i.e., Cases *i-q*) are located in APPENDIX C.

Table 5.28: Tractor cabin CG maximum accelerations for semi-rigid median barrier impacts

Barrier	Impact Side	Maximum x-, y-, and z-axis accelerations (*g*)					
		Flat Median			Sloped Median		
		x	y	z	x	y	z
W-beam Guardrail	Front-side	5.1	8.6	13.5	-4.7	14.8	21.2
	Backside	-	-	-	-5.1	6.3	9.0
Wood-blockout Thrie-beam Guardrail	Front-side	-5.4	7.9	-26.0	-6.2	18.8	-19.1
	Backside	-	-	-	5.6	-8.9	19.1
Steel-blockout Thrie-beam Guardrail	Front-side	-3.6	-10.3	-20.6	-7.2	-10.0	-17.3
	Backside	-	-	-	-6.1	-10.3	-23.2

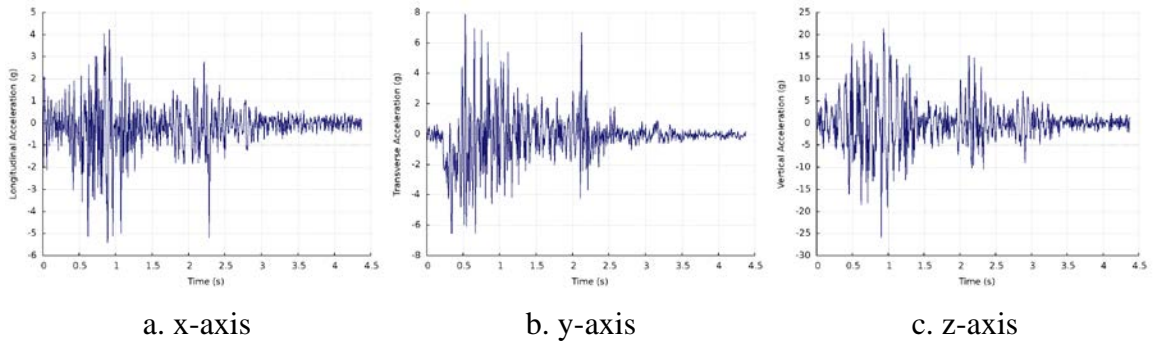a. x-axis   b. y-axis   c. z-axis

Figure 5.17: Case *j*: time histories of the tractor cabin CG x-, y-, and z-axis accelerations for the flat median wood-blockout Thrie-beam guardrail front-side impact

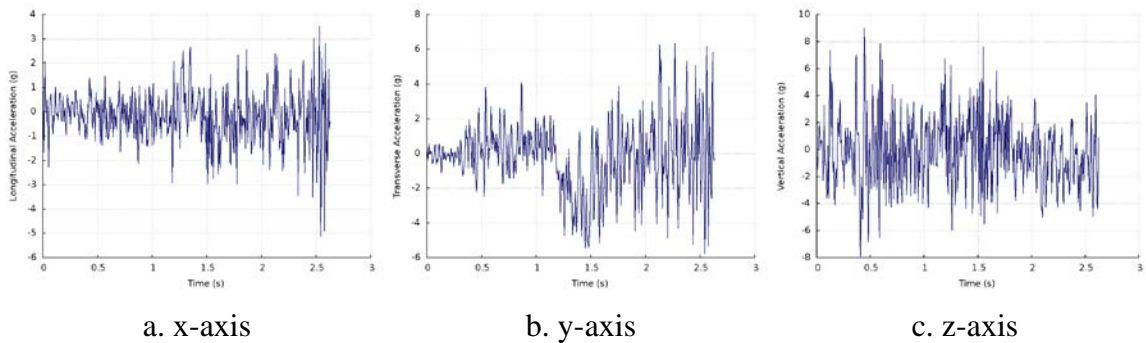a. x-axis   b. y-axis   c. z-axis

Figure 5.18: Case *m*: time histories of the tractor cabin CG x-, y-, and z-axis accelerations for the sloped median W-beam guardrail backside impact

The tractor cabin CG acceleration profiles were used to evaluate the OIV and corresponding ORA in the longitudinal and lateral directions. A potential limitation of the OIV and ORA criteria, as well as the THIV and PHD, is the exclusion of the vertical acceleration component. The exclusion of the vertical acceleration component was based on the requirement of passenger vehicles remaining upright throughout impact scenarios. None the less, the aforementioned evaluation criteria were evaluated and tabulated. Table 5.29 shows the calculated OIV_x and OIV_y for the tractor cabin CG during the semi-rigid median barrier impacts. Table 5.30 shows the corresponding ORA_x and ORA_y after the respective OIV_x and OIV_y was determined. All OIV and ORA values were far below the allowable threshold values (i.e., OIV < 30 ft/s (9.1 m/s) and ORA < 15 g), which signifies a low chance of occupant injury, although the influence the vertical acceleration would impart on the OIV and ORA values is currently unknown. The primary concern for occupant safety in a rollover scenario is the crushing of the roof into the occupant compartment resulting in neck and head injuries, which predominantly occurs during half-turn (i.e., 180°) rollovers. Rollovers greater than quarter-turn are uncommon for tractor-trailer rollovers, as seen from impact Cases k-q; therefore, the occupant injury risk is substantially decreased.

Table 5.29: Tractor cabin CG OIV_x and OIV_y for semi-rigid median barrier impacts

Barrier	Impact Side	OIV (ft/s (m/s))			
		Flat Median		Sloped Median	
		OIV_x	OIV_y	OIV_x	OIV_y
W-beam Guardrail	Front-side	-8.76 (-2.67)	12.43 (3.79)	-6.79 (-2.07)	4.3 (1.31)
	Backside	-	-	-3.97 (-1.21)	-12.4 (-3.78)
Wood-blockout Thrie-beam Guardrail	Front-side	-9.61 (-2.93)	11.45 (3.49)	-7.87 (-2.40)	6.92 (2.11)
	Backside	-	-	-1.08 (-0.33)	3.71 (1.13)
Steel-blockout Thrie-beam Guardrail	Front-side	-6.76 (-2.06)	8.86 (2.70)	-1.25 (-0.38)	3.97 (1.21)
	Backside	-	-	-1.51 (-0.46)	2.82 (0.86)

Table 5.30: Tractor cabin CG ORA_x and ORA_y for semi-rigid median barrier impacts

Barrier	Impact Side	ORA (g)			
		Flat Median		Sloped Median	
		ORA_x	ORA_y	ORA_x	ORA_y
W-beam Guardrail	Front-side	1.83	4.40	-1.34	-2.22
	Backside	-	-	-2.68	2.66
Wood-blockout Thrie-beam Guardrail	Front-side	4.45	1.07	0.71	-2.53
	Backside	-	-	-1.34	-0.27
Steel-blockout Thrie-beam Guardrail	Front-side	-1.90	-1.13	-2.07	1.77
	Backside	-	-	3.21	-1.02

The ASI does not have the limitation that the other occupant risk evaluation criteria has in excluding the vertical acceleration component, since the ASI utilizes all three acceleration (x, y, and z) profiles in its formulation. Consequently, the occupant injury risk of a rollover scenario can be assessed by taking into account the tractor-trailer motion in all directions. Figure 5.19 shows the ASI time histories for Cases *j* and *m* and Table 5.31

shows the ASIs of the tractor cabin CG for the semi-rigid median barrier impact scenarios.

The ASI time histories for the remaining cases are shown in APPENDIX D. The tractor

cabin experienced larger ASI values compared to those in the flexible median barrier

impacts, with two impact scenarios, Cases *j* and *o*, having ASI values greater than the

preferred allowable limit of 1.0. Although, these two impact scenarios' ASI values were

below the maximum allowable limit of 1.4, which indicate a possibility of occupant injury.

Considering the *RO* outcome impact scenarios, the ASI values were, on average, below the

preferred allowable limit of 1.0.

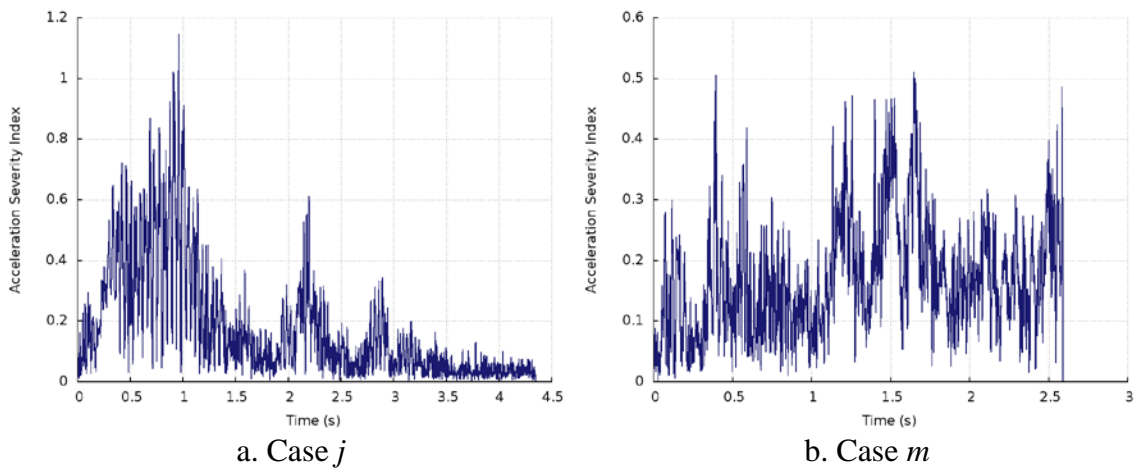a. Case *j*   b. Case *m*

Figure 5.19: ASI profiles of tractor-trailer impacts on semi-rigid median barriers

Table 5.31: Tractor cabin CG ASI for semi-rigid median barrier impacts

Barrier	Impact Side	ASI	
		Flat Median	Sloped Median
W-beam Guardrail	Front-side	0.78	0.93
	Backside	-	0.51
Wood-blockout Thrie-beam Guardrail	Front-side	1.14	0.87
	Backside	-	1.01
Steel-blockout Thrie-beam Guardrail	Front-side	0.60	0.92
	Backside	-	0.79

The THIV and PHD values for the tractor-trailer impacts on semi-rigid median barrier are shown in Table 5.32 and Table 5.33, respectively. All impact scenarios had THIV and PHD values well below the threshold limits, THIV < 30 ft/s (9.1 m/s) and PHD < 20 *g*, which signifies low occupant injury risk potential. It should be noted, THIV and PHD consider only longitudinal and lateral accelerations, as well as yaw rotation, and omit vertical accelerations like the OIV and ORA calculations.

Table 5.32: Tractor cabin CG THIV for semi-rigid median barrier impacts

Barrier	Impact Side	THIV (ft/s (m/s))	
		Flat Median	Sloped Median
W-beam Guardrail	Front-side	12.43 (3.79)	7.48 (2.28)
	Backside	-	8.89 (2.71)
Wood-blockout Thrie-beam Guardrail	Front-side	13.42 (4.09)	10.17 (3.10)
	Backside	-	3.64 (1.11)
Steel-blockout Thrie-beam Guardrail	Front-side	10.37 (3.16)	3.02 (0.92)
	Backside	-	2.79 (0.85)

Table 5.33: Tractor cabin CG PHD for semi-rigid median barrier impacts

Barrier	Impact Side	PHD (*g*)	
		Flat Median	Sloped Median
W-beam Guardrail	Front-side	8.60	7.93
	Backside	-	11.22
Wood-blockout Thrie-beam Guardrail	Front-side	7.58	8.64
	Backside	-	12.58
Steel-blockout Thrie-beam Guardrail	Front-side	7.22	7.58
	Backside	-	7.70

The CEN impact severity levels for the tractor-trailer impacts against semi-rigid median barriers were classified as *A*, except for the two impact Cases (*j* and *o*) that had ASI values greater than 1.0, see Table 5.34. Considering the size and weight of the tractor-trailer, and the fact that the strong link between vehicle rollover and occupant injury for passenger vehicles isn't present in heavy vehicles (MASH 2009), it may be concluded that the *RO* impact cases would provide relatively safe conditions for an occupant, assuming the restraint system (i.e., seat belt) is used. In light of this occupant safety evaluation, combined with the semi-rigid median barrier's ability to prevent vehicle overriding on flat and sloped medians, the semi-rigid median barriers performed adequately during impacts from tractor-trailers using MASH TL-5 impact conditions.

Table 5.34: CEN impact severity for tractor-trailer impacts on semi-rigid median barriers

Barrier	Impact Side	CEN Impact Severity Level	
		Flat Median	Sloped Median
W-beam Guardrail	Front-side	*A*	*A*
	Backside	-	*A*
Wood-blockout Thrie-beam Guardrail	Front-side	*B*	*A*
	Backside	-	*B*
Steel-blockout Thrie-beam Guardrail	Front-side	*A*	*A*
	Backside	-	*A*

5.4 Tractor-Trailer Impacts on Rigid Median Barriers

Combining the ISOL tractor-trailer FE model discussed in Section 3.4 as well as the concrete median barriers from Section 4.4, two impact scenarios were conducted: one flat and one sloped median impact. Due to the symmetry of the front and back side of the concrete median barrier model, the front-side and backside impact cases were assumed to be identical; therefore, the need to conduct the flat backside impact case was eliminated. Additionally, as mentioned previously in CHAPTER 4, the placement of the concrete barrier is only applicable on flat terrain. Hence, only a backside impact is possible in which the tractor-trailer traverses through the sloped median prior to impacting the backside of the concrete barrier (see Figure 4.2b). Table 5.35 shows the simulation matrix of the tractor-trailer impacts on rigid median barriers, (Cases *r* and *s*), and summarizes the impact performance based on tractor-trailer behavior.

Table 5.35: Tractor-trailer responses for rigid median barrier impacts

Barrier	Impact Side	Impact Outcomes	
		Flat Median	Sloped Median
Concrete Barrier	Front-side	*r. R*	-
	Backside	-	*s. R*

5.4.1 Tractor-Trailer Impact Response

Both of the impact scenarios against the concrete median barriers resulted in redirections (*R*) as can be seen in Figure 5.20. Due to rigid constraint of the concrete barriers, no deflection was present in the barrier and the tractor-trailer was redirected quickly in both impact scenarios. Table 5.36 shows the interaction durations in which the tractor-trailer was in contact with the concrete barrier for each impact case. The rigid median barrier impacts resulted in the shortest interaction times compared to the flexible and semi-rigid median barrier impact cases.

a. Case *r*   b. Case *s*
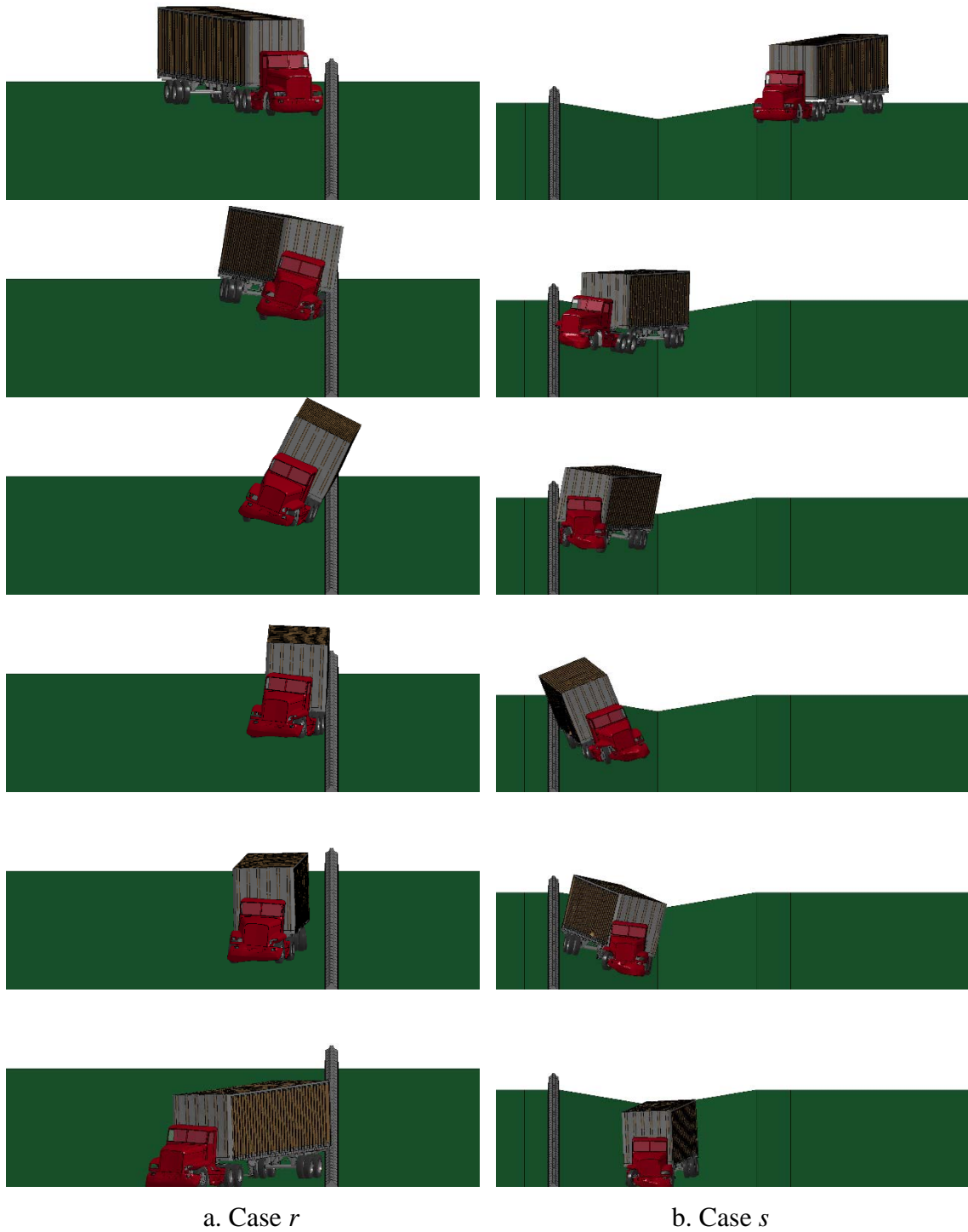
Figure 5.20: Front view sequences of tractor-trailer impacts on rigid median barriers

Table 5.36: Tractor-trailer to rigid median barrier impact interaction time

Barrier	Impact Side	Impact Interaction Time (s)	
		Flat Median	Sloped Median
Concrete Barrier	Front-side	1.37	-
	Backside	-	1.11

Since the rigid median barriers were rigidly constrained, no barrier deflection nor damage length was recorded; therefore, those tables were omitted for the tractor-trailer impacts on rigid median barriers. Instead, the longitudinal length of interaction between the tractor-trailer and barrier was recorded in Table 5.37.

Table 5.37: Longitudinal length of interaction between the tractor-trailer and rigid median barriers

Barrier	Impact Side	Longitudinal Interaction Length (ft (m))	
		Flat Median	Sloped Median
Concrete Barrier	Front-side	77.0 (23.5)	-
	Backside	-	22.3 (6.8)

Both front-side and backside impact cases on flat and sloped medians were redirected with low exit angles (see Table 5.38) and passed the MASH exit box criteria (see Table 5.39). The post-impact trajectories of Cases *r* and *s* are shown in Figure 5.21a-b with the exit boxes placed at the last point of contact during the initial redirection. The backside impact, where the tractor-trailer traversed through the entire sloped median before impacting the concrete barrier, was redirected back into the sloped median traveling longitudinally along the concrete barrier indicating a low probability of reentering the roadway.

Table 5.38: Tractor and trailer exit angles for rigid median barrier impacts

Barrier	Impact Side	Tractor and Trailer Exit Angles (°)	
		Flat Median	Sloped Median
Concrete Barrier	Front-side	21.5/1.2	-
	Backside	-	20.4/3.7

Table 5.39: Tractor-trailer exit box criteria for rigid median barrier impacts

Barrier	Impact Side	Tractor-trailer Exit Box Criteria	
		Flat Median	Sloped Median
Concrete Barrier	Front-side	Pass	-
	Backside	-	Pass
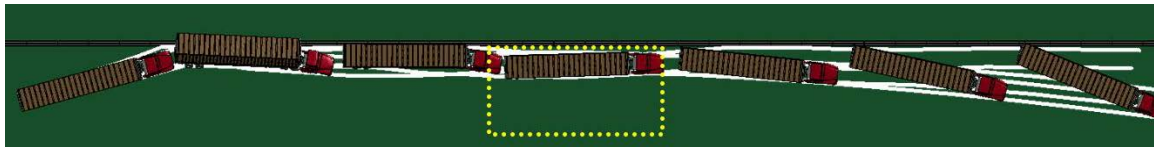
a. Case r: flat median concrete median barrier front-side impact
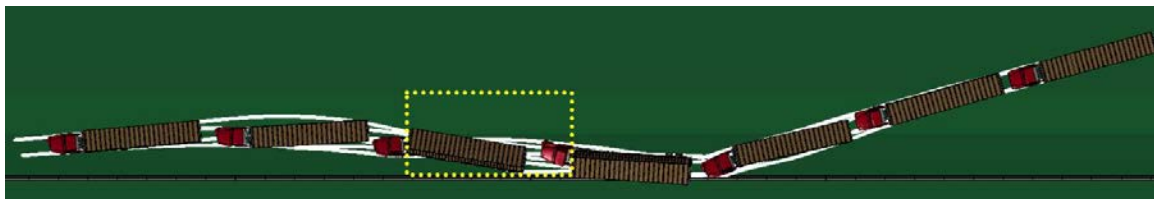
b. Case *s*: sloped median concrete median barrier backside impact

Figure 5.21: Tractor-trailer post-impact trajectories of rigid median barriers with MASH exit boxes placed

Considering all impact scenarios where the tractor-trailer remained upright during flexible, semi-rigid, and rigid median barrier impacts, the tractor-trailer experienced the largest roll angles when impacting the rigid barriers due to their inability to deform or deflect. Table 5.40 and Table 5.41 show the maximum yaw, pitch, and roll angles of the tractor and trailer, respectively. Figure 5.22 shows the yaw, pitch, and roll angles for the

flat median concrete median barrier front-side impact (i.e., Case *r*) and Figure 5.23 shows the yaw, pitch, and roll angles for the sloped median concrete median barrier backside impact (i.e., Case *s*).

Table 5.40: Tractor maximum rotational angles for rigid median barrier impacts

| Barrier | Impact Side | Tractor Maximum Rotational Angles (°) | | | | | |
| | | Flat Median | | | Sloped Median | | |
		Yaw	Pitch	Roll	Yaw	Pitch	Roll
Concrete Barrier	Front-side	-36.0	-9.61	-30.7	-		
	Backside	-			-29.5	-6.7	-20.5

Table 5.41: Trailer maximum rotational angles for rigid median barrier impacts

| Barrier | Impact Side | Trailer Maximum Rotational Angles (°) | | | | | |
| | | Flat Median | | | Sloped Median | | |
		Yaw	Pitch	Roll	Yaw	Pitch	Roll
Concrete Barrier	Front-side	-43.4	-6.3	-29.0	-		
	Backside	-			-24.2	6.6	-21.9

a. Tractor cabin CG   b. Trailer tandem axle
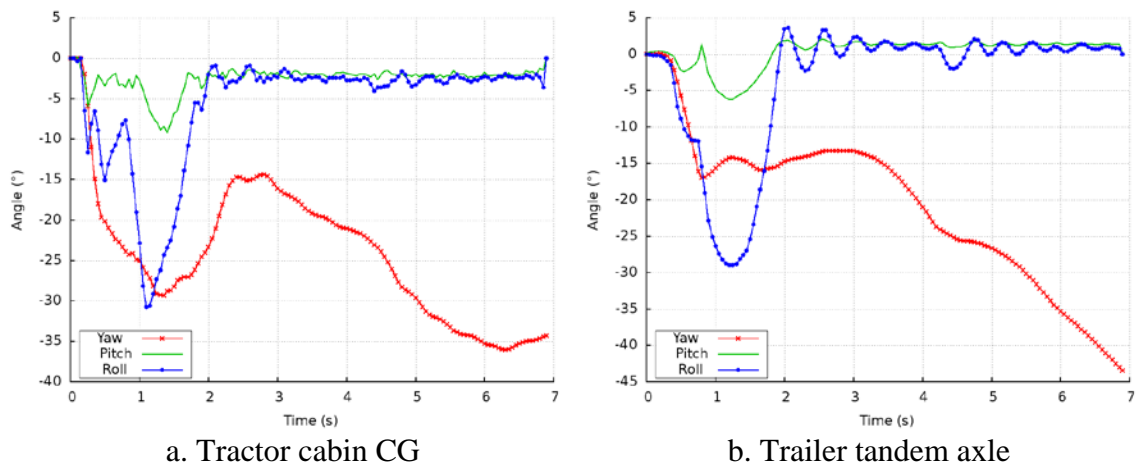
Figure 5.22: Case *r*: yaw, pitch, and roll angles for the flat median concrete median barrier front-side impact
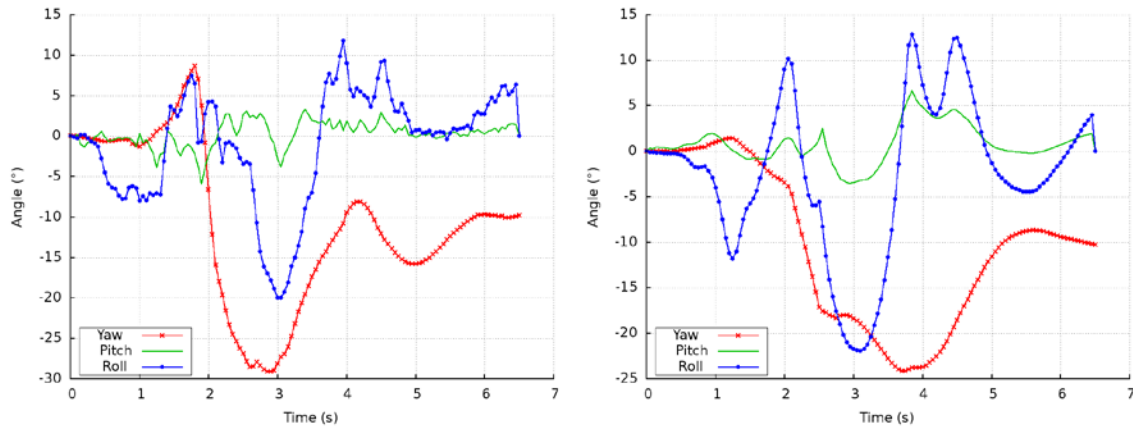
a. Tractor cabin CG   b. Trailer tandem axle

Figure 5.23: Case *s*: yaw, pitch, and roll angles for the sloped median concrete
median barrier backside impact

The residual velocities of both concrete median barrier impacts were nearly identical, see Table 5.42, with the majority of the velocity component in the longitudinal direction. The residual velocity direction, along with the post-impact trajectory and low exit angles, all support the notion of a low possibility of reentering the travel lane and causing a secondary collision.

Table 5.42: Tractor-trailer residual velocity for rigid median barrier impacts

Barrier	Impact Side	Post-Impact Residual Velocity (mph (km/h))	
		Flat Median	Sloped Median
Concrete Barrier	Front-side	38.1 (61.3)	-
	Backside	-	38.3 (61.7)

5.4.2 Occupant Risk Evaluation

The tractor-cabin CG three-dimensional acceleration profiles are shown in Figure 5.24 and Figure 5.25, for Cases *r* and *s*, respectively. Table 5.43 lists the maximum accelerations experienced in the x, y, and z directions for both concrete median barrier impacts. The maximum accelerations that the tractor cabin experienced during the rigid median barrier impacts were comparable to the maximum accelerations that the redirected semi-rigid median barrier impacts developed.

a. x-axis b. y-axis c. z-axis
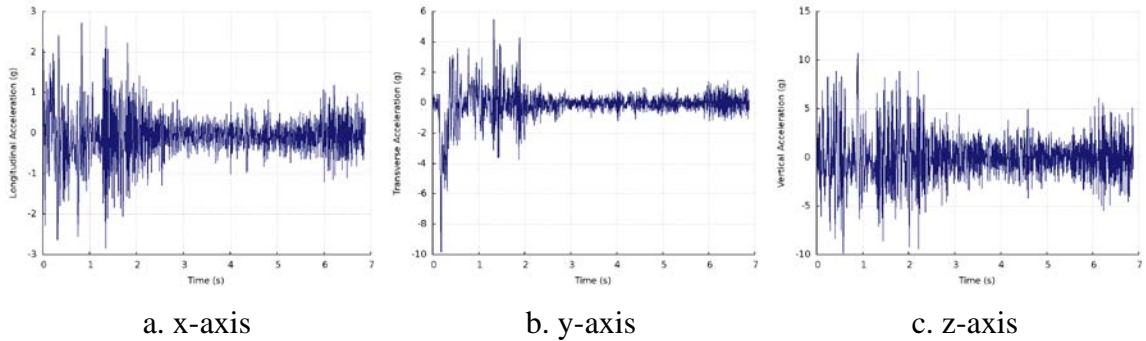
Figure 5.24: Case *r*: time histories of the tractor cabin CG x-, y-, and z-axis accelerations for the flat median concrete median barrier front-side impact

a. x-axis b. y-axis c. z-axis
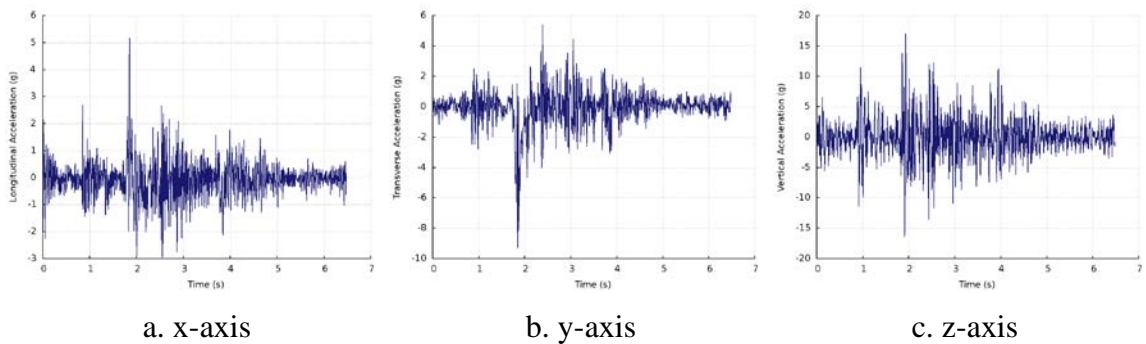
Figure 5.25: Case *s*: time histories of the tractor cabin CG x-, y-, and z-axis accelerations for the sloped median concrete median barrier backside impact

Table 5.43: Tractor cabin CG maximum accelerations for rigid median barrier impacts

Barrier	Impact Side	Maximum x-, y-, and z-axis accelerations (g)					
		Flat Median			Sloped Median		
		x	y	z	x	y	z
Concrete Barrier	Front-side	-2.8	-9.8	10.7	-		
	Backside	-			5.1	-9.3	17.0

The tractor cabin longitudinal and transverse accelerations were used to calculate the OIVs and ORAs of the rigid median barrier impacts, shown in Table 5.44 and Table 5.45, respectively. The rigid response of the concrete barriers did not cause higher OIV and ORA values; however, it did reduce the time in which the OIVs, and subsequent ORAs, occurred. All OIV and ORA values were well within the allowable threshold values (i.e., OIV < 30 ft/s (9.1 m/s) and ORA < 15 g) signifying a low occupant injury risk.

Table 5.44: Tractor cabin CG OIV_x and OIV_y for rigid median barrier impacts

Barrier	Impact Side	OIV (ft/s (m/s))			
		Flat Median		Sloped Median	
		OIV_x	OIV_y	OIV_x	OIV_y
Concrete Barrier	Front-side	-2.33 (-0.71)	-5.61 (-1.71)	-	
	Backside	-		-0.82 (-0.25)	3.12 (0.95)

Table 5.45: Tractor cabin CG ORA_x and ORA_y for rigid median barrier impacts

Barrier	Impact Side	ORA (g)			
		Flat Median		Sloped Median	
		ORA_x	ORA_y	ORA_x	ORA_y
Concrete Barrier	Front-side	2.11	-1.16	-	
	Backside	-		0.44	1.13

The time histories of the ASIs for Cases *r* and *s* are shown in Figure 5.26. Consistent with the previous occupant risk evaluation criteria, the ASI values for the concrete median barrier impacts occurred soon after initial impact. However, the maximum ASIs were not greater as a result of the quick redirection and were consistent with the ASI values of the flexible median barrier impacts as seen in Table 5.46.

a. Case *r*   b. Case *s*
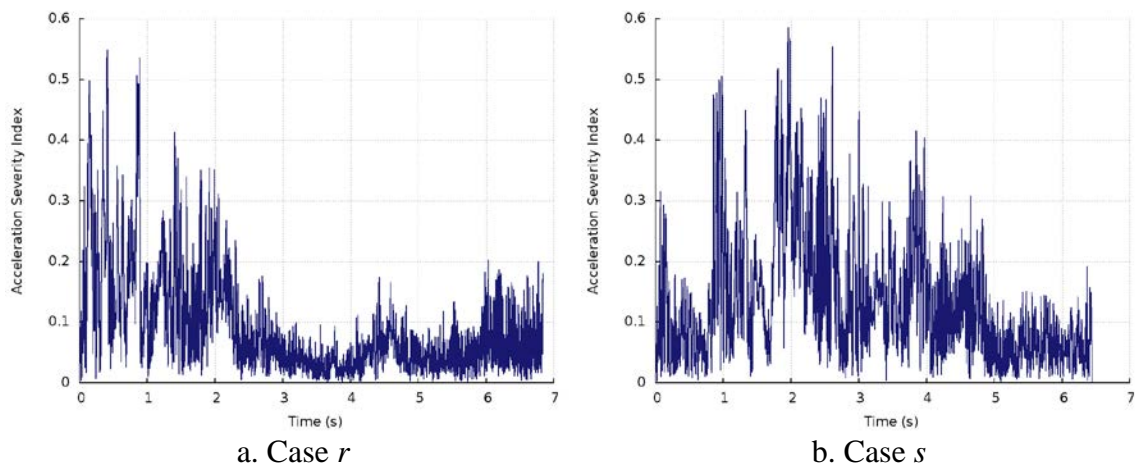
Figure 5.26: ASI profiles of tractor-trailer impacts on rigid median barriers

Table 5.46: Tractor cabin CG ASI for rigid median barrier impacts

Barrier	Impact Side	ASI	
		Flat Median	Sloped Median
Concrete Barrier	Front-side	0.55	-
	Backside	-	0.59

The THIV and PHD values for the concrete barrier impacts seen in Table 5.47 and Table 5.48, respectively, were all below the threshold limits, THIV < 30 ft/s (9.1 m/s) and PHD < 20 *g*, which signifies low occupant injury risk potential.

Table 5.47: Tractor cabin CG THIV for rigid median barrier impacts

Barrier	Impact Side	THIV (ft/s (m/s))	
		Flat Median	Sloped Median
Concrete Barrier	Front-side	3.35 (1.02)	-
	Backside	-	9.81 (2.99)

Table 5.48: Tractor cabin CG PHD for rigid median barrier impacts

Barrier	Impact Side	PHD (g)	
		Flat Median	Sloped Median
Concrete Barrier	Front-side	4.49	-
	Backside	-	4.89

Combining the ASI and THIV values to assess the CEN impact severity level for the tractor-trailer impacts against the rigid median barriers resulted in a classification of the lowest severity levels (i.e., *A*) for both impact cases (See Table 5.49). Considering the vehicle post-impact behavior, rigid median barrier performance, and occupant risk evaluation criteria, it may be concluded the concrete median barriers are capable of safely containing and redirecting tractor-trailers impacts under MASH TL-5 conditions.

Table 5.49: CEN impact severity for tractor-trailer impacts on rigid median barriers

Barrier	Impact Side	CEN Impact Severity Level	
		Flat Median	Sloped Median
Concrete Barrier	Front-side	*A*	-
	Backside	-	*A*

CHAPTER 6: ANALYSIS OF TRACTOR-TRAILER IMPACT SCENARIOS

In the previous chapter, the tractor-trailer impacts on various median barriers were shown and evaluated against the other impact scenarios on the same median barrier type. It was shown that the flexible, semi-rigid, and rigid median barriers installed on flat and sloped terrain were capable of containing and/or redirecting tractor-trailer impacts under MASH TL-5 conditions, while minimizing the occupant injury risk, even if the vehicle failed to remain upright. In this chapter, the tractor-trailer impact scenarios on all three median barrier types are analyzed relative to each other by comparing the tractor-trailer impact behavior, guardrail performance, and occupant risk.

6.1 Tractor-Trailer Post-Impact Behavior

Summarizing all of the tractor-trailer impact scenarios evaluated in this research, Table 6.1 restates the alphabetical labels assigned to each impact case in Sections 5.2, 5.3, and 5.4. Assessing the post-impact behavior of the tractor-trailer for all median barrier types, Figure 6.1 compiles all impact cases and denotes the simulation outcome plotted against the MASH exit box criteria. All impact scenarios that were redirected, with the exception of two impacts (i.e., Cases *d* and *h*), were redirected by their respective median barrier with a low enough exit angle to pass the MASH exit box criteria and signify a low probability of causing a secondary collision by reentering the roadway.

Table 6.1: Simulation matrix of all tractor-trailer impact cases

Barrier	Impact Side	Impact Scenario Case Labels	
		Flat Median	Sloped Median
Three-CMB	Front-side	*a.*	*e.*
	Backside	*b.*	*f.*
Four-CMB	Front-side	*c.*	*g.*
	Backside	*d.*	*h.*
W-beam Guardrail	Front-side	*i.*	*l.*
	Backside	-	*m.*
Wood-blockout Thrie-beam Guardrail	Front-side	*j.*	*n.*
	Backside	-	*o.*
Steel-blockout Thrie-beam Guardrail	Front-side	*k.*	*p.*
	Backside	-	*q.*
Concrete Barrier	Front-side	*r.*	-
	Backside	-	*s.*
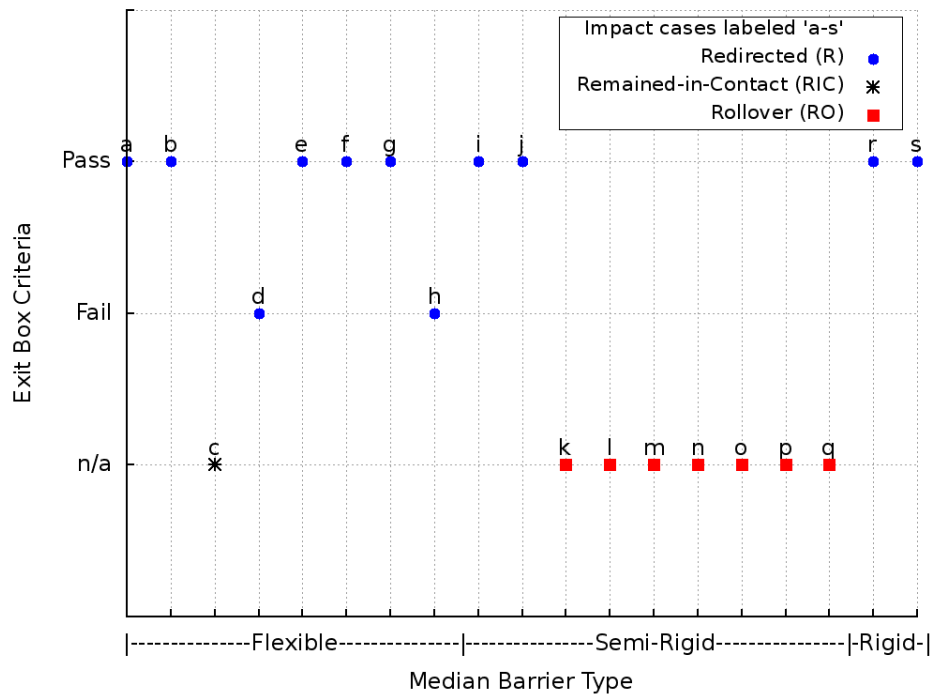
Figure 6.1: Exit box results for all impact scenario outcomes

The stiffness of the median barriers evaluated under tractor-trailer impacts directly relates to the amount of time the tractor-trailer is in contact with the barrier as well as the length of barrier sections damaged. Figure 6.2 shows the strong correlation between the tractor-trailer-to-barrier engagement times against the length of barrier that was damaged during the impact scenario. It should be noted, for the rigid barrier impacts (i.e., Cases *r* and *s*), the longitudinal damage length in Figure 6.2 refers to the length of interaction between the tractor-trailer and concrete barrier. The rigid median barrier impacts had engagement times below 1.5 seconds with the length of interactions less than 79 ft (24 m). The semi-rigid median barrier impacts, (i.e., Cases *i-q*), had engagement times ranging between 1.5-2.7 seconds and longitudinal damage lengths varying between 111-177 ft (34-54 m). Lastly, the flexible median barrier impacts, (i.e., Cases *a-h*), had engagement times greater than 3.6 seconds with longitudinal damage lengths between 190-364 ft (58-111 m). The flexible median barrier impacts had the longest engagement times which resulted in the largest lengths of damaged barrier sections that would need to be repaired or replaced. It should also be noted that the damage lengths for the flexible median barrier impacts only refers to the length of damage caused by direct impact, while omitting the potential damage caused to posts and J-bolts from the cable disengagement, upstream and downstream from the impact region.
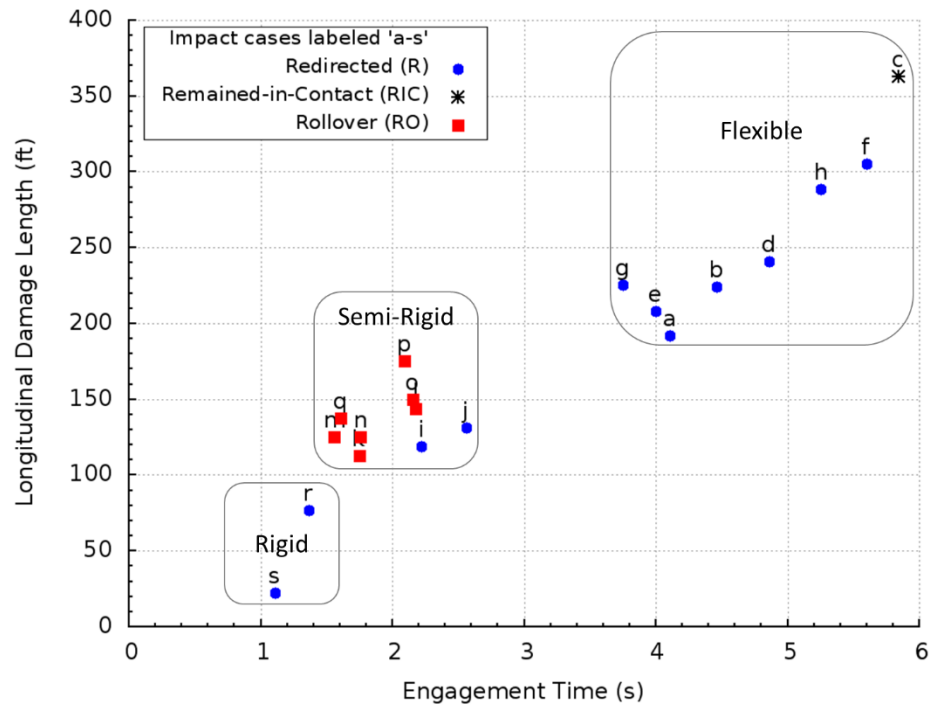
Figure 6.2: Length of longitudinal barrier damage

Figure 6.3 follows the same general trend as Figure 6.2, where the maximum deflection of the barrier is a function of the barrier flexibility. The concrete median barriers were rigidly constrained, thus impact Cases *r* and *s* had no observable deflection. Assessing the various semi-rigid median barriers, based on the degree of flexibility, the W-beam, wood-blockout Thrie-beam, and steel-blockout Thrie-beam guardrails average maximum transverse dynamic deflections were: 8.3 ft (2.5 m), 5.5 ft (1.7 m), and 3.4 ft (1.0 m), respectively. For the flexible median barrier impacts, the three-CMB had an average maximum transverse dynamic deflection of 20.1 ft (6.1 m), while the four-CMB deflected slightly less with an average maximum transverse dynamic deflection of 19.4 ft (5.9 m).
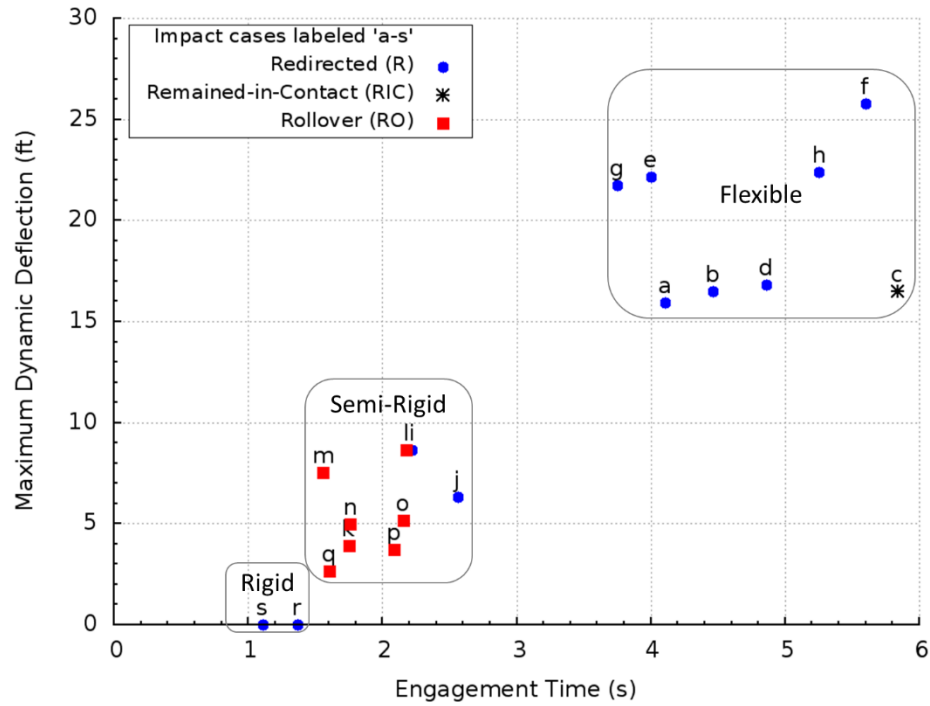
Figure 6.3: Maximum dynamic barrier deflection

The maximum dynamic deflection can be viewed as a function of the longitudinal barrier damage. The longer the damage length, the greater the barrier deflection as shown in Figure 6.4. Considering the flexible and semi-rigid median barrier impacts, the backside impacts on flat or sloped medians resulted in longer damage lengths with larger deflections compared to their front-side impact counterpart.
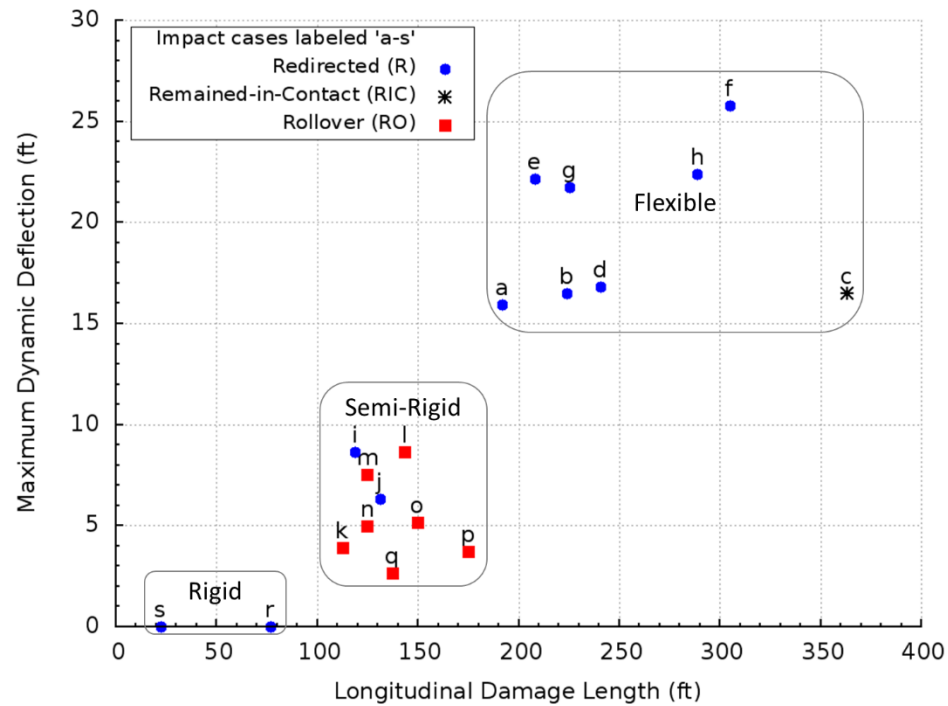
Figure 6.4: Maximum dynamic deflection vs length of longitudinal barrier damage

6.2 Occupant Injury Risk Evaluation from Tractor-Trailer Impact Responses

Due to the absence of an ATD in full-scale and simulated crash tests, researchers often evaluate the risk of occupant injury using vehicle responses. The injury risk of an occupant is based on the assumption that the greater the impact severity, the more likely an occupant would get injured. The occupant injury risk evaluation criteria were exclusively based on vehicle responses, in particular the acceleration profiles of the tractor cabin CG.

A measure of impact severity using the x-, y-, and z-axis acceleration profiles is the ASI, which defines the overall impact severity throughout the impact, but the maximum value is typically taken as the single non-dimensional ASI. An ASI value of 1.0

corresponds to "light injury, if any", although a value of 1.4 is acceptable. Figure 6.5 shows the ASI for the tractor-trailer impacts on all median barriers. The semi-rigid barrier impacts resulted in the largest ASIs, compared to the flexible and rigid median barrier impacts, with an average ASI of 0.84, compared to 0.5 and 0.57, respectively. The front-side impacts resulted in a marginally higher average ASI of 0.72, when compared to the backside impact's average ASI of 0.6. There was no variation in the average ASIs when comparing front-side to backside impacts for all median barriers.
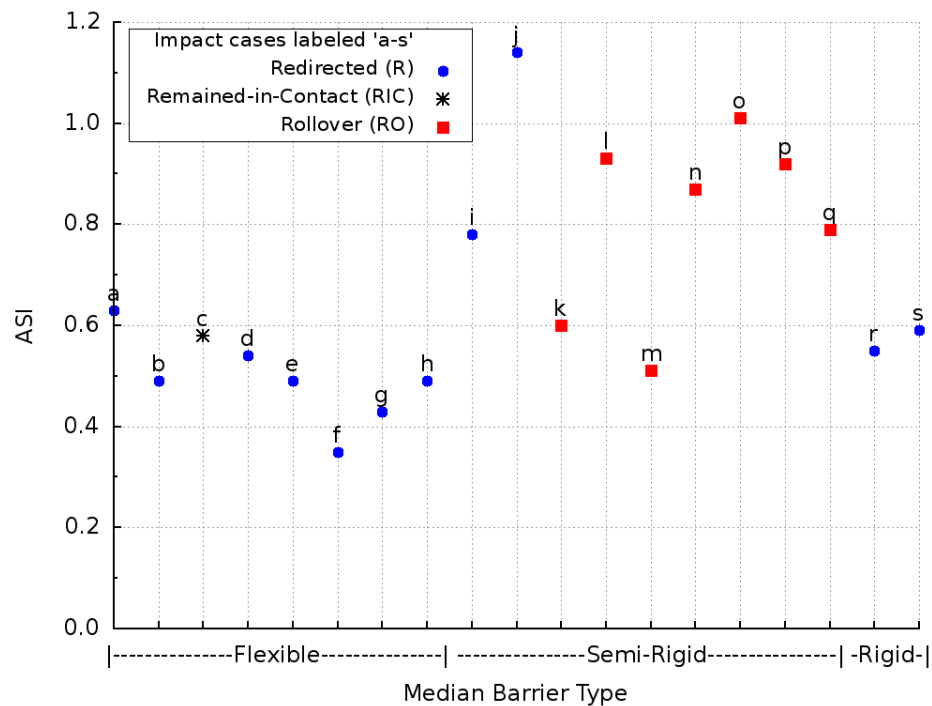
Figure 6.5: ASI of all tractor-trailer impact scenarios

Figure 6.6a shows the ASI plotted against the post-impact residual velocity for each impact scenario. Although no conclusive trend is visible, it can be seen that, for the flexible

median barrier impacts, even though the post-impact residual velocity varied from 28.5 mph (46 km/h) to 41.6 mph (67 km/h), the variation in the ASI was minimal with an average ASI of 0.5. Due to the majority of the tractor-trailers failing to remain upright (i.e., 90° rollover) for impacts on the semi-rigid median barriers, larger ASIs occurred, with an average ASI of 0.84 and average residual velocity of 40 mph (58 km/h). The rigid median barrier impacts had the largest average residual velocity of 38 mph (61.5 km/h) and average ASI of 0.57. When comparing the ASIs against the tractor cabin CG maximum resultant acceleration, a strong correlation can be made. In general, the larger the maximum resultant acceleration of the tractor cabin, the higher the ASI will be, as seen in Figure 6.6b

a. ASI vs residual velocity   b. ASI vs maximum resultant acceleration
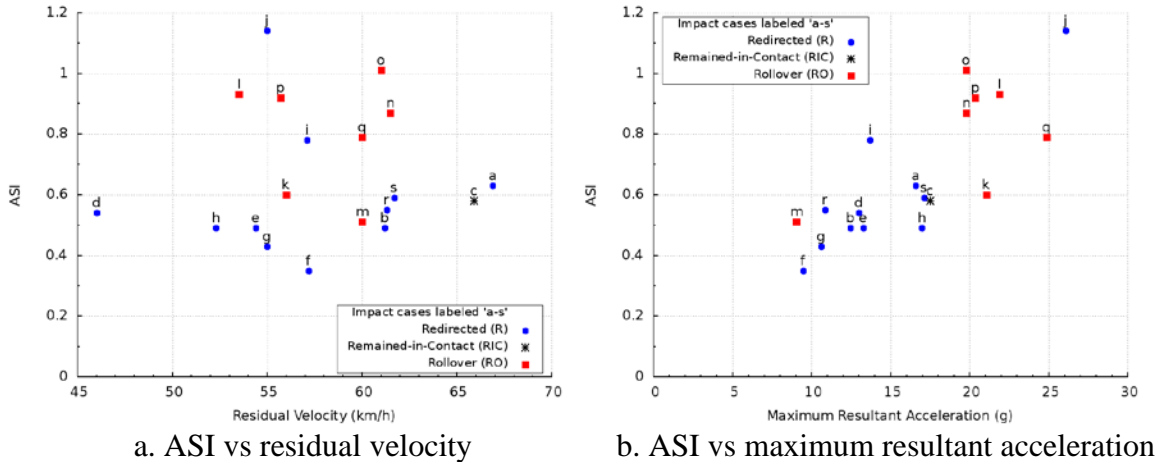
Figure 6.6: ASI comparisons

The velocity at which a hypothetical occupant would make contact with the vehicle interior compartment is the OIV and the maximum acceleration the occupant experiences after contact occurs is the ORA. The larger the OIV and ORA values, the higher the impact

severity and the more likely an occupant would experience injuries. MASH specifies a preferred allowable OIV limit of 30 ft/s (9.1 m/s) and ORA of 15.0 g; although a maximum allowable OIV limit of 40 ft/s (12.2 m/s) and ORAs of 20 g are acceptable. Additionally, the CEN utilizes THIV, which calculates the impact velocity similar to OIV, except the yaw rotation of the vehicle is considered and the resultant of the x- and y- axis accelerations are used to define a singular THIV. The THIV restricts the maximum allowable impact velocity to 30 ft/s (9.1 m/s).

It should be noted, the OIV_x, OIV_y, and THIV occupant injury risk evaluation criteria omit the vertical acceleration profile which could be more predominant during impact scenarios on sloped medians or for vehicles that fail to remain upright. By reason of thoroughly evaluating occupant injury risk, the criteria were assessed and the OIV_x and OIV_y for all tractor-trailer impacts are shown in Figure 6.7. The OIV_x and OIV_y in all impacts were well below the allowable limits specified in MASH. The semi-rigid median barrier impacts had the largest average OIVs in both directions compared to the flexible and rigid median barrier impacts. Assessing the OIVs in terms of the flat and sloped median impacts, the sloped median impacts resulted in lower OIV_x and OIV_y compared to the flat median impacts. A possible source for the difference between the flat and sloped median OIVs could be attributed to the tractor-trailer traversing the slope prior to impacting the median barrier, compared to the shorter distance traveled prior to impacting the flat median barriers.

a. OIV$_x$ b. OIV$_y$
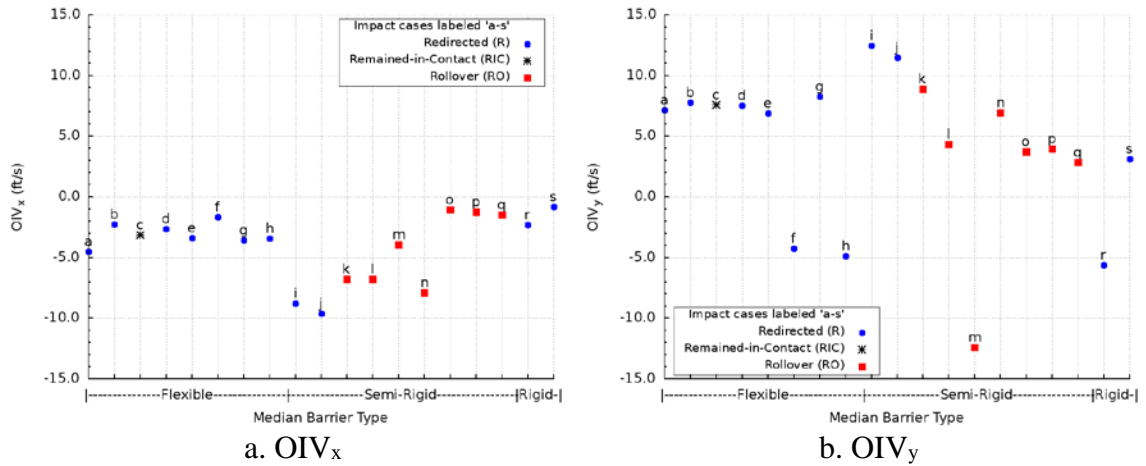
Figure 6.7: OIV outcomes

The THIV values are shown in Figure 6.8a adjacent to the manually determined resultant OIV in Figure 6.8b for comparison. The THIV for all tractor-trailer impact scenarios were within the acceptable range (i.e., below 30 ft/s (9.1 m/s)) with the semi-rigid median barrier impacts resulting in some of the largest THIVs. Similar to the OIV outcomes, when assessing the THIV based on median type, the flat median barrier impacts resulted in larger impact velocities than those of the sloped median barrier impacts. The average flat median barrier impact THIV was 8.5 ft/s (2.6 m/s) compared to 4.9 ft/s (1.5 m/s) for the sloped median barrier impacts.

a. THIV   b. Resultant OIV
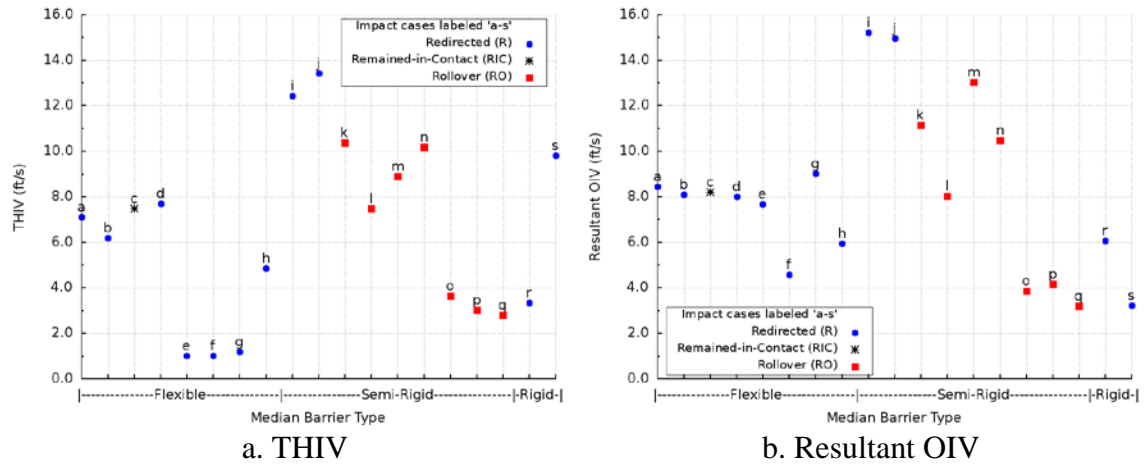
Figure 6.8: Resultant occupant impact velocity criteria

Figure 6.9 shows the correlation between the THIV and resultant OIV results for all impact cases. Note, three outlying impact cases, Cases *e*, *g*, and *s*, which do not follow the general trend of the other impact scenarios. Comparing the THIV values to the resultant OIV values in Figure 6.9, both evaluation criteria correlated well with each other. In all cases, excluding Cases *e*, *f*, *g*, and *s*, the impact velocities reported by THIV and the resultant OIV were within 15.9% of each other, on average. The four excluded aforementioned cases had reported impact velocities that varied by an average of 79% between the THIV and resultant OIV criteria.
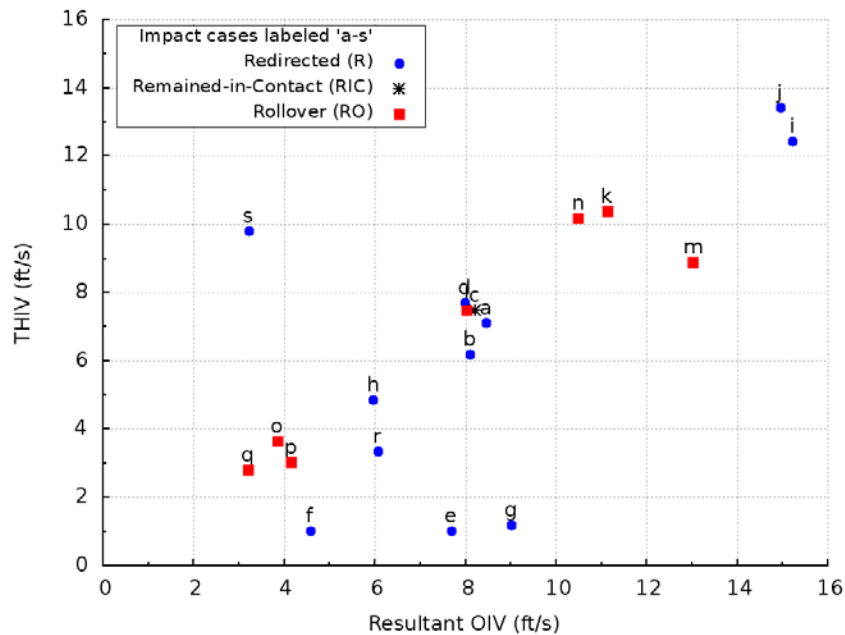
Figure 6.9: THIV vs resultant OIV

The maximum acceleration the occupant experiences after contact occurs is the ORA. The subsequent ORA_x and ORA_y in the longitudinal and lateral directions, respectively, are determined as the maximum 10-ms moving average tractor cabin CG acceleration after OIV occurs. MASH specifies a preferred ORA limit of 15.0 g; although a maximum ORA limit of 20 g is acceptable. The now defunct PHD evaluation criteria, which was previously required in CEN EN 1317-2, calculates the resultant maximum acceleration after the THIV occurs. The PHD, which is still recommended by MASH, prescribes a maximum post-impact acceleration limit of 20 g.

Assessing the longitudinal and transverse ORAs for the tractor-trailer impacts on all median barrier types, all impact cases resulted in ORAs of less than a third of the MASH preferred allowable limit (i.e., less than 15.0 g) in both directions, as shown in Figure 6.10.

Similar to the trends present in the OIVs, the semi-rigid median barrier impacts had the largest ORAs compared to the flexible and rigid median barrier impacts. Additionally, the flat median impact cases resulted in larger average absolute ORAs compared to sloped median impact cases.

a. ORA$_x$ b. ORA$_y$
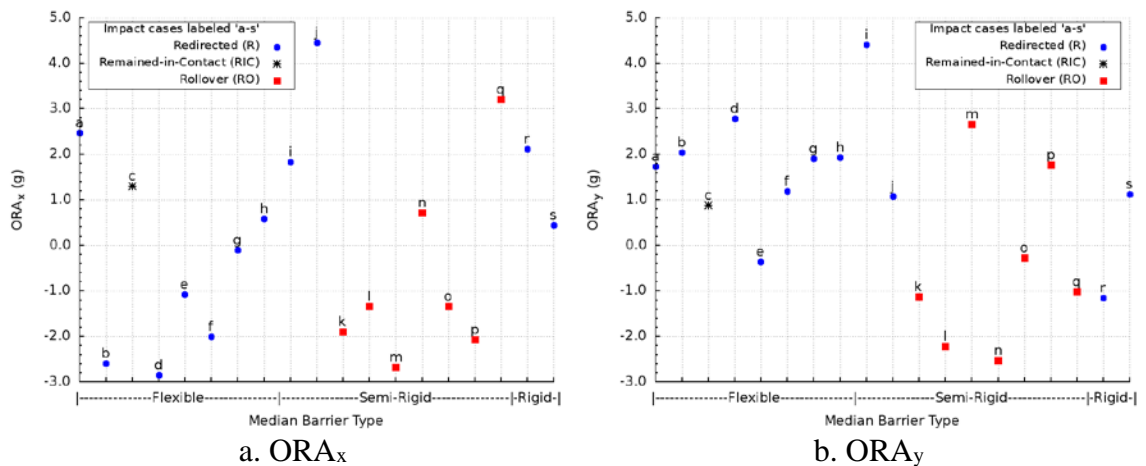
Figure 6.10: ORA outcomes

Figure 6.11a shows the PHD occupant injury risk evaluation criteria for all tractor-trailer impact cases, adjacent to the manually determined resultant ORA in Figure 6.11b for comparison. All impact cases were below the CEN maximum allowable PHD value of 20 g. Consistent with the individual component ORA evaluation, the semi-rigid median barrier impacts were the most severe, resulting in the largest maximum post-impact accelerations (i.e., PHD) of any median barrier type. Contrary to the ORA results, the sloped median impact cases had a larger average PHD of 7.25 g compared to the average PHD of 6.31 g for the flat median impact cases. Similarly, the backside impact cases, with

an average PHD of 7.32 *g*, were slightly more severe than the front-side impact cases with an average PHD of 6.52 *g*. The resultant ORAs showed no variation between the front-side and backside average maximum post-impact acceleration.

a. PHD   b. Resultant ORA
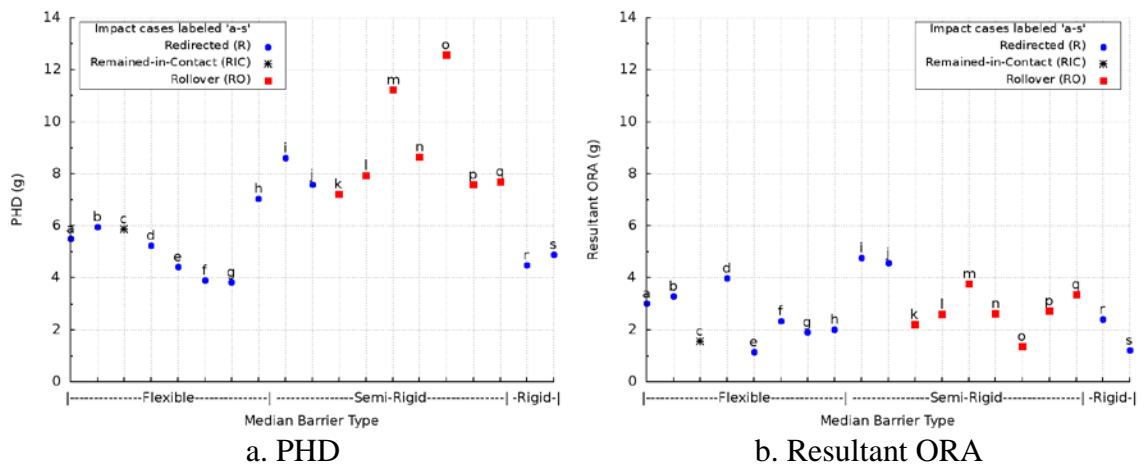
Figure 6.11: Resultant occupant maximum acceleration criteria

Comparing the PHD values to the resultant ORA values in Figure 6.12, the PHD evaluation criteria consistently reported larger maximum post-impact accelerations compared to the resultant ORA values. In all tractor-trailer impact cases, the maximum post-impact acceleration reported by PHD were on average 58.5% larger than the resultant ORA. The smallest variation between PHD and resultant ORA values occurred with Case *d* (24%) and the largest variation was with Case *o* (89.1%). A potential source for the discrepancy between the PHD and resultant ORA values is the time instance at which the maximum post-impact acceleration was determined and the application of the standardized low-pass Butterworth filtering to the PHD values.
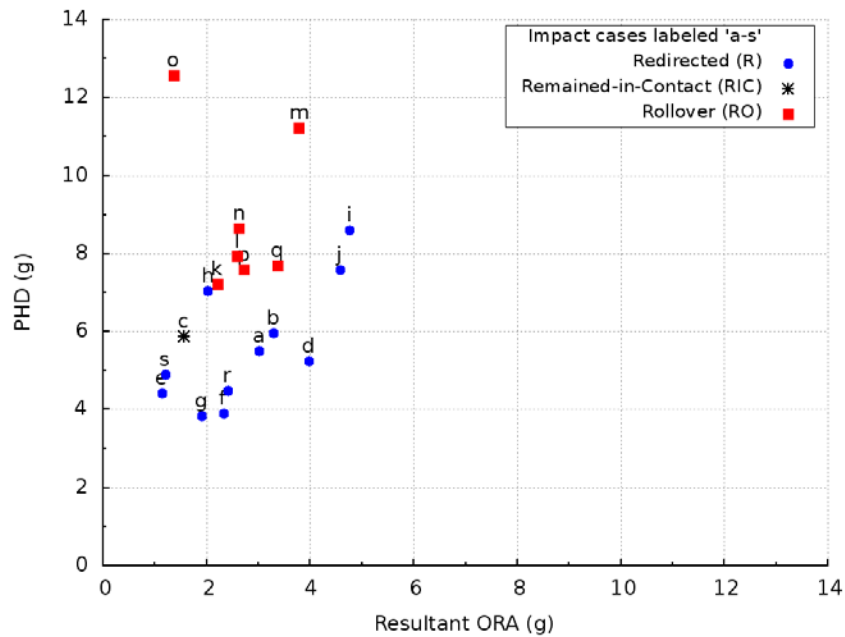
Figure 6.12: PHD vs resultant ORA

Regardless of the discrepancies between the MASH and CEN evaluation criteria, all occupant injury risk evaluation criteria were successful in utilizing the tractor-cabin CG acceleration profiles to correlate impact severity to occupant safety. The computed indices show that, due to the size of the tractor-trailer, an occupant located in the tractor cabin is at a low risk for injury, regardless of whether or not the vehicle remains upright throughout a redirective impact on flexible, semi-rigid, and rigid median barriers installed on flat or sloped terrain.

Table 6.2 summarizes the MASH TL-5 compliance of each flexible, semi-rigid, and rigid barrier, assessed based on the barrier performance, post-impact vehicle behavior, and occupant risk evaluation criteria.

Table 6.2: MASH TL-5 evaluation compliance

Barrier	Impact Side	Impact Scenarios	
		Flat Median	Sloped Median
Three-CMB	Front-side	*a.* PASS	*e.* PASS
	Backside	*b.* PASS	*f.* PASS
Four-CMB	Front-side	*c.* FAIL	*g.* PASS
	Backside	*d.* FAIL	*h.* FAIL
W-beam Guardrail	Front-side	*i.* PASS	*l.* PASS
	Backside	-	*m.* PASS
Wood-blockout Thrie-beam Guardrail	Front-side	*j.* PASS	*n.* PASS
	Backside	-	*o.* PASS
Steel-blockout Thrie-beam Guardrail	Front-side	*k.* PASS	*p.* PASS
	Backside	-	*q.* PASS
Concrete Barrier	Front-side	*r.* PASS	-
	Backside	-	*s.* PASS

CHAPTER 7: CONCLUSIONS

Full-scale crash tests are required to evaluate the performance of redirection-type roadway hardware systems before they can be used on federal and state highway systems in the United States. Redirection-type roadway hardware systems are categorized into three classes of barriers, flexible, semi-rigid, and rigid, based on the stiffness of the barrier system and the amount of energy the barrier can dissipate while redirecting an errant vehicle. Depending on the type of barrier system, different full-scale crash tests are required to meet the classifications specified in the AASHTO's Manual for Assessing Safety Hardware (MASH). Most flexible and semi-rigid barrier systems are tested under MASH Test Level 3 (TL-3) impact conditions, which require the use of a small passenger sedan and a large pick-up truck. Most rigid barriers are tested under MASH TL-5 or TL-6 impact conditions, which use the two aforementioned vehicles with the addition of a tractor-trailer to evaluate the barrier performance. Due to the lower testing requirements of flexible and semi-rigid barrier systems, most CMBs, W-beam, and Thrie-beam guardrails installed along roadways today have not been evaluated for impacts from larger vehicles such as single-unit trucks or tractor-trailers.

In recent years, with the further advancements in numerical modeling and simulation capabilities, finite element (FE) models of vehicles from every weight class have been developed and have been used to simulate crash tests on roadway hardware

systems to achieve multiple objectives. The FE models are used primarily in three areas: 1) as an additional resource during the development and design stage of a new redirection hardware system to evaluate barrier designs before manufacturing and production begins; 2) as a research tool to investigate the performance of barrier systems installed in locations and configurations not currently evaluated by full-scale crash tests to assess vehicle behavior in different impact scenarios; and 3) to investigate the performance of already approved or in-service roadway hardware systems to provide barrier performance characteristics, determine vehicle redirection behavior, and evaluate occupant injury risk. To that end, in this research, the FE model of a full-scale tractor-trailer was improved, validated, and used to simulate its impacts at MASH TL-5 conditions on flexible, semi-rigid, and rigid median barriers installed on flat and sloped terrain. The simulation results are analyzed to evaluate the barrier performance, vehicle's post-impact behavior, and occupant injury risk of the most commonly used barrier systems throughout the United States.

The FE model of the tractor used in this study was initially created at the National Crash Analysis Center (NCAC) and was further extended and validated against a tractor-only impact by the National Transportation Research Center (NTRCI). The FE model of the tractor used in this research was based on the NTRCI model and further improved due to the presence of a large number of modeling issues including initial penetrations, improper contact definitions, and inaccurately modeled components. The revised model, which was developed at the Impact and Structural Optimization Library (ISOL) at UNC Charlotte, was then validated against the full-scale tractor-only crash test and compared to

the initial NTRCI FE model. This analysis showed the tractor's kinematics and acceleration profiles correlated well with the full-scale test data and were improved relative to the NTRCI simulation data.

In order to simulate full-scale tractor-trailer impacts, the FE models of a 48-ft (14.6-m) dry-box trailer and a 50,000-lb (22,680-kg) ballast load, were obtained from NTRCI and improved upon by fixing the numerical modeling issues, similar to those present in the tractor FE model. The FE models of the tractor, trailer, and ballast were combined to create the complete 80,000-lb (36,287-kg) ISOL tractor-trailer FE model that was modified from the NTRCI models and validated against the most recent full-scale test conducted at MwRSF. The ISOL tractor-trailer FE model was shown to be in good agreement with the tractor and trailer kinematics as well as the occupant safety evaluation criteria calculated from the full-scale crash test data. The comparisons showed that the revised ISOL tractor-trailer FE model had improved accuracy over the NTRCI model.

The validated ISOL tractor-trailer FE model was used to simulate tractor-trailer impacts on cable median barriers (CMBs) with three and four cables, a 31-in (787-mm) double-faced W-beam guardrail, 31-in (787-mm) double-faced wood- and steel-blockout Thrie-beam guardrails, and a 42-in (1.1-m) concrete barrier installed on flat and 6H:1V sloped medians. The CMBs, W-beam, and Thrie-beam guardrails were impacted from the front-side and backside when placed on flat median and on a sloped median at 4 ft (1.3 m) from the slope ditch centerline. However, for W-beam and Thrie-beam guardrails and the concrete barrier on a flat median, only a front-side impact was considered due to the longitudinal symmetry of the barrier. For the backside concrete barrier impact on a sloped

median, the tractor-trailer traversed through the entire sloped median before impacting the barrier installed on the opposite shoulder breakpoint. In each impact scenario, the tractor-trailer began at the roadway median shoulder with MASH TL-5 impact conditions, i.e., at a 15° impact angle and 50-mph (80.5-km/h) impact speed.

In simulations of the tractor-trailer impacting the various median barrier systems, barrier and tractor-trailer responses were extracted from the simulation results to evaluate the barrier's safety performance, vehicle redirection characteristics, and occupant injury risks that are assumed to be proportional to impact severity. The barrier performance was assessed by classifying the redirection ability and evaluating the maximum dynamic deflection as well as the length of damage along the longitudinal axis of the barrier system. The tractor-trailer's redirection characteristics were classified by assessing the post-impact behavior using the residual velocity, yaw, pitch, and roll angles, and exit angle combined with the MASH exit box criteria to determine the chance of the vehicle returning to the roadway and potentially causing a secondary accident. To assess the occupant injury risk, occupant safety evaluation criteria including the OIV, ORA, THIV, PHD, and ASI, were computed based on the tractor cabin CG acceleration histories for all impact scenarios.

For all of the impact scenarios for the tractor-trailer on the flexible median barriers on flat and sloped terrain, the three- and four-CMBs successfully redirected the tractor-trailer on the impacting side of the barrier, except for one case in which the tractor-trailer remained in contact with the barrier through the duration of the impact. For the two backside impacts on the four-CMB on flat and sloped medians, the tractor-trailer was successfully redirected by the barrier, but the growing yaw rotation of the tractor-trailer

resulted in the post-impact trajectory failing the exit box criteria. The maximum dynamic deflections of the CMBs were the most severe of all impact scenarios in this research. In front-side impacts, the CMBs had an average deflection of 16.4 ft (5 m), whereas in the backside impacts, the average deflection was 23 ft (7 m). The CMBs also resulted in the longest interaction times with the tractor-trailer, which translated to the largest longitudinal sections of barriers being affected. Since the cables were designed to be released from their supports to allow further deflection, the length of the damaged longitudinal section of barriers typically extended the entire span of the cable barrier system. Based on the barrier response of evaluated length-of-need (LON) section of the flexible barrier systems, an increased LON section would be recommended for future evaluations to decrease the influence of the terminal anchor points. The results of all occupant safety evaluation criteria indicated a very low probability of occupant injury.

For impacts on 31-in (787-mm) double-faced W-beam guardrails and 31-in (787-mm) double-faced wood- and steel-blockout Thrie-beam guardrails on flat and sloped medians, all, except for two scenarios, resulted in the tractor-trailer rolling 90° onto the barrier after impact. When assessing these aforementioned rollover impact scenarios solely based on barrier performance, the median barriers were adequate in preventing the vehicle from penetrating through the barrier; and performed satisfactorily according to MASH, which does not require heavy vehicles (i.e., tractor-trailers) to remain upright during impacts. In such impact scenarios involving vehicle rollovers, the barrier performance was not evaluated using the MASH exit box criteria. The two scenarios that did not result in the vehicle failing to remain upright were the front-side impacts on the W-beam and wood-

blockout Thrie-beam guardrails, where the tractor-trailers were successfully redirected with small exit angles and passed the MASH exit box criteria. The longitudinal length of damage received and total engagement time from the tractor-trailer impacts on semi-rigid median barriers were significantly less than those on the flexible median barriers with the damage primarily located at the regions directly impacted. The maximum dynamic deflections were also less than those of the flexible median barriers, with the semi-rigid barriers deflecting an average of 7.5 ft (2.3 m) in cases with no rollover, and the remaining barriers deflecting an average of 5.2 ft (1.6 m) in cases with rollovers. All of the tractor-trailer impact scenarios on the semi-rigid median barriers, including the cases with rollover, resulted in acceptable values from the occupant injury risk evaluation, indicating a low risk of occupant injury.

For tractor-trailer impacts on the 42-in (1.1-m) concrete barrier, the simulation results showed that the barrier was effective for impacts on flat median as well as traversing through sloped median prior to impact. The concrete barriers were rigidly constrained; therefore, no deflection was present. The total engagement length and time of the tractor-trailer with the concrete barrier were the shortest duration and smallest interaction length, respectively. Both impact scenarios resulted in the tractor-trailer remaining upright, with small exit angles, and passing the MASH exit box criteria. The occupant injury risk evaluation criteria did not indicate a risk of occupant injury.

This research demonstrated the practicality, usefulness, and feasibility of utilizing FE modeling and simulations for research in assessing and evaluating roadway safety hardware, specifically with the use of a full-scale tractor-trailer FE model. Given the

complexity of heavy articulating vehicles, combined with the challenges involved in maintaining adept highway barrier systems to keep up with the ever-evolving vehicle designs, extensive resources should be devoted to further improve the numerical accuracy and efficiency. Although the tractor-trailer FE model used in this research implemented extensive numerical improvements, additional numerical enhancements would be beneficial in reducing the computational cost of conducting full-scale crash test simulations.

The MASH TL-5 80,000-lb (36,287-kg) tractor-trailer FE model, consisting of, a day-cab tractor, 48-ft (14.6-m) dry-box trailer, and 50,000-lb (22,680-kg) ballast trailer payload, could be improved upon further and employed to investigate other impact scenarios such as vehicle to vehicle collisions or other stationary roadside objects like portable work-zone crash cushions, terminals, bridge pillars, tree trunks, or utility poles. Furthermore, an ATD (anthropomorphic test device), i.e., crash test dummy, may be implemented in the tractor-trailer FE model to more accurately quantify the occupant injury risk during redirective-type impact scenarios. As the current occupant injury risk evaluation criteria used in this research only provides the probability of occupant injury based on impact severity.

REFERENCES

AASHTO. (2006). *Roadside Design Guide* American Association of State Highway and Transportation Officials (AASHTO). Washington, D.C.

AASHTO. (2016). *Manual for Assessing Safety Hardware (MASH-2) - 2nd Edition*. American Association of State Highway and Transportation Officials (AASHTO). Washington, D.C.

Abad, J., Valladares, D., Malon, H., Miralbes, R. and Martin, C. (2013). *Experimental Validation of a Three-Axle Semi-trailer Finite Element Model for Subsequent Dynamic Analyses*. International Journal of Vehicle Systems Modelling and Testing **8**(3): 209-227.

AFDC. (2012). *Vehicle Weight Classes & Categories*. Alternative Fuels Data Center (AFDC). Energy Efficiency & Renewable Energy, United States Department of Energy. Washington, D.C.

Alberson, D. C., Zimmer, R. A. and Menges, W. L. (1997). *NCHRP Report 350 Compliance Test 5-12 of the 1.07-m Vertical Wall Bridge Railing. (Report No. FHWA-RD-96-199)*. Turner-Fairbank Highway Research Center. Federal Highway Administration. McLean, VA. (Prepared by Texas Transportation Institute (TTI). Texas A&M University System. College Station, TX).

Alicandri, E. (2017). *An Open Letter To All In The Highway Safety Hardware And Roadside Design Community*. U.S. Department of Transportation. Federal Highway Administration. Washington, D.C.

Allen, K. (2010). *The Effectiveness of Underride Guards for Heavy Trailers (Report No. DOT HS 811 37)*. National Highway Traffic Safety Administration. Office of Vehicle Safety. U.S. Department of Transportation, Federal Highway Administration. Washington, D.C.

ASTM. (2008). *ASTM A148/A148M-08: Standard Specification for Steel Castings, High Strength, for Structural Purposes*. ASTM International.

ASTM. (2009). *ASTM A536-84(2009): Standard Specification for Ductile Iron Castings*. ASTM International.

ATA. (2016). *American Trucking Trends*. American Trucking Associations (ATA).

Atahan, A. O. and Cansiz, O. F. (2005). *Impact Analysis of a Vertical Flared Back Bridge Rail-To-Guardrail Transition Structure using Simulation*. Finite Elements in Analysis and Design **41**(4): 371-396.

Bala, S. (2001). *Contact Modeling in LS-DYNA*. Livermore Software Technology Corporation. Livermore, CA.

Bean, J. D., Kahane, C. J., Mynatt, M., Rudd, R. W., Rush, C. J. and Wiacek, C. (2009). *Fatalities in Frontal Crashes Despite Seat Belts and Air Bags – Review of All CDS Cases – Model and Calendar Years 2000-2007 – 122 Fatalities (Report No. DOT HS 811 202)*. National Highway Traffic Safety Administration. Office of Vehicle Safety. U.S. Department of Transportation, Federal Highway Administration. Washington, D.C.

Beason, W. L. and Hirsch, T. J. (1989). *Measurement of Heavy Vehicle Impact Forces and Inertia Properties. (Report No. FHWA/RD-89/120)*. Turner-Fairbank Highway Research Center. Federal Highway Administration. McLean, VA. (Prepared by Texas Transportation Institute (TTI). Texas A&M University System. College Station, TX).

Benson, D. J. and Hallquist, J. O. (1990). *A Single Surface Contact Algorithm for the Post-Buckling Analysis of Shell Structures*. Computer methods in applied mechanics and engineering **78**(2): 141-163.

Blair, M. and Stevens, T. (1995). *Steel Castings Handbook*. Steel Founders' Society of America.

Bligh, R. P. (2001). *NCHRP 22-14: Improvement of the Procedures for the Safety-Performance Evaluation of Roadside Features*. Transportation Research Board. National Cooperative Highway Research Program. National Academies of Sciences, Engineering, and Medicine. Washington, D.C.

Blower, D. and Woodrooffe, J. (2013). *Heavy-Vehicle Crash Data Collection and Analysis to Characterize Rear and Side Underride and Front Override in Fatal Truck Crashes (Report DOT HS 811 725)*. The University of Michigan Transportation Research Institute (UMTRI). Office of Applied Vehicle Safety Research. National Highway Traffic Safety Administration. Washington, D.C.

Bois, P. D., Chou, C. C., Fileta, B. B., Khalil, T. B., King, A. I., Mahood, H. F., Mertz, H. F. and Wismans, J. (2004). *Vehicle Crashworthiness and Occupant Protection*. ,Southfield, MI.

Bronstad, M. E. and Michie, J. D. (1974). *NCHRP Report 153: Recommended Procedures for Vehicle Crash Testing of Highway Appurtenances*. Transportation Research Board. National Cooperative Highway Research Program. National Academies of Sciences, Engineering, and Medicine. Washington, D.C.

Brumbelow, M. L. (2012). *Potential Benefits of Underride Guards in Large Truck Side Crashes*. Traffic Injury Prevention **13**(6): 592-599.

Bullard Jr, D. L., Bligh, R. P., Menges, W. L. and Haug, R. R. (2010). *NCHRP 22-14 (03): Volume I: Evaluation of Existing Roadside Safety Hardware using Updated Criteria—Technical Report*. Transportation Research Board. National Cooperative Highway Research Program. National Academies of Sciences, Engineering, and Medicine. Washington, D.C.

Buth, C., Hirsch, T. and Menges, W. (1997-A). *Testing of New Bridge Rail and Transition Designs. Volume X: Appendix I - 42-in.(1.07-m) Concrete Parapet Bridge Railing. (Report No. FHWA-RD-93-067)*. Turner-Fairbank Highway Research Center. Federal Highway Administration. McLean, VA. (Prepared by Texas Transportation Institute (TTI). Texas A&M University System. College Station, TX).

Buth, C. E., Hirsch, T. J. and Menges, W. L. (1997-B). *Testing of New Bridge Rail and Transition Designs. Volume XI: Appendix J - 42-in (1.07-m) F-Shape Bridge Railing. (Report No. FHWA-RD-93-068)*. Turner-Fairbank Highway Research Center. Federal Highway Administration. McLean, VA. (Prepared by Texas Transportation Institute (TTI). Texas A&M University System. College Station, TX).

Buth, C. E. and Menges, W. L. (1999). *NCHRP Report 350 Test 4-12 of the Modified Thrie Beam Guardrail (Report FHWA-RD-99-065)*. Texas Transportation Institute (TTI). Texas A&M University. College Station, TX.

Campise, W. L. and Buth, C. E. (1986). *Performance Limits of Longitudinal Barrier Systems, Volume III-Appendix B: Details of Full-Scale Crash Tests on Longitudinal Barriers*. Texas Transportation Institute (TTI). Texas A&M University. College Station, TX.

Carrigan, C. E., Ray, M. H. and Ray, A. M. (2017). *Evaluating the Performance of Roadside Hardware*. Transportation Research Board 96th Annual Meeting Compendium of Papers, Transportation Research Board. National Academies of Sciences, Engineering, and Medicine. Washington, D.C.

CEN. (2010). *BS EN 1317-2:2010: Road Restraint Systems. Performance Classes, Impact Test Acceptance Criteria And Test Methods For Safety Barriers Including Vehicle Parapets*. European Committee for Standardization (CEN). British Standards Institution (BSI). London, UK.

Cinar, A. (2012). *Heavy Truck 5th Wheel Modelling Techniques in Finite Element and Their Effect on Stress Distribution*. ASME 2012 11th Biennial Conference on Engineering Systems Design and Analysis.

Clausius, R. A. (2016). *Letter of Eligibility B-267: ArcelorMittal TL5 Steel High Containment Median Barrier - FHWA Federal-Aid Reimbursement Eligibility Process for Safety Hardware Devices*. U.S. Department of Transportation. Federal Highway Administration. Washington, D.C.

Cole, D. J. and Cebon, D. (1992). *Validation of an Articulated Vehicle Simulation*. Vehicle System Dynamics **21**(1): 197-223.

Cook, A. G. M. (2016). *Front Underride Protection Devices: Design Methodology for Heavy Vehicle Crashworthiness* Master of Applied Science in Mechanical Engineering University of Ontario Institute of Technology.

Council, F. M. and Stewart, J. R. (1993). *Attempt to Define Relationship Between Forces to Crash-Test Vehicles and Occupant Injury in Similar Real-world Crashes*. Transportation Research Record (1419)78-85. U.S. Department of Transportation. Federal Motor Carrier Safety Administration. Analysis, Research, and Technology Division. Washington, D.C.

Dhoshi, N. P., Ingole, N. K. and Gulhane, U. D. (2011). *Analysis and Modification of Leaf Spring of Tractor Trailer using Analytical and Finite Element Method*. International Journal of Modern Engineering Research (IJMER) **1**(2): 719-722.

Dobrovolny, C. S., Schulz, N. D., Blower, D. and Benedetti, M. (2015). *Identifying the Potential of Improved Heavy-Truck Crashworthiness to Reduce Death and Injury for Truck Drivers*. Center for Advancing Transportation Leadership and Safety (ATLAS Center). U.S. Department of Transportation. Office of the Assistant Secretary for Research and Transportation. University Transportation Centers Program (DTRT13-G-UTC54).

Faller, R. K. (2017). *AASHTO Accreditation Inter-laboratory Collaborations Participation List* AASHTO-AGC-ARTBA Task Force 13: Subcommittee #7 - Certification of Test Facilities.

Fancher, P. S., Ervin, R. D., Winkler, C. B. and Gillespie, T. D. (1986). *A Factbook of the Mechanical Properties of the Components for Single Unit and Articulated Heavy Trucks. (Report Number: UMTRI86-12).* Texas Transportation Institute(TTI). Texas A&M University System. College Station, TX.

Fang, H., Gutowski, M., Li, N. and DiSogra, M. (2013). *Performance Evaluation of NCDOT W-beam Guardrails under MASH TL-2 Conditions*. North Carolina Department of Transportation. Raleigh, NC.

Fang, H., Gutowski, M., Palta, E., Kuvilla, D., Baker, R. and Li, N. (2015). *Performance Evaluation of 29-inch and 31-inch W-beam Guardrails on Six-lane, 46-foot Median Divided Freeways*. North Carolina Department of Transportation. Raleigh, NC.

Fang, H., Li, N., DiSogra, M., Gutowski, M. and Weggel, D. C. (2012). *Recommendations for Placement of Cable Median Barriers on 6:1 and 4:1 Sloped Medians with Horizontal Curvatures*. North Carolina Department of Transportation. Raleigh, NC.

Fang, H., Li, N. and Tian, N. (2010). *Median Barrier Placement on Six-lane, 46-Foot Median Divided Freeways*. North Carolina Department of Transportation. Raleigh, NC.

Fang, H., Weggel, D. C., Bi, J. and Martin, M. E. (2009). *Finite Element Evaluation of Two Retrofit Options to Enhance the Performance of Cable Median Barriers*. North Carolina Department of Transportation. Raleigh, NC.

FAST. (2015). *Fixing America's Surface Transportation Act (FAST Act).* . Public Law 114 - 94; 114th United States Statutes at Large; Page 1311.

FEDERAL. (1956). *Federal Aid Highway Act of 1956*. Public Law 84-627; 70th United States Statutes at Large; Page 374.

FEDERAL. (1974). *Federal-Aid Highway Amendments of 1974*. Public Law 93-643; 88th United States Statutes at Large; Page 2281.

Fiacco, A. V. and McCormick, G. P. (1964). *The Sequential Unconstrained Minimization Technique for Nonlinear Programing, a Primal-dual Method*. Management Science **10**(2): 360-366.

Fiacco, A. V. and McCormick, G. P. (1966). *Extensions of SUMT for Nonlinear Programming: Equality Constraints and Extrapolation*. Management Science **12**(11): 816-828.

Friedman, K., Bui, K., Hutchinson, J., Stephens, M. and Gonzalez, F. (2016). *Advanced Heavy Truck Frame Design and Opportunities for Fuel System Impact Protection*. SAE Technical Paper 2016-01-8049. Society of Automotive Engineers (SAE).

Gadala, M. E., Elmadany, M. M. and Gadala, M. S. (1986). *Finite Element and Analytical Modelling of a Tractor-semitrailer Vehicle*. Computers & Structures **23**(6): 831-836.

Galipeau-Bélair, P., El-Gindy, M., Ghantae, S., Critchley, D. and Ramachandra, S. (2013). *Development of a Regulation for Testing the Effectiveness of a Rigid Side Underride Protection Device (SUPD)*. International Journal of Crashworthiness **19**(1): 89-103.

GAO. (1996). *CFR 571.121 - FMVSS No. 121; Air Brake Systems.* U.S. Government Accountability Office (U.S. GAO). Washington, D.C. **5**(49): 374-396.

GAO. (1998). *CFR 393.55 - Antilock brake systems*. U.S. Government Accountability Office (U.S. GAO). Washington, D.C. **5**(49): 411-412.

GAO. (2005). *Report to Congressional Committees: Large Truck Safety : Federal Enforcement Efforts Have Been Stronger Since 2000, But Oversight of State Grants Needs Improvement*. U.S. Government Accountability Office (U.S. GAO). Washington, D.C.

GAO. (2015-A). *49 CFR Part 571.136 - FMVSS 136: Electronic Stability Control Systems for Heavy Vehicles - Final Rule. (Docket No. NHTSA-2015-0056)*. U.S. Government Accountability Office (U.S. GAO). Washington, D.C. **80**(120): 36049-36110.

GAO. (2015-B). *49 CFR 571 - FMVSS - Automatic Emergency Braking (Docket No. NHTSA-2015-0099)*. U.S. Government Accountability Office (U.S. GAO). Washington, D.C. **80**(200): 62487-62488.

GAO. (2016). *FMVSS; FMCSR; Parts and Accessories Necessary for Safe Operation; Speed Limiting Devices*. U.S. Government Accountability Office (U.S. GAO). Washington, D.C. **81**(173): 61942-61972.

Ghodake, A. P. and Patil, K. N. (2013). *Analysis of Steel and Composite Leaf Spring for Vehicle*. IOSR Journal of Mechanical and Civil Engineering (IOSR-JMCE) **5**(4): 68-76.

Hallquist, J. O. (1976). *Preliminary User's Manuals for DYNA3D and DYNAP (Nonlinear Dynamic Analysis of Solids in Three Dimensions)*. Lawrence Livermore National Laboratory. Livermore, CA.

Hallquist, J. O. (2017). *LS-DYNA Theory Manual Rev. 8339.* Livermore Software Technology Corporation. Livermore, CA.

Hallquist, J. O., Goudreau, G. L. and Benson, D. J. (1985). *Sliding Interfaces with Contact-impact in Large-scale Lagrangian Computations*. Computer methods in applied mechanics and engineering **51**(1-3): 107-137.

Hirsch, T. and Fairbanks, W. L. (1984). *Bridge Rail to Restrain and Redirect 80,000-lb Trucks (Report No. 2-15D-83-911)*. Texas State Department of Highways & Public Transportation. Austin, TX. (Prepared by Texas Transportation Institute (TTI). Texas A&M University System. College Station, TX).

Hirsch, T. J., Fairbanks, W. L. and Buth, C. E. (1986). *Concrete Safety Shape with Metal Rail on Top to Redirect 80,000-lb Trucks (Report No. FHWA/TX-83)*. Texas State Department of Highways & Public Transportation. Austin, TX. (Prepared by Texas Transportation Institute (TTI). Texas A&M University System. College Station, TX)(HS-039 939).

Högberg, D. (2001). *Use of Finite Element Method in Trailer Deck Design*. Journal of Materials Processing Technology **117**(1): 238-243.

Hoge, K. (1996). *Influence of Strain Rate on Mechanical Properties Of 6061-T6 Aluminum under Uniaxial and Biaxial States of Stress*. Experimental Mechanics **6**(4): 204-211.

HRB. (1962). *HRB Circular 482: Proposed Full Scale-testing Procedures for Guardrails*. Highway Research Correlation Service Circular 482. Highway Research Board. Washington, D.C.

Hubbell, J. (2012). *Transportation Research Circluar E-C172: Can EN 1317 and NCHRP 350–MASH Be Used Interchangeably?* Roadside Safety Design and Devices International Workshop. Milan, Italy.

Ibrahim, I. M. (1999). *Finite Element Multibody System Control of Tractor Semi-Trailers with Active Suspension and Controller Time Delay*. SAE Technical Paper 1999-01-0726. International Congress & Exposition. Society of Automotive Engineers (SAE).

Ibrahim, I. M. (2004). *A Generally Applicable 3D Truck Ride Simulation with Coupled Rigid Bodies and Finite Element Models*. International Journal of Heavy Vehicle Systems **11**(1): 67-85.

IIHS. (2017). *IIHS Tests Show Benefits of Side Underride Guards for Semitrailers*. Insurance Institute for Highway Safety (IIHS). Arlington, VA.

Kawabe, T. and Kawai, S. (1973). *Brake Pressure Regulator*. Aisin Seiki Kabushiki Kaisha, Japan, United States Patent and Trademark Office. Washington, D.C.

Kikuchi, N. and Oden, J. T. (1988). *Contact Problems in Elasticity: A Study of Variational Inequalities and Finite Element Methods*. Society for Industrial and Applied Mathematics (SIAM).

Kirkpatrick, S. W., Simons, J. W. and Antoun, T. H. (1999). *Development and Validation of High Fidelity Vehicle Crash Simulation Models*. International Journal of Crashworthiness **4**(4): 395-406.

Kurdi, O., Rahman, R. A. and Tamin, M. N. (2008). *Stress Analysis of Heavy Duty Truck Chassis using Finite Element Method*. 2nd Regional Conference on Vehicle Engineering & Technology. Kuala Lumpur.

Lakshmi, B. V. and Satyanarayana, I. (2012). *Static and Dynamic Analysis on Composite Leaf Spring in Heavy Vehicle*. International Journal of Advanced Engineering Research and Studies **2**(1): 80-84.

Laursen, T. A. (2003). *Computational Contact and Impact Mechanics: Fundamentals of Modelling Interfacial Phenomena in Nonlinear Finite Element Analysis*. Meccanica **38**(3): 393-394.

Li, H., Kwasniewski, L., Malachowski, J. and Wekezer, J. (2006). *Development of Finite Element Models of Heavy Vehicles*. 9th International Symposium on Heavy Vehicle Weights and Dimensions. International Forum for Road Transport Technology.

LSTC. (2017). *LS-DYNA Keyword User's Manual, Volume I, Version R9.0 (r:7883)*. Livermore Software Technology Corporation. Livermore, CA.

Magoci, J. (2017). *The Rise of Semi Trailer Trucks – History and Industry Impact.* FuelLoyal Inc. Bloomingdale, Il.

Mak, K. K., Beason, W. L., Hirsch, T. J. and Campise, W. L. (1988). *Oblique Angle Crash Tests of Loaded Heavy Trucks into an Instrumented Wall. (Report No. DOT HS 807 256).* Texas Transportation Institute (TTI). Texas A&M University. College Station, TX.

Mak, K. K. and Campise, W. L. (1990). *Test and Evaluation of Ontario 'Tall Wall' Barrier with an 80,000-pound Tractor-trailer. (Project No. 4221-9089-534).* Texas Transportation Institute (TTI). Texas A&M University. College Station, TX.

MAP-21. (2012). *Moving Ahead for Progress in the 21st Century Act (MAP-21).* U.S. Department of Transportation. Federal Highway Administration. Washington, D.C.

Marzougui, D. (2003). *Freightliner into 42 in. F-Shape Concrete Barrier at 25 Degrees. (Report No. 03008).* Federal Outdoor Impact Laboratory (FOIL). National Crash Analysis Center (NCAC). McLean, VA.

Marzougui, D., Mohan, P., Kan, C. and Opiela, K. (2007). *Performance evaluation of low-tension three-strand cable median barriers.* Transportation Research Record: Journal of the Transportation Research Board(2025): 34-44.

Marzougui, D., Samaha, R. R., Cui, C., Kan, C. and Opiela, K. S. (2012). *Extended Validation of the Finite Element Model for the 2010 Toyota Yaris Passenger Sedan. (Report # NCAC 2011-T-001).* National Crash Analysis Center, George Washington University, Washington, DC.

MatWeb. (2009). *MatWeb: material property data.* Automation Creations Inc. <matweb.com>.

Michie, J. D. (1981). *Collision Risk Assessment Based on Occupant Flail-space Model.* Transportation Research Record (796)1-9. U.S. Department of Transportation. Federal Motor Carrier Safety Administration. Analysis, Research, and Technology Division. Washington, D.C.

Michie, J. D. (1981). *NCHRP Report 230: Recommended Procedures for the Safety Performance Evaluation of Highway Appurtenances.* Transportation Research Board. National Cooperative Highway Research Program. National Academies of Sciences, Engineering, and Medicine. Washington, D.C.

Miele, C. R., Plaxico, C., Stephens, D. and Simonovic, S. (2010). *U26: Enhanced Finite Element Analysis Crash Model of Tractor-Trailers (Phase C).* NTRCI University Transportation Center. U.S. Department of Transportation Research and Innovative Technology Administration Grant #DTRT06G-0043. Federal Highway Administration Purchase Order #DTFH61-07-P-00235.

Mohan, P., Marzougui, D., Meczkowski, L. and Bedewi, N. (2005). *Finite Element Modeling and Validation of a 3-Strand Cable Guardrail System*. International Journal of Crashworthiness **10**(3): 267-273.

Moosbrugger, C. (2002). *Atlas of Stress-Strain Curves - 2nd Edition*. ASM International Technical Book Committee. ASM International. Materials Park, OH.

MOTOR. (1935). *Motor Carrier Act of 1935*. Public Law 74-255; 49th United States Statutes at Large. Page 543.

MOTOR. (1980). *Motor Carrier Act of 1980*. Public Law 96-296. 94th United States Statutes at Large. Page 793.

MOTOR. (1999). *Motor Carrier Safety Improvement Act of 1999*. Public Law 106-159; 113th United States Statutes at Large; Page 1748.

Mullins, J. D. (1990). *Ductile Iron Data for Design Engineers*. Ductile Iron Data Society, Soremetal Technical Services, Rio Tinto Iron & Titanium Inc.: 5.7-5.16.

Nawrocki, A. and Labrosse, M. (2000). *A Finite Element Model for Simple Straight Wire Rope Strands*. Computers & Structures **77**(4): 345-359.

NCDOT. (2002). *Roadway Design Manual*. North Carolina Department of Transportation, Raleigh, NC.

NCDOT. (2012). *Roadway Standard Drawings*. North Carolina Department of Transportation, Raleigh, NC.

NCSA. (2016). *Summary of Motor Vehicle Crashes (Early Edition): 2015 Data; Traffic Safety Facts. (Report No. DOT HS 812 376)*. National Highway Traffic Safety Administration. National Center for Statistics and Analysis. U.S. Department of Transportation, Federal Highway Administration. Washington, D.C.

NHSTA. (2015-A). *Preliminary Regulatory Evaluation: FMVSS No. 223 Rear Impact Guards and FMVSS No. 224 Rear Impact Protection* National Highway Traffic Safety Administration. Office of Regulatory Analysis and Evaluation. National Center for Statistics and Analysis. U.S. Department of Transportation, Federal Highway Administration. Washington, D.C.

NHSTA. (2015-B). *The Need for Additional Heavy Truck Crashworthiness Standards. The Moving Ahead for Progress in the 21st Century Act (MAP-21) Report to the House Committee on Transportation and Infrastructure and the Senate Committee on Commerce, Science, and Transportation* National Highway Traffic Safety Administration. U.S. Department of Transportation, Federal Highway Administration. Washington, D.C.

NHSTA. (2015-C). *Truck Crashworthiness Data Special Study (APPENDIX). The Moving Ahead for Progress in the 21st Century Act (MAP-21) Report to the House Committee on Transportation and Infrastructure and the Senate Committee on Commerce, Science, and Transportation.* National Highway Traffic Safety Administration. U.S. Department of Transportation, Federal Highway Administration. Washington, D.C.

Nicholas, T. (1981). *Tensile Testing of Materials at High Rates of Strain.* Experimental Mechanics **21**(5): 177-185.

NSC. (2015). *Injury Facts 2015 Edition.* Research and Safety Management Solutions Group, National Safety Council, Itasca, IL.

Opiela, K., Kan, S. and Marzougui, D. (2007). *Development of a Finite Element Model for W-Beam Guardrails (No. NCAC 2007-T-004).* National Highway Traffic Safety Administration. National Center for Statistics and Analysis. U.S. Department of Transportation, Federal Highway Administration. Washington, D.C.

Parnell, T. K., White, C. V. and Day, S. E. (1999). *Finite Element Simulation of 180° Rollover For Heavy Truck Vehicles.* Exponent Failure Analysis Associates. Menlo Park, CA.

Paul, I. D., Sarange, S. M., Bhole, G. P. and Chaudhari, J. R. (2012). *Structural Analysis of Truck Chassis using Finite Element Method.* International Journal of Multidisciplinary Research and Advances in Engineering (IJMRAE) **4**: 85-98.

Plaxico, C., Kennedy, J., Simonovic, S. and Zisi, N. (2007). *U01: Enhanced Finite Element Analysis Crash Model of Tractor-Trailers (Phase A).* NTRCI University Transportation Center. U.S. Department of Transportation Research and Innovative Technology Administration Grant #DTRT06G-0043.

Plaxico, C., Miele, C. R., Kennedy, J., Simonovic, S. and Zisi, N. (2009). *U08: Enhanced Finite Element Analysis Crash Model of Tractor-Trailers (Phase B).* NTRCI University Transportation Center. U.S. Department of Transportation Research and Innovative Technology Administration Grant #DTRT06G-0043. Federal Highway Administration Purchase Order #DTFH61-07-P-00235.

Plaxico, C. A. and Ray, M. H. (2015). *Impact and Quasi-Static Pier Capacity.* NCHRP 12-90 Guidelines for Shielding Bridge Piers - Ongoing Project. AASHTO Subcommittee on Bridges and Structures Annual Meeting. Roadsafe LLC.

Polivka, K. A., Faller, R. K., Holloway, J. C., Rohde, J. R. and Sicking, D. L. (2005). *Development, Testing, and Evaluation of NDOR's TL-5 Aesthetic Open Concrete Bridge Rail. (Report No. TRP-03-148-05).* Midwest Roadside Safety Facility (MwRSF), University of Nebraska-Lincoln. Lincoln, NE.

Ray, M. H., Plaxico, C. A. and Carrigan, C. E. (2012). *NCHRP 12-90: Guidelines for Shielding Bridge Piers*. Transportation Research Board. National Cooperative Highway Research Program. National Academies of Sciences, Engineering, and Medicine. Washington, D.C.

Rosenbaugh, S. K., Schmidt, J. D., Larsen, H. P., Faller, R. K. and Pankratz, A. (2016). *Development and Testing of the Manitoba Constrained Width Tall Wall Barrier*. Transportation Research Record: Journal of the Transportation Research Board(2638): 55-64.

Rosenbaugh, S. K., Sicking, D. L. and Faller, R. K. (2007). *Development of a TL-5 Vertical Faced Concrete Median Barrier Incorporating Head Ejection Criteria. (Report No. TRP-030194-07)*. Midwest Roadside Safety Facility (MwRSF), University of Nebraska-Lincoln. Lincoln, NE.

Ross Jr, H. E., Sicking, D. L., Zimmer, R. A. and Michie, J. D. (1993). *NCHRP Report 350: Recommended Procedures for the Safety Performance Evaluation of Highway Features* Transportation Research Board. National Cooperative Highway Research Program. National Academies of Sciences, Engineering, and Medicine. Washington, D.C.

SAE. (1997). *Heavy Truck Crashworthiness Cooperative Research Project CRP-013*. Society of Automobile Engineers (SAE) International.

Saez, D., Maddah, L., Bligh, R., Mirdamadi, A. and Briaud, J.-L. (2015). *Full Scale Crash Test of a 36-Ton Truck Against a Barrier on Top of an MSE Wall*. International Foundations Congress and Equipment Expo (IFCEE) 2015 **GSP**(256): 2462-2471.

Shoffner, B., Allen, J., El-Gindy, M., Evenson, W. and Scaglione, M. A. (2007). *Prediction of Kingpin/Fifthwheel Forces for Tractor-Semitrailers During Typical Operating Maneuvers*. ASME 2007 International Design Engineering Technical Conferences and Computers and Information in Engineering Conference. American Society of Mechanical Engineers: 1027-1040.

Shoffner, B. W. (2008). *Development and Validation of a Finite Element Analysis Model Used to Analyze Coupling Reactions Between a Tractor's Fifthwheel and a Semitrailer's Kingpin*. Mechanical Engineering Pennsylvania State University.

Sicking, D. L. (2008). *NCHRP 22-14(02): Improved Procedures for Safety-Performance Evaluation of Roadside Features*. Transportation Research Board. National Cooperative Highway Research Program. National Academies of Sciences, Engineering, and Medicine. Washington, D.C.

Sicking, D. L., Mak, K. K., Rohde, J. R. and Reid, J. D. (2009). *Manual For Assessing Safety Hardware (MASH)*. American Association of State Highway and Transportation Officials (AASHTO). Washington, D.C.

Smith, S. (2017). *FMCSA Research Activities: Update on FAST Act Projects, Planned Research, and NAS Recommendations*. Transportation Research Board Forum Presentation. U.S. Department of Transportation. Federal Motor Carrier Safety Administration. Analysis, Research, and Technology Division. Washington, D.C.

STAA. (1982). *Highway Improvement Act of 1982. (Surface Transportation Assistance Act of 1982)*. Public Law 97-424; 96th United States Statutes at Large; Page 2097.

Stelzmann, U. (2012). *Robust and Efficient Contact Modeling in LS-DYNA: How Good are the New Options?* 30th CADFEM ANSYS Simulation Conference: The Simulation Driven Product Development Conference. Kassel, Germany.

Suh, M. W., Park, Y. K. and Kwon, S. J. (2002). *Braking Performance Simulation for a Tractor-Semitrailer Vehicle With an Air Brake System*. Proceedings of the Institution of Mechanical Engineers, Part D: Journal of Automobile Engineering **216**(1): 43-54.

Szurgott, P., Kwaśniewski, L. and Wekezer, J. W. (2010). *Example of Experimental Validation and Calibration of a Finite Element Model of a Heavy Vehicle*. Journal of KONES Powertrain and Transport. **17**(1): 433-440.

Tobler, W. E. and Krauter, A. I. (1972). *Tractor-Semitrailer Dynamics: Design of the Fifth Wheel*. Vehicle System Dynamics **1**(2): 123-160.

Tohti, G., Mahemuti, D. and Tursun, M. (2012). *Finite Element Analysis to Stringer of a Semi-Trailer*. Key Engineering Materials **522**: 400-405.

URL1. *<truckingnewsonline.com/news/detroit-diesel-starts-production-on-integrated-truck-powertrain/6293/>*.

USDOT. (1998). *ACTION: National Cooperative Highway Research Program (NCHRP) Report 350 Hardware Compliance Dates*. U.S. Department of Transportation. Federal Highway Administration. Washington, D.C.

USDOT. (2016). *AASHTO/FHWA Joint Implementation Agreement for Manual for Assessing Safety Hardware (MASH)*. U.S. Department of Transportation. Federal Highway Administration. Washington, D.C.

Vallejo, R. (2008). *Full Frame Fatigue Test on Heavy Trucks and their Set up Using Finite Element Simulation*. SAE Technical Paper 2008-01-2667. Commercial Vehicle Engineering Congress & Exhibition. Society of Automotive Engineers (SAE).

Walton, C. and Opar, T. (1981). *Iron Castings Handbook*. Iron Castings Society, Inc.

WHO. (2015). *Global Status Report on Road Safety 2015*. World Health Organization. Geneva, Switzerland.

Williams, A. F. and Lund, A. K. (1986). *Seat Belt Use Laws and Occupant Crash Protection in the United States*. American journal of public health **76**(12): 1438-1442.

Williams, W. F., Ries, J., Bligh, R. and Odell, W. (2015). *Design & Full Scale Testing of Aesthetic TXDOT Type T224 Bridge Rail for MASH TL-5 Applications (TRB committee AFB00 Section)*. Transportation Research Board Paper. National Academies of Sciences, Engineering, and Medicine. Washington, D.C.

Woodrooffe, J., Blower, D., Flannagan, C. A. C., Bogard, S. E. and Bao, S. (2013). *Effectiveness of a Current Commercial Vehicle Forward Collision Avoidance and Mitigation Systems*. SAE Technical Paper 2013-01-2394. Society of Automotive Engineers (SAE) International.

Yarmohamadi, H. and Berbyuk, V. (2013). *Kinematic and Dynamic Analysis of a Heavy Truck with Individual Front Suspension*. Vehicle System Dynamics **51**(6): 877-905.

Zhong, Z.-H. and Mackerle, J. (1992). *Static Contact Problems—A Review*. Engineering Computations **9**(1): 3-37.

APPENDIX A: MAXIMUM DYNAMIC DEFLECTIONS
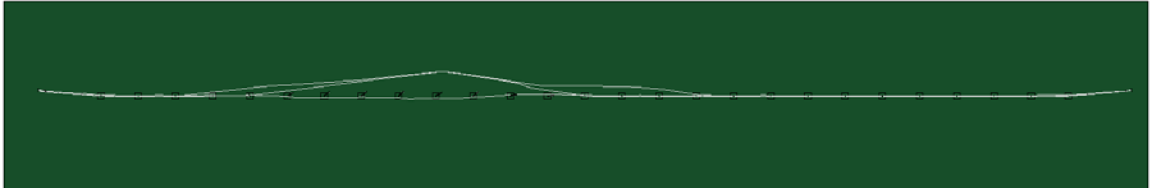
Figure A.1: Case *a*: maximum dynamic deflection, 10.7 ft (3.3 m), for the flat
median three-CMB front-side impact
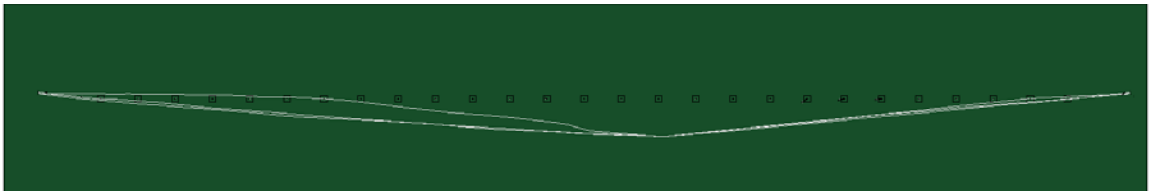
Figure A.2: Case *b*: maximum dynamic deflection, 16.5 ft (5.0 m), for the flat
median three-CMB backside impact
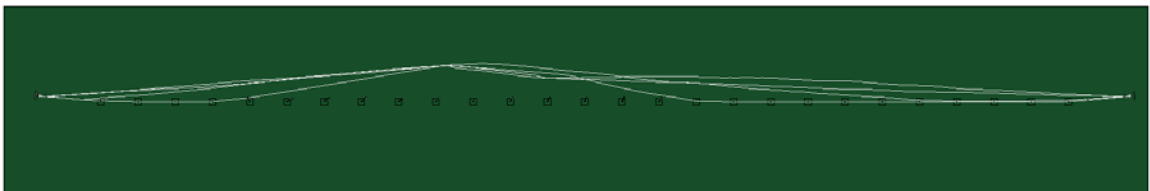
Figure A.3: Case *c*: maximum dynamic deflection, 16.5 ft (5.0 m), for the flat
median four-CMB front-side impact
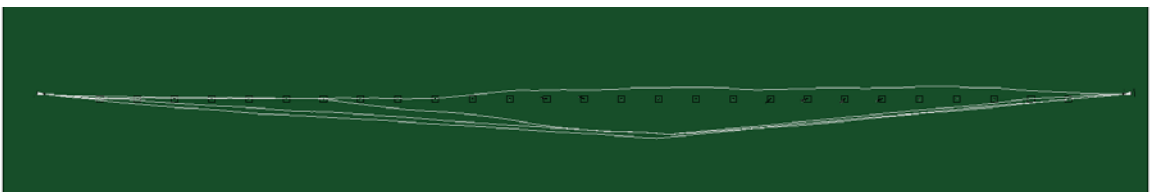
Figure A.4: Case *d*: maximum dynamic deflection, 16.8 ft (5.1 m), for the flat
median four-CMB backside impact

Figure A.5: Case *e*: maximum dynamic deflection, 22.2 ft (6.8 m), for the sloped median three-CMB front-side impact
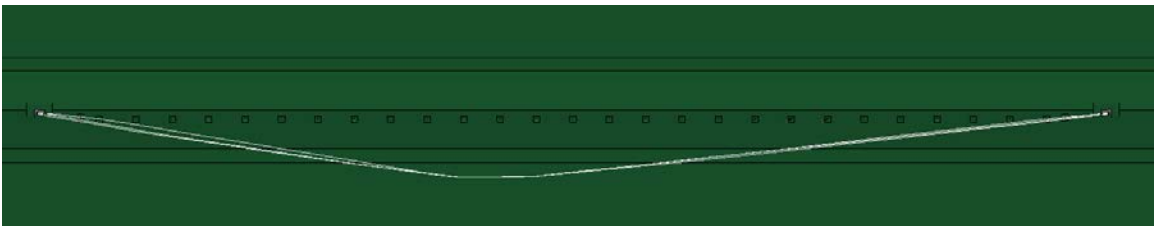
Figure A.6: Case *f*: maximum dynamic deflection, 25.8 ft (7.9 m), for the sloped median three-CMB backside impact
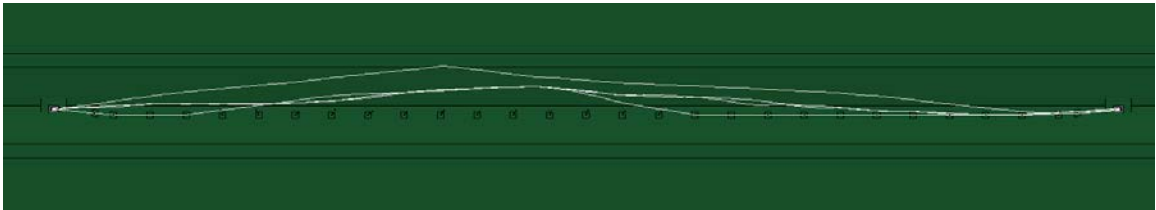
Figure A.7: Case *g*: maximum dynamic deflection, 21.7 ft 6.6 m), for the sloped median four-CMB front-side impact

Figure A.8: Case *h*: maximum dynamic deflection, 22.4 ft (6.8 m), for the sloped median four-CMB backside impact

Figure A.9: Case *i*: maximum dynamic deflection, 8.6 ft (2.6 m), for the flat median W-beam guardrail front-side impact
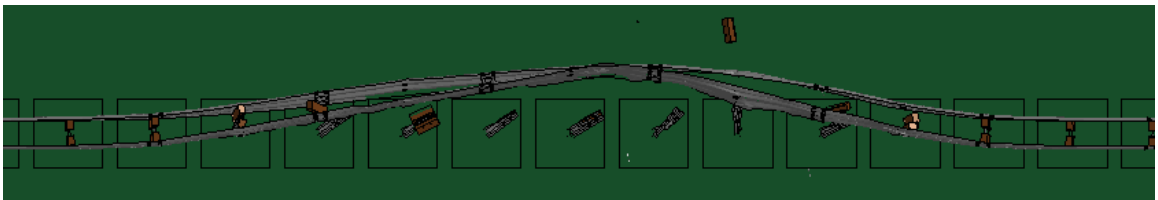
Figure A.10: Case *j*: maximum dynamic deflection, 6.3 ft (1.9 m), for the flat median wood-blockout Thrie-beam guardrail front-side impact
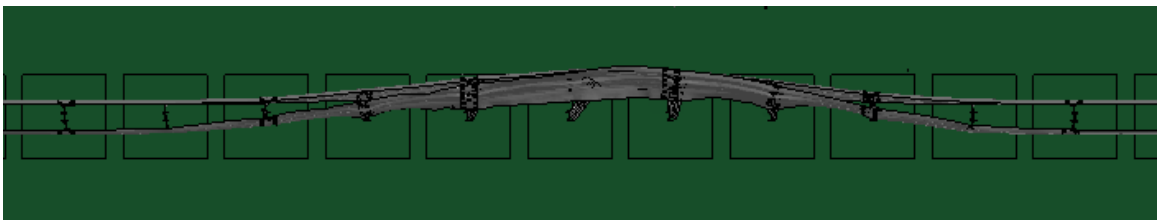
Figure A.11: Case *k*: maximum dynamic deflection, 3.9 ft (1.2 m), for the flat median steel-blockout Thrie-beam guardrail front-side impact
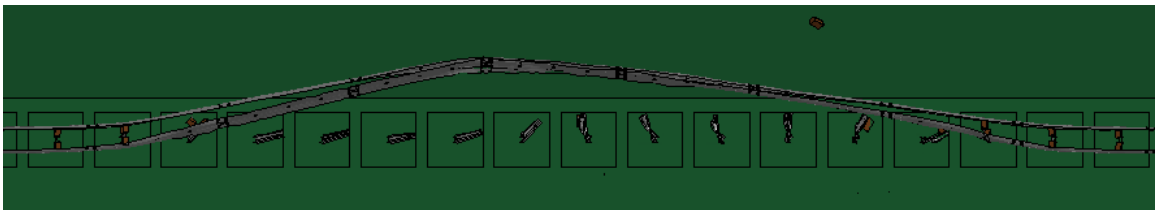
Figure A.12: Case *l*: maximum dynamic deflection, 8.6 ft (2.6 m), for the sloped median W-beam guardrail front-side impact
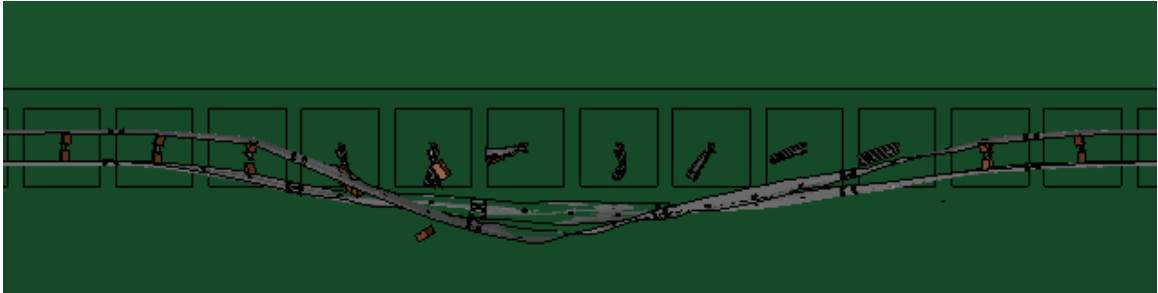
Figure A.13: Case *m*: maximum dynamic deflection, 7.5 ft (2.3 m), for the
sloped median W-beam guardrail backside impact
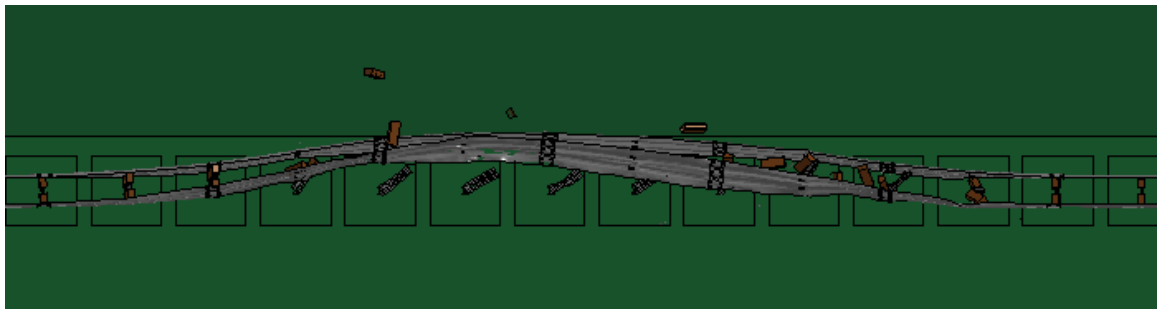
Figure A.14: Case *n*: maximum dynamic deflection, 5.0 ft (1.5 m), for the sloped
median wood-blockout Thrie-beam guardrail front-side impact
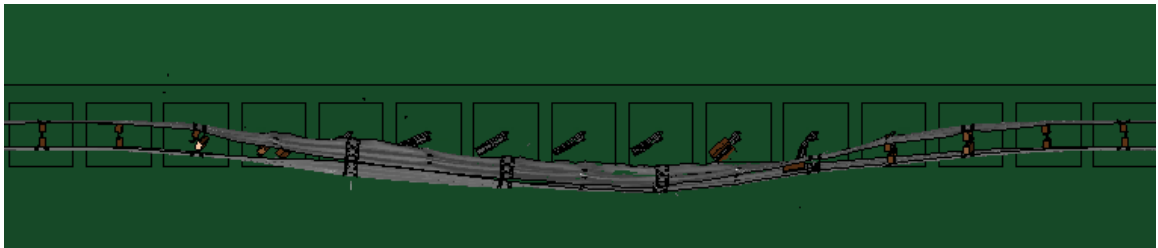
Figure A.15: Case *o*: maximum dynamic deflection, 5.2 ft (1.6 m), for the sloped
median wood-blockout Thrie-beam guardrail backside impact
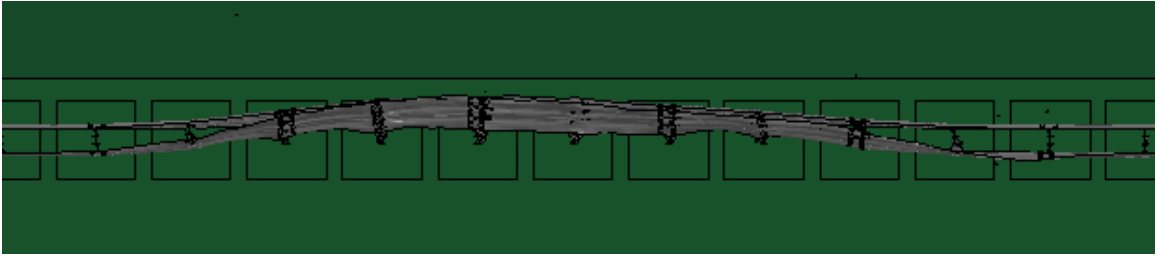
Figure A.16: Case *p*: maximum dynamic deflection, 3.7 ft (1.1 m), for the sloped median steel-blockout Thrie-beam guardrail front-side impact
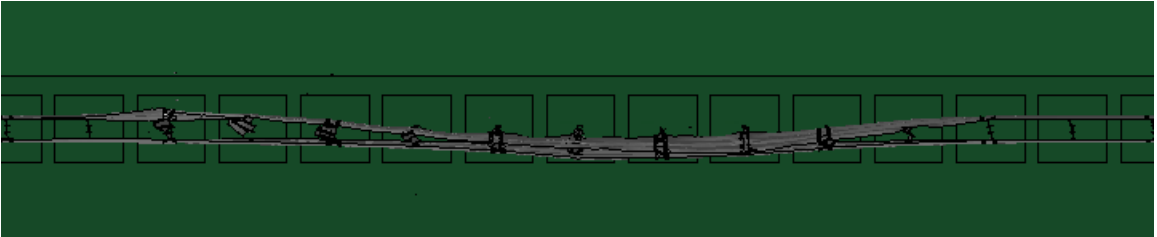
Figure A.17: Case *q*: maximum dynamic deflection, 2.6 ft (0.8 m), for the sloped median steel-blockout Thrie-beam guardrail backside impact

APPENDIX B: YAW, PITCH, AND ROLL ANGLES

a. Tractor cabin CG

b. Trailer tandem axle
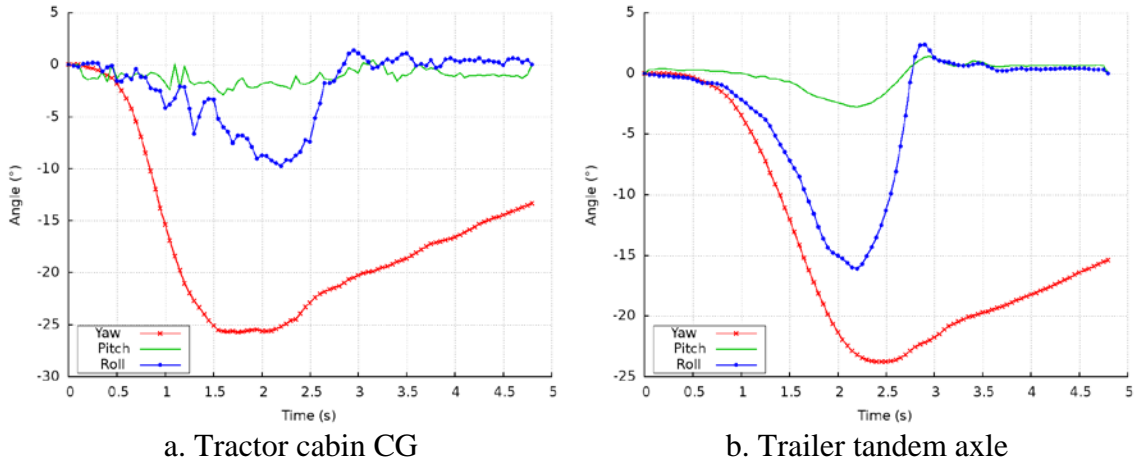
Figure B.1: Case *a*: yaw, pitch, and roll angles for the flat median three-CMB front-side impact

a. Tractor cabin CG

b. Trailer tandem axle
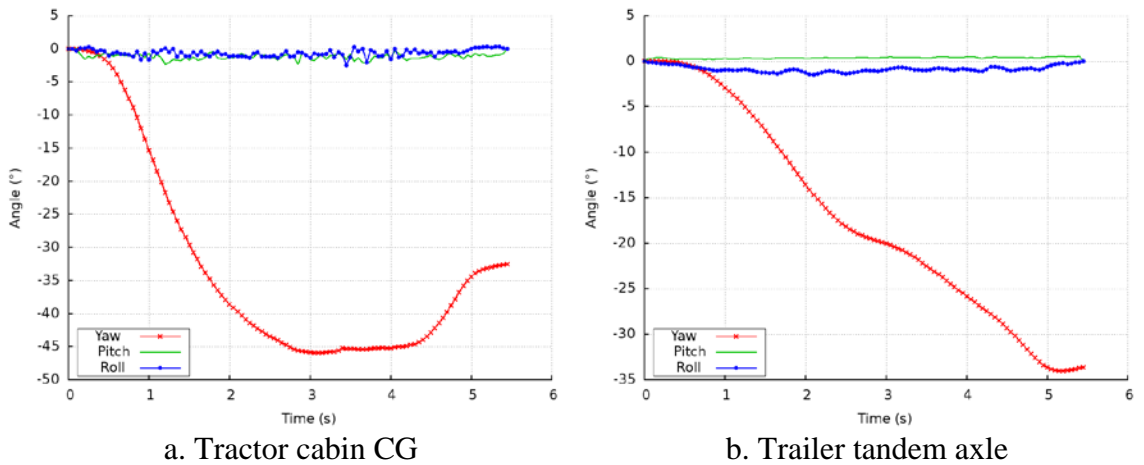
Figure B.2: Case *b*: yaw, pitch, and roll angles for the flat median three-CMB backside impact
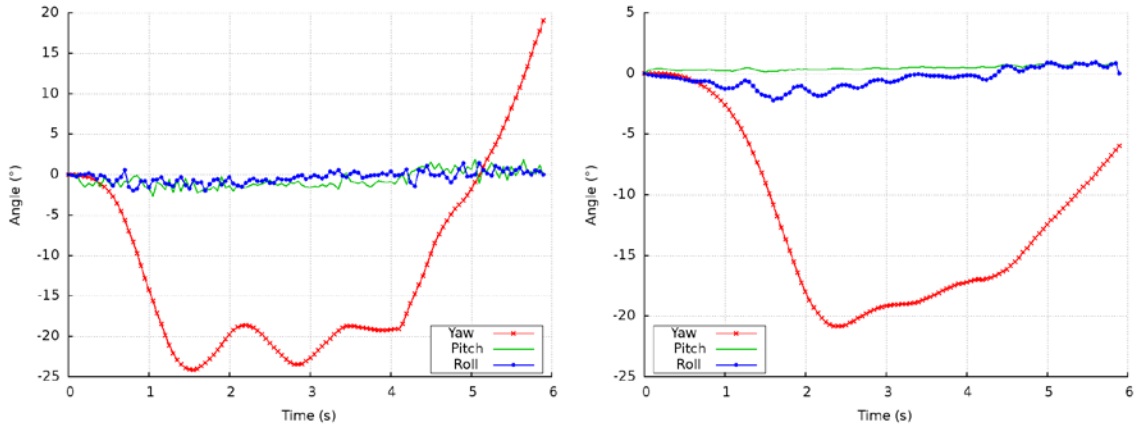
a. Tractor cabin CG   b. Trailer tandem axle

Figure B.3: Case *c*: yaw, pitch, and roll angles for the flat median four-CMB front-side impact
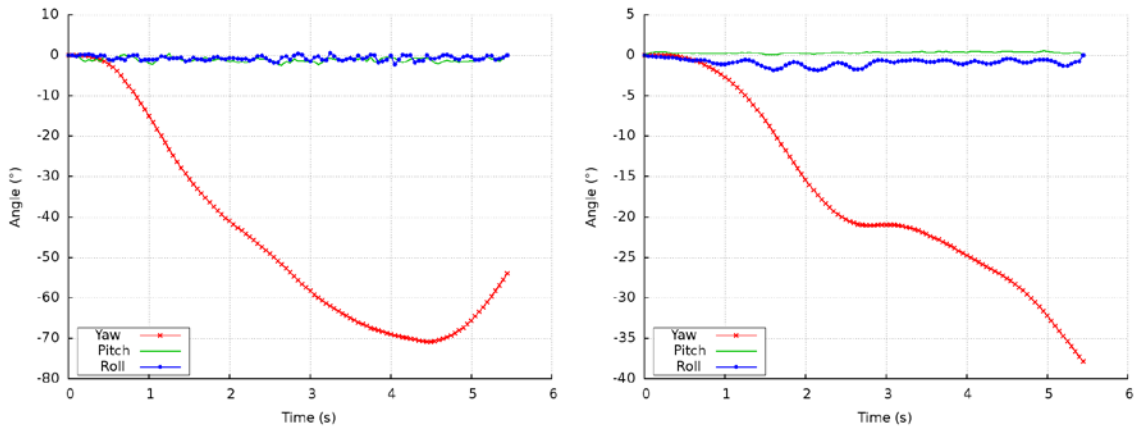
a. Tractor cabin CG   b. Trailer tandem axle

Figure B.4: Case *d*: yaw, pitch, and roll angles for the flat median four-CMB backside impact
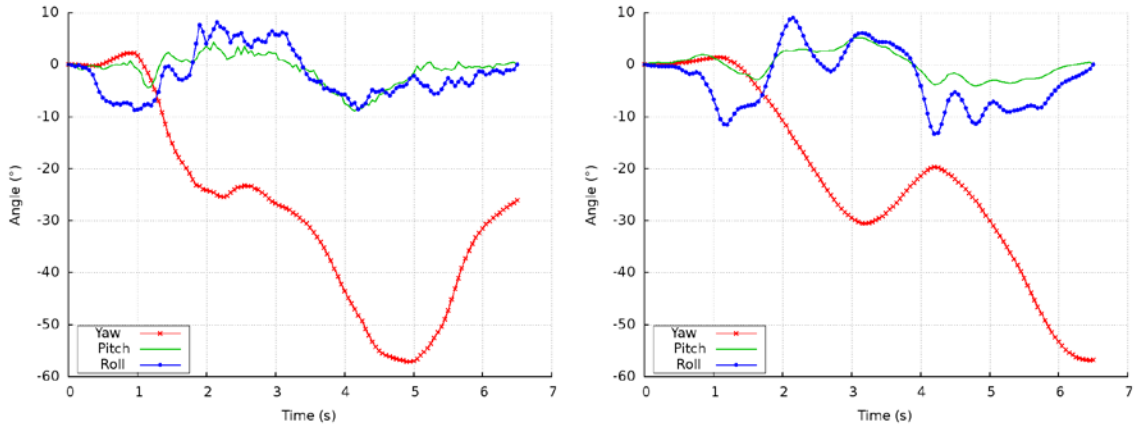
a. Tractor cabin CG   b. Trailer tandem axle

Figure B.5: Case *e*: yaw, pitch, and roll angles for the sloped median three-CMB
front-side impact
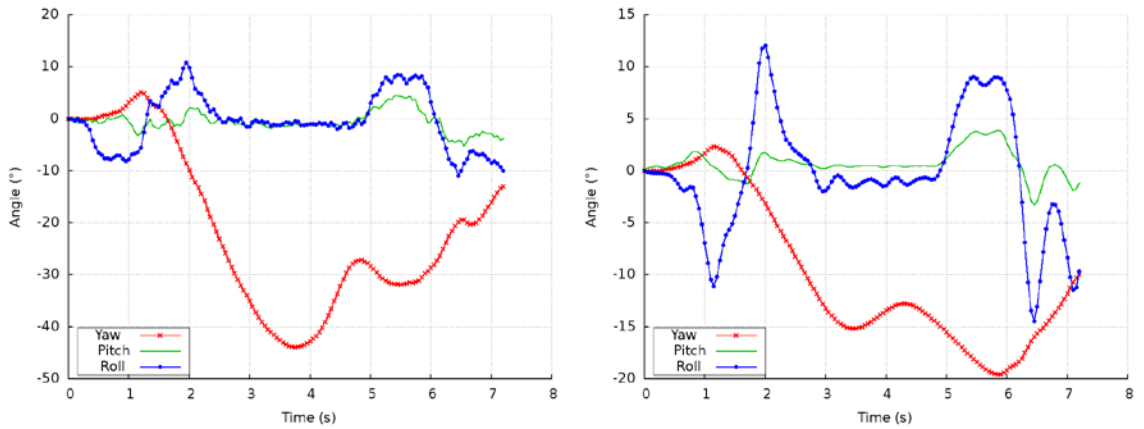
a. Tractor cabin CG   b. Trailer tandem axle

Figure B.6: Case *f*: yaw, pitch, and roll angles for the sloped median three-CMB
backside impact
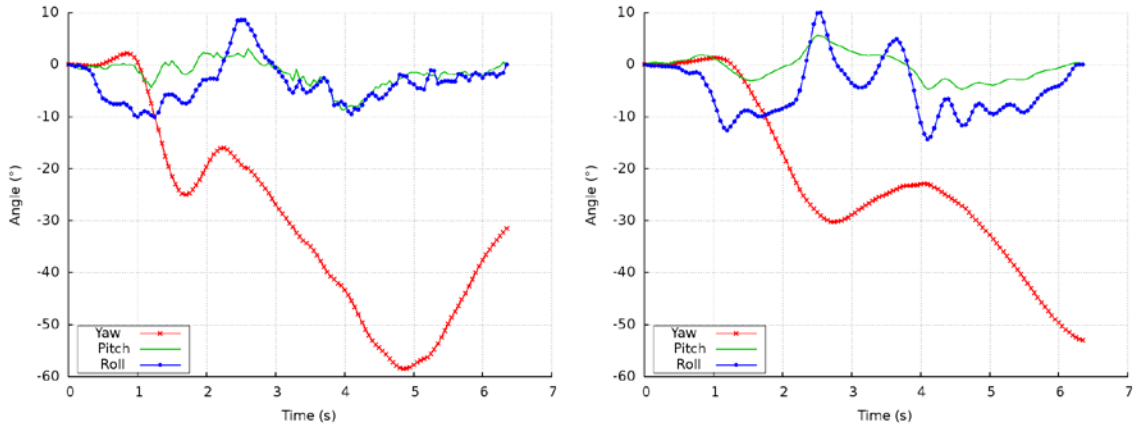
a. Tractor cabin CG   b. Trailer tandem axle

Figure B.7: Case *g*: yaw, pitch, and roll angles for the sloped median four-CMB
front-side impact
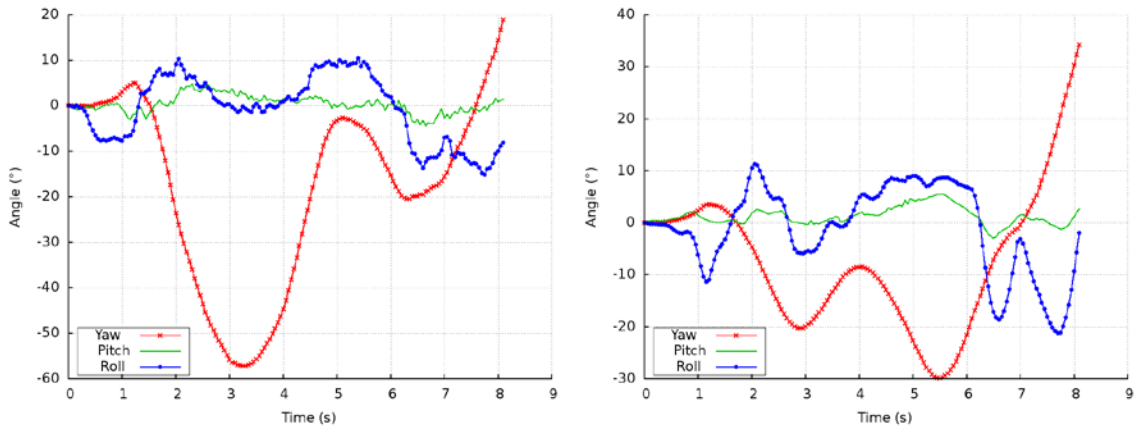
a. Tractor cabin CG   b. Trailer tandem axle

Figure B.8: Case *h*: yaw, pitch, and roll angles for the sloped median four-CMB
backside impact
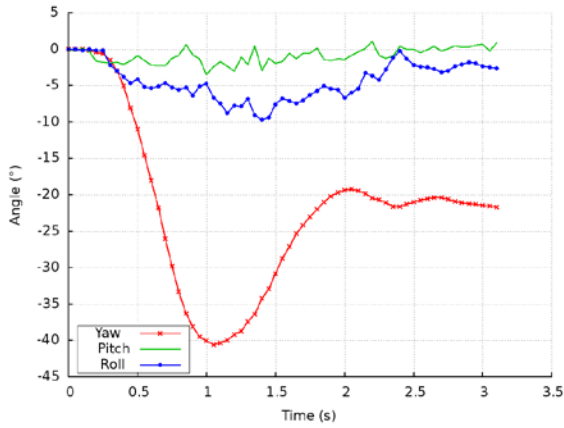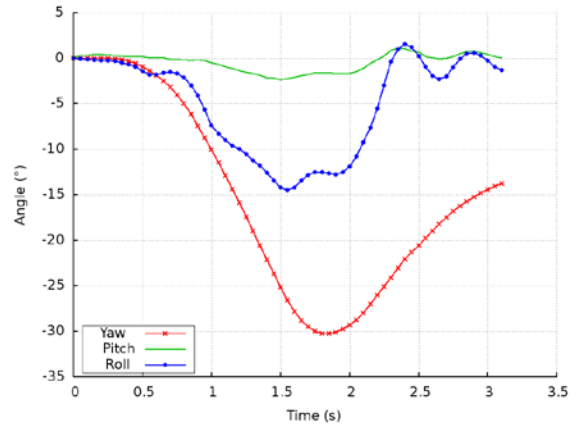
a. Tractor cabin CG

b. Trailer tandem axle

Figure B.9: Case *i*: yaw, pitch, and roll angles for the flat median W-beam guardrail front-side impact
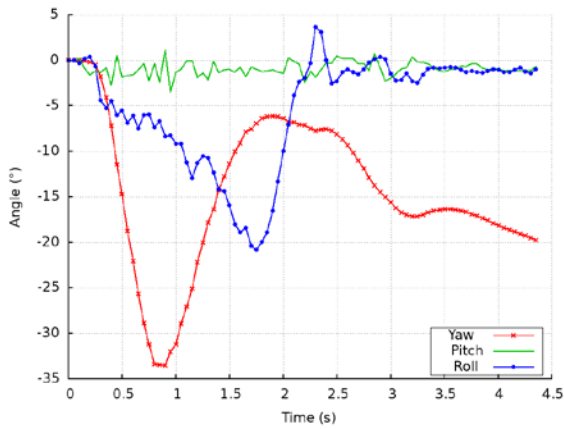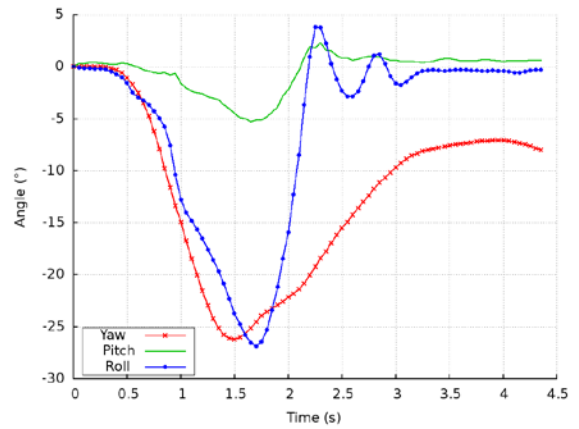
a. Tractor cabin CG

b. Trailer tandem axle

Figure B.10: Case *j*: yaw, pitch, and roll angles for the flat median wood-blockout Thrie-beam guardrail front-side impact
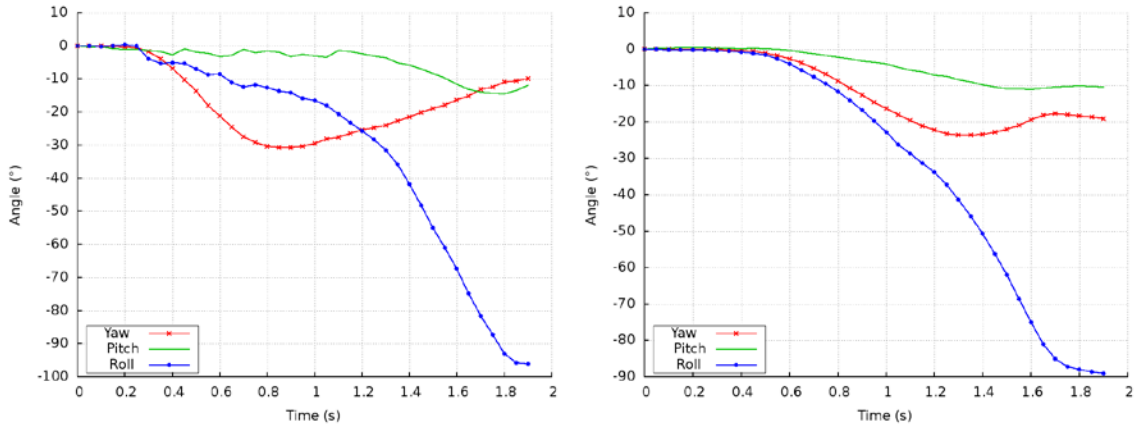
a. Tractor cabin CG   b. Trailer tandem axle

Figure B.11: Case *k*: yaw, pitch, and roll angles for the flat median steel-blockout Thrie-beam guardrail front-side impact
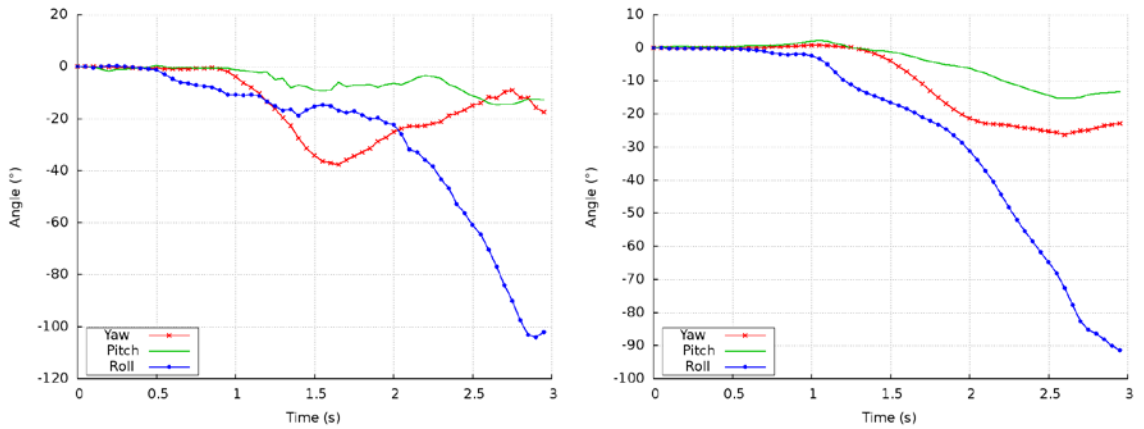
a. Tractor cabin CG   b. Trailer tandem axle

Figure B.12: Case *l*: yaw, pitch, and roll angles for the sloped median W-beam guardrail front-side impact
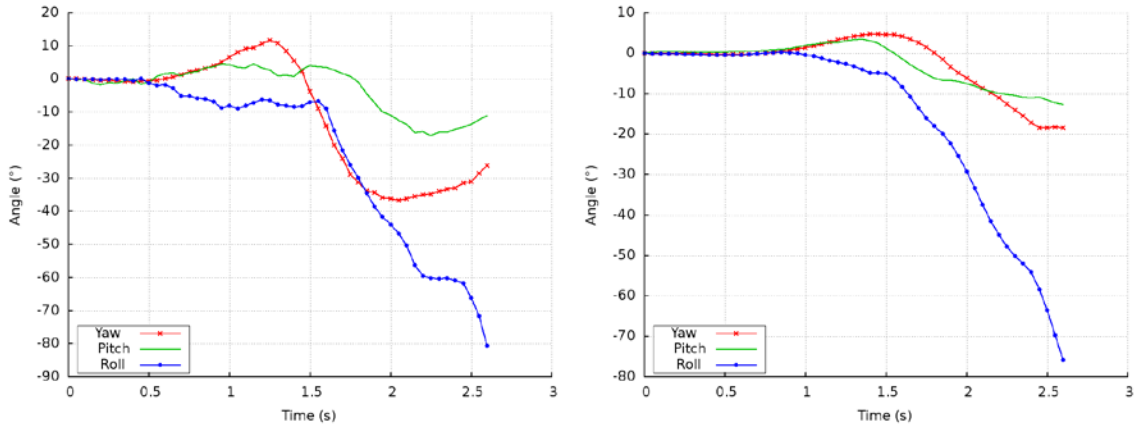
a. Tractor cabin CG   b. Trailer tandem axle

Figure B.13: Case *m*: yaw, pitch, and roll angles for the sloped median W-beam guardrail backside impact
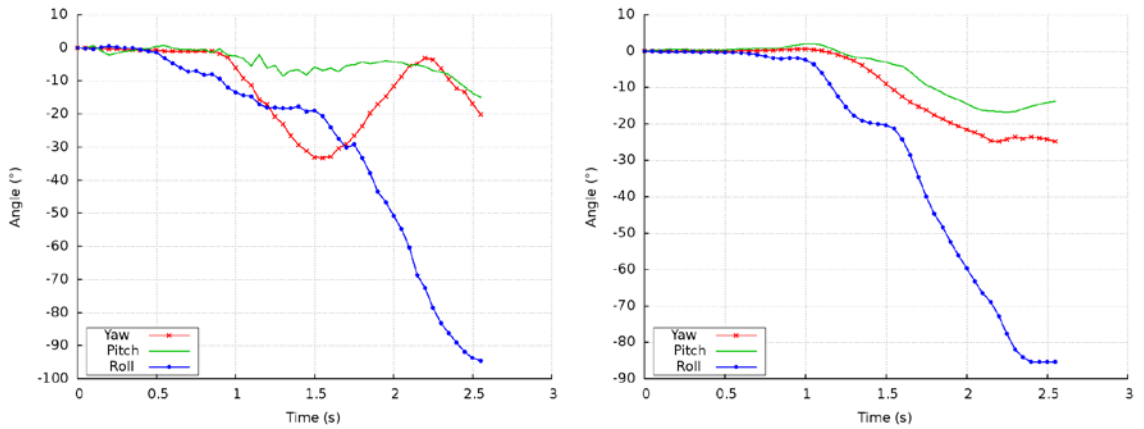
a. Tractor cabin CG   b. Trailer tandem axle

Figure B.14: Case *n*: yaw, pitch, and roll angles for the sloped median wood-blockout Thrie-beam guardrail front-side impact
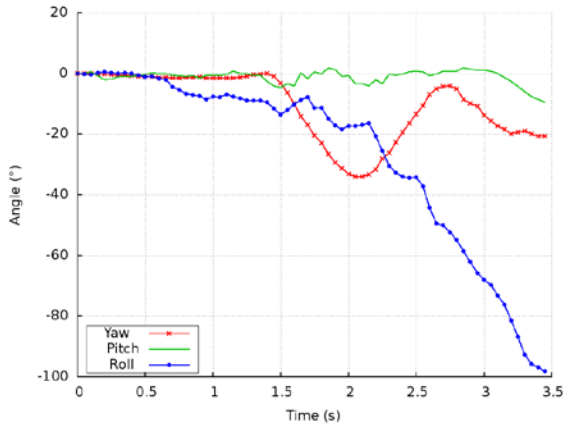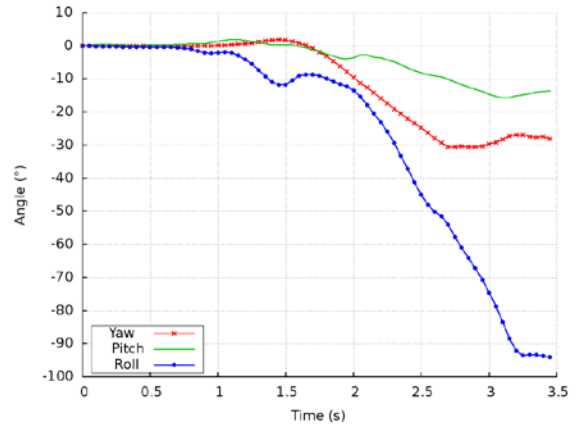
a. Tractor cabin CG

b. Trailer tandem axle

Figure B.15: Case *o*: yaw, pitch, and roll angles for the sloped median wood-blockout Thrie-beam guardrail backside impact
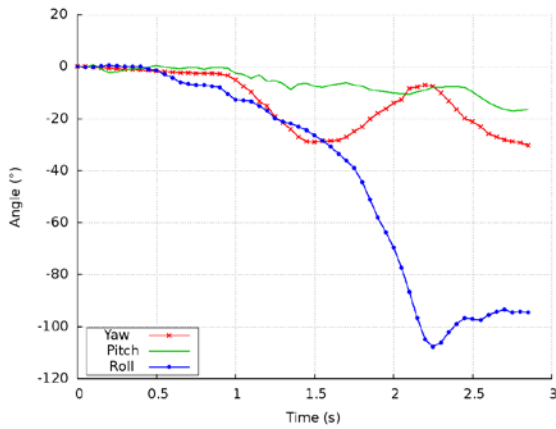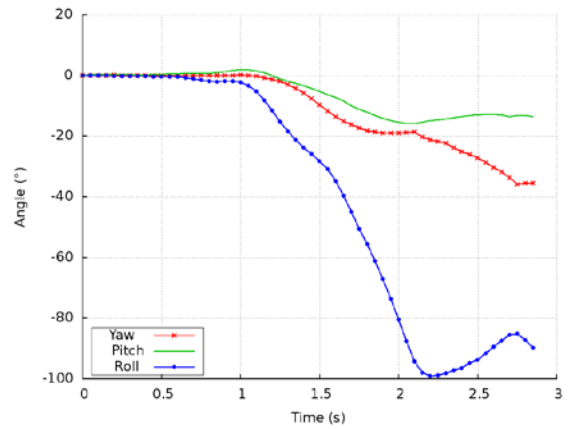
a. Tractor cabin CG

b. Trailer tandem axle

Figure B.16: Case *p*: yaw, pitch, and roll angles for the sloped median steel-blockout Thrie-beam guardrail front-side impact
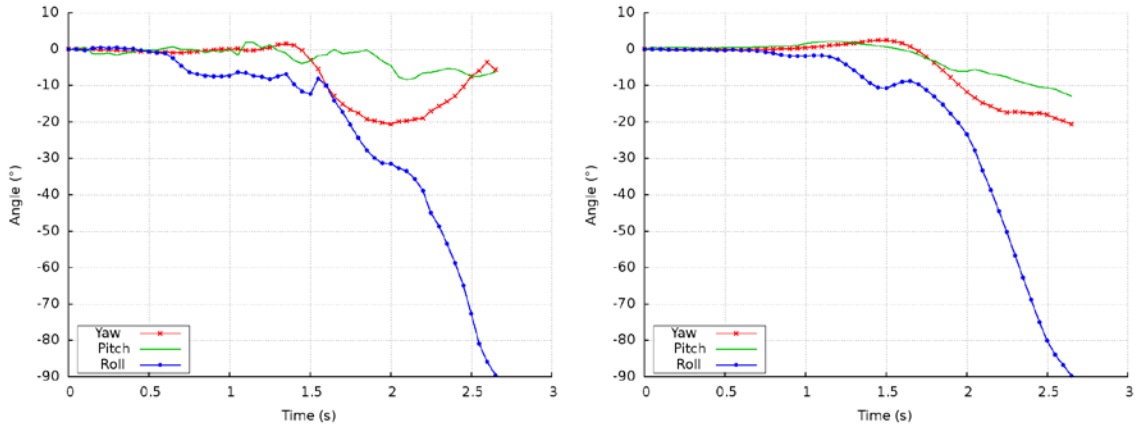
a. Tractor cabin CG   b. Trailer tandem axle

Figure B.17: Case *q*: yaw, pitch, and roll angles for the sloped median steel-blockout Thrie-beam guardrail backside impact
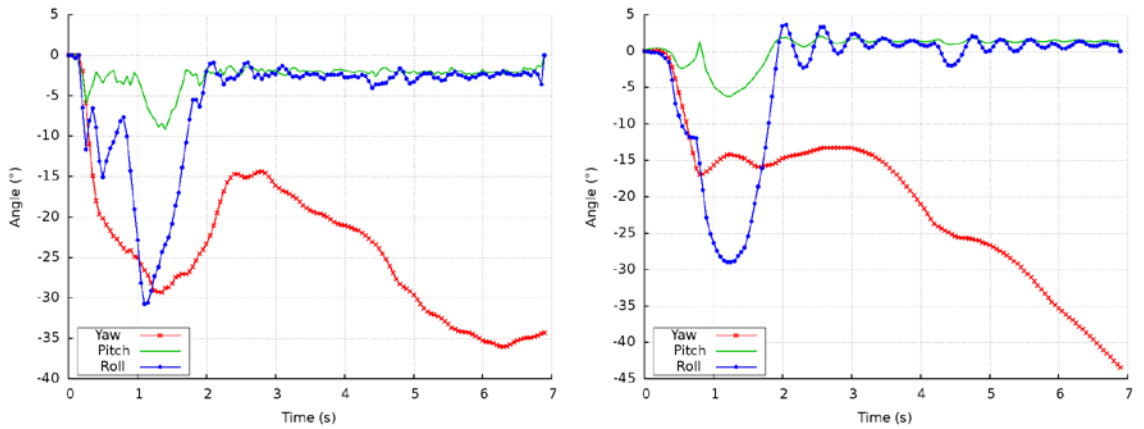
a. Tractor cabin CG   b. Trailer tandem axle

Figure B.18: Case *r*: yaw, pitch, and roll angles for the flat median concrete median barrier front-side impact
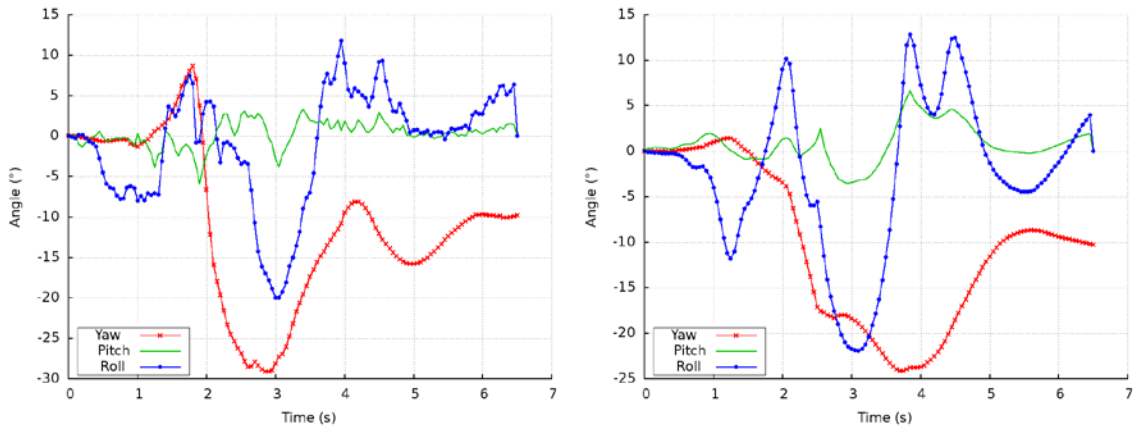
a. Tractor cabin CG

b. Trailer tandem axle

Figure B.19: Case *s*: yaw, pitch, and roll angles for the sloped median concrete median barrier backside impact

APPENDIX C: TRACTOR CABIN CG ACCELERATION PROFILES
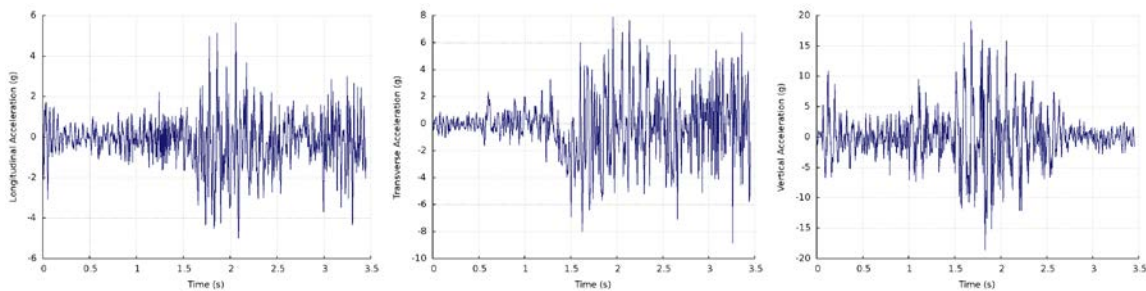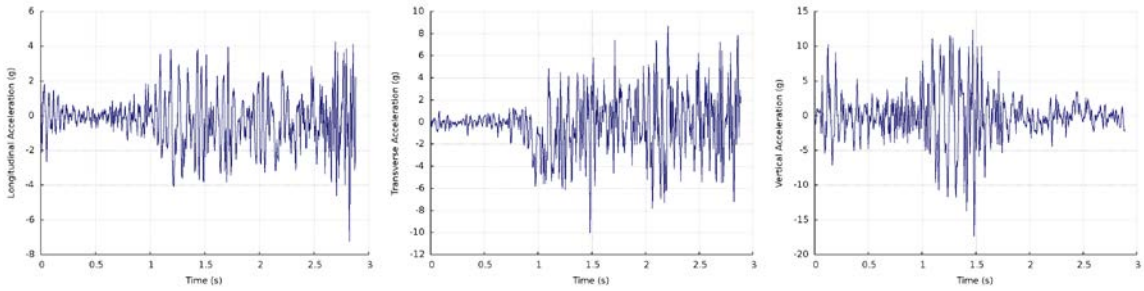

a. x-axis   b. y-axis   c. z-axis
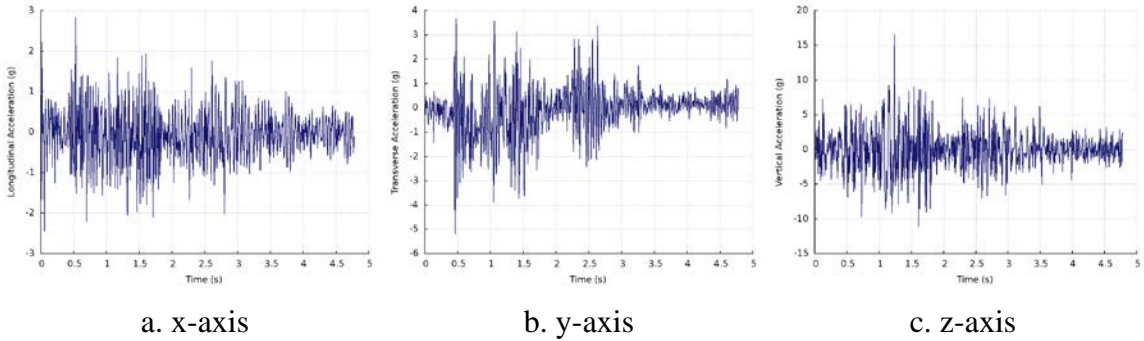
Figure C.1: Case *a*: time histories of the tractor cabin CG x-, y-, and z-axis
accelerations for the flat median three-CMB front-side impact

a. x-axis   b. y-axis   c. z-axis
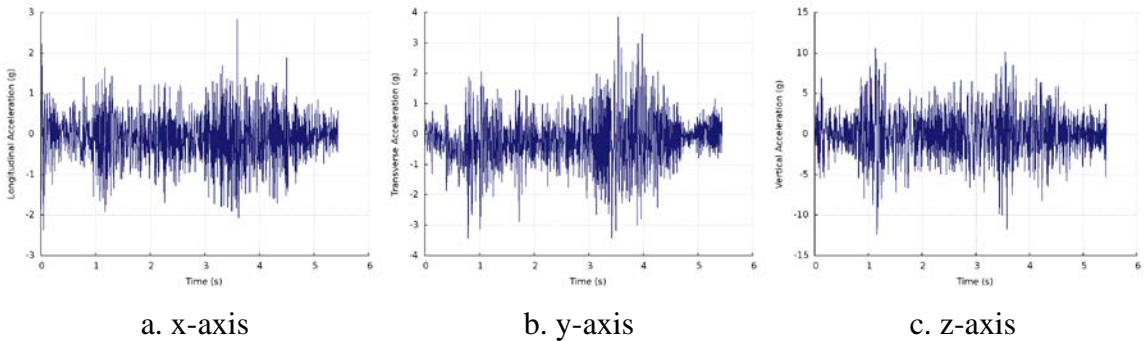
Figure C.2: Case *b*: time histories of the tractor cabin CG x-, y-, and z-axis
accelerations for the flat median three-CMB backside impact
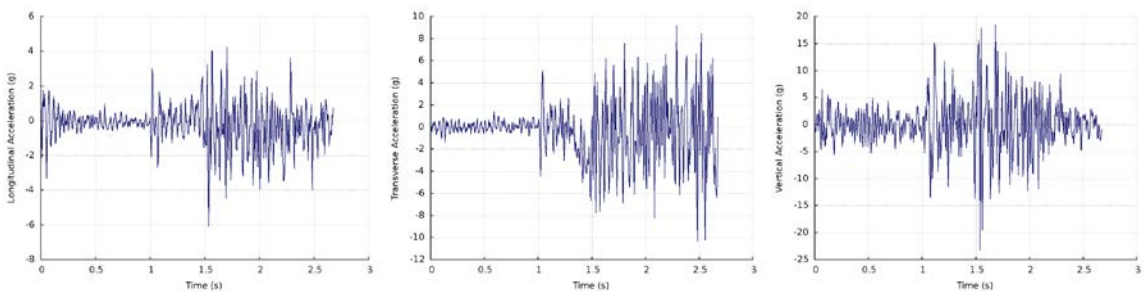

a. x-axis   b. y-axis   c. z-axis
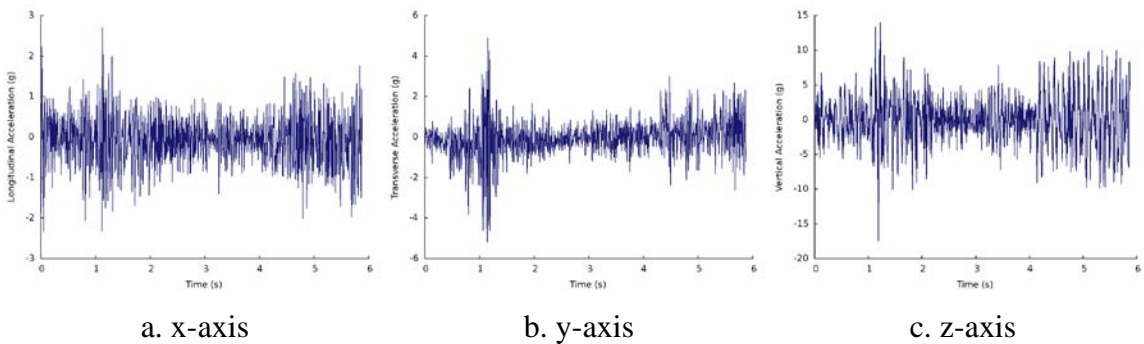
Figure C.3: Case *c*: time histories of the tractor cabin CG x-, y-, and z-axis
accelerations for the flat median four-CMB front-side impact
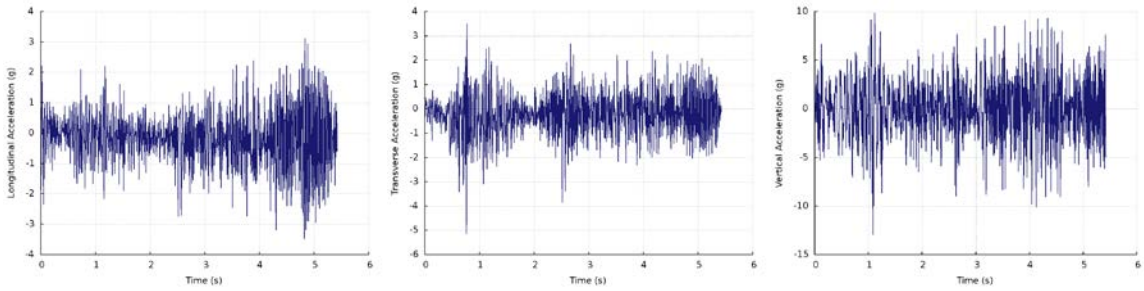
| a. x-axis | b. y-axis | c. z-axis |

Figure C.4: Case *d*: time histories of the tractor cabin CG x-, y-, and z-axis accelerations for the flat median four-CMB backside impact
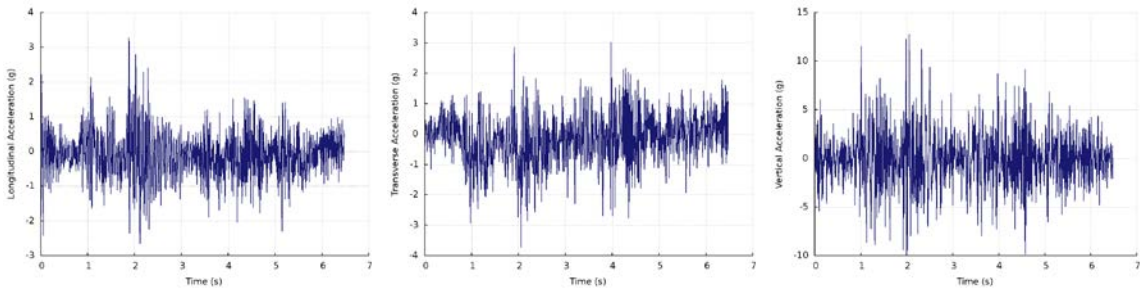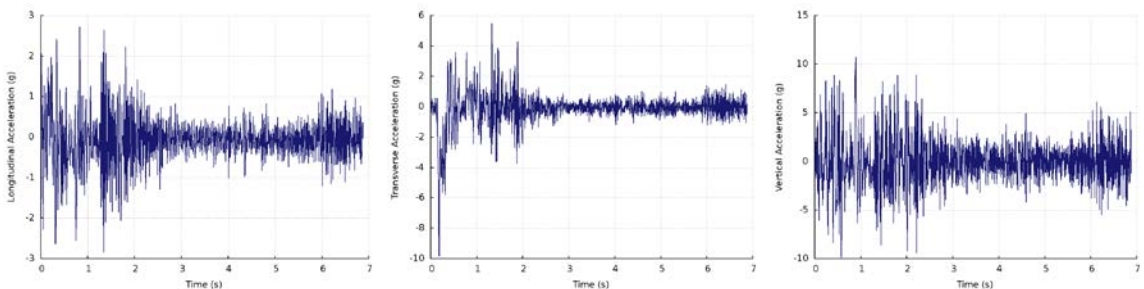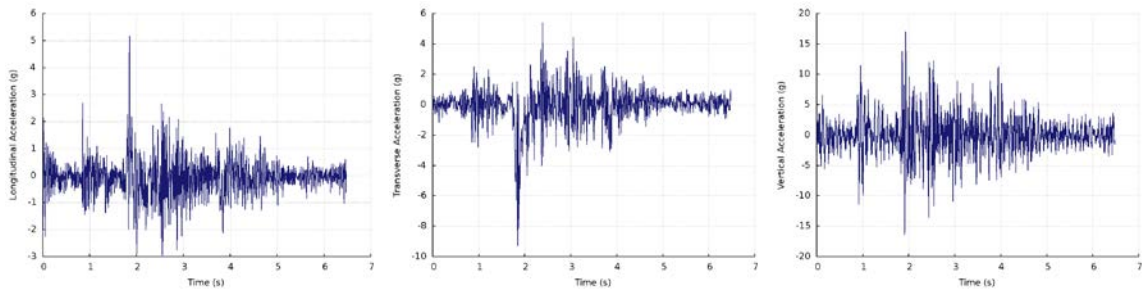

| a. x-axis | b. y-axis | c. z-axis |

Figure C.5: Case *e*: time histories of the tractor cabin CG x-, y-, and z-axis accelerations for the sloped median three-CMB front-side impact
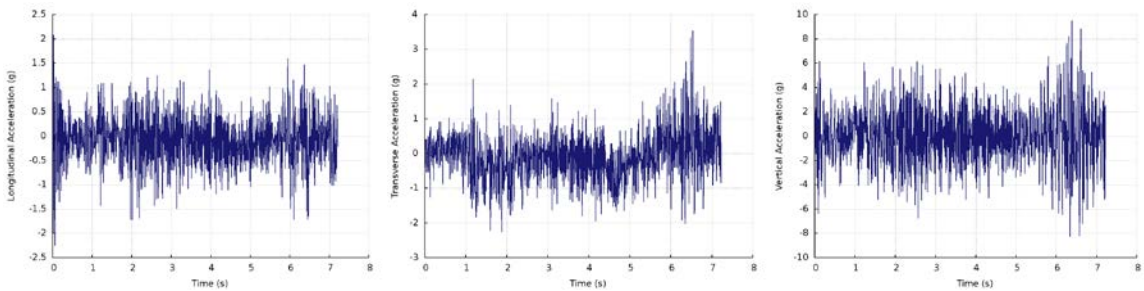
| a. x-axis | b. y-axis | c. z-axis |

Figure C.6: Case *f*: time histories of the tractor cabin CG x-, y-, and z-axis accelerations for the sloped median three-CMB backside impact
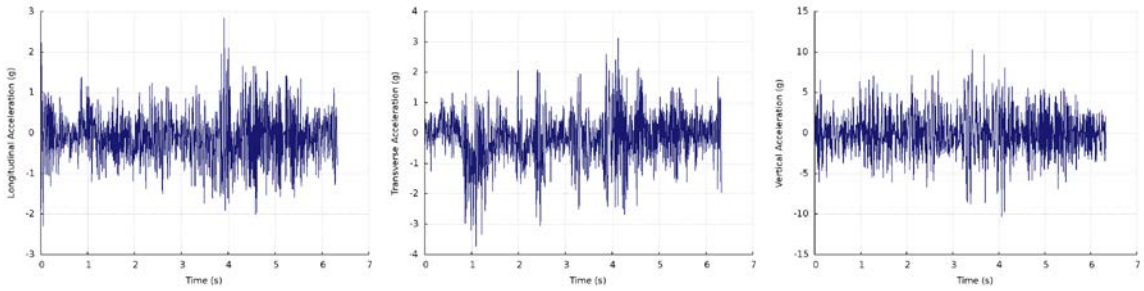
a. x-axis   b. y-axis   c. z-axis

Figure C.7: Case *g*: time histories of the tractor cabin CG x-, y-, and z-axis accelerations for the sloped median four-CMB front-side impact
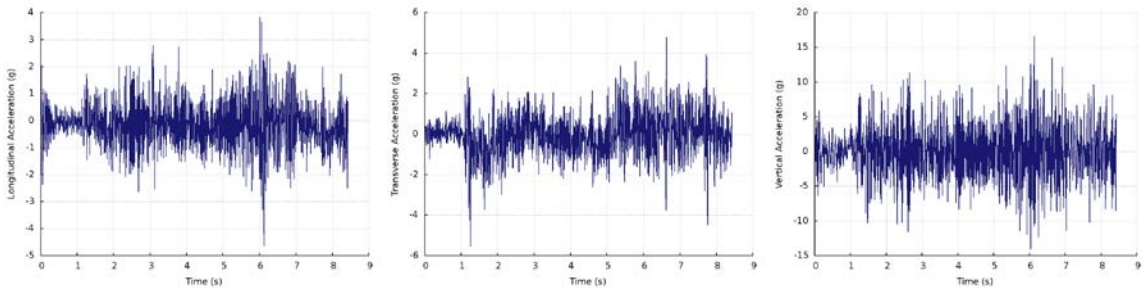
a. x-axis   b. y-axis   c. z-axis

Figure C.8: Case *h*: time histories of the tractor cabin CG x-, y-, and z-axis accelerations for the sloped median four-CMB backside impact
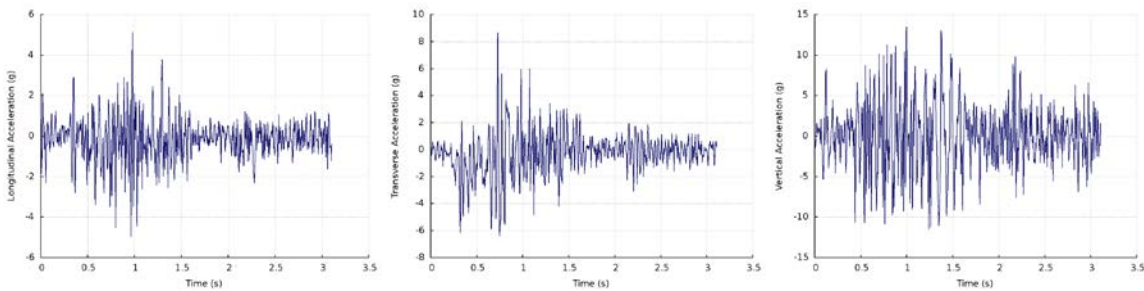
a. x-axis   b. y-axis   c. z-axis

Figure C.9: Case *i*: time histories of the tractor cabin CG x-, y-, and z-axis accelerations for the flat median W-beam guardrail front-side impact
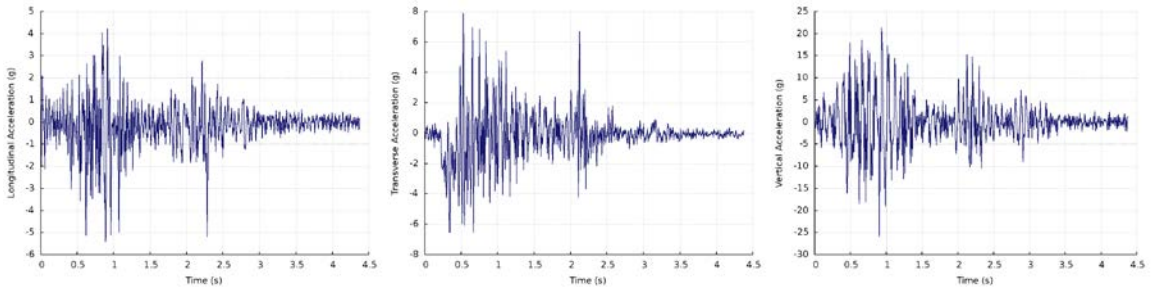
a. x-axis   b. y-axis   c. z-axis

Figure C.10: Case *j*: time histories of the tractor cabin CG x-, y-, and z-axis accelerations for the flat median wood-blockout Thrie-beam guardrail front-side impact
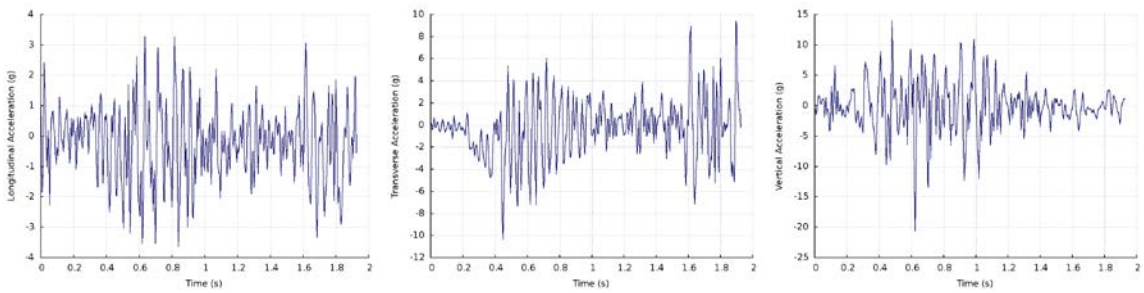
a. x-axis   b. y-axis   c. z-axis

Figure C.11: Case *k*: time histories of the tractor cabin CG x-, y-, and z-axis accelerations for the flat median steel-blockout Thrie-beam guardrail front-side impact
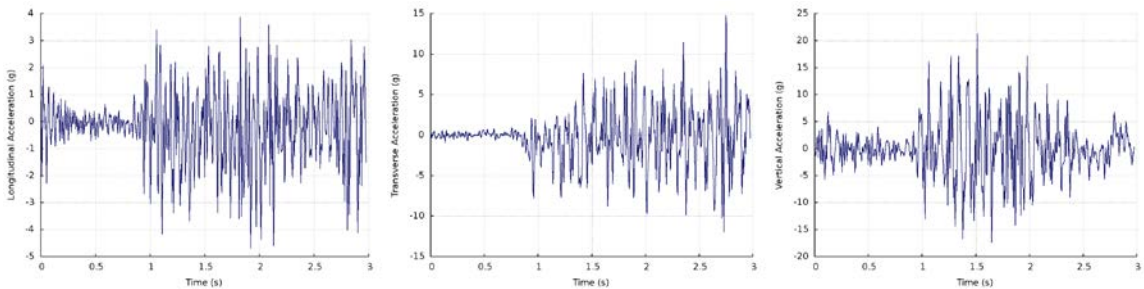
a. x-axis   b. y-axis   c. z-axis

Figure C.12: Case *l*: time histories of the tractor cabin CG x-, y-, and z-axis accelerations for the sloped median W-beam guardrail front-side impact
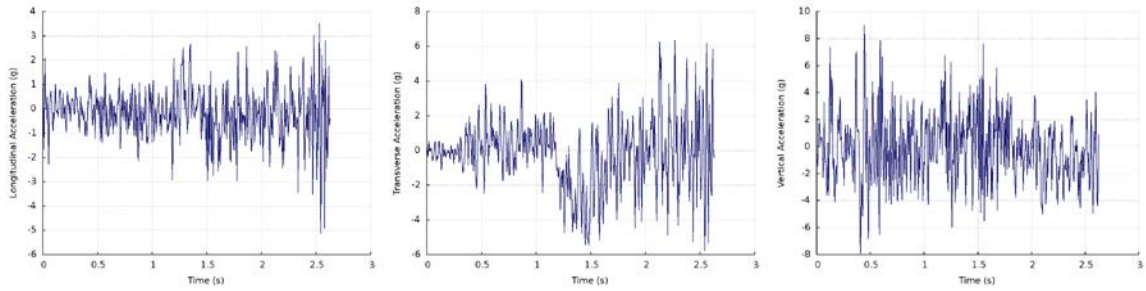
a. x-axis   b. y-axis   c. z-axis

Figure C.13: Case *m*: time histories of the tractor cabin CG x-, y-, and z-axis accelerations for the sloped median W-beam guardrail backside impact
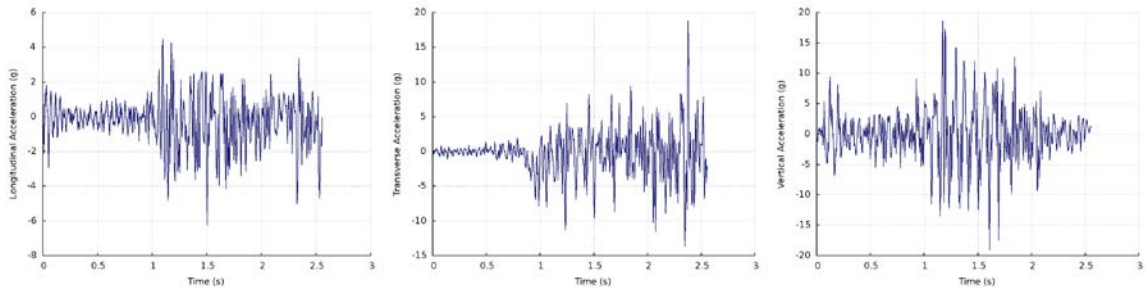
a. x-axis   b. y-axis   c. z-axis

Figure C.14: Case *n*: time histories of the tractor cabin CG x-, y-, and z-axis accelerations for the sloped median wood-blockout Thrie-beam guardrail front-side impact

a. x-axis   b. y-axis   c. z-axis

Figure C.15: Case *o*: time histories of the tractor cabin CG x-, y-, and z-axis accelerations for the sloped median wood-blockout Thrie-beam guardrail backside impact

a. x-axis   b. y-axis   c. z-axis

Figure C.16: Case *p*: time histories of the tractor cabin CG x-, y-, and z-axis accelerations for the sloped median steel-blockout Thrie-beam guardrail front-side impact

a. x-axis   b. y-axis   c. z-axis

Figure C.17: Case *q*: time histories of the tractor cabin CG x-, y-, and z-axis accelerations for the sloped median steel-blockout Thrie-beam guardrail backside impact

a. x-axis   b. y-axis   c. z-axis

Figure C.18: Case *r*: time histories of the tractor cabin CG x-, y-, and z-axis accelerations for the flat median concrete median barrier front-side impact

a. x-axis　　　　　　　b. y-axis　　　　　　　c. z-axis

Figure C.19: Case *s*: time histories of the tractor cabin CG x-, y-, and z-axis accelerations for the sloped median concrete median barrier backside impact

APPENDIX D: ACCELERATION SEVERITY INDICES
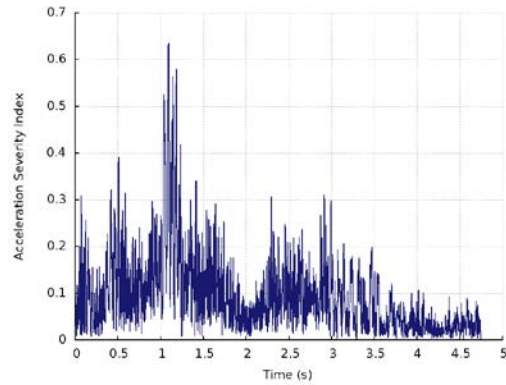
Figure D.1: Case *a*: ASI profile of the tractor cabin CG for the flat median three-CMB front-side impact
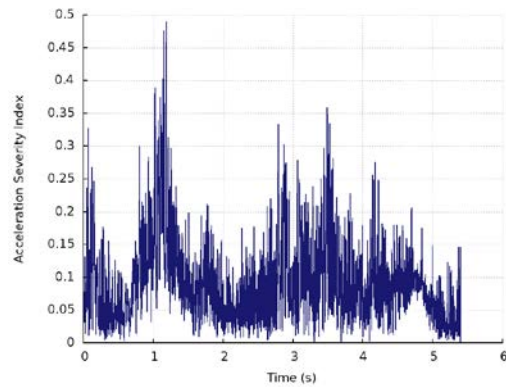
Figure D.2: Case *b*: ASI profile of the tractor cabin CG for the flat median three-CMB backside impact
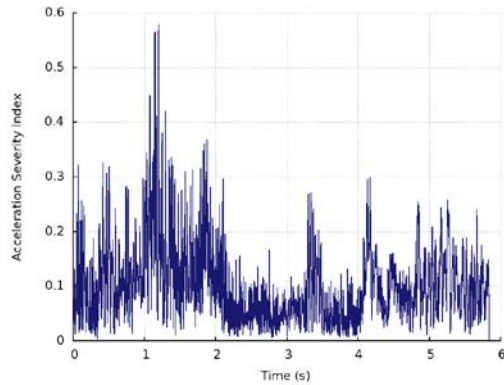
Figure D.3: Case *c*: ASI profile of the tractor cabin CG for the flat median front-side four-CMB impact
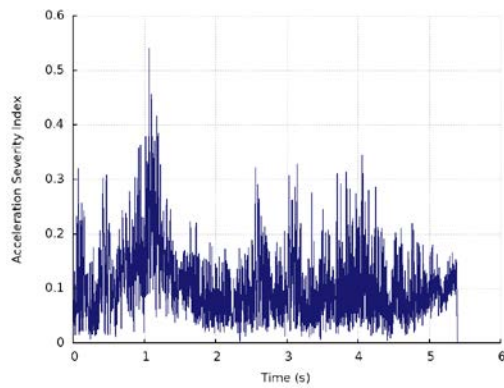
Figure D.4: Case *d*: ASI profile of the tractor cabin CG for the flat median backside four-CMB impact
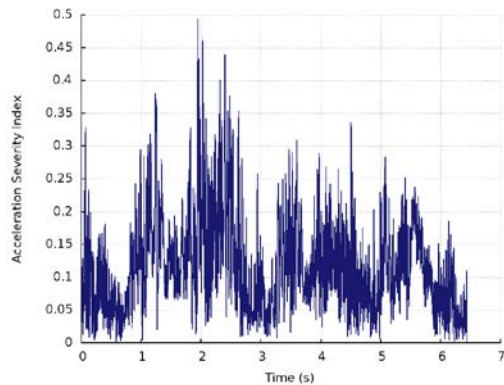
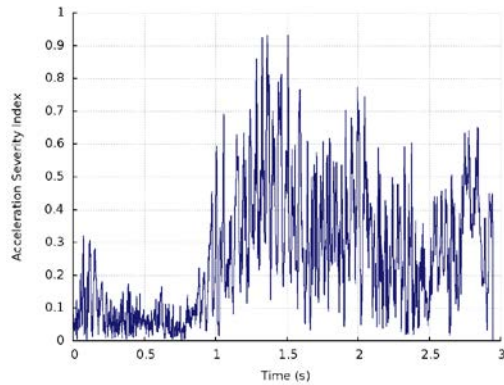

Figure D.5: Case *e*: ASI profile of the tractor cabin CG for the sloped median three-CMB front-side impact
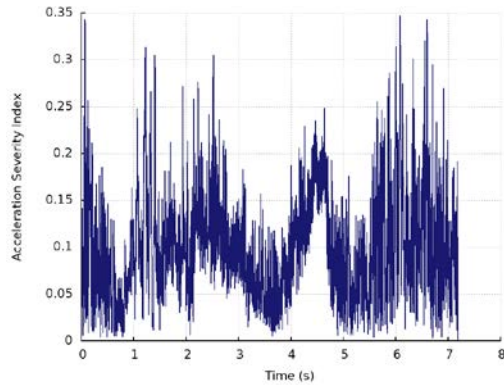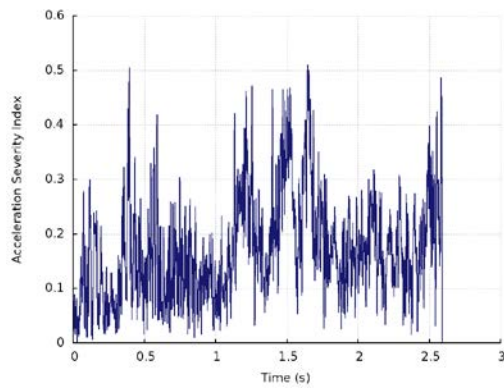
Figure D.6: Case *f*: ASI profile of the tractor cabin CG for the sloped median three-CMB backside impact
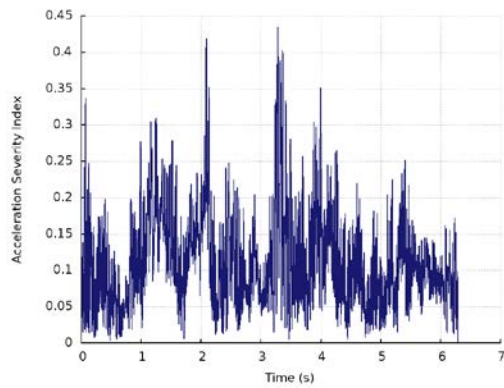
Figure D.7: Case *g*: ASI profile of the tractor cabin CG for the sloped median four-CMB front-side impact
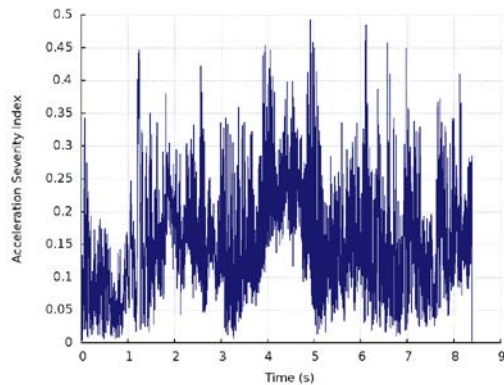
Figure D.8: Case *h*: ASI profile of the tractor cabin CG for the sloped median four-CMB backside impact
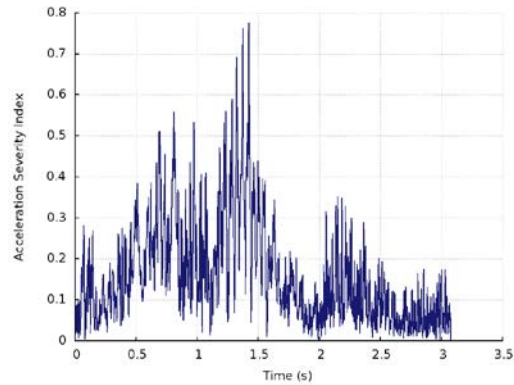
Figure D.9: Case *i*: ASI profile of the tractor cabin CG for the flat median W-beam guardrail front-side impact
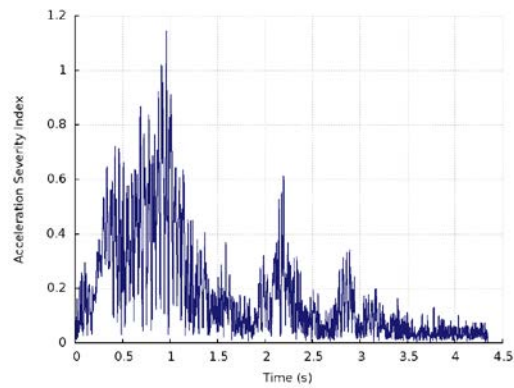
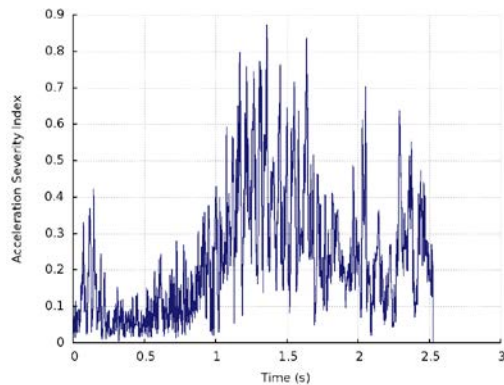Figure D.10: Case *j*: ASI profile of the tractor cabin CG for the flat median wood-blockout Thrie-beam guardrail front-side impact
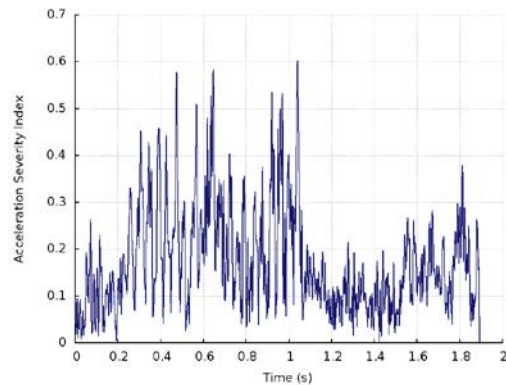
Figure D.11: Case *k*: ASI profile of the tractor cabin CG for the flat median steel-blockout Thrie-beam guardrail front-side impact

Figure D.12: Case *l*: ASI profile of the tractor cabin CG for the sloped median
W-beam guardrail front-side impact

Figure D.13: Case *m*: ASI profile of the tractor cabin CG for the sloped median
W-beam guardrail backside impact

Figure D.14: Case *n*: ASI profile of the tractor cabin CG for the sloped median
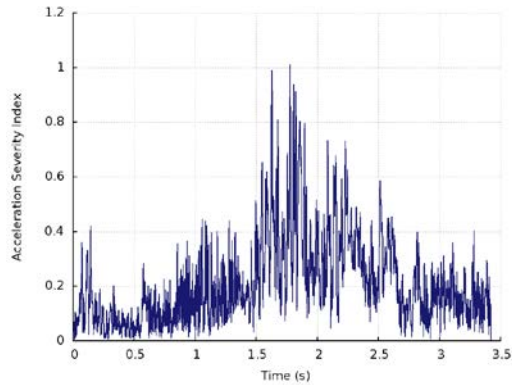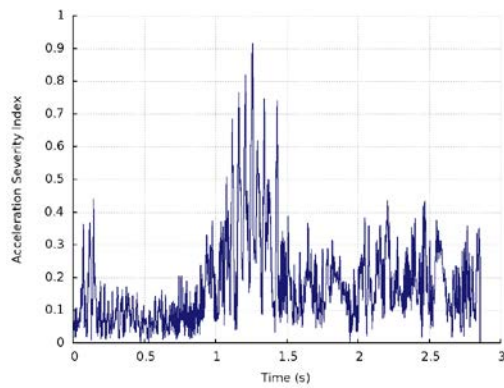wood-blockout Thrie-beam guardrail front-side impact

Figure D.15: Case *o*: ASI profile of the tractor cabin CG for the sloped median
wood-blockout Thrie-beam guardrail backside impact

Figure D.16: Case *p*: ASI profile of the tractor cabin CG for the sloped median
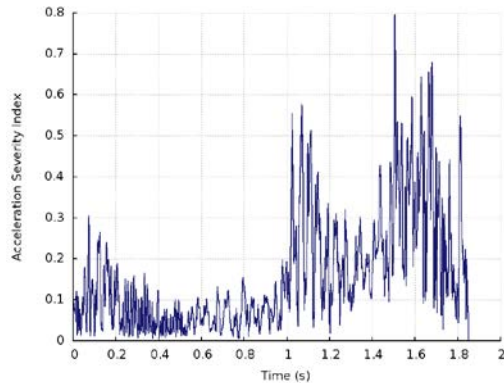steel-blockout Thrie-beam guardrail front-side impact

Figure D.17: Case *q*: ASI profile of the tractor cabin CG for the sloped median
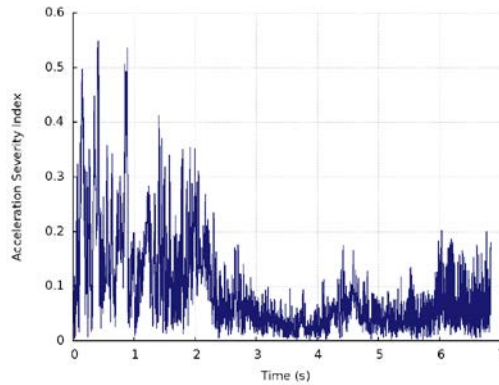steel-blockout Thrie-beam guardrail backside impact

Figure D.18: Case *r*: ASI profile of the tractor cabin CG for the flat median concrete median barrier front-side impact
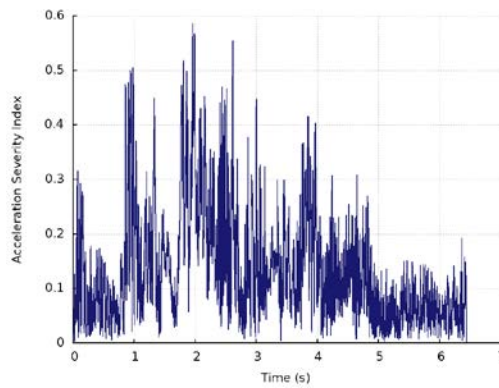

Figure D.19: Case *s*: ASI profile of the tractor cabin CG for the sloped median concrete median barrier backside impact